

**Sustainable Management of  
Flowback Water during  
Hydraulic Fracturing of  
Marcellus Shale for Natural Gas  
Production**

**April 2015**

**Final Technical Report**

**January 1, 2010 – January 24, 2015**

**Principal Author:  
Radisav D. Vidic**

**Grant Number: DE-FE0000975**

**Submitted to:**

**U.S. Department of Energy  
National Energy Technology Laboratory  
626 Cochrans Mill Road  
Pittsburgh, PA 15236-0940**

**Submitted by:**

**University of Pittsburgh  
Department of  
Civil and Environmental Engineering  
Pittsburgh, PA 15261-2294**

**Disclaimer:** This report was prepared as an account of work sponsored by an agency of the United States Government. Neither the United States Government nor any agency thereof, nor any of their employees, makes any warranty, express or implied, or assumes any legal liability or responsibility for the accuracy, completeness, or usefulness of any information, apparatus, product, or process disclosed, or represents that its use would not infringe privately owned rights. Reference herein to any specific commercial product, process, or service by trade name, trademark, manufacturer, or otherwise does not necessarily constitute or imply its endorsement recommendation, or favoring by the United States Government or any agency thereof. The views and opinions of authors expressed herein do not necessarily state or reflect those of the United States Government or any agency thereof.

## ABSTRACT

This study evaluated the feasibility of using abandoned mine drainage (AMD) as make-up water for the reuse of produced water for hydraulic fracturing. There is an abundance of AMD sources near permitted gas wells as documented in this study that can not only serve as makeup water and reduce the demand on high quality water resources but can also as a source of chemicals to treat produced water prior to reuse.

The assessment of AMD availability for this purpose based on proximity and relevant regulations was accompanied by bench- and pilot-scale studies to determine optimal treatment to achieve desired water quality for use in hydraulic fracturing.

Sulfate ions that are often present in AMD at elevated levels will react with  $Ba^{2+}$  and  $Sr^{2+}$  in produced water to form insoluble sulfate compounds. Both membrane microfiltration and gravity separation were evaluated for the removal of solids formed as a result of mixing these two impaired waters. Laboratory studies revealed that neither AMD nor barite formed in solution had significant impact on membrane filtration but that some produced waters contained submicron particles that can cause severe fouling of microfiltration membrane. Coagulation/flocculation was found to be an effective process for the removal of suspended solids and both bench- and pilot-scale studies revealed that optimal process conditions can consistently achieve the turbidity of the finished water below 5 NTU. Adjusting the blending ratio of AMD and produced water can achieve the desired effluent sulfate concentration that can be accurately predicted by chemical thermodynamics.

Co-treatment of produced water and AMD will result in elevated levels of naturally occurring radioactive materials (NORM) in the solid waste generated in this process due to radium co-precipitation with barium sulfate.

Laboratory studies revealed that the mobility of barite that may form in the subsurface due to the presence of sulfate in the fracturing fluid can be controlled by the addition of appropriate antisclalants.

## ACKNOWLEDGEMENTS

This work was supported by the U.S. Department of Energy under Award Number DE-FE0000975. We thank the following individuals for serving on our Project Advisory Committee: Bob Garland (Universal Well Services), Dave Cercone (Consol Energy), Albert Aloia (Consol Energy), Mark Gannon (Tetra Tech), Steve Hughes (Tetra Tech), Kashi Banerjee (Veolia Water Services), Vince Yantko (Pennsylvania Department of Environmental Protection), Brendan McLaughlin (CDM), Tony Gaudlip (Range Resources) and Pete Miller (Range Resources). We are grateful to Aquatech International Corporation (Canonsburg, PA) for providing access to the wastewater treatment facility in Tioga County for pilot-scale testing and for their assistance in that part of the project. We also thank Department of Conservation and Natural Resources and Susquehanna River Basin Commission for permitting the use of abandoned mine discharge for pilot-scale study.

## TABLE OF CONTENTS

<b>1.0</b>	<b>INTRODUCTION</b> .....	1-1
1.1	Unconventional Shale Gas Extraction .....	1-2
1.2	Flowback Water Management .....	1-4
1.3	Abandoned Mine Drainage .....	1-6
1.4	Utilization of AMD for Flowback Water Reuse.....	1-7
1.4.1	Co-treatment of Flowback Water and AMD.....	1-7
1.4.2	Concerns with AMD Use in Unconventional Gas Extraction .....	1-8
1.4.2.1	Compatibility with Hydraulic Fracturing Chemical Additives.....	1-8
1.4.2.2	Impact on Well Productivity .....	1-9
1.4.2.3	Potential for Bacterial Activity.....	1-10
1.4.2.4	Management of Solid Wastes .....	1-11
1.4.2.5	Regulatory Concerns .....	1-13
1.5	Study Objectives .....	1-14
1.6	Organization of the Report .....	1-15
1.7	References .....	1-15
<b>2.0</b>	<b>GIS AMD DATABASE</b> .....	2-1
2.1	Location of Flowback Water and AMD .....	2-1
2.1.1	Flowback Water Location .....	2-1
2.1.2	AMD Location.....	2-4
2.2	Identification AMD Sites with GIS Database.....	2-6
2.3	References .....	2-8

<b>3.0</b>	<b>SPATIAL AND TEMPORAL CORRELATION OF WATER QUALITY PARAMETERS OF PRODUCED WATERS FROM DEVONIAN-AGE SHALE FOLLOWING HYDRAULIC FRACTURING</b>	3-1
<b>3.1</b>	<b>Materials and Methods</b>	3-1
3.1.1	Flowback Water Sampling	3-1
3.1.2	Analytical Methods	3-2
3.1.3	Other Data Sources	3-2
<b>3.2</b>	<b>Results and Discussion</b>	3-3
3.2.1	Composition of Flowback Water Recovered with Time	3-3
3.2.2	Origin of Salinity in the Produced Water	3-8
3.2.3	Spatial Trends in Flowback Water Chemistry in Pennsylvania	3-17
<b>3.3</b>	<b>References</b>	3-22
<b>4.0</b>	<b>TREATABILITY STUDIES WITH SYNTHETIC AND ACTUAL WASTEWATERS</b>	4-1
<b>4.1</b>	<b>Precipitation of Ba and Sr as Sulfates</b>	4-1
4.1.1	Materials and Methods	4-1
4.1.1.1	Flowback Water Characteristics	4-1
4.1.1.2	Experiment Protocol	4-2
4.1.1.3	Chemical Equilibrium Models	4-2
4.1.2	Results and Discussion	4-6
4.1.2.1	Kinetics of Barite and Celestite Precipitation in Synthetic Flowback Water	4-6
4.1.2.2	Equilibrium Predictions for Synthetic Flowback Waters	4-12
4.1.2.3	Comparison of Barite and Celestite Precipitation in Synthetic and Real Flowback Waters	4-16
4.1.3	Conclusions	4-19
4.1.4	References	4-20

<b>4.2</b>	<b>Precipitation of Ba and Sr with AMD</b> .....	4-24
4.2.1	Materials and Methods .....	4-24
4.2.1.1	Flowback Water and AMD Sampling .....	4-24
4.2.1.2	Mixing Experiments and Analytical Method .....	4-25
4.2.1.3	Radium Leaching Test .....	4-25
4.2.2	Results and Discussion .....	4-25
4.2.2.1	Mixing Experiments and Equilibrium Prediction .....	4-25
4.2.2.2	Celestite Precipitation .....	4-28
4.2.2.3	Empirical Kinetic Model for BaSO <sub>4</sub> Precipitation .....	4-31
4.2.2.4	Radium Leaching Test .....	4-35
4.2.3	Conclusion.....	4-36
4.2.4	References .....	4-36
<b>4.3</b>	<b>Evaluation of Membrane Microfiltration for Solids Separation</b> .....	4-38
4.3.1	Materials and Methods .....	4-38
4.3.1.1	Feed Water .....	4-38
4.3.1.2	Fouling Mechanism Theory.....	4-40
4.3.1.3	Particle Size Distribution Analysis.....	4-41
4.3.1.4	Membrane Filtration Experiment.....	4-42
4.3.1.5	Stability Evaluation.....	4-43
4.3.2	Results and Discussion .....	4-44
4.3.2.1	Membrane Filtration of the Mixture of AMD and Flowback Water.....	4-44
4.3.2.2	Fouling Mechanism Identification.....	4-46
4.3.2.3	Membrane Fouling Analysis.....	4-56
4.3.2.4	Stability of Colloidal Suspension .....	4-61
4.3.3	Conclusions.....	4-64
4.3.4	References .....	4-65

<b>4.4</b>	<b>Evaluation of Coagulation/Flocculation for Solids Removal</b>	4-67
4.4.1	Materials and Methods	4-67
4.4.1.1	Feed Water Characteristics	4-67
4.4.1.2	Conventional Coagulation/Flocculation Process	4-68
4.4.1.3	Ballasted Flocculation	4-71
4.4.1.4	Settling characteristics of the sludge	4-71
4.4.2	Results and Discussion	4-72
4.4.2.1	Conventional Coagulation/Flocculation Jar Tests – Mixture 1	4-72
4.4.2.2	Conventional Coagulation/Flocculation Jar Tests – Mixtures 2, 3 and 4	4-74
4.4.2.3	Conventional Coagulation/Flocculation Jar Tests – Mixtures 5 and 6	4-76
4.4.2.4	Ballasted Flocculation – Mixture 1	4-78
4.4.2.5	Ballasted Flocculation – Mixtures 2, 3 and 4	4-80
4.4.2.6	Ballasted Flocculation – Mixtures 5 and 6	4-82
4.4.2.7	Settling properties of the sludge	4-83
4.4.3	Conclusion	4-84
4.4.4	References	4-85
<b>5.0</b>	<b>FIELD DEMONSTRATION OF THE TREATMENT SYSTEM</b>	5-1
<b>5.1</b>	<b>Materials and Methods</b>	5-1
5.1.1	Characteristics of Flowback Water and AMD	5-1
5.1.2	Pilot-scale Operation	5-3
5.1.3	Analytical Methods	5-5
<b>5.2</b>	<b>Results and Discussion</b>	5-6
5.2.1	Sulfate Removal	5-6
5.2.2	AMD as a source of coagulant	5-8
<b>5.3</b>	<b>Conclusions</b>	5-10
<b>5.4</b>	<b>References</b>	5-11



<b>6.0 COMPATIBILITY OF AMD WATER WITH HYDRAULIC FRACTURING OF MARCELLUS SHALE</b> .....	6-1
<b>6.1 Impact of Antiscalants on the Fate of Barite in the Unconventional Wells</b> .....	6-2
6.1.1 Materials and Methods .....	6-3
6.1.1.1 Granular Porous Media .....	6-3
6.1.1.2 Feed Solution .....	6-3
6.1.1.3 Column Experiment.....	6-4
6.1.1.4 Single Collector Efficiency Model .....	6-5
6.1.2 Results and Discussion .....	6-7
6.1.2.1 Characterization of Barium Sulfate Particles.....	6-7
6.1.2.2 Mobility of BaSO <sub>4</sub> through Proppant .....	6-12
6.1.2.3 Impact of Antiscalants on the Mobility of BaSO <sub>4</sub> through Proppant .....	6-14
6.1.2.4 Impact of Antiscalants on the Mobility of BaSO <sub>4</sub> through Shale Core .....	6-17
6.1.3 Conclusions.....	6-20
<b>6.2 Affinity of Barium Sulfate for the Casing Material</b> .....	6-21
6.2.1 Materials and Methods .....	6-21
6.2.1.1 Bench-scale Recirculating System.....	6-21
6.2.1.2 Feed Solution .....	6-21
6.2.1.3 Theoretical Calculation of the Forces Acting on Barite Particles.....	6-22
6.2.2 Results and Discussion .....	6-24
6.2.2.1 Theoretical Calculation of the Total Force .....	6-24
6.2.2.2 Impact of Temperature on Barite Deposition .....	6-25
6.2.2.3 Deposition of Freshly Precipitated Barite in the Absence of Antiscalants...6-26	
6.2.2.4 Deposition of Freshly Precipitated Barite in the Presence of Antiscalants..6-27	
6.2.3 Conclusions.....	6-30
<b>6.3 References</b> .....	6-30
<b>Appendix GIS Database User Manual</b> .....	A-1

## EXECUTIVE SUMMARY

Unconventional (shale) gas extraction produces large amount of wastewater (i.e., flowback and produced water) that is typically disposed in Class II Underground Injection Control (UIC) wells. Due to the lack of such wells in Pennsylvania, flowback and produced waters are generally reused for hydraulic fracturing. Because only 10-40% of the hydraulic fracturing fluid returns to the surface during the flowback period, it is necessary to supplement this impaired water to be able to fracture the next well. This study evaluated the feasibility of using abandoned mine drainage (AMD) as a make up water for hydraulic fracturing in Marcellus Shale. As AMD is often available in the vicinity of planned natural gas wells, this approach can reduce the need for fresh water utilization and the cost for water transport.

The overall objective of this study was to evaluate the feasibility of using AMD for flowback water reuse. Specific objectives of the research were as follows:

- (a) Evaluate the location of AMD in Pennsylvania and compile these data into a geographic information system (GIS);
- (b) Evaluate spatial and temporal characteristics of Marcellus Shale produced water;
- (c) Conduct bench-scale experiments to characterize the kinetics and equilibrium of chemical reactions that may occur when flowback water and AMD are mixed;
- (d) Evaluate potential separation processes to remove suspended solids formed by mixing flowback and AMD and optimize the treatment process in the laboratory;
- (e) Demonstrate the feasibility of the proposed treatment process in pilot-scale treatment system; and
- (e) Evaluate the affinity of barium sulfate to attach and form scales on the production casing, proppant surface or shale core.

### GIS-based Database

Locations of AMD sites in Pennsylvania were compiled in a GIS-based database that can be searched to identify all known AMD locations in the vicinity of a proposed location. The database includes the quantity and quality of the AMD source water if such information is

publicly available. Spatial analysis of available data indicated that multiple AMD sources are typically available near permitted and proposed shale gas wells.

### **Spatial and Temporal Correlation of Flowback Water Quality Parameters**

Chemical analyses of 160 flowback and produced water samples collected from hydraulically fractured Marcellus Shale gas wells in Pennsylvania were correlated with spatial and temporal information to reveal underlying trends. Chloride was used as a reference for the comparison as its concentration varies with time of contact with the shale. Most major cations (i.e., Ca, Mg, Sr) were well-correlated with chloride concentration while barium exhibited strong influence of geographic location (i.e., higher levels in the northeast than in southwest). Comparisons against brines from adjacent formation provided insight into the origin of salinity in produced waters from Marcellus Shale. Major cations exhibited variations that cannot be explained by simple dilution of existing formation brine with the fracturing fluid, especially during the early flowback production when the composition of the fracturing fluid and solid-liquid interactions influence the quality of the produced water. Water quality analysis in this study may help guide water management strategies for the development of unconventional gas resources.

### **Treatability Study for Ba and Sr Precipitation as Sulfates**

Flowback water from natural gas extraction in Marcellus Shale contains very high concentrations of inorganic salts and organic chemicals. Potential reuse of this water in subsequent hydraulic fracturing operations may be limited by high concentrations of divalent cations (e.g., Ba, Sr and Ca).

Kinetics of barite and celestite precipitation in flowback waters from different well sites was evaluated in this study. Ba reacted rapidly with sulfate and reached equilibrium within 30 min while Sr reacted slowly and it required several days to reach equilibrium.

Equilibrium concentrations of Ba and Sr predicted by thermodynamic models were compared with experimental results. Activity corrections based on Pitzer equation provided the best agreement with experimental data for both Ba and Sr.

Comparison of barite and celestite precipitation kinetics in actual and synthetic flowbackwater revealed that there was no observable impact of organics and other minor components in actual flowback water on barite precipitation rate. This was mainly due to the fact that barite precipitation occurred relatively quickly due to high saturation indices utilized in this

study. On the other hand, lattice poisoning and complexation with organic matter had profound impact on comparatively slower celestite precipitation. The presence of organic matter in actual flowback water increased Sr concentration in solution and contributed to the discrepancy between measured and predicted concentrations.

### **Treatability Study for Ba and Sr Precipitation Using AMD**

Sulfate concentrations predicted by PHREEQC software were very close to those measured after 60 min of reaction, which was due to rapid barite precipitation and minimal impact of celestite precipitation. Barium sulfate precipitation was found to follow the second order reaction with respect to barium and sulfate concentrations, respectively. Linear regression was performed to correlate the reaction rate constant  $k$  and homogenous nucleation rate to allow accurate prediction of barite precipitation kinetics for any combination of barium and sulfate in the reactor.

Radium that is present in the flowback water will be incorporated in barite in proportion to barium removal from solution. Ra leaching from barite was found to be negligible, which demonstrates that potential migration of Ra may not be of major concern. The low-level radioactive solid wastes formed in this process can be disposed in municipal solid waste landfills in accordance with state regulations.

### **Separation of Solids Formed by Mixing Flowback and AMD**

Feasibility of microfiltration to separate solids created by mixing actual flowback water and AMD was evaluated using a bench-scale setup. Hydrophilic polyvinylidene fluoride (PVDF) membrane with a pore size of 0.22  $\mu\text{m}$  was used as a model polymeric microfiltration membrane. Severe membrane fouling occurred during the first 5 minutes of filtration with one flowback/AMD mixture while no significant fouling was observed for a different mixture. It was discovered that iron-based colloids with an average particles size of 0.2  $\mu\text{m}$  were the main reason for rapid and severe membrane fouling. These colloids were not formed by mixing flowback water containing high barium concentration with AMD rich in sulfate but were originally present in the flowback water, especially in the samples collected early in the flowback period. Stability of these sub-micron colloidal particles at high ionic strength of the flowback water is attributed to organic coating on the particle surface.

Conventional coagulation/flocculation process was optimized for solids removal with respect to mixing/settling time, pH and coagulant dose. The conventional process was compared with ballasted flocculation that has smaller footprint and may be better suited for a mobile treatment system. The treated water quality from the conventional and ballasted flocculation systems were comparable with turbidity below 5 NTU despite the fact that the contact time required for the ballasted flocculation was just 10 min compared to 1 hour required for conventional treatment process.

### **Field Demonstration of the Treatment System**

Pilot-scale study was conducted to demonstrate the feasibility of the treatment process optimized under laboratory conditions. Flowback water and AMD from northeast Pennsylvania were co-treated in a 5 gpm pilot-scale treatment system consisting of rapid mixing reactor, flocculation tank and sedimentation tank. Sulfate concentration in the finished water can be reduced to below 100 mg/L by adjusting the mixing ratio of flowback water to AMD. Ferric iron in AMD could serve as coagulant to assist with solids removal, during which total iron is reduced to below 0.3 mg/L.

### **Compatibility of AMD for Hydraulic Fracturing of Marcellus Shale**

If the effluent from the proposed treatment process containing sulfate is used for hydraulic fracturing, it will result in the formation of barium sulfate in the shale formation. Therefore, the fate of BaSO<sub>4</sub> particles was studied in a laboratory-scale system. Specifically, transport of barite particles through porous shale core and proppant sand media and scaling on the production casing was evaluated under relevant process conditions. BaSO<sub>4</sub> particles formed under high ionic strength (>0.5 M) have larger size when compared to those formed in deionized water and very high affinity to both quartz sand and shale surface. Therefore, BaSO<sub>4</sub> formed in the subsurface will be unlikely to move back to surface during the flowback period.

The presence of antiscalants cannot prevent rapid formation of BaSO<sub>4</sub> at high supersaturation levels that may occur in the subsurface. Ethylene glycol, which is often used as a chemical additive to inhibit particle deposition, does not influence the size or the mobility of BaSO<sub>4</sub> through the porous media. However, BaSO<sub>4</sub> particles formed in the presence of polymeric antiscalants (e.g., polymaleic acid, phosphino carboxylic acid) have much smaller

size and greater mobility through the shale core and proppant sand media. Furthermore, these antisclalants will also prevent attachment of barite to the production casing.

### **Overarching Impact**

This project evaluated the feasibility of an alternative management option for wastewater generated from Marcellus shale gas extraction. The use of AMD as a make-up water source for produced water reuse will reduce the adverse environmental impact of both wastewaters simultaneously. This novel water management solution is beneficial for unconventional gas production from the Marcellus Shale and potentially any shale or coal bed methane development where produced water must be actively managed and/or freshwater withdrawals may be limited. In addition, application of this water management solution will greatly reduce the volume of concentrated brine that must be disposed, minimize withdrawals of freshwater and reduce associated pumping costs, and add value to AMD that is abundant and often located in the proximity of gas well in Marcellus Shale .

## 1.0 Introduction

Natural gas has recently emerged as an energy source that offers the opportunity for a number of regions around the world to reduce their reliance on energy imports or strive towards energy independence. Natural gas is a more environmentally benign fossil energy source compared with coal in terms of combustion byproducts and pollutant emissions. It may be a potential transition fuel that will allow for the shift from coal to renewable energy resources while helping to reduce the emissions of CO<sub>2</sub>, criteria pollutants and mercury by the power sector (MIT, 2011).

Development of continental shale gas reservoirs is a growing source of natural gas to meet the energy needs of the United States. The Marcellus Shale of the Appalachian Basin has recently been estimated to contain 262-500 Tcf (trillion cubic feet) of natural gas reserves and is one of the largest underdeveloped reservoirs of shale gas in the US (Engelder and Lash, 2008; Milici and Swezey, 2006). Based on the U.S. Energy Information Administration (EIA) projections, shale gas production will grow to 16.6 trillion cubic feet in 2040, which will account for 50 % of total U.S. natural gas production (EIA, 2013).

The Marcellus Shale underlies most of Northern and Western Pennsylvania, including about 70% of the state (de Witt et al., 1993). The recoverable volume of gas from the Marcellus formation is difficult to predict and estimates vary over several orders of magnitude. However, the resource certainly represents many years of natural gas needs for the eastern U.S. (Pletcher, 2008). Although shale gas production has been ongoing since the early 1800's, a lack of technology confounded development of deep shale reservoirs such as Marcellus. However, recent advances in horizontal drilling and multi-stage hydraulic fracturing technology have enabled development of highly productive gas wells in Marcellus Shale (Harper, 2008).

While shale gas is an attractive energy source that may reduce the reliance on energy imports for a number of regions in the world, it comes with its own environmental challenges in terms of water resources and flowback/produced water management. Extraction of natural gas from the shale rock requires large amounts of water for hydraulic fracturing (2-5 million gallons/well) and generates significant quantities of wastewater during the flowback period. The most dominant management approach for this wastewater is the disposal in Class II Underground Injection Control (UIC) wells (Gregory et al., 2011). However, this is not a viable option in Pennsylvania that sits on top of one of the largest shale gas reservoirs in the world while it only has seven Class II UIC wells (Vidic et al., 2013). Moreover, high salinity of the flowback water from Marcellus Shale precludes the use of conventional desalination processes

(e.g., reverse osmosis) and would require energy-demanding thermal processes (e.g., distillation, crystallization) to meet the total dissolved solids (TDS) limits (i.e., 500 mg/L) prescribed by the Pennsylvania Department of Environmental Protection (DEP) for discharge to the environment.

Abandoned mine drainage (AMD) is an environmental legacy from another energy-related industry (i.e., coal mining) and is one of the most significant threats to water quality in Pennsylvania. Considering that AMD sites in Pennsylvania are often located in the vicinity of shale gas extraction sites, it would be truly beneficial to use AMD as source water for hydraulic fracturing operations to alleviate pressure on fresh water sources while at the same time helping to reduce environmental impact of AMD.

This study points to the synergy in solving environmental problems associated with unconventional shale gas extraction technology and abandoned mine drainage in Marcellus Shale region as archetypical example of rapidly growing shale gas development in the US. Opportunities and concerns with direct use of AMD water for hydraulic fracturing are discussed together with potential process for co-treatment of AMD and flowback water to reuse in shale gas development.

## **1.1 Unconventional Shale Gas Extraction**

Shales typically have extremely low permeability (< 0.1 microDarcy), which limits the flow of gas to a wellbore (Soeder, 1988; Ameri et al., 1985). With recent innovations in drilling and hydraulic fracturing (fracking), shale gas production that was originally considered not to be economical has now become quite viable (US DOE, 2009). The success in gas extraction from Barnett Shale served to promote natural gas development in United States.

Advancements in horizontal drilling make it feasible to drill multiple wells from a single pad with each horizontal leg being even more than a mile long. This allows access to as much as 1 square mile of shale located more than a mile deep from a single well pad. Once horizontal drilling is completed, the well casing is placed into a wellbore and is sealed with cement to ensure that produced water and natural gas do not contaminate other subsurface layers, including groundwater. Hydraulic fracturing fluid is then pumped downhole at high pressure to widen the pre-existing fractures and creates new fractures that increases the permeability of shale formation. Together with the fracturing fluid, more than 1,000 t of proppant (most commonly silica sand) is pumped into these fractures to prevent them from closing once water is evacuated from the wellbore and pressure is relieved.



Once the hydraulic fracturing is completed, the valve on the wellhead is opened and fracturing fluid is allowed to flow back to the surface. The fluid recovered during this period is called flowback water. As illustrated in Figure 1.1, the flow rate during this period experiences a sharp decline and stabilizes after about two weeks. Typically, 10% - 30% of the injected fracturing fluid returns to the surface during this period. Water that continues to flow to surface during the life of a well is referred to as “produced water” (Kidder et al., 2011).

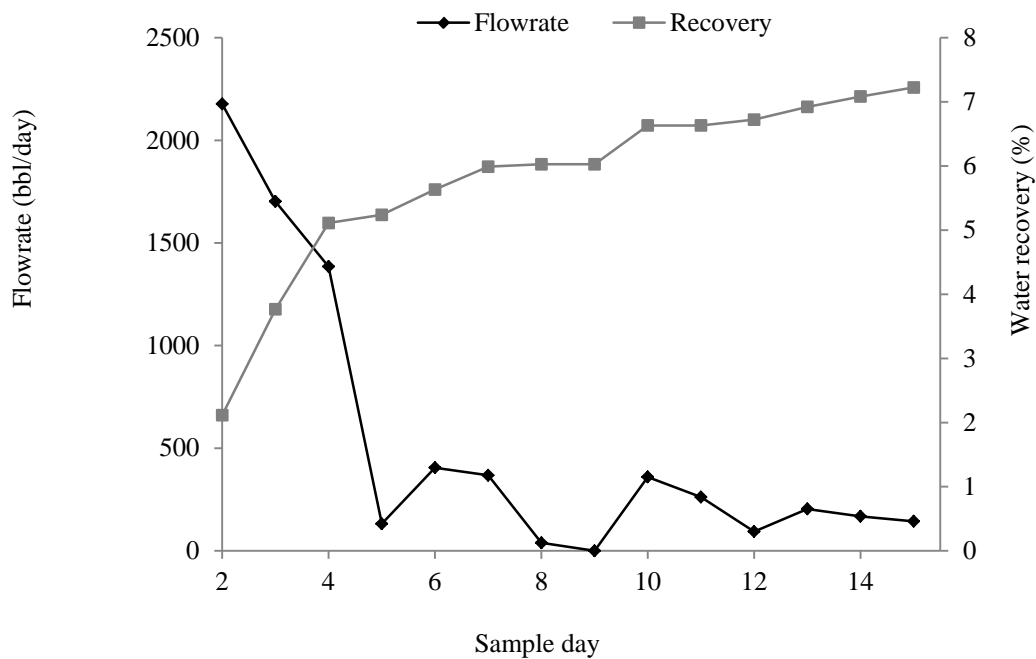


**Figure 1.1** Variation of flowrate and water recovery during the flowback period

The key characteristics of flowback water are governed by the mixing of injected fluid and the formation brine (Barbot et al., 2013). Management of flowback and produced water from Marcellus Shale formation causes growing public concern due to its high total dissolved solids (TDS), radioactive elements and organic matter. It is important to note that the flowback water from Marcellus Shale has much higher barium and much lower sulfate concentration compared with that from Barnett Shale, which is likely due to profound differences in geochemical characteristics of the two formations (Miller et al., 2013). High TDS concentrations and lack of Class II underground injection control wells in Pennsylvania pose a great challenge for flowback water management (Arthur et al., 2008; Kargbo et al., 2010).

## 1.2 Flowback Water Management

Flowback and produced water generated by shale gas extraction raised significant health and environmental concerns due to its chemical characteristics. Produced water generated in Marcellus Shale is characterized by high concentrations of total dissolved solids (TDS), metals (e.g., Ba, Sr), organic matter and NORM (Barbot et al., 2013). For example, the average barium concentration in the flowback water exceeds the drinking water regulation by more than 1,000 times. Presence of NORM in the produced water is of particular concern because of the potential health effect for on-site workers and long-term soil and water contamination.

Because of the high salinity, toxicity and radioactivity of the produced water, the most common management approach is disposal by deep well injection. The approximately 144,000 Class II wells in operation in the United States are injecting over 2 billion gallons of brine every day. Due to the abundance of Class II disposal wells in Texas and low cost of deep well injection, water reuse in TX accounts for only 5% of the total amount of water that is used for shale gas extraction (Nicot and Scanlon, 2012). Although water usage for shale gas extraction is less 1% of the total statewide water withdrawals in Texas, the impact of water use for hydraulic fracturing on the local water resource may be significant for the arid regions at peak time of well completion activities (Arthur et al., 2008; Nicot and Scanlon, 2012). In contrast, there are only seven Class II wells that are available for produced water disposal in Pennsylvania (Gregory et al., 2011), which limits the available management options.

In the early stages of Marcellus Shale development, discharge of produced water into publicly owned treatment works (POTWs) was allowed under certain conditions (i.e., less than 1% of the average daily flow). However, typical treatment processes employed by POTWs (e.g., sedimentation, biological treatment, filtration) are not capable of removing dissolved solids and the TDS contained in the produced water was only diluted with municipal wastewater and discharged into the receiving waterways. As a result, level of barium in the POTW effluent and salt loading in the rivers in Pennsylvania increased during this period (Ferrar et al., 2013). It was reported that disposal of flowback water into POTWs resulted in elevated bromide levels in the Allegheny River, which is a health concern because of a potential to create brominated disinfection by-products (Wilson and Vanbriesen, 2012). In addition, increased Ra concentration was found in river sediments downstream of a waste treatment facility that received produced water (Warner et al., 2013). Aiming to resolve these environmental concerns, the disposal of water produced from unconventional gas wells into POTWs has been curtailed by the Pennsylvania Department of Environmental Protection since 2010 (PADEP, 2010).

Because of the lack of disposal options, close to 90% of the produced water generated in Pennsylvania is reused for hydraulic fracturing (Vidic et al., 2013). Figure 1.2 summarizes the dominant produced water management approach in Pennsylvania. Impoundments or storage tanks are often constructed near well sites to store produced water for subsequent treatment and reuse and a small fraction is shipped for disposal in Class II wells in neighboring states (i.e., Ohio and West Virginia).

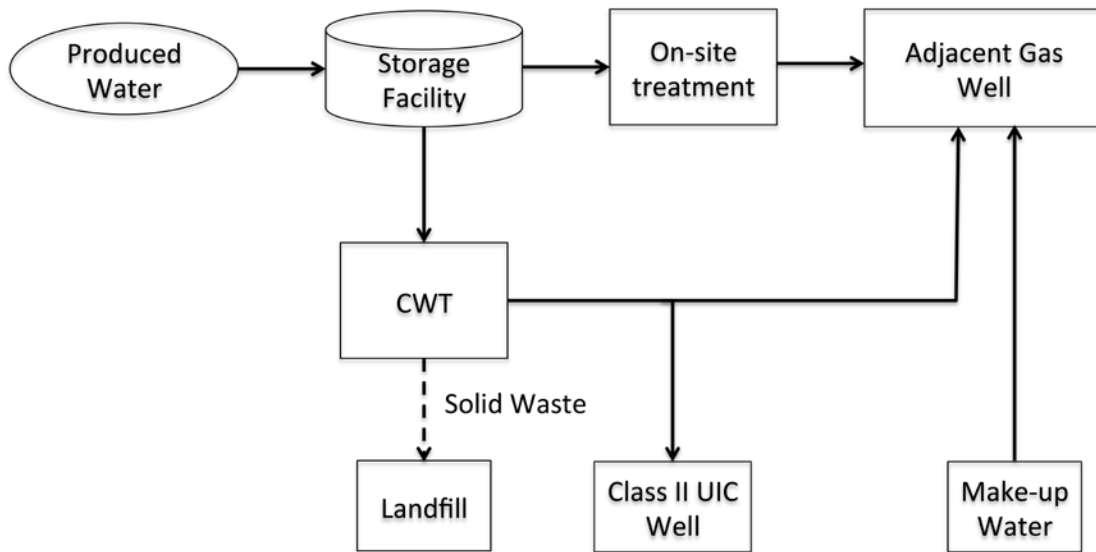


**Figure 1.2** Dominant Marcellus Shale produced water management approach in Pennsylvania

On-site treatment may include filtration to remove coarse suspended solids from the produced water and enable unrestricted use in subsequent hydraulic fracturing operations. Regional centralized wastewater treatment plants (CWTs) play an important role in managing wastewater from unconventional shale gas extraction activities. In comparison to POTWs, the CWTs are equipped to remove barium and strontium using sulfate precipitation. This process removes over 90% of barium, strontium and radium (He et al., 2013), but the major dissolved ions (i.e., Na, Ca and Cl) are not affected and the TDS of the finished water cannot meet the requirements for the discharge into surface streams. Therefore, the only options for treated wastewater include reuse for hydraulic fracturing and disposal by deep well injection.

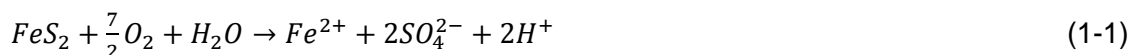
It is important to note that wastewater reuse for hydraulic fracturing represents a temporary solution in Pennsylvania because the capacity to reuse this wastewater is limited by the development of new wells. When the well fields mature and the drilling of new wells slows

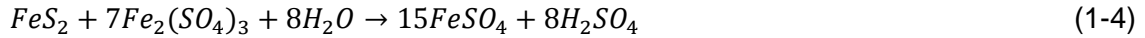
considerably, it will not be possible to reuse all produced water generated by the existing gas wells. It is difficult to predict when a given well field will become a net water producer because of the unique well completion schedule for each field and the estimates range from 12-20 years (Kuijvenhoven et al., 2011; Vidic et al., 2011; Silva et al., 2012). In the absence of a large number of Class II disposal wells that are distributed throughout Pennsylvania, it would be necessary to employ effective and economical technologies for separation of dissolved salts, including NORM, from produced water so that the treated effluent would meet regulatory limits for unrestricted disposal to surface waters. This is a formidable challenge considering that there are currently no operating desalination facilities in this region. In addition, it will be necessary to develop industrial capacity that would use around 7 million tons of chloride salts (e.g., NaCl and CaCl<sub>2</sub>) that could be recovered annually from estimated 80,000 Marcellus Shale gas wells that are likely to be eventually developed in Pennsylvania when each well is generating approximately 8 bbl/day (1.3 m<sup>3</sup>/day) of produced water. This significant industrial development will be needed to ensure continued use of this important natural resource in an environmentally responsible manner.

### 1.3 Abandoned Mine Drainage

Environmental concerns with AMD come from elevated concentration of metals and metalloids, high sulfate content and potentially acidic nature of the discharge which all have adverse impacts on surface and groundwater quality in the coal mining region (Johnson, 2003; Gary, 1998). AMD typically has orange color which is due to the precipitation of ferric hydroxide (Fe(OH)<sub>3</sub>(s)) when pH is above 3.5.

Abandoned mine drainage is sourced from mine waste rock, tailings, and mine structures, and its quality depends on the mineralogy of rock material and availability of water and oxygen (US EPA, 2004). When pyrite or other sulfidic minerals are exposed to both oxygen and water, oxidation of these minerals (mainly pyrite) would govern the quality of AMD. The mechanism of pyrite oxidation has been widely studied (Johnson, 2003; Singer and Stumm, 1970; Moses and Herman, 1991; Evangelou, 1995):





As shown by Equations 1-4, ferric iron and oxygen both serve as pyrite oxidants. Oxidation by ferric iron is the dominant process at pH below 4.5, while O<sub>2</sub> is the primary pyrite oxidant at neutral or alkaline pH (Johnson, 2003; Evangelou, 1995).

AMD from coal mining operations represent difficult and costly environmental problems in the U.S (EPA, 2004). In Pennsylvania, AMD influences the quality of more than 3,000 miles of streams and associated ground water and is demonstrated to be the most critical source of water contamination (USGS, 1999). Remediation of AMD in Pennsylvania is estimated to cost up to 15 billion dollars (Berghorn and Hunzeker, 2001).

## **1.4 Utilization of AMD for Flowback Water Reuse**

### **1.4.1 Co-treatment of Flowback Water and AMD**

Currently, many operators are practicing flowback water reuse for hydraulic fracturing of adjacent wells (latest review of PA DEP data reveals that about 90% of flowback water generated in Pennsylvania is reused). The flowback water is generally pretreated to remove suspended solids and, occasionally, metals (calcium, barium, strontium) that have the potential to create mineral scales (e.g., sulfates, carbonates) and is stored before reuse. Pretreated flowback water is then mixed with fresh water to make up for the fraction of the fracturing fluid that is not recovered during the flowback period and to control the salinity of this mixture for subsequent utilization.

The advantage of using AMD as makeup water is that it is located in the vicinity of shale gas extraction site, which reduces the overall water transportation costs and reduces the total greenhouse gas emissions of the unconventional gas industry (i.e., reduces the CO<sub>2</sub> emissions generated by water transport). Figure 1.3 depicts the locations of permitted Marcellus Shale gas extraction wells in 2010 and known AMD sites in Pennsylvania. As illustrated by this figure, there is an abundance of AMD sources near permitted gas wells, especially in Western Pennsylvania. AMD can not only serve as makeup water for hydraulic fracturing operations and reduce the demand on high quality water resources but it also provides a source of chemicals that can be used to treat the flowback water and remove divalent cations that could form mineral scales and reduce permeability of gas wells. Sulfate ions that are often present in AMD at elevated levels can react with Ba<sup>2+</sup>, Sr<sup>2+</sup>, and Ca<sup>2+</sup> in the flowback water to precipitate them as their insoluble sulfate forms. In addition, some AMD sources are net alkaline, which would lead

to additional precipitation of metal carbonates. The removal of divalent cations depends on the concentrations of species of interest (i.e.,  $Ba^{2+}$ ,  $Sr^{2+}$ ,  $Ca^{2+}$  and  $SO_4^{2-}$ ) that are related to flowback time, quality of AMD and blending ratio. The blending ratio can be adjusted to achieve the desired final hydraulic fracturing fluid quality. After mixing of these two waters, a simple gravity separation process may be used to remove the suspended solids created by chemical reactions so that the quality of the finished water would be suitable for hydraulic fracturing.

Although AMD and flowback water co-treatment is certainly beneficial, there are still some concerns and barriers for the use of AMD in unconventional gas extraction.

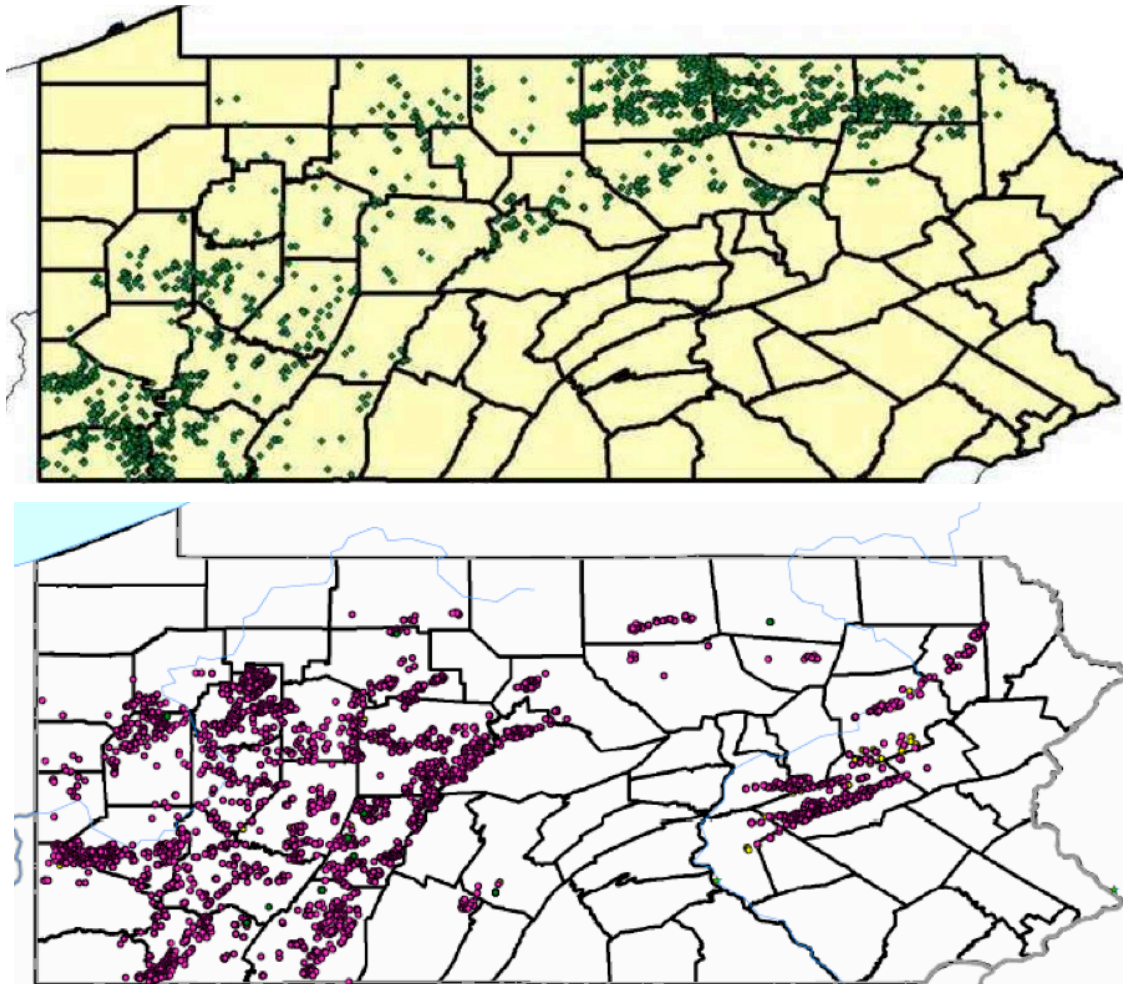


**Figure 1.3** Location of permitted shale gas wells (top) and AMD (bottom) in Pennsylvania in 2010

## 1.4.2 Concerns with AMD Use in Unconventional Gas Extraction

### 1.4.2.1 Compatibility with Hydraulic Fracturing Chemical Additives

Quality of AMD varies with locations and is influenced by underlying geology of coal

formation and environmental conditions in the abandoned mine. Analysis of 140 AMD samples demonstrated that pH varies in a wide range (2.7 - 7.3) with a bimodal distribution in the acidic pH (2.5-4) and near-neutral pH (6-7) range (Cravotta, 2008). Low pH of AMD would exacerbate corrosion of production casing and may prevent its use in hydraulic fracturing operations. However, low-pH AMDs are often equipped with active (e.g., lime addition) or passive (e.g., limestone ponds or channels) treatment systems to neutralize acidity.

Friction reducers are high molecular weight polymers added to the fracturing fluid to reduce the pumping losses during hydraulic fracturing operations, which in turn reduces the operating costs. Several studies have demonstrated that high TDS of fracturing fluid can impair the effectiveness of polyacrylamide-based friction reducers (Tam and Tiu, 1990; Kamel and Shah, 2009). As the TDS concentration of AMD is between 1,000-2,000 mg/L, it is not expected that the use of AMD as make up water will add to the concerns about the effectiveness of friction reducers because the flowback water normally has 2 orders of magnitude higher salt content than AMD. In addition, high salinity tolerant friction reducers have been developed to overcome these problems and it is currently feasible to use water with TDS as high as 100,000 mg/L without compromising the effectiveness of friction reducers (Paktinat et al., 2011).

Additional concern regarding AMD quality for use in hydraulic fracturing is the dissolved iron content that may interfere with gel cross-linking if gel systems are used to increase the viscosity of fracturing fluid and enhance its ability to carry proppant into deeper fractures. Commonly acceptable iron concentration in cross-linked systems is 10-20 mg/L. Because AMD could have several hundred mg/L of dissolved iron, it may be necessary to implement iron removal (e.g., aeration and sedimentation) to address this concern. In the case of slickwater fracturing, which is typically used in Marcellus shale, the concern about the iron presence is not as pronounced and much higher concentrations can be tolerated (total divalent cation concentration as high as 15,000 mg/L is acceptable).

#### *1.4.2.2 Impact on Well Productivity*

One of the key issues related to AMD use in hydraulic fracturing is its sulfate concentration because of the scaling potential that exists in barium-rich Marcellus Shale formation (Barbot et al., 2013; Rassenfoss, 2011). Dissolved sulfate in the fracturing fluid will inevitably react with barium in the subsurface to precipitate barium sulfate (barite), which could potentially cause the scaling on production casing, proppant pack or the shale itself and reduce production of natural gas from the well. Strontium and calcium sulfate are less likely to

precipitate because barite has much lower solubility product compared to celestite and gypsum. Barite scale is very tenacious (not soluble in concentrated hydrochloric acid) and difficult to remove. This is of particular concern in situation with continuous supply of scale forming ions as the growth of barite scale can lead to complete plugging of pipes or fractures. However, this is not the case in Marcellus Shale formation where sulfate concentration in the flowback water ranges from non-detect to several mg/L (Barbot et al., 2013). The most likely fate of barite particles that would form downhole is that they would be captured in the proppant pack that would serve as a granular filter media (typical proppant sand is 40/70 U.S. Mesh) during the flowback period. This means that the key concern with high levels of sulfate in the frack fluid would be permeability reduction of the proppant pack due to plugging with freshly precipitated barite.

The volume of freshly precipitated barite that would form in a well can be estimated assuming that there is sufficient barium in the shale to facilitate complete sulfate removal. Assuming that a total of 3 million gallons of fracturing fluid containing 800 mg/L of sulfate is injected together with 9 wt.% of proppant, the maximum volume of barite that can potentially precipitate downhole would be 4.9 m<sup>3</sup>. This volume of barite is less than 0.5% of the total volume of proppant injected in the well. Hence, it can be concluded that the total volume of barite solids formed downhole is negligible compared to the volume of proppant remaining downhole and that the well-plugging due to high sulfate in the fracturing fluid may be limited.

#### *1.4.2.3 Potential for Bacterial Activity*

Sulfate reducing bacteria (SRB) use simple organic acids or molecular H<sub>2</sub> as energy source while reducing sulfate to hydrogen sulfide. Typically, the temperature in Marcellus Shale formation is between 35 °C to 51 °C, which is optimal for certain SRB species (Kargbo et al., 2010; Philips and Lappin-Scott, 1997). Any sulfate that is present in the fracturing fluid as free ion would promote growth of SRB under anaerobic conditions that are prevalent in Marcellus Shale formation. Hydrogen sulfide that would form as a result of SRB activity can contaminate (sour) natural gas and increase the cost of gas purification. Hydrogen sulfide would also promote precipitation of ferrous sulfide that could lead to plugging of the production casing, proppant pack and/or shale fractures and would accelerate corrosion of iron and steel pipes (Cord-Ruwisch et al., 1987).

As indicated earlier, any sulfate that is present in the fracturing fluid will likely be precipitated as barium sulfate due to fairly high concentration of barium in Marcellus Shale.



Therefore, the availability of free sulfate ions in solution to promote SRB activity will likely be very limited. Several studies suggested that *Desulfovibrio desulfuricans* can utilize limited amounts of barite solids as electron acceptor to dissolve Ba and Ra that co-precipitated with barite (Baldi et al., 1996; Philips et al., 2001). It is then important to ensure that the biocides that are typically added with the fracturing fluid remain active in the subsurface as long as possible to prevent proliferation of *Desulfovibrio desulfuricans*. If not, excessive biological growth would not only reduce the quality of gas produced from this well but could also reduce well productivity.

#### 1.4.2.4 Management of Solid Wastes

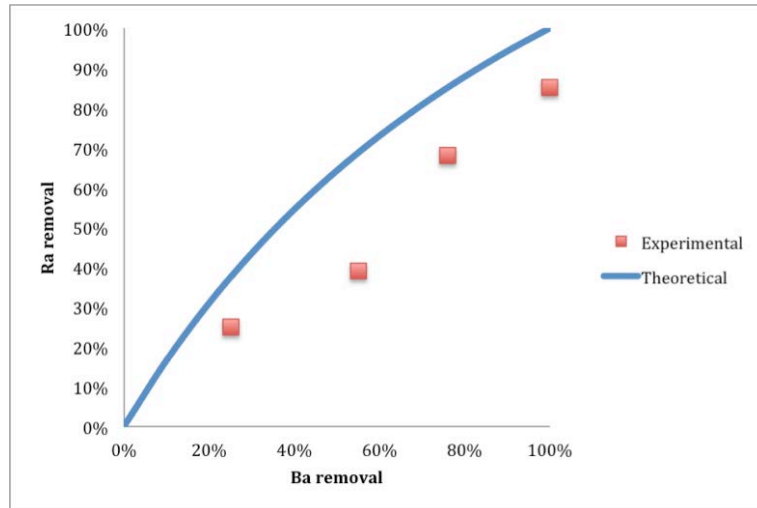
Radium is a naturally occurring radioactive material (NORM) that is often present in Marcellus Shale flowback water at levels ranging from several hundred to several thousand pCi/L. Ra-226 with a half-life of 1622 years is one of the major radium isotopes and it dominates radioactivity in the flowback water. When flowback water is mixed with AMD in above-surface treatment process, radium and barium sulfate will co-precipitate despite the fact that the solubility product of  $\text{RaSO}_4$  ( $K_{\text{sp,RaSO}_4} = 10^{-10.38}$ ) is almost never exceeded under typical process conditions (Langmuir and Riese, 1985). Solids generated as a result of adding AMD to flowback water could have appreciable radioactivity and even exceed the RCRA-D (Resource Conservation and Recovery Act, Subtitle D) non-hazardous landfill disposal limit of 25 pCi/g that is stipulated in Pennsylvania (RPSEA, 2012). Since AMD and flowback water mixture is a dilute solution, the extent of Ra that would be incorporated into the barite solids can be estimated by Nernst-Berthelot Equation (Doerner and Hoskins, 1925):

$$\frac{\text{RaSO}_4}{\text{BaSO}_4} = K_d \frac{\text{Ra}^{2+}}{\text{Ba}^{2+}} \quad (1-5)$$

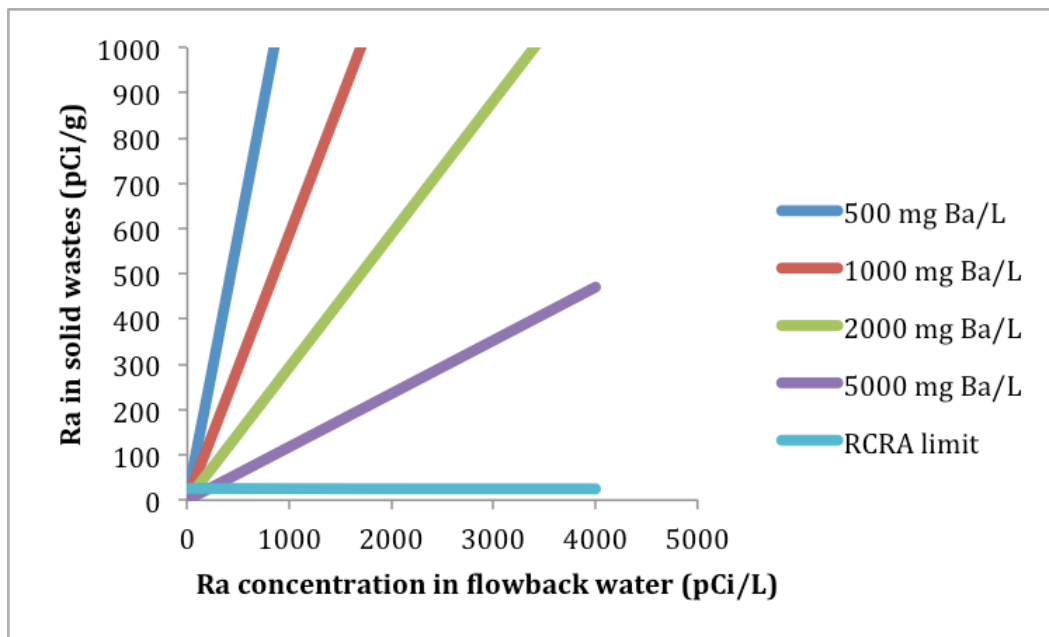
where,  $K_d$  is the equilibrium distribution coefficient,  $\text{BaSO}_4$  and  $\text{RaSO}_4$  are the concentrations of barium and radium carriers in the solid solution, and  $\text{Ba}^{2+}$  and  $\text{Ra}^{2+}$  are dissolved ion concentrations in the liquid phase.

Figure 1.4 depicts relationship between Ra and Ba removal during co-precipitation of barium and radium sulfate as predicted by Nernst-Berthelot Equation and verified by experimental studies. In the case of excess sulfate in solution, barium removal by precipitation would be almost complete because of low barite solubility and theoretical calculations indicate that all Ra in solution will also be incorporated into the solids that would precipitate. Figure 1.5 shows Ra concentration in solids (pCi/g) that would precipitate after mixing high-sulfate AMD

with flowback water as a function of Ra and Ba concentration in the flowback water. As can be seen in Figure 1.5, it is very likely that the Ra concentration in solid waste generated by this process would exceed the landfill disposal limit, which could be a major concern for managing solid waste that would be created by this process.



**Figure 1.4** Relationship between Ra and Ba removal during co-precipitation of barium and radium sulfate



**Figure 1.5** Radium activity in solids that would precipitate when high-sulfate AMD is mixed with flowback water as a function of Ba concentration in flowback water

#### 1.4.2.5 Regulatory Concerns

Water withdrawals for Marcellus Shale drilling activities are under the jurisdiction of either interstate basin commissions or state agencies. The Code of Federal Regulations states that water withdrawal must be limited in both quantity and rate to avoid any adverse impact on water level, competing supplies, aquifer storage capacity, water quality, fish and wildlife, and low flow of perennial streams (18 C.F.R. § 806.23). Based on the water demand, a minimum passby flow may be required to maintain adequate health of the stream ecosystem. Withdrawal of AMD falls under the same legislation as surface and ground water, although it is technically a waste and the key source of surface water pollution in Pennsylvania.

For the operators who intend to use AMD for natural gas extraction activities, one of the key concerns is the potential for long-term liability for AMD “treatment” (withdrawal and use can be construed as treatment) as claimed in The Clean Streams Law. Recently, the Pennsylvania Department of Environmental Protection (PA DEP) published a “white paper” to encourage the use of AMD for hydraulic fracturing. Two possible solutions for the liability concern associated with the use of AMD for hydraulic fracturing have been proposed by PA DEP. One option is to treat the project that uses AMD for fracturing within the Environmental Good Samaritan Act (EGSA), which is a law intended to encourage pollution abatement caused by abandoned mines. Based on EGSA, participants in a water pollution abatement project are not responsible for any pollution coming from the water treatment facilities used to treat AMD. The other option is to use a Consent Order of Agreement where PA DEP could agree to exempt the operators who use AMD for hydraulic fracturing from long-term liability of the treatment.

Alternatives for AMD storage stipulated by PA DEP include non-jurisdictional impoundments, centralized impoundment and on-site pits and tanks. If AMD is to be stored in non-jurisdictional impoundment it must meet water quality standards listed in Table 1.1, while this standard is not enforced for centralized impoundment and on-site pits. In other words, storage of AMD in large non-jurisdictional surface impoundments is not permitted unless substantial treatment of AMD is implemented. In addition, existing AMD treatment facilities, such as polishing ponds or wetlands, can also serve as AMD storage prior to hydraulic fracturing.

**Table 1.1** Storage standards for MIW stored in non-jurisdictional impoundments (DEP, 2013)

Parameter	Units	MIW Storage Standards for Non-jurisdictional Impoundment
Alkalinity	mg/L	Minimum of 20 mg/L
Aluminum	mg/L	0.2
Ammonia	mg/L	1.0
Arsenic	µg/L	10.0
Barium	mg/L	2.0
Bromide	mg/L	0.2
Cadmium	µg/L	5.0
Chloride	mg/L	250
Chromium	µg/L	100
Copper	mg/L	1.0
Iron	mg/L	0.3
Lead	µg/L	15
Manganese	mg/L	0.5
Nickel	µg/L	470
pH		6.5-8.5
phenol	µg/L	5.0
Selenium	µg/L	50
Conductivity	µmho/cm	1,000
Sulfate	mg/L	250
TDS	mg/L	500
TSS	mg/L	45
Zinc	mg/L	5.0

MIW, mine influenced water

## 1.5 Study Objectives

The overall objective of this study was to evaluate the feasibility and benefits associated with application of acid mine drainage for flowback water reuse.

Specific objectives of the study were as follows:

(a) Evaluate the locations of AMD and shale gas well sites in Pennsylvania and compile these data into geographic information system (GIS);

(b) Evaluate spatial and temporal correlations of water quality parameters of Marcellus Shale flowback and produced water;

(c) Conduct bench-scale experiments to establish the kinetics and thermodynamics of chemical reactions that would occur when flowback water and AMD are mixed;

(d) Evaluate the separation processes to remove suspended solids in the mixture

flowback water and AMD and optimize the treatment process in the laboratory;

(e) Demonstrate the feasibility of using AMD for flowback water reuse in a pilot-scale treatment system; and

(e) Evaluate the affinity of barium sulfate to attach to production casing, proppant sands and shale cores.

## 1.6 Organization of the Report

The report contains eight major chapters following the Introduction. Chapter 2 is focused on locations of AMD and shale gas well sites in Pennsylvania. Chapter 3 discusses water quality parameters of Marcellus Shale produced water and their spatial and temporal correlations. Chapter 4 discusses laboratory efforts to optimize the treatment process for the co-treatment of flowback water and AMD. Chapter 5 presents an overview of the pilot-scale study on the feasibility of using AMD for flowback water reuse. Chapter 6 evaluates the affinity of barium sulfate to attach to production casing, proppant sands and shale core.

## 1.7 References

Ameri, S., Aminian, K., Miller, J. A., Doricich, D. and Yost, A. B. (1985). A Systematic Approach for Economic Development of the Devonian Shale Gas Resources. In SPE Eastern Regional Meeting. Society of Petroleum Engineers.

Arthur, J. D., Bohm, B. and Layne, M. (2008). Hydraulic fracturing considerations for natural gas wells of the Marcellus Shale. The Ground Water Protection Council 2008 Annual Forum, Cincinnati, OH.

Barbot, E., Vidic, N. S., Gregory, K. B. and Vidic, R. D. (2013). Spatial and temporal correlation of water quality parameters of produced waters from devonian-age shale following hydraulic fracturing. *Environmental science & technology*, 47(6), 2562-2569.

Berghorn, G. H. and Hunzeker, G. R. (2001). Passive Treatment Alternatives for Remediating Abandoned Mine Drainage. *Remediation Journal*, 11(3), 111-127.

Cravotta, C. A. (2008). Dissolved metals and associated constituents in abandoned coal-mine discharges, Pennsylvania, USA. Part 1: Constituent quantities and correlations. *Applied Geochemistry*, 23(2), 166-202.

DEP (2013). White paper: Utilization of mine influenced water for natural gas extraction activities.

EIA (2013). Annual Energy Outlook 2013. United States Department of Energy, Energy Information Administration, DOE/EIA-0383.

Evangelou, V. P. (1995). Pyrite oxidation and its control: Solution chemistry, surface chemistry, acid mine drainage (AMD), molecular oxidation mechanisms, microbial role, kinetics, control, ameliorates and limitations, microencapsulation. Boca Raton, FL, CRC Press.

Ferrar, K. J., Michanowicz, D. R., Christen, C. L., Mulcahy, N., Malone, S. L. and Sharma, R. K. (2013). Assessment of effluent contaminants from three facilities discharging Marcellus Shale wastewater to surface waters in Pennsylvania. *Environmental science & technology*, 47(7), 3472-3481.

Gray, N. F. (1998). Acid mine drainage composition and the implications for its impact on lotic systems. *Water Research*, 32(7), 2122-2134.

Gregory, K. B., Vidic, R. D. and Dzombak, D. A. (2011). Water management challenges associated with the production of shale gas by hydraulic fracturing. *Elements*, 7(3), 181-186.

He, C., Zhang, T. and Vidic, R. D. (2013). Use of abandoned mine drainage for the development of unconventional gas resources. *Disruptive Science and Technology*, 1(4), 169-176.

Johnson, D. B. (2003). Chemical and microbiological characteristics of mineral spoils and drainage waters at abandoned coal and metal mines. *Water, Air and Soil Pollution: Focus*, 3(1), 47-66.

Kamel, A. and Shah, S. N. (2009). Effects of salinity and temperature on drag reduction characteristics of polymers in straight circular pipes. *Journal of petroleum Science and Engineering*, 67(1), 23-33.

Kargbo, D. M., Wilhelm, R. G. and Campbell, D. J. (2010). Natural gas plays in the Marcellus shale: Challenges and potential opportunities. *Environmental Science & Technology*, 44(15), 5679-5684.

Kidder, M., Palmgren, T., Ovale, A. and Kapila, M. (2011) . Treatment options for reuse of frac flowback and produced water from shale. *Industry Report/Produced Water Society*, 232.

Kuijvenhoven, C., Sun, P., Padmasiri, S., Fedotov, V., Hassing, T., Hagemeijer, P., Meyer, C. (2011). Treatment of water from fracturing operations for unconventional gas production. *Shale Gas Water Management*.

Miller, D. J., Huang, X., Li, H., Kasemset, S., Lee, A., Agnihotri, D., Hayes, T., Paul, D.R. and Freeman, B. D. (2013). Fouling-resistant membranes for the treatment of flowback water from hydraulic shale fracturing: A pilot study. *Journal of Membrane Science*, 437, 265-275.

Moses, C. O. and Herman, J. S. (1991). Pyrite oxidation at circumneutral pH. *Geochimica et Cosmochimica Acta*, 55(2), 471-482.

Nicot, J. P. and Scanlon, B. R. (2012). Water use for shale-gas production in Texas, US. *Environmental science & technology*, 46(6), 3580-3586.

Paktinat, J., O'Neil, B. J., Aften, C. W. and Hurd, M. D. (2011). Critical evaluation of high brine tolerant additives used in shale slickwater fracs. In *SPE Production and Operations Symposium*. Society of Petroleum Engineers.

Rassenfoss, S. (2011). From flowback to fracturing: Water recycling grows in the Marcellus shale. *Journal of Petroleum Technology*, 63(7), 48-51.

Singer, P. C. and Stumm, W. (1970). Acidic mine drainage: the rate-determining step. *Science*, 167(3921), 1121-1123.

Silva, J.M., Matis, H., Kostedt IV, W. and Watkins, V. (2012). Produced water pretreatment for water recovery and salt production. RPSEA Final Report, 08122-36.

Soeder, D.J. (1988). Porosity and permeability of eastern Devonian gas shale. *SPE Formation Evaluation*. 3(01), 116-124.

Tam, K. C. and Tiu, C. (1990). Role of ionic species and valency on the steady shear behavior of partially hydrolyzed polyacrylamide solutions. *Colloid and polymer science*, 268(10), 911-920.

U.S. Department of Energy (2009). Modern Shale Gas Development in the United States: A Primer. [http://energy.gov/sites/prod/files/2013/03/f0/ShaleGasPrimer\\_Online\\_4-2009.pdf](http://energy.gov/sites/prod/files/2013/03/f0/ShaleGasPrimer_Online_4-2009.pdf)

U.S. Environmental Protection Agency. Acid Mine Drainage Prediction. 2004:EPA530-R-94-036.

Vidic, R. D., Brantley, S. L., Vandenbossche, J. M., Yoxtheimer, D. and Abad, J. D. (2013). Impact of shale gas development on regional water quality. *Science*, 340(6134), 1235009.

Vidic, R.D., Hayes, T.D. and Hughes, S. (2011). Techno-economic assessment of water management solutions: Assessing the economics of technologies, and emerging solutions for shale gas water management. Shale Gas Water Management Marcellus Initiative. Pittsburgh, PA, April 13-14.

Warner, N. R., Christie, C. A., Jackson, R. B. and Vengosh, A. (2013). Impacts of shale gas wastewater disposal on water quality in western Pennsylvania. *Environmental science & technology*, 47(20), 11849-11857.

Wilson, J. M. and VanBriesen, J. M. (2012). Oil and gas produced water management and surface drinking water sources in Pennsylvania. *Environmental Practice*, 14(04), 288-300.

## **2.0 GIS AMD Database**

This study evaluated the feasibility of using AMD water as a source of sulfate for precipitation of metals of concern in the flowback water based on geographic proximity. A list of AMD locations was identified and compiled to develop the GIS-based database. Water quality information for flowback water and AMD is included into the database to help target the desired AMD sites for evaluation. The database allows the user to input a set of coordinates and locate AMD sites from a selected database within a specified distance and with a specified flow rate. The AMD locations and accompanying water quality data can be exported as both Excel files and an ArcGIS layer. The database can provide developers with a valuable tool that enables them to consider AMD water for hydraulic fracturing operations.

### **2.1 Location of Flowback Water and AMD**

#### **2.1.1 Flowback Water Location**

The location of permitted gas wells in the Marcellus shale is incorporated in the ArcGIS database. The GIS can display permitted sites for horizontal wells, vertical wells or both. The information in this database may facilitate the forecast of water needs in a given region but is not adequate to determine the quantity and quality of flowback water because many of the permitted sites have not been developed. The PADEP website provides a list of drilled wells each month. However, no geographical information is included except the county where the well is located. The location of drilled wells can be found by comparing the site API number in the table listing the permits with the table listing the actually drilled wells. Different excel files have been created combining the information about the drilled wells with the information about the permitted sites for the years 2008, 2009 and 2010. These excel files have been incorporated into the database as layers. Figure 2.1 shows the wells permitted until 09/30/2010, while Figure 2.2 shows the wells drilled during the year 2010.



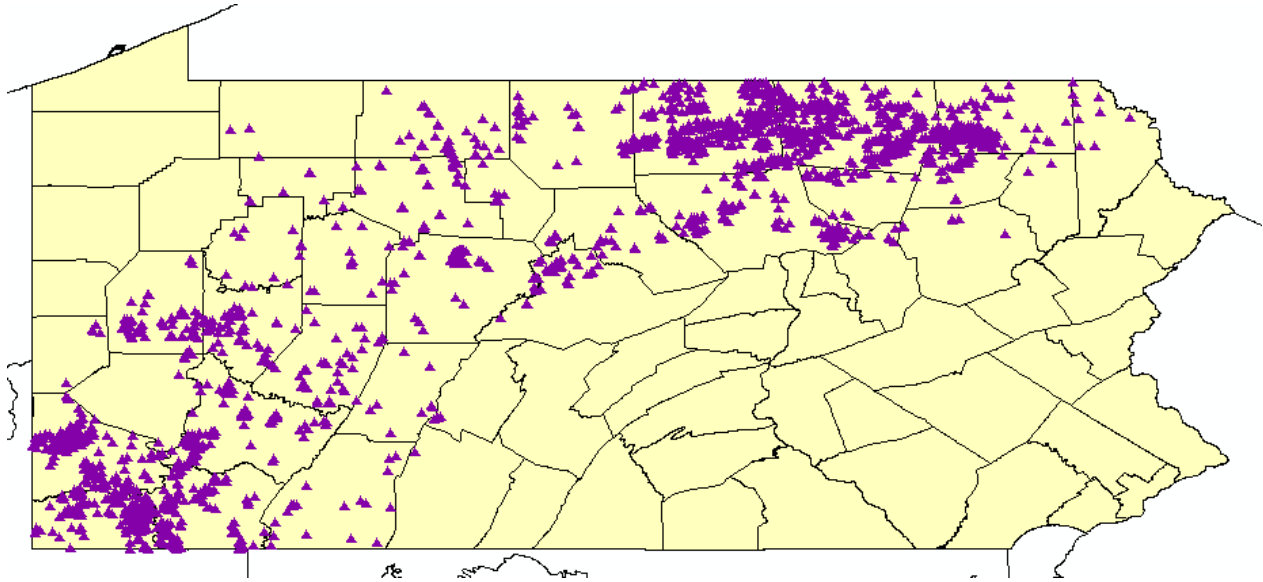


**Figure 2.1** Marcellus shale wells permitted in PA as of September 30, 2010

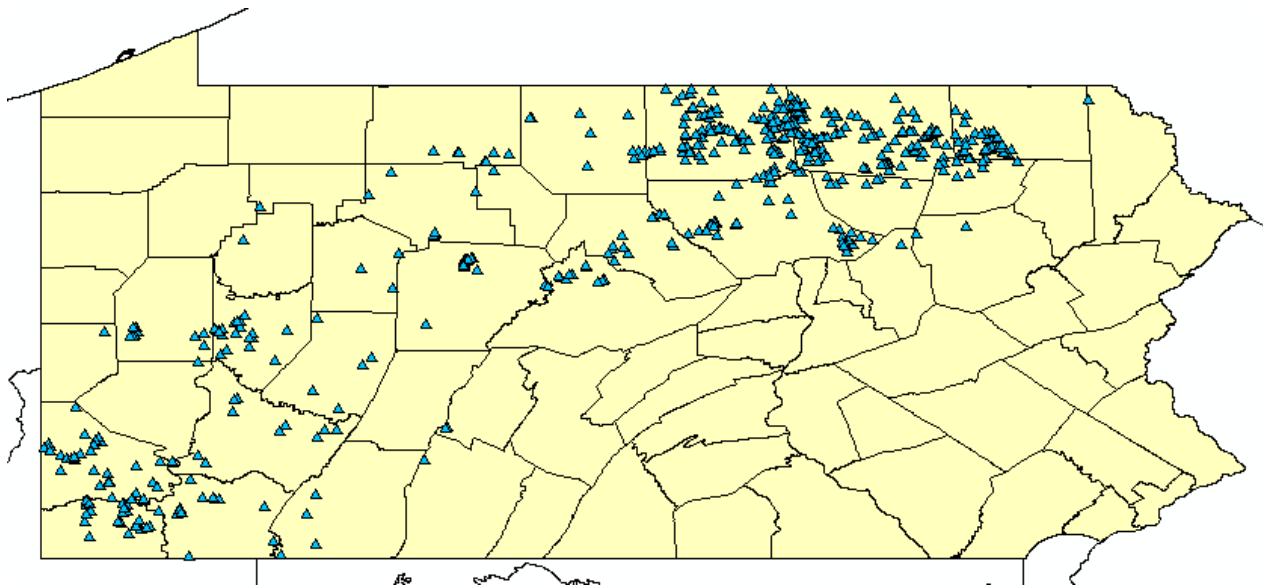


**Figure 2.2** Marcellus shale wells drilled from January 2010 until September 2010

Data available from the Bureau of Oil and Gas Management (BOGM) are included in this database. Flowback water samples were collected on 41 sites and a complete set of analysis comprising inorganics, volatile organics, glycols and radioactivity was performed. The wells sampled can be found in this database together with flowback water (Figure 2.3). Although it is very detailed in terms of water quality analysis, the BOGM data set presents the flowback water composition at one time only. In addition, some samples were collected in impoundments where the flowback water was generally mixed with produced water, drilling muds and fresh water. The Marcellus Shale Coalition (MSC), a group of owner/operators in the Marcellus, has released information on flowback water composition. Seventeen wells were sampled across Pennsylvania at different times after hydraulic fracturing treatment and these data are also included in the database.

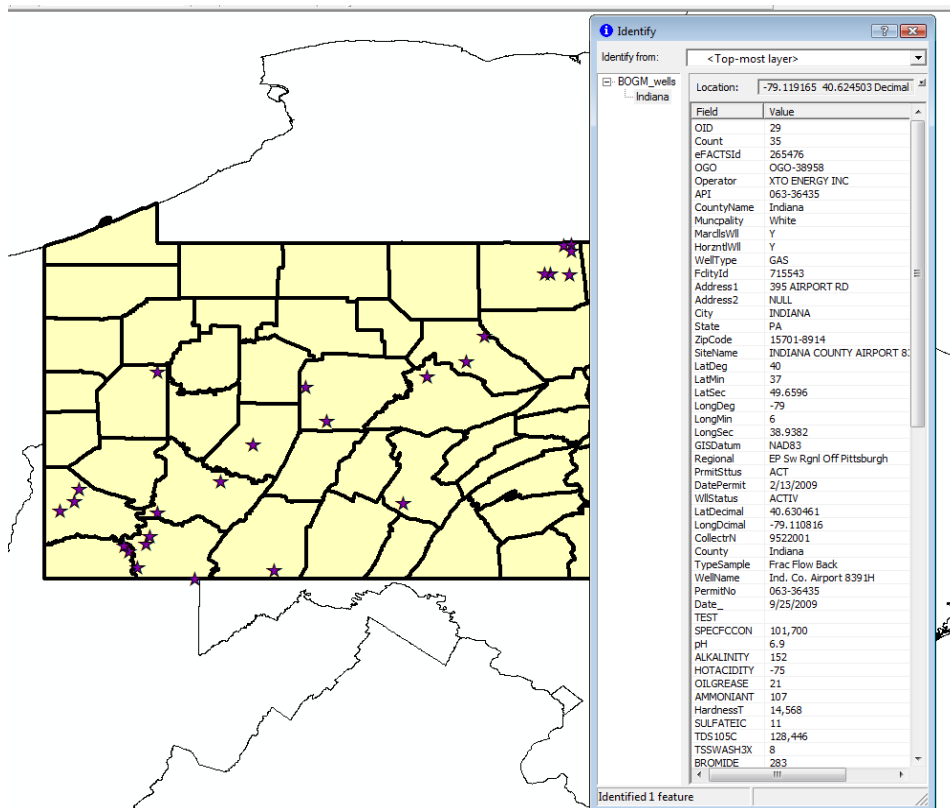


**Figure 2.3** Maps of well sites in Pennsylvania where flowback water was analyzed by the BOGM, with an example of inorganic water composition

Knowing the number of permits, the number of wells already drilled, and the average volume of water used to fracture either a vertical or a horizontal well, it is possible to approximate the water consumption across the state (Table 2.1) assuming that 1.7 and 3.8

million gallons of water is needed to fracture vertical and horizontal wells, respectively (Hayes, 2009). The calculated value is a rough estimate since it does not take into account flowback water reuse.

**Table 2.1** Drilled wells and estimated water consumption for the year 2009 and 2010 in PA

	2009	2010
Total wells drilled	734	1105
Horizontal wells	523	988
Vertical wells	211	117
Estimated water consumption (MM Gal)	2346.1	3953.3
Estimated flowback water volume (MM Gal)	540.96	830.44

### 2.1.2 AMD Location

Information about AMD sites registered with the PA-DEP is included in the database developed in this study. Comparing Figures 2.1 and 2.4 indicates that natural gas drilling is regionally well collocated with many AMD sites in the southeast. However, central and northeastern locations are not as well coordinated, raising concerns regarding trucking and/or pipeline capital costs. Figures 2.5 and 2.6 show concentrations of total iron and sulfate at selected AMD sites, respectively. Sulfate can indeed pose a problem if AMD is used for hydraulic fracturing because of the potential to stimulate sulfate reducing bacteria growth in the well, which would lead to souring of the produced gas. Depending on the pH, iron present in AMD may precipitate as iron hydroxides that may cause reduction in well permeability. Therefore, total iron and sulfate are of primary importance for ongoing and future analyses of the suitability of AMD waters for dilution and treatment of flowback water.

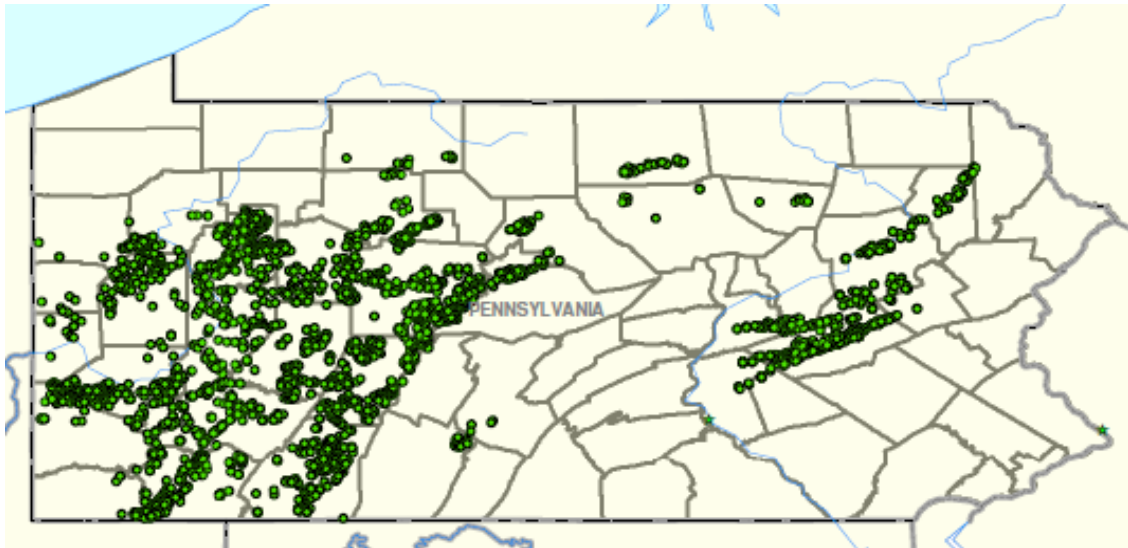


**Figure 2.4** AMD Sites through February 2010. Locations were obtained from PA-DEP databases.

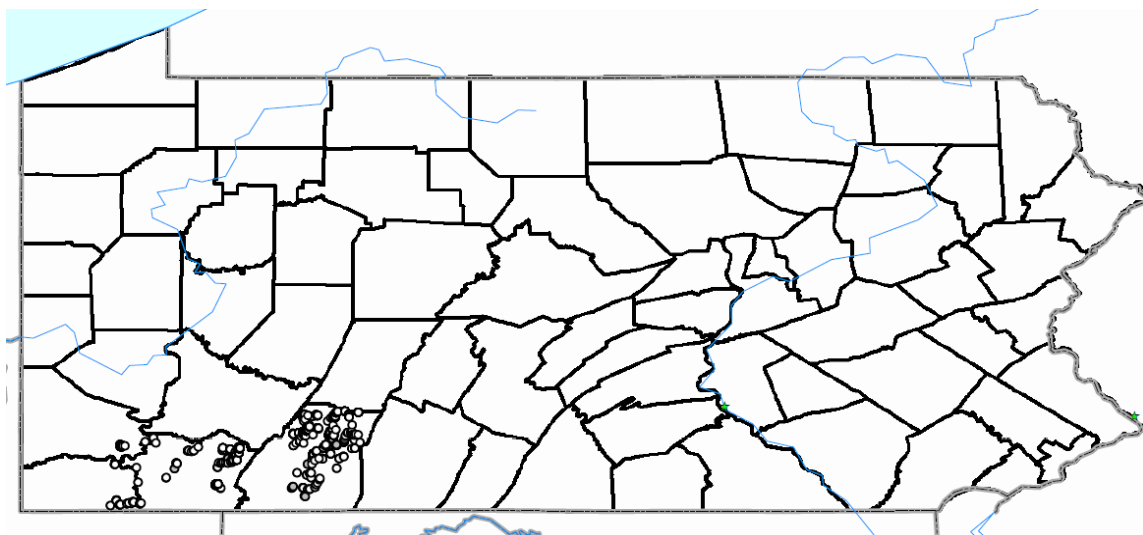


**Figure 2.5** Total iron concentrations at AMD Sites as of February 2010. Data were obtained from PA DEP database and laboratory analyses. Dark circles represent concentrations above 100 mg/L and light circles represent concentrations below 100 mg/L

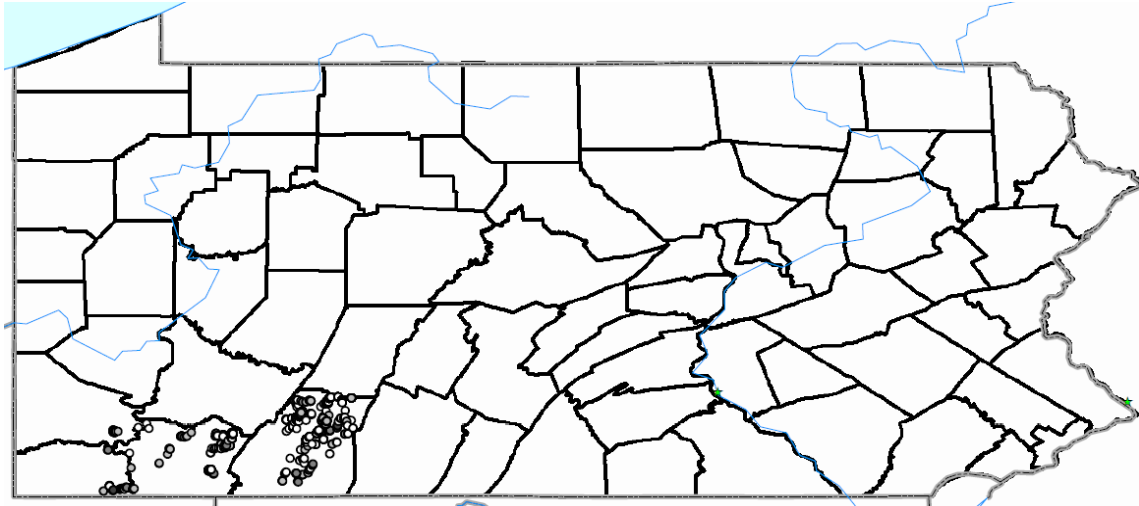


**Figure 2.6** Sulfate concentrations in AMD from sites analyzed as of February 2010. Data were obtained from PA DEP database and laboratory analyses. Dark circles represent concentrations above 800 mg/L and light circles represent concentrations below 800 mg/L

## 2.2 Identification AMD Sites with GIS Database

After all the data were compiled and entered into the GIS database, the database can be used to identify the potential AMD sites that may serve as water sources for fracturing a shale gas well or for a centralized waste treatment facility that processes and supplies water for shale gas development. The database includes a python script that allows the user to input a set of coordinates and locate AMD sites from a selected database within a specified distance and with a specified flow rate. The AMD locations and accompanying water quality data can be exported as both Excel files and an ArcGIS layer. The information on water quality depends on the available data in the GIS database. Figure 2.7 illustrates working window of the Python script that enables the search of the database with specified parameters. An example of AMD sites identified for a specific location is shown in Figure 2.8.

The database can provide developers with a valuable tool that enables them to consider AMD water for hydraulic fracturing operations. The operation manual for the use of the GIS database with python script is shown in the Appendix I.

```
Model.py - C:\Users\Hannah\Desktop\Marcellus Shale data\GDB and Maps\Database Script\Model.py
File Edit Format Run Options Windows Help
# -*- coding: #
# -----
# Model.py
# Created on:
# (by Hannah
# Description:
# -----

# Import arcpy module
import arcpy
import os
arcpy.ImportToolbox("C:\Users\Hannah\Desktop\Marcellus Shale data\GDB and Maps\Toolboxes\Additional Conversion - Generic Tools.tbx")

# Load required toolboxes
arcpy.env.workspace = "C:\Users\Hannah\Desktop\Marcellus Shale data\GDB and Maps\Database Script\Shapefiles"

# Local variables:

Select_Layer = "Select_Layer"
WQ_lyr= "WQ_lyr"
Delete_Me3_lyr = "Delete_Me3_lyr"
Delete_Me="C:\Users\Hannah\Desktop\Marcellus Shale data\GDB and Maps\Delete_Me.shp"
Delete_Me2="C:\Users\Hannah\Desktop\Marcellus Shale data\GDB and Maps\Delete_Me2.shp"
Delete_Me3="C:\Users\Hannah\Desktop\Marcellus Shale data\GDB and Maps\Delete_Me3.shp"
Delete_Me4="C:\Users\Hannah\Desktop\Marcellus Shale data\GDB and Maps\Delete_Me4.shp"
Delete_Me5="C:\Users\Hannah\Desktop\Marcellus Shale data\GDB and Maps\Delete_Me5.shp"
Output = "C:\Users\Hannah\Desktop\Marcellus Shale data\GDB and Maps\Output.shp"
Final_Output = "C:\Users\Hannah\Desktop\Marcellus Shale data\GDB and Maps\Final_Output.shp"
Final_Output_csv= "C:\Users\Hannah\Desktop\Marcellus Shale data\GDB and Maps\Final_Output_csv.csv"
Final_Output2_csv= "C:\Users\Hannah\Desktop\Marcellus Shale data\GDB and Maps\Final_Output2_csv.csv"

while True:

    rows = arcpy.UpdateCursor("C:\Users\Hannah\Desktop\Marcellus Shale data\GDB and Maps\Marcellus.gdb\Marcellus_Wells\Update_Cursor")
    for row in rows:
        latitude = float(row_input('Latitude: '))
        longitude = float(row_input('Longitude: '))
        row.Shape = arcpy.PointGeometry(arcpy.Point(longitude, latitude))
        row.Latitude = latitude
        row.Longitude = longitude
```

Figure 2.7 The interface of the python script

### Sample Locations within 25 Miles of Franklin

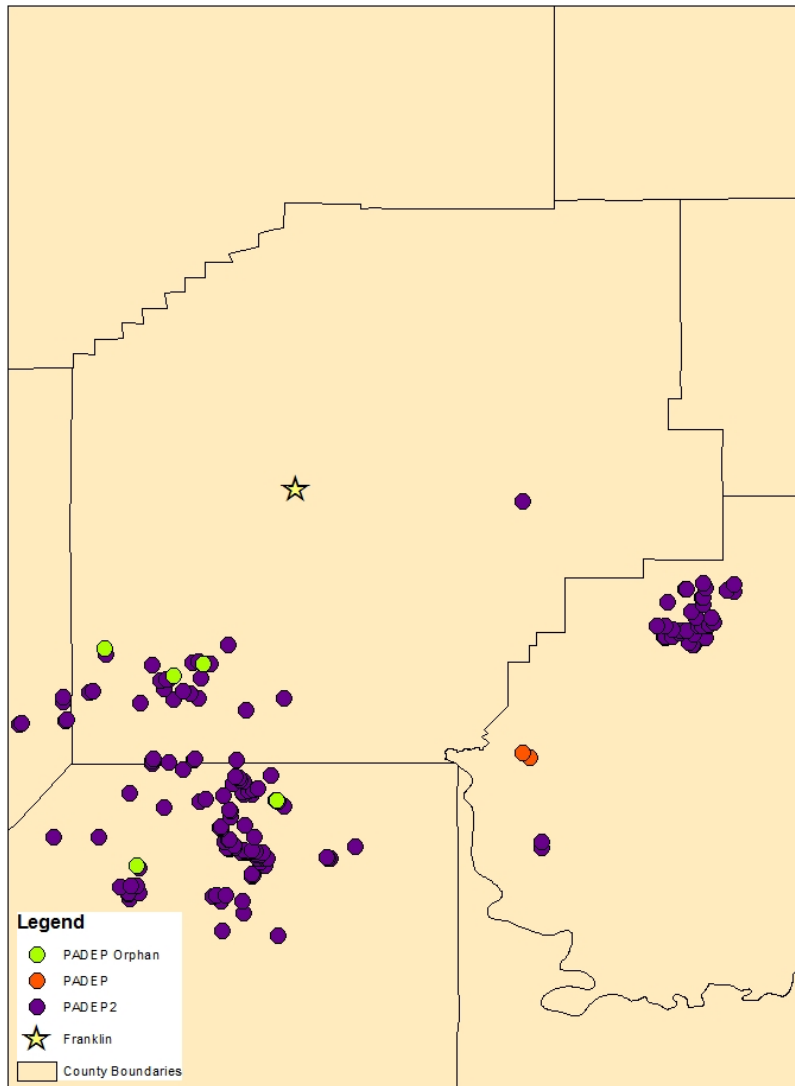


**Figure 2.8** An example using GIS-based database for the selection of available AMD sites

## 2.3 References

Hayes, T. (2009). Sampling and analysis of water streams associated with the development of Marcellus shale gas, Final report prepared for the Marcellus Shale Coalition.

### **3.0 Spatial and Temporal Correlation of Water Quality Parameters of Produced Waters from Devonian-age Shale following Hydraulic Fracturing**

The exponential increase in fossil energy production from Devonian-age shale in the Northeastern United States has highlighted the management challenges for produced waters from hydraulically fractured wells. Confounding these challenges is a scant availability of critical water quality parameters for this wastewater. Chemical analyses of 160 flowback and produced water samples collected from hydraulically fractured Marcellus Shale gas wells in Pennsylvania were correlated with spatial and temporal information to reveal underlying trends. Chloride was used as a reference for the comparison as its concentration varies with time of contact with the shale. Most major cations (i.e., Ca, Mg, Sr) were well-correlated with chloride concentration while barium exhibited strong influence of geographic location (i.e., higher levels in the northeast than in southwest). Comparisons against brines from adjacent formation provide insight into the origin of salinity in produced waters from Marcellus Shale. Major cations exhibited variations that cannot be explained by simple dilution of existing formation brine with the fracturing fluid, especially during the early flowback water production when the composition of the fracturing fluid and solid-liquid interactions influence the quality of the produced water. Water quality analysis in this study may help guide water management strategies for development of unconventional gas resources.

### **3.1 Materials and Methods**

#### **3.1.1 Flowback Water Sampling**

Flowback water samples have been collected at three well sites in southwest Pennsylvania (Sites A, B1 and B2). Site A includes 5 horizontal wells on a single pad that were hydraulically fractured within a short period of time using similar fracturing fluid. The fracturing fluid was a mix of flowback water from previously completed wells and fresh water, but the exact composition of the fluid was unknown. The five wells were fractured stage by stage simultaneously and the water flowed back to the surface at the same time from all five wells. Flowback water samples were collected at various times from day 1 to day 20 (day 1 referring to the first day the water was allowed to flow). On this particular site, the wells were shut in for 11 days between the end of the hydraulic fracturing event and the beginning of the flowback. Sites B1 and B2 are separated by 0.9 km and are characterized by a single well on a pad and no lag time between the end of the hydraulic fracturing and flowback. Hence, they present similarities



in geographic location and in depth, length, number of stages and volume of fracturing fluid injected. Samples were collected from day 1 to 29 on site B1 and from day 1 to 16 on site B2.

### **3.1.2 Analytical Methods**

Total dissolved solids (TDS) and total suspended solids (TSS) were determined using the Standard Methods 2540C and 2540D, respectively. Alkalinity measurements were performed following the Standard Method 2320B (APHA, 2000). Prior to cation analysis by atomic absorption (GBC908, GBC Scientific Equipment LLC, Hampshire, IL and Perkin Elmer model 1000 AAS) the samples were filtered through 0.45 µm nylon filter, acidified to pH below 2 using nitric acid and kept at 4°C. Samples for total iron analysis were prepared by dissolving the sample in 1N H<sub>2</sub>SO<sub>4</sub> before filtration. For Ca, Ba and Sr analysis, the samples were diluted in 2% metal grade nitric acid and 0.15% KCl was added to the solution to limit ionization interferences. An air-acetylene flame was used for Na, Mg, Fe analysis while a nitrous oxide-acetylene flame was used for Ba, Sr and Ca analysis to limit chemical interferences. Cation analysis was also performed by ICP-OES for several samples to verify AA methods. The two analytical methods were in very good agreement. Anions were analyzed using ion chromatograph (Dionex DX-500) with Dionex IonPac® AS14A column at a flowrate of 1mL/min.

### **3.1.3 Other Data Sources**

Several flowback/produced water data sources were used in this study, including the PADEP Bureau of Oil and Gas Management analyses of flowback/produced water from more than 40 sources and the Marcellus Shale Coalition sampling and analyses of flowback water from several wells (Hayes, 2009). In addition, data shared by production companies were included in analyses. For all samples, charge balance was checked and any sample exhibiting a charge balance below 85% was discarded. The location of sampled sites is indicated on Figure 3.1 and shows the number of wells sampled and the number of samples collected for each county.

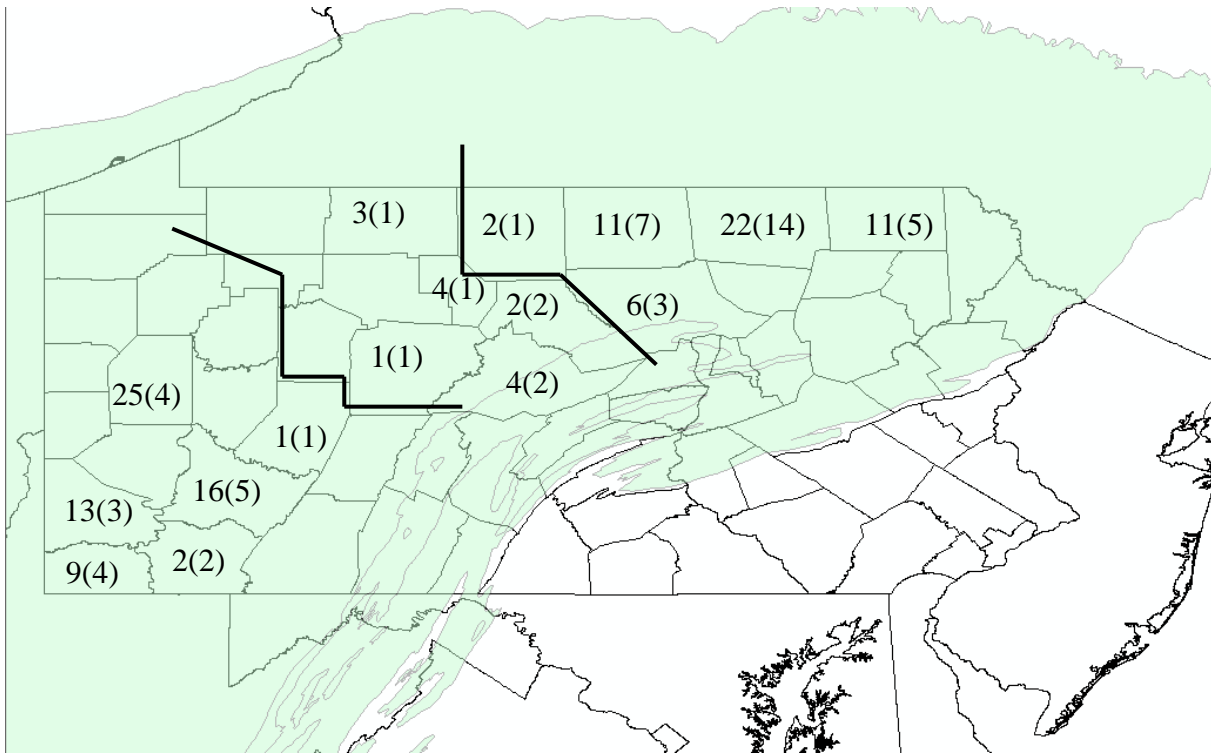


**Figure 3.1** Map of Pennsylvania counties and underlying Marcellus Shale, with number of samples collected and in between brackets number of wells sampled (geospatial data from the USGS, available at [www.pasda.psu.edu](http://www.pasda.psu.edu)). Black bold lines separate the Northeast, Central and Southwest areas of the state.

## 3.2 Results and Discussion

### 3.2.1 Composition of Flowback Water Recovered with Time

Flowback water is dominated by Cl-Na-Ca with elevated bromide, magnesium, barium and strontium content and very low sulfate and carbonate. Its chemistry varies greatly during the first weeks of collection. A summary of the key water quality parameters for samples examined in this study is presented in Table 3.1 and TDS profiles for the well sites sampled for this study are shown on Figure 3.2. Sites B1 and B2 exhibited much lower TDS content than site A, which is likely due to shorter residence time in the formation and the use of municipal drinking water as fracturing fluid rather than a mixture of freshwater and produced water as was the case for site A.

**Table 3.1** Summary of Marcellus Shale produced water quality in Pennsylvania

	Minimum	Maximum	Average	Number of samples
TDS (mg/L)	680	345,000	106,390	129
TSS (mg/L)	4	7,600	352	156
Oil and grease (mg/L)	4.6	802	74	62
COD (mg/L)	195	36,600	15,358	89
TOC (mg/L)	1.2	1530	160	55
pH	5.1	8.42	6.56	156
Alkalinity (mg/L as CaCO <sub>3</sub> )	7.5	577	165	144
SO <sub>4</sub> (mg/L)	0	763	71	113
Cl (mg/L)	64.2	196,000	57,447	154
Br (mg/L)	0.2	1,990	511	95
Na (mg/L)	69.2	117,000	24,123	157
Ca (mg/L)	37.8	41,000	7,220	159
Mg (mg/L)	17.3	2,550	632	157
Ba (mg/L)	0.24	13,800	2,224	159
Sr (mg/L)	0.59	8,460	1,695	151
Fe dissolved (mg/L)	0.1	222	40.8	134
Fe total (mg/L)	2.6	321	76	141
Gross Alpha <sup>1</sup> (pCi/L)	37.7	9,551	1,509	32
Gross Beta <sup>1</sup> (pCi/L)	75.2	597,600	43,415	32
Ra <sup>228</sup> (pCi/L)	0	1,360	120	46
Ra <sup>226</sup> (pCi/L)	2.75	9,280	623	46
U <sup>235</sup> (pCi/L)	0	20	1	14
U <sup>238</sup> (pCi/L)	0	497	42	14

<sup>1</sup> Data for Northeast Pennsylvania only

Chloride and sodium are the primary constituent ions, followed by calcium, barium, magnesium and strontium and their increase with time was similar to that of TDS (Figure 3.3). Concentration of strontium and magnesium in the flowback water from site A ranged from 1,300 mg/L on day 11 to 2,100 mg/L on day 30, while the concentration of barium reached only 380 mg/L on day 30. In contrast, barium concentration in the flowback water from sites B1 and B2 increased to 3,000 mg/L on day 30, while magnesium concentration reached only 670 mg/L on the same day. For the two sites close to each other (site B1 and B2), the flowback water had

similar concentration ranges for ions, demonstrating a strong correlation between geographic location and flowback water composition.

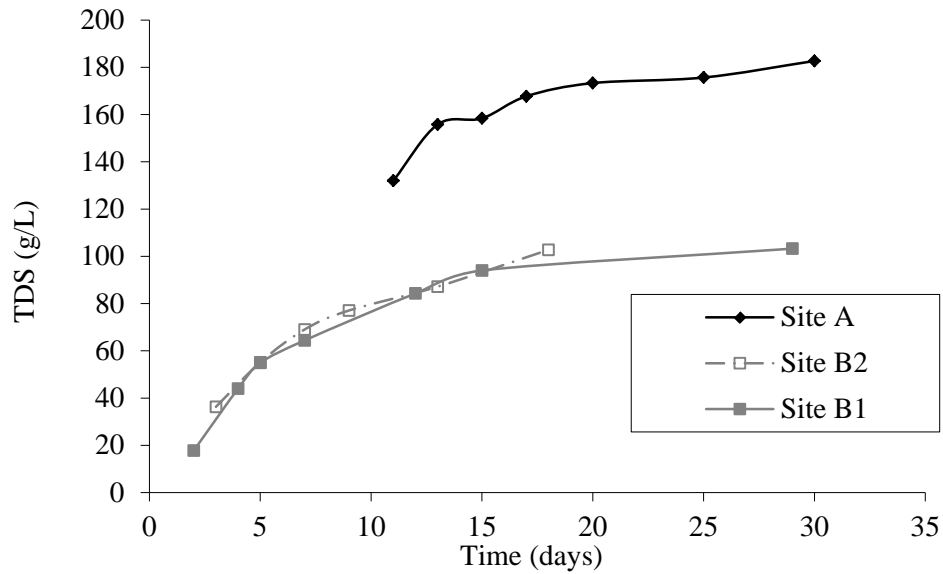


**Figure 3.2** Variation of total dissolved solids concentration in flowback water versus time for sites A, B1 and B2. Day 0 corresponds to the end of the hydraulic fracturing process.

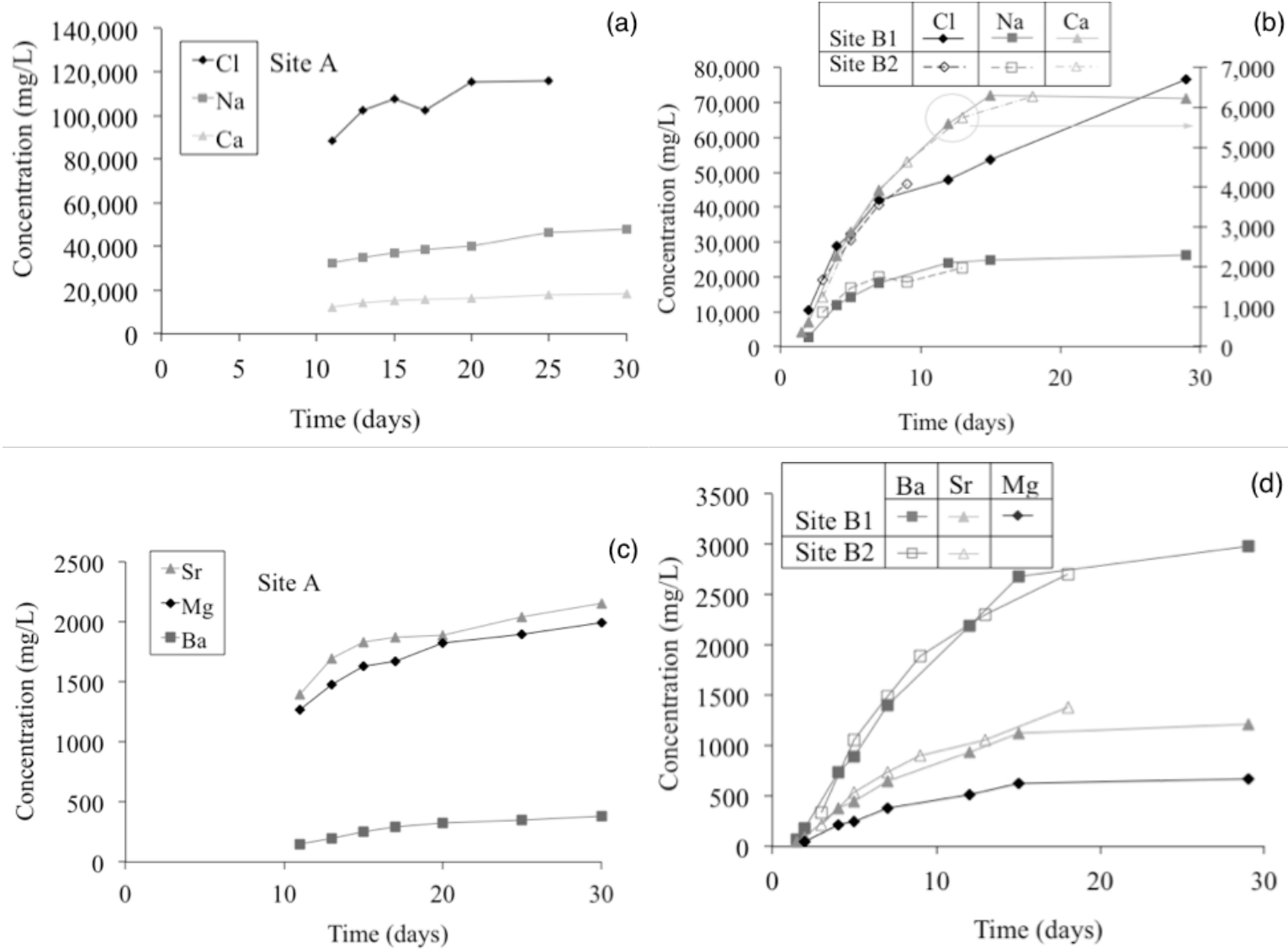


**Figure 3.3** Concentration profiles of Na, Cl, Ca (a and b), and Mg, Sr, Ba (c and d) for site A and sites B1 and B2, respectively. Day 0 corresponds to the end of the hydraulic fracturing process

The decrease in pH and alkalinity with time (Figure 3.4 and 3.5) as well as the decline of Ca/Mg ratio (Figure 3.5) suggests precipitation of calcium carbonate within the formation. Equilibrium calculations were performed using the software Phreeqc and the Pitzer activity coefficient model. Calcite saturation index for Site A decreased from 0.83 to -0.15, indicating that this flowback water is essentially equilibrated with respect to calcium carbonate within 30 days. However, calcite saturation index for Site B1 ranged from 1.94 on day 2 to 1.02 on day 29, indicating that calcite continues to precipitate in the brine. Site A flowback water had much lower alkalinity in comparison with site B1. This difference may be due to a greater extent of calcium carbonate precipitation driven by the higher initial calcium content in Site A flowback water. Sulfate concentrations in flowback samples collected from Site A were close to detection limit while sulfate concentrations in flowback water from Site B1 decreased from 28.6 mg/L on the first day to 2 mg/L after 30 days. Reduction in sulfate concentration can be explained by barium sulfate precipitation and the fact that very little sulfate is present in the formation. Equilibrium calculations revealed that barite saturation index decreasing from 2.15 on day 2 to 1.61 on day 29, confirming slow precipitation of BaSO<sub>4</sub>. Such behavior is in agreement with previous studies that revealed fairly slow barite precipitation when the saturation index is below 2.6 (Barbot and Vidic, 2011).

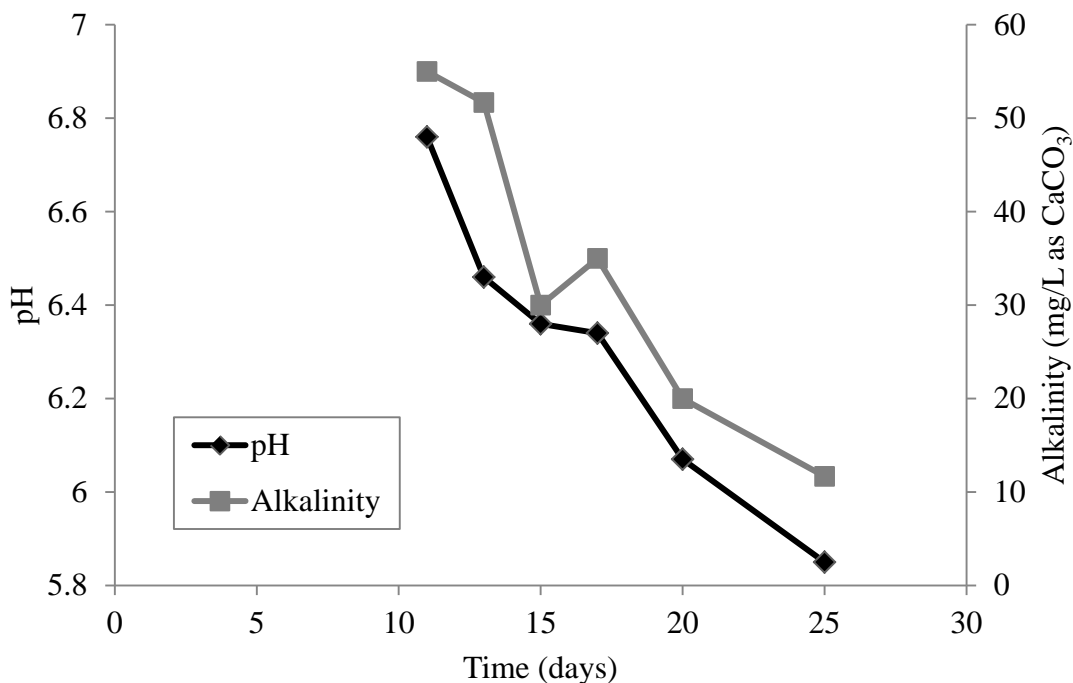


**Figure 3.4** Variation of pH and alkalinity with time for flowback water from site A. Day 0 corresponds to the end of the hydraulic fracturing process.

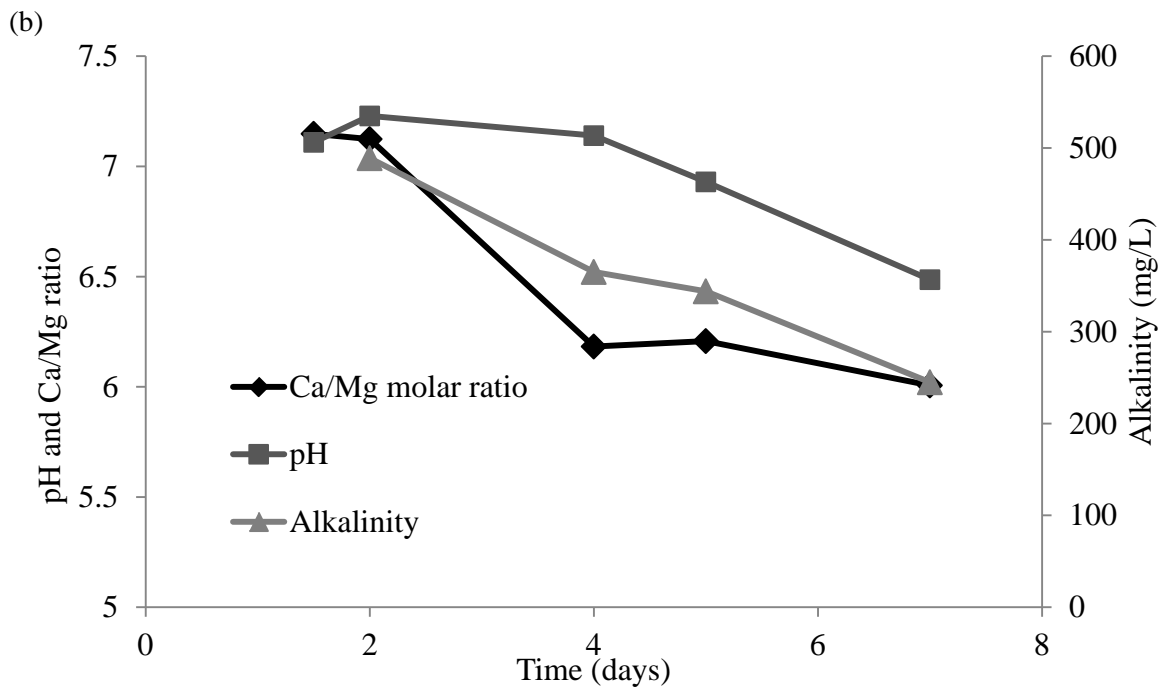


**Figure 3.5** Variation of Ca/Mg molar ratio, pH and alkalinity with time for flowback water from site B1. Day 0 corresponds to the end of the hydraulic fracturing process.

### 3.2.2 Origin of Salinity in the Produced Water

When injected in the wellbore, the fracturing fluid may mix with formation brine that exists in the target formation (Marcellus Shale in this case) or from adjacent formations should fractures extend outside the target formation. The Marcellus Shale is widely regarded as a dry formation, but there is a single report in the literature with three formation brine analyses (Osborn and McIntosh, 2010). The second salinity source can be the formation itself. XRD analysis of core samples revealed that shale from the Marcellus Shale is composed (by decreasing fraction) of quartz, clays, pyrite and calcite (Roen, 1984; Boyce, 2010). Blauch et al. describe salt layers containing calcium, sodium, potassium, iron, magnesium, barium and strontium, that may dissolve and contribute to salinity in flowback and produced water (Blauch et al., 2009). However, there are no other reports that describe salt layers, suggesting that they may not be present throughout the formation.

Inorganic constituents of produced from the Marcellus Shale were compared with the Marcellus Shale formation brines described previously, Bradford Formation brines located in the Upper Devonian, and produced water from oil and gas wells in Western Pennsylvania from

horizons ranging from Lower Silurian to Upper Devonian (Osborn and McIntosh, 2010; Dresel and Rose, 2010). Most of the reports on produced water analyses from the Marcellus Shale used in this study are missing some critical information that is required for detail understanding of the produced water chemistry. For example, the PADEP Bureau of Oil and Gas Management (BOGM) data provides exact sampling location but gives no information about the time of contact between the water and the formation, or about the initial fracturing fluid quality. In addition, only one sample was collected per site, representing either the composition at a given time or mixed flowback/produced water collected over several days. The Marcellus Shale Coalition report (Hayes, 2009) includes initial water quality and variation of flowback water composition with time but no information on the contact time with the formation. Despite the lack of precise information in these reports, the data can be used to analyze general trends in the geochemistry of produced water and provide information that is critical when evaluating potential management strategies for these wastewaters, especially in the Appalachian basin where water reuse for hydraulic fracturing is the preferred management alternative.

Chloride concentration was chosen as reference for other key ions as it is the major anion in flowback water and is strongly correlated with TDS independently of the location and sampling time ( $R^2 = 0.90169$ ). The concentrations of key ions of interest (i.e., Na, Ba, Mg, Sr, Br) were compared to chloride concentrations for Marcellus Shale but the data were divided into 3 geographical zones: Southwest (SW), Central (C), and Northeast (NE) to assess the impact of geographic location on these correlations (Figure 3.1). Due to the small sample size, analyses of data from wells in Central Pennsylvania were not performed.

Marcellus Shale produced water exhibits Na:Cl ratio similar to other brines from Pennsylvania (Figure 3.6). However, it differentiates itself from other brines by the concentration of divalent cations. Produced water from Marcellus Shale wells had slightly less Ca (Figure 3.7), much less Mg (Figure 3.8), and much more Sr (Figure 3.9) than are found in any other brines from PA. Although Ba data for produced water from all other formations are not available, indications are that the produced water from Marcellus Shale contains much more Ba compared to Lower Silurian and Upper Devonian formations. Furthermore, the produced water from Marcellus Shale does not exhibit the same trends in Ca:Cl and Mg:Cl ratios as other produced waters, especially during the early stages of the flowback period indicated by lower chloride concentrations. This behavior indicates that mixing with the formation brine cannot completely explain the salinity of the produced water over the entire life of a well.



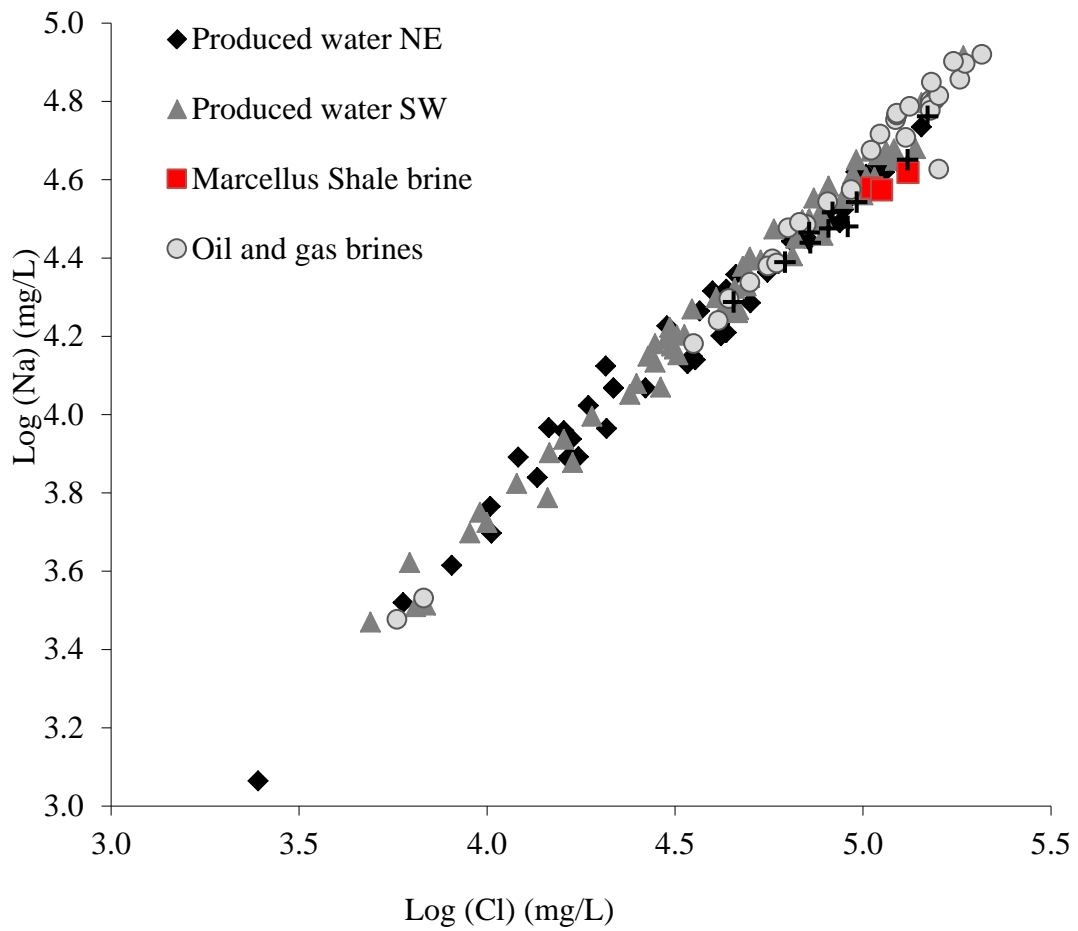


**Figure 3.6** Correlation of Na with Cl in the produced water from Marcellus Shale, oil and gas brines from conventional reservoirs in southwest Pennsylvania, Marcellus Shale brine, and Bradford Formation brine.

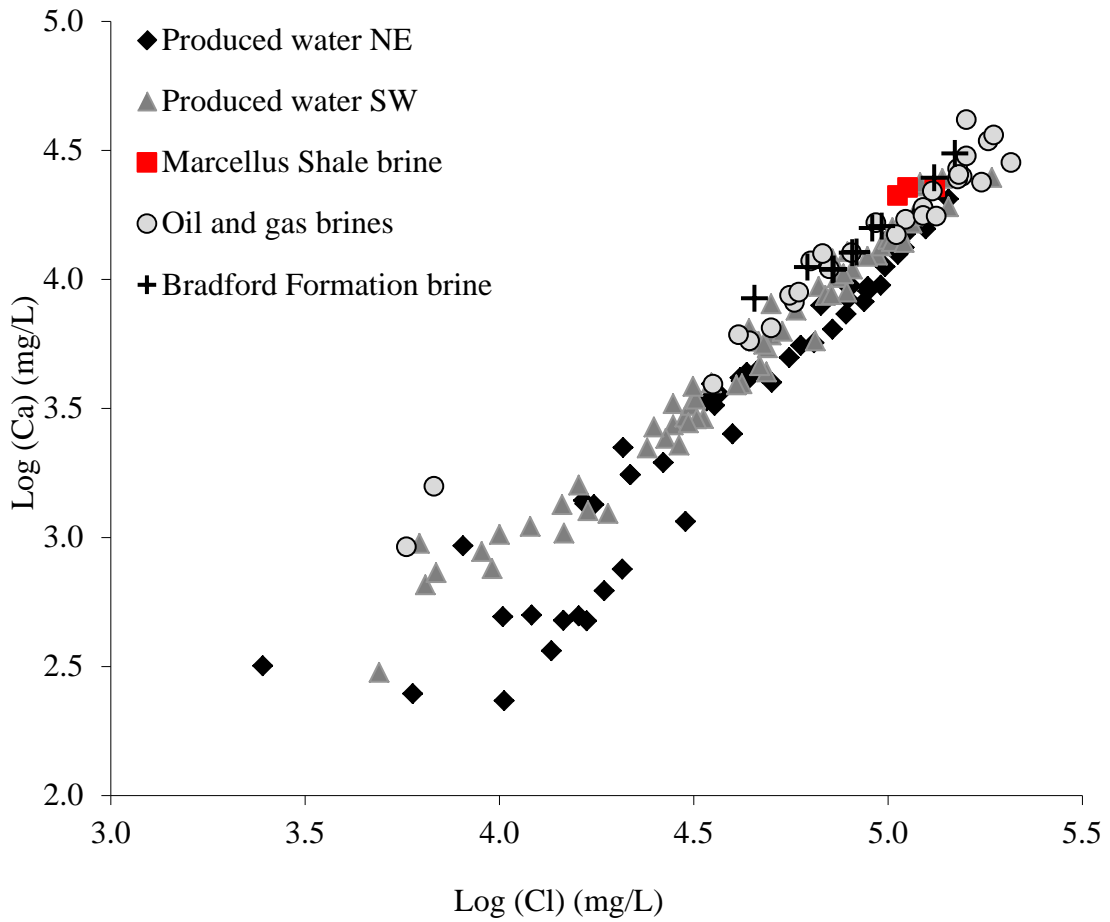


**Figure 3.7** Correlation of Na with Cl in the produced water from Marcellus Shale, oil and gas brines from conventional reservoirs in southwest Pennsylvania, Marcellus Shale brine, and Bradford Formation brine.

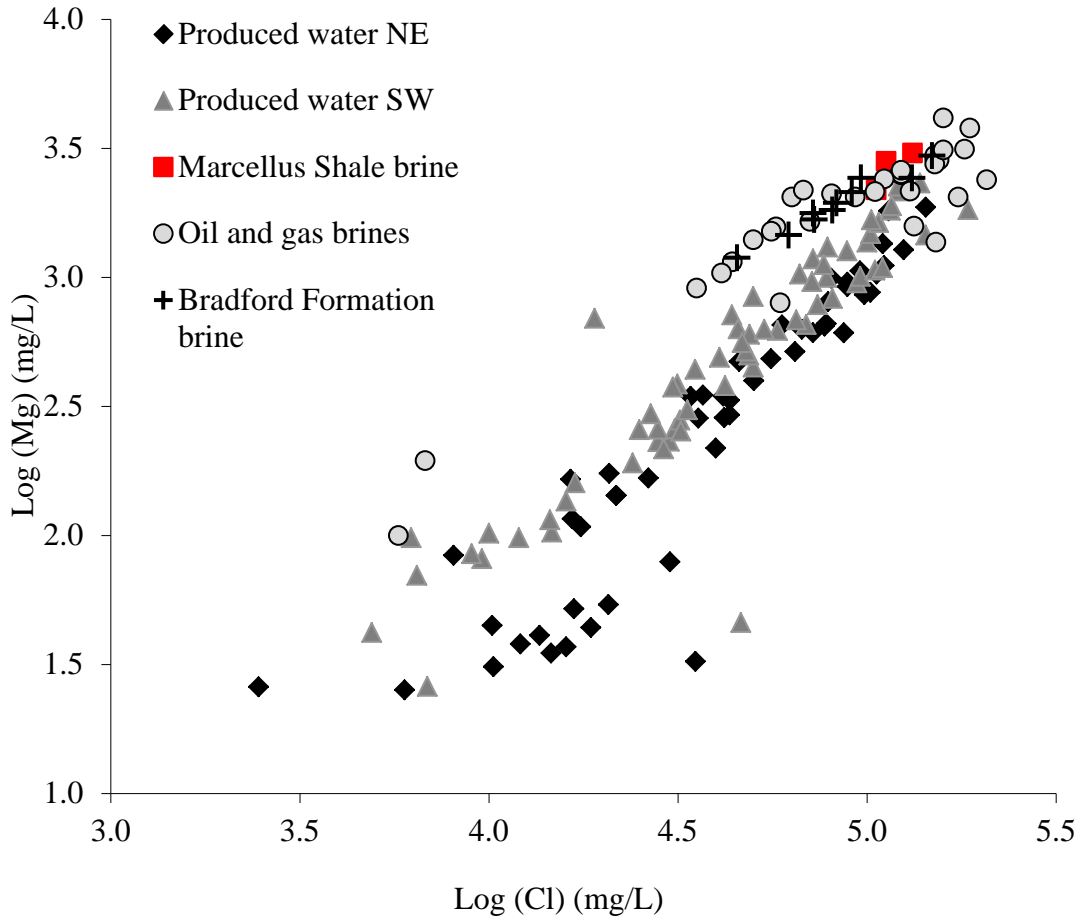


**Figure 3.8** Correlation of Na with Mg in the produced water from Marcellus Shale, oil and gas brines from conventional reservoirs in southwest Pennsylvania, Marcellus Shale brine, and Bradford Formation brine.

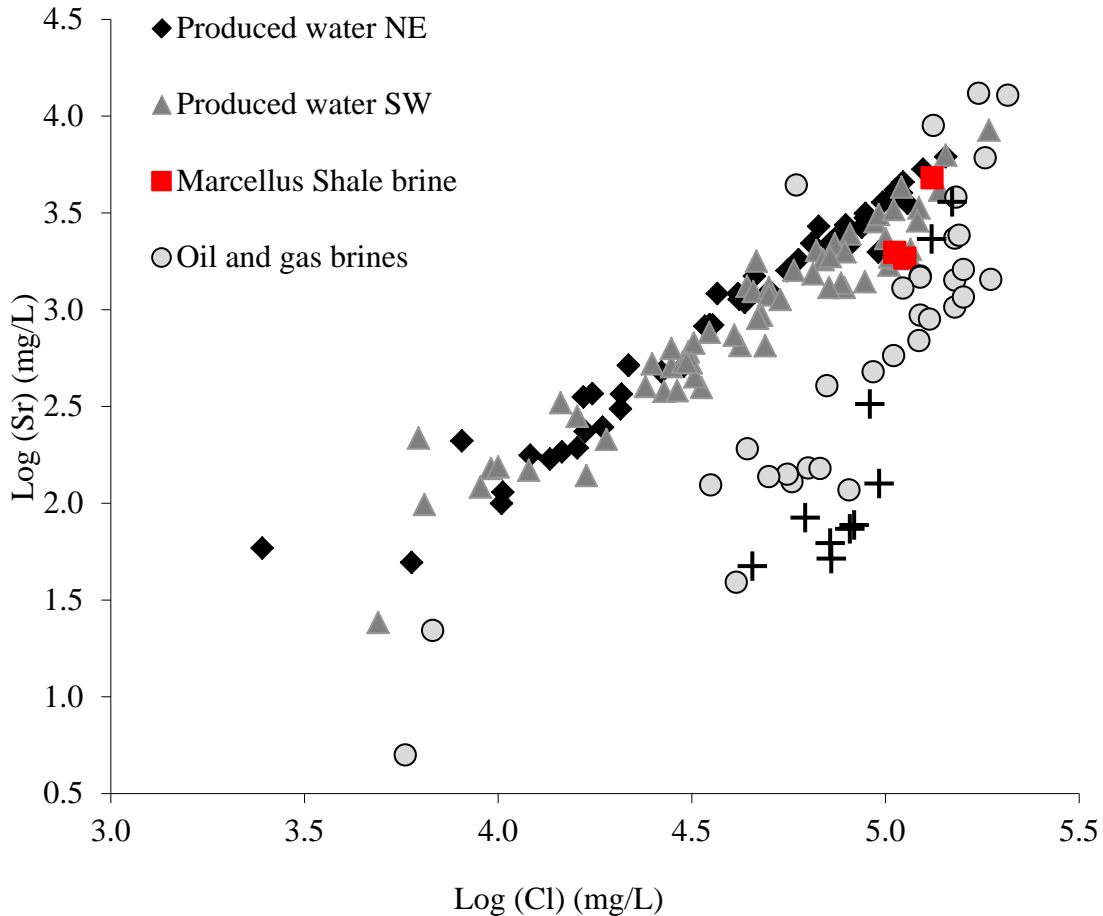


**Figure 3.9** Correlation of Na with Sr in the produced water from Marcellus Shale, oil and gas brines from conventional reservoirs in southwest Pennsylvania, Marcellus Shale brine, and Bradford Formation brine.

The origin of the salinity in the produced water is better understood using ion concentrations that are plotted versus bromide concentration, as bromide in solution is normally conserved during water evaporation (Carpenter, 1978). The conservative parameter  $MCl_2$  is valuable when determining the chemical origin of chloride-rich brines.  $MCl_2$  is calculated as follows:

$$MCl_2 \text{ (meq/L)} = Ca^{2+} + Mg^{2+} + Ba^{2+} + Sr^{2+} - SO_4^{2-} - CO_3^{2-} \quad (3-1)$$

$MCl_2$  is a conservative quantity during seawater evaporation (up to the point of  $KMgCl_3$  precipitation).  $MCl_2$  remains constant during precipitation of sulfates, carbonates and NaCl.

During seawater evaporation, the plot of  $\log[MCl_2] = f(\log[Br])$  is a straight line of slope 1:1. It is represented by the following equation (Carpenter, 1978):

$$\log (MCl_2) = \log [Br] + 0.011 \quad (3-2)$$

Oil and gas brines from conventional reservoirs in SW Pennsylvania (Dresel and Rose, 2010) follow the trend of seawater evaporation (Figure 3.10) while the produced water from the Marcellus Shale shows an unusual relationship. High-salinity water samples closely match the seawater evaporation line, which suggests that the salinity of the produced water originates from the concentrated seawater. On the other hand, less concentrated produced water samples deviate from the expected relationship and exhibit either bromide enrichment or depletion of  $MCl_2$  with respect to concentrated seawater. With time, produced water becomes concentrated in Ca, Mg, Ba and Sr cations while sulfate and carbonate concentrations decrease. For the lowest salinity samples, the  $MCl_2$  and bromide relationship deviates significantly from the 1:1 slope, indicating that the characteristics of these samples were influenced by the quality of the fracturing fluid and/or chemical reactions that may be occurring in the formation during the contact with the shale.

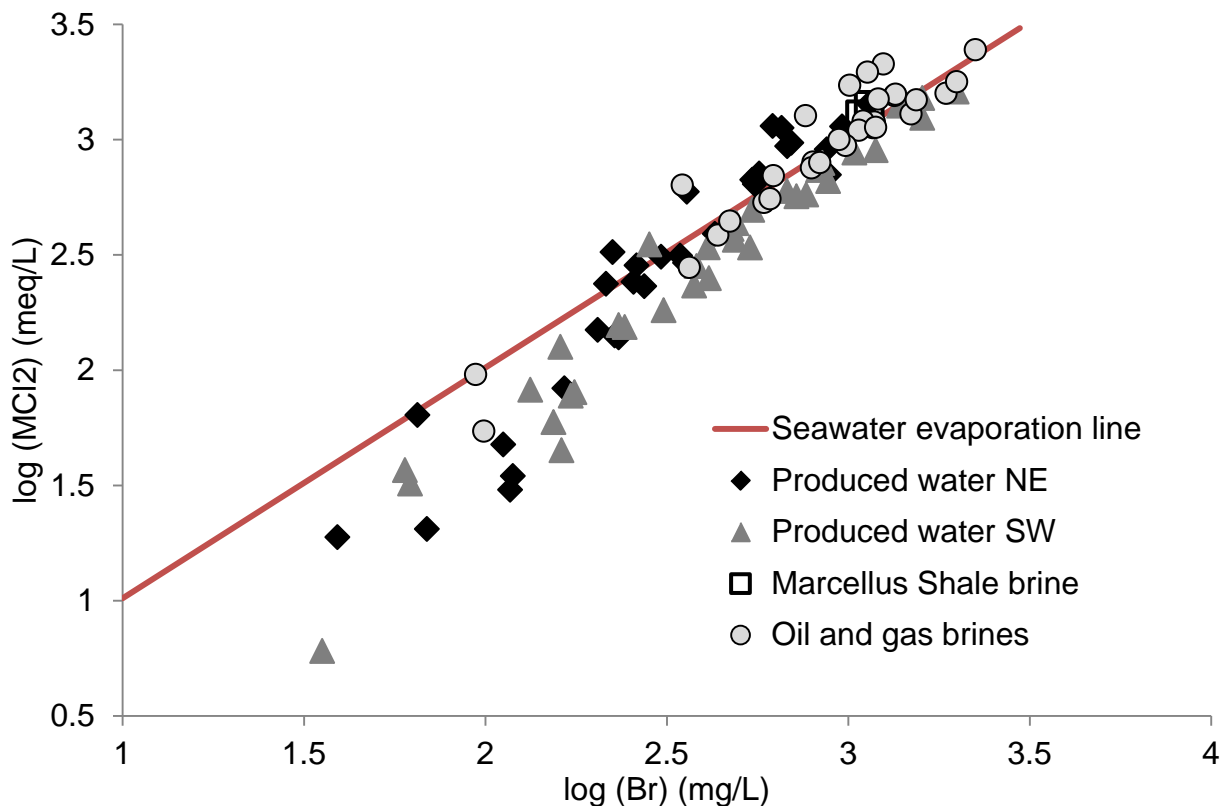


**Figure 3.10** Correlation of  $\log[MCl_2]$  versus  $\log[Br]$  for various Pennsylvania brines.

The plot  $\log[\text{Cl}] = f(\log[\text{Br}])$  for Marcellus Shale produced water samples exhibits a straight line with the slope that is very close to 1:1 for both Northeast and Southwest region of Pennsylvania (Figure 3.11). This finding suggests mixing of relatively dilute fracturing fluid with a brine concentrated beyond the point of halite saturation, which then exhibits a chloride:bromide ratio below that for seawater (Dresel and Rose, 2010).

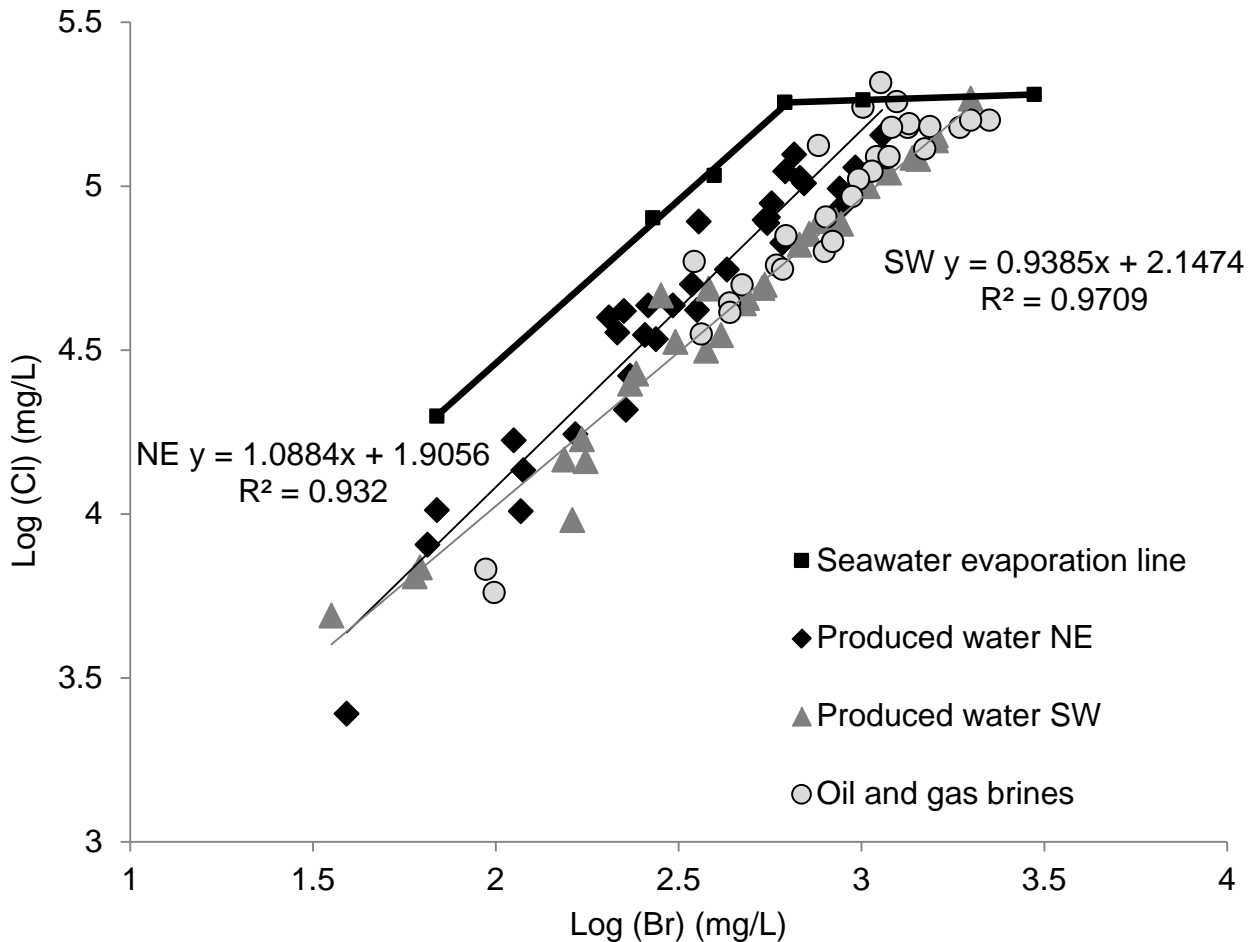


**Figure 3.11** Correlation of  $\log[\text{Cl}]$  versus  $\log[\text{Br}]$  for various Pennsylvania brines.

Finally, the logarithmic plot of  $[\text{Cl}]$  versus  $[\text{MCl}_2]$  for Marcellus Shale produced water is a straight line with slope of approximately 0.7, which suggests that  $\text{MCl}_2$  and  $\text{Cl}$  concentrations in flowback water are not governed by the simple dilution of the concentrated formation brine, as is the case for oil and gas brines from conventional reservoirs (Figure 3.12). To better understand how flowback water composition evolves with time, the plot of  $[\text{Cl}]$  versus  $[\text{MCl}_2]$  was constructed for the data collected from wells A and B1 (Figure 3.13). The average slope for both wells was

again found to be around 0.7. With time, the flowback water salinity continues to increase, but is enriched in alkaline earths (or depleted in chloride) as compared to the trend expected for seawater evaporation. If the fracturing fluid was simply being mixed with the formation brine, the resulting plot of flowback water at different times would follow a straight line with the slope of 1:1. The slope exhibited by the flowback from these Marcellus Shale wells suggests that other mechanisms are involved and that the salinity of the early flowback water cannot be entirely explained by mixing of the fracturing fluid with existing formation water.

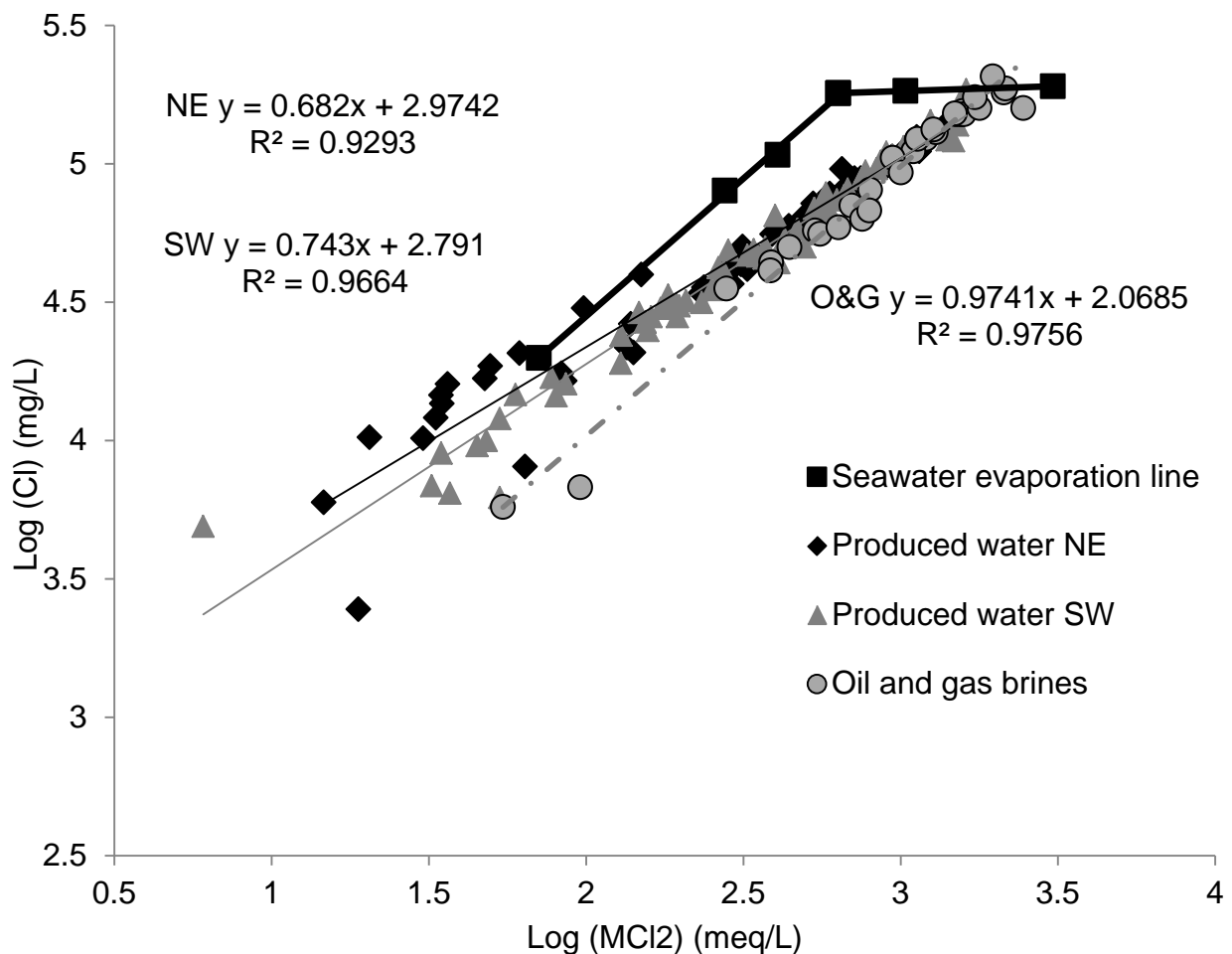


**Figure 3.12** Correlation of log[Cl] versus log[MCl<sub>2</sub>] for all Marcellus Shale produced water samples and oil and gas brines

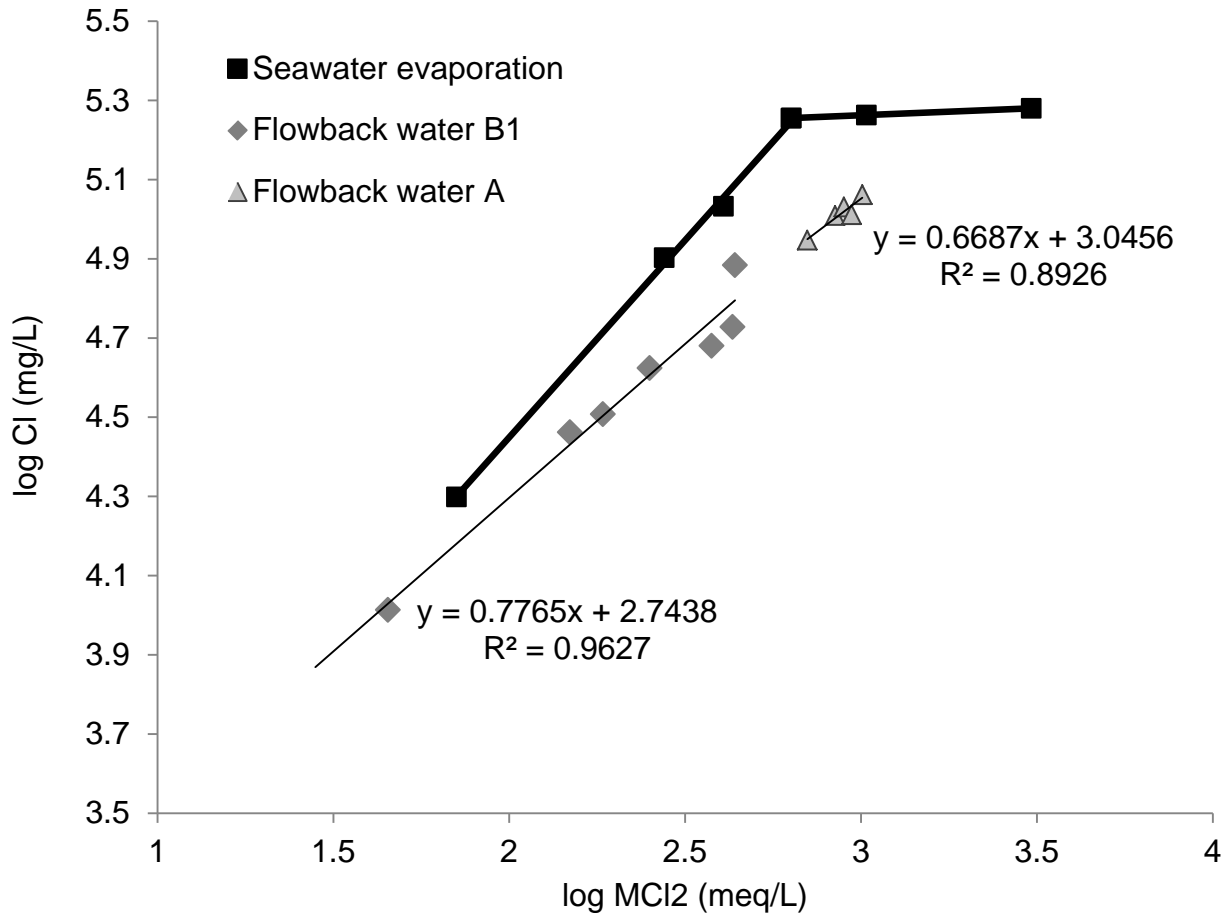


**Figure 3.13** Correlation of log[Cl] versus log[MCl<sub>2</sub>] for flowback water samples from sites A and B1.

### 3.2.3 Spatial Trends in Flowback Water Chemistry in Pennsylvania

Although the flowback water chemistries from wells that were in close proximity exhibited similar trends (i.e., wells B1 and B2), it is difficult to predict composition of the flowback/produced water as it varies with time, location, and quality of the fracturing fluid. Nevertheless, it is important to estimate the concentrations of major cations of interest to reusing the flowback/produced water for hydraulic fracturing based on easily measurable water quality parameters. Therefore, all major cations included in this study were initially fitted to the following non-linear regression model:

$$Y = \beta_0 X^{\beta_1} \epsilon \quad (3-3)$$



where, Y is the concentration of cation of interest, X is the chloride concentration,  $\beta_0$  and  $\beta_1$  are fitting constants, and  $\epsilon$  is the error term.

The regression model was found to fit the data reasonably well with the data collected in SW being different from those collected in NE. However, the plots of residuals revealed non constant variance as well as non-symmetrical distribution, suggesting that the model did not satisfy basic assumptions that the errors are normally distributed variables with zero mean and constant variance. In order to satisfy the normally distributed assumption and eliminate non-constant variance, logarithmic transformations were performed as follows:

$$Y' = \log Y \quad (3-4)$$

$$X' = \log [Cl] \quad (3-5)$$

The resulting linear model,

$$Y' = \log(\beta_0) + \beta_1 X' + \log(\epsilon) \quad (3-6)$$

was then tested and the residuals were normally distributed with mean equal to zero and constant variance indicating that the assumptions about error normality were correct.

Aside from chloride concentration, the intent was to determine if location is a significant regressor. Therefore, geographic location was incorporated in the linear model (6) as an indicator variable to identify if differences in composition between data from NE and SW were statistically significant. The following model was fitted to the data:

$$\log(Y) = C_1 + C_2 \times \log[Cl] + C_3 \times X_1 \times \log[Cl] + C_4 \times X_1 + \log(\epsilon) \quad (3-7)$$

where  $C_1$ ,  $C_2$ ,  $C_3$ ,  $C_4$  are fitting constants and  $X_1 = 0$  if the observation is from SW and 1 if it is from NE.

Two equations were then obtained for the two geographical locations:

$$\log(Y_{SW}) = C_1 + C_2 * \log[Cl_{SW}] \quad (3-8)$$

$$\log(Y_{NE}) = (C_1 + C_4) + (C_2 + C_3) * \log[Cl_{NE}] \quad (3-9)$$

Results of this analysis are summarized in Table 3.2. The significance of regression was tested to determine if at least one regression coefficient was different from zero. The null hypothesis was that all  $C_i = 0$  against the alternative hypothesis that at least one  $C_i$  is different from zero. All tests were performed using alpha equal to 0.05.  $C_3$  and  $C_4$  are the constants that differentiate the NE data from the SW data. p-values greater than 0.05 for these constants would mean that  $C_3 = C_4 = 0$ , and therefore no statistically significant difference exists between data from NE and SW. On the contrary, p-value below 0.05 for either or both  $C_3$  and  $C_4$  would indicate that the ion concentrations follow a different model for data from NE and SW.

The p-values obtained for the significance of regression are infinitely small for all cases, meaning that at least one  $C_i$  is different from zero. In addition, high values for the coefficient of determination ( $R^2$ ) indicate that the chloride concentration is a good predictor for the variations in concentrations of other ions. p-values for  $C_3$  and  $C_4$  for sodium are particularly large, showing no statistical difference in the correlations with chloride concentrations between SW and NE. On the other hand, regressions for strontium and bromide reveal significant difference for the correlations between SW and NE with p-values for  $C_3$  and  $C_4$  much below 0.05. For barium and calcium, p-values for  $C_3$  are greater than 0.05 while p-values for  $C_4$  are lower than 0.05. The difference between SW and NE for these two ions relies on the multiplying constant but not the exponent of the power law. Magnesium, like sodium, does not exhibit statistically different behavior between SW and NE, but the p-value for  $C_4$  is only slightly above the significance level. Overall, the concentrations of calcium, magnesium and bromide are higher in the southwest part of Pennsylvania than in the northeast, while the opposite is true for barium and strontium. The opposite trend for strontium and calcium might indicate the transformation of strontium-containing aragonite into calcite through the precipitation of calcium ions and release of strontium ions (Katz et al., 1972).

Among all the ions studied, barium in SW locations exhibited the lowest determination coefficient (51%) with particularly wide confidence intervals. Chloride concentration was not a sufficient predictor of the variation of barium. The results of the multiple regression displayed in Table 3.2 clearly indicated higher barium content for flowback water from the northeast part of the state, with concentrations reaching as high as 14,000 mg/L, while low concentrations were measured in the southwest even for samples containing high chloride concentrations. The geographic trend is illustrated by the heat map of Ba/Cl weight ratio shown in Figure 3.14. An average Ba/Cl ratio was calculated for each investigated county, and reported on a Pennsylvania map using the ArcGIS software. Counties located in the far northeast part of PA exhibited Ba/Cl ratio above 6%, while southwest counties had ratios up to 3%.

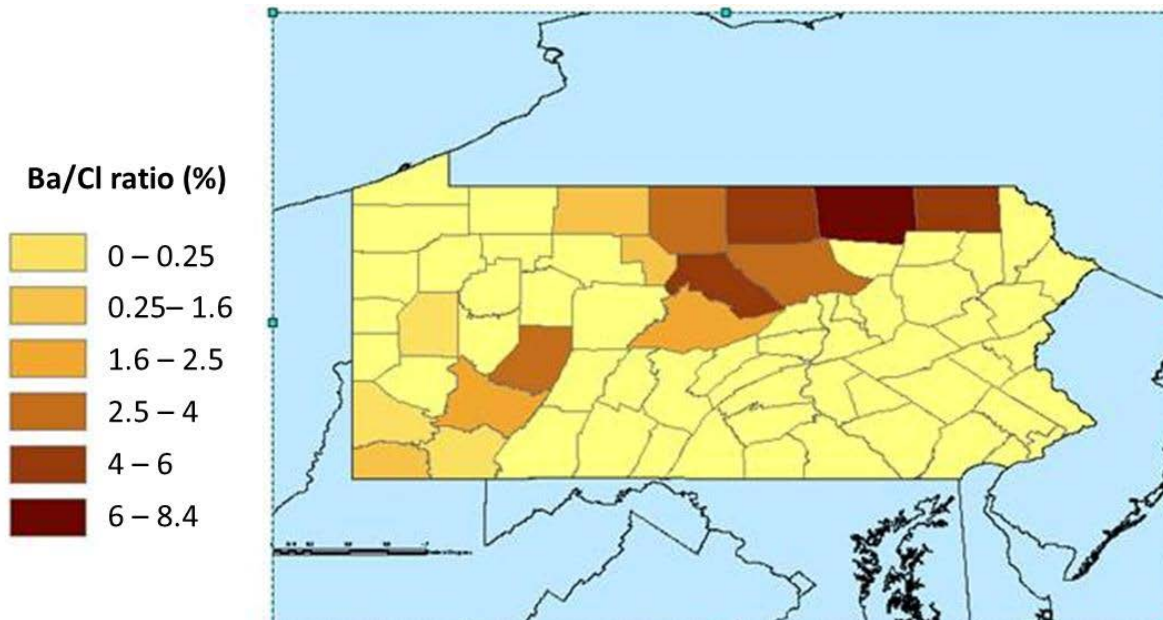


**Figure 3.14** Heat map of [Ba]/[Cl] ratio in produced water from Marcellus Shale

**Table 3.2** Fitting constants for the log-log multiple regression model

	$C_1$	p	$C_2$	p	$C_3$	p	$C_4$	p	$R^2$
Sodium	0.176	0.012	0.888	<0.001	-0.024	0.257	0.097	0.331	0.983
Calcium	-1.841	<0.001	1.195	<0.001	0.119	0.061	-0.687	0.020	0.936
Magnesium	-2.692	<0.001	1.157	<0.001	0.147	0.132	-0.866	0.055	0.86
Barium	-6.070	<0.001	1.761	<0.001	-0.389	0.125	3.107	0.009	0.744
Strontium	-2.879	<0.001	1.254	<0.001	0.212	<0.001	-0.892	0.001	0.957
Bromide	-2.299	<0.001	1.066	<0.001	-0.238	<0.001	0.976	<0.001	0.956

p-values in bold are greater than 0.05, indicating that the associated constant  $C_i$  is not a significant predictor

### 3.3 References

APHA, AWWA-WPCF (2000). Standard methods for the examination of water and drinking water, 20th Edition.

Barbot, E. and Vidic, R. (2012). Potential for abandoned mine drainage as water supply for hydraulic fracturing in the Marcellus Shale, 244th ACS National Meeting & Exposition, August 19-23, Philadelphia, Pennsylvania.

Blauch, M.E., Myers, R.R., Lipinski, B.A. and Houston, N.A. (2009). Marcellus Shale post-frac flowback waters – where is all the salt coming from and what are the implications? SPE 125740, Society of Petroleum Engineers.

BOGM, Bureau of Oil and Gas Management, Frac and flowback water analytical data, inorganics, spreadsheet, available at [http://www.bfenvironmental.com/pdfs/PADEP\\_Frac\\_Flow\\_Back\\_Water\\_Study\\_\\_Presence\\_of\\_Inorganics.pdf](http://www.bfenvironmental.com/pdfs/PADEP_Frac_Flow_Back_Water_Study__Presence_of_Inorganics.pdf), last access on 06/20/2012.

Boyce, M.L. (2010). Sub-surface stratigraphy and petrophysical analysis of the Middle Devonian interval of the central Appalachian basin; West Virginia and southwest Pennsylvania, Thesis, West Virginia University, , 159 pages.

Carpenter, A.B. (1978). Origin and chemical evolution of brines in sedimentary basins, Oklahoma Geological Survey Circular, (79), 60-76.

Dresel, P.E and Rose, A.W. (2010). Chemistry and origin of oil and gas well brines in western Pennsylvania: Pennsylvania Geological Survey, 4th ser., Open-File Report OFOG 10-01.0, 48 p.

Hayes, T. (2009). Sampling and analysis of water streams associated with the development of Marcellus Shale gas, Final report prepared for the Marcellus Shale Coalition, December 31.

Katz, A., Sass, E., Starinsky, A. and Holland, H.D. (1972). Strontium behavior in the aragonite-calcite transformation: An experimental study at 40–98°C, *Geochim. Cosmochim. Acta*, 36(4), 481-496.

Osborn, S.G. and McIntosh, J.C. (2010). Chemical and isotopic tracers of the contribution of microbial gas in Devonian organic-rich shales and reservoir sandstones, northern Appalachian Basin, *Appl. Geochem*, 25(3) 456-471.

Roen, J.B. (1984). Geology of the Devonian black shales of the Appalachian Basin, *Org. Geochem*, 5(4) 241-254.

## 4.0 Treatability Studies with Synthetic and Actual Wastewaters

### 4.1 Precipitation of Ba and Sr as Sulfates

Flowback water from natural gas extraction in Marcellus Shale contains very high concentrations of inorganic salts and organic chemicals. Potential reuse of this water in subsequent hydraulic fracturing operations may be limited by high concentrations of divalent cations (e.g., Ba, Sr and Ca).

Kinetics of barite and celestite precipitation in flowback waters from different well sites was evaluated in this study. Ba reacted rapidly with sulfate and reached equilibrium within 30 min while Sr reacted slowly and took days to reach equilibrium.

Equilibrium concentrations of Ba and Sr predicted by thermodynamic models were compared with experimental results. Activity corrections based on Pitzer equation provided the best agreement with experimental data for both Ba and Sr.

Comparison of barite and celestite precipitation kinetics in actual and synthetic flowbackwater revealed that there was no observable impact of organics and other minor components in actual flowback water on barite precipitation rate. This was mainly due to the fact that barite precipitation occurred relatively quickly due to high saturation levels utilized in this study. On the other hand, lattice poisoning and complexation with organic matter had profound impact on comparatively slower celestite precipitation. The presence of organic matter in actual flowback water increased Sr concentration in solution and contributed to the discrepancy between measured and predicted equilibrium concentrations.

#### 4.1.1 Materials and Methods

##### 4.1.1.1 Flowback Water Characteristics

The chemical composition of flowback water varies with location and well completion practice (Barbot et al., 2013). Flowback water used in this study came from three representative well sites located in southwest Pennsylvania: Site A, Site B, and Site C. The key characteristics of flow-composite flowback water sample used in this study are shown in Table 4.1. In general, they are all concentrated brines with ionic strength ranging from 0.91 M to 3.41 M. Sodium, calcium, barium and strontium are the major cations while chloride is the major anion in Marcellus Shale flowback water. The flowback water from Site A is characterized by low Ba and Sr concentrations and medium Ca content; Site B has high Ba and Sr concentrations but low Ca content; Ba concentration in Site C is very low but Sr and Ca contents are very high.

**Table 4.1** Key inorganic constituents of Flowback Water used in this study [mg/L]

Constituent	Site A	Site B	Site C
Na <sup>+</sup>	16518	32327.8	46130.7
Ca <sup>2+</sup>	2224	449.1	15021
Mg <sup>2+</sup>	220	119.9	1720
Ba <sup>2+</sup>	730	2530	236
Sr <sup>2+</sup>	367	1387	1817
Cl <sup>-</sup>	29000	52913.5	104300
Ionic Strength/M	0.91	1.55	3.41

#### 4.1.1.2 Experiment Protocol

The synthetic flowback waters were prepared in 1-liter volumetric flask using high purity chemicals. Synthetic or actual flowback water was placed into 250ml volumetric flasks and sulfate was added as anhydrous NaSO<sub>4</sub> (J.T. Baker, Phillipsburg, NJ) to simulate the treatment practice in centralized wastewater treatment plants in Pennsylvania. Reactants were mixed with magnetic bar at 400 rpm.

Unless specified otherwise, samples from each 250-ml volumetric flask were collected at predetermined time intervals and filtered through 0.45 μm nylon filters. Ba and Sr were measured using atomic adsorption spectrometer (Perkin-Elmer model 1000 AAS) with a nitrous-acetylene flame. To eliminate the interference from ionization and retard the kinetics of reaction, all samples were immediately diluted using 0.15% KCl and 2% HNO<sub>3</sub> solution after filtration (EPA method 208.1 (EPA, 1974); Agilent Technology, Inc, 2010). Each cation analysis was performed at least three times and the average value was used if the standard deviation was below 10%.

#### 4.1.1.3 Chemical Equilibrium Models

MINEQL+ (Westall et al., 1976) and Phreeqcl (Parkhurst, 1999) were used to calculate equilibrium distribution for the ions of interest (i.e. Ba<sup>2+</sup> and Sr<sup>2+</sup>). MINEQL+ uses Davis equation (Davis, 1962) to calculate activity coefficients, while Phreeqcl software package allows the selection between “Wateq” Debye-Hückel (Truesdell and Jones, 1974) and Pitzer equation (Pitzer, 1973 and 1991).

Because of high ionic strength of flowback water, it is important to accurately estimate activity coefficients of different components and species that may be involved in chemical reactions of interest. Davis equation is valid for  $I < 0.5$  and is defined as:

$$\log(\gamma_i) = -A \cdot Z_i^2 \left( \frac{\sqrt{I}}{1+\sqrt{I}} - 0.2I \right) \quad (4-1)$$

“Wateq” Debye-Hückel model is valid for  $I < 1$  and is defined as:

$$\log(\gamma_i) = \frac{-A \cdot Z_i^2 \cdot \sqrt{I}}{1+B \cdot a_i \cdot \sqrt{I}} + b_i \cdot I \quad (4-2)$$

where,

$$A = \frac{1.82483 \cdot 10^6 \cdot \sqrt{d}}{(\varepsilon \cdot T_k)^{3/2}}$$

$$B = \frac{50.2916 \cdot \sqrt{d}}{(\varepsilon \cdot T_k)^{1/2}} \text{ (Merkel and Planer-Friedrich, 2008)}$$

$a_i$  and  $b_i$  are ion-specific parameters determined by the ion size (Table 4.2)

$d$  = density of water,

$\varepsilon$  = dielectric constant,

$T_k$  = temperature in Kelvin,

$I$  = ionic strength.



**Table 4.2** Ion-specific parameters  $a_i$  and  $b_i$  (after Parkhurst et al., 1980 and Truesdell and Jones, 1974)

Ion	$a_i$ [Å]	$b_i$ [Å]	Ion	$a_i$ [Å]	$b_i$ [Å]
H <sup>+</sup>	4.78	0.24	Fe <sup>2+</sup>	5.08	0.16
Li <sup>+</sup>	4.76	0.20	Co <sup>2+</sup>	6.17	0.22
Na <sup>+</sup>	4.32	0.06	Ni <sup>2+</sup>	5.51	0.22
K <sup>+</sup>	3.71	0.01	Zn <sup>2+</sup>	4.87	0.24
Cs <sup>2+</sup>	1.81	0.01	Cd <sup>2+</sup>	5.80	0.10
Mg <sup>2+</sup>	5.46	0.22	Pb <sup>2+</sup>	4.80	0.01
Ca <sup>2+</sup>	4.86	0.15	OH <sup>-</sup>	10.65	0.21
Sr <sup>2+</sup>	5.48	0.11	F <sup>-</sup>	3.46	0.08
Ba <sup>2+</sup>	4.55	0.09	Cl <sup>-</sup>	3.71	0.01
Al <sup>3+</sup>	6.65	0.19	ClO <sub>4</sub> <sup>-</sup>	5.30	0.08
Mn <sup>2+</sup>	7.04	0.22	SO <sub>4</sub> <sup>2-</sup>	5.31	-0.07

Another semi-empirical model based on ion interaction theory was developed for high ionic strength conditions (Pitzer, 1973). Compared to ion association theory or ion-pair theory, the ion interaction model considers all charged ions to be fully separated as free ions. This model was later edited (Pitzer, 1991) to incorporate ion association models to solve some inaccuracies for weak electrolytes. General equations used for calculating the activity coefficient by Pitzer equations for cations and anions are listed below (Aniceto, 2012):

$$\ln \gamma_M = z_M^2 F + \sum_a m_a (2B_{Ma} + (2\sum_c m_c z_c) C_{Ma}) + \sum_c m_c (2\phi_{Mc} + \sum_a m_a \Psi_{Mca}) + \frac{1}{2} \sum_a \sum_{<a'} m_a m_{a'} \Psi_{Maa'} + \sum_c \sum_a m_c m_a (z_M^2 B'_{ij} + |z_M| C_{ca}) \quad (4-3)$$

$$\ln \gamma_X = z_X^2 F + \sum_c m_c (2B_{cX} + (2\sum_a m_a z_a) C_{cX}) + \sum_a m_a (2\phi_{cX} + \sum_c m_c \Psi_{Xca}) + \frac{1}{2} \sum_c \sum_{<c'} m_c m_{c'} \Psi_{Xcc'} + \sum_c \sum_a m_c m_a (z_X^2 B'_{ij} + |z_X| C_{ca}) \quad (4-4)$$

where, subscripts M and X stand for cation and anion of interests, respectively. The subscripts c and a indicate other cations and anions. In these equations, F is a derived Debye-Hückel function, which is dependent on Debye-Hückel parameter A and ionic strength. Other terms in these equations are determined based on six types of temperature-dependent empirical

parameters (i.e.,  $\beta^{(0)}_{MX}$ ,  $\beta^{(1)}_{MX}$ ,  $\beta^{(2)}_{MX}$ ,  $C^{(0)}_{MX}$ ,  $\Phi_{ij}$ ,  $\Psi_{ijk}$ ). The first three terms, namely  $\beta^{(0)}_{MX}$ ,  $\beta^{(1)}_{MX}$ ,  $\beta^{(2)}_{MX}$ , describe the interaction of oppositely charged ions pairs in mixed electrolyte solutions.  $C^{(0)}_{MX}$  accounts for short-range interaction of ions and is of importance at high concentration.  $\Phi_{ij}$  are mixed electrolyte parameters for interaction between ions of the same charge.  $\Psi_{ijk}$  describe interactions for cation-cation-anion and anion-anion-cation in the mixed electrolyte solutions (Pitzer and Mayorga, 1973; Pitzer and Kim, 1974; Pitzer, 1974; Pitzer, 1991). Table 4.3 lists empirical parameters that were used to supplement the database available in Phreeqcl.

**Table 4.3** Ion interaction parameters in Pitzer equation

Parameter	Value	Reference
$\beta^{(0)}$ Ba-SO4	-1.0	Monnin & Galinier, 1988
$\beta^{(0)}$ Sr-SO4	-0.43	Monnin & Galinier, 1988
$\beta^{(0)}$ Mg-SO4	0.221	Pabalan & Pitzer, 1987
$\beta^{(0)}$ Ca-SO4	0.2	Greenberg & Moller, 1989
$\beta^{(0)}$ Ba-SO4	12.6	Monnin & Galinier, 1988
$\beta^{(0)}$ Sr-SO4	5.7	Monnin & Galinier, 1988
$\beta^{(1)}$ Mg-SO4	3.343	Harvie et al., 1984
$\beta^{(1)}$ Ca-SO4	3.1973	Greenberg & Moller, 1989
$\beta^{(2)}$ Ba-SO4	-153.4	Monnin & Galinier, 1988
$\beta^{(2)}$ Sr-SO4	-94.2	Monnin & Galinier, 1988
$\beta^{(2)}$ Mg-SO4	-37.23	Pabalan & Pitzer, 1987
$\beta^{(2)}$ Ca-SO4	-54.24	Greenberg & Moller, 1989
$\Psi$ Na-Ca-Cl	-0.003	Holmes et al., 1987
$\Psi$ Na-Ca-SO4	-0.012	Greenberg & Moller, 1989
$\Psi$ Na-Ba-Cl	0.0128	Monnin, 1999
$\Psi$ Cl-SO4-Mg	-0.008	Harvie et al., 1984
$\Phi$ SO4-Cl	0.07	Greenberg & Moller, 1989

Pitzer's equation is more advantageous over other prediction models in two aspects. First, Pitzer's equation is applicable under ionic strength of up to 6M (Burkin, 2001). Second, as Pitzer's equation is based on ion interaction model, it takes account the impact of all ions that

are presents in solution. Therefore, activity coefficient will vary with dissolved ion composition even for identical ionic strength.

## 4.1.2 Results and Discussion

### 4.1.2.1 Kinetics of Barite and Celestite Precipitation in Synthetic Flowback Water

Previous studies (He et al., 1995; Risthaus et al., 2000; Jones et al., 2004; Shen et al., 2009; Fan et al., 2010) have shown that a number of parameters, including temperature, pressure, saturation index, ionic strength and scale inhibitors, have significant impact on the kinetics of barite and celestite precipitation. In this study, the temperature and pressure were at standard conditions (atmospheric pressure and room temperature of  $22\pm 1^\circ\text{C}$ ) and the focus was on the impact of water quality on these reactions. Mineral precipitation involves two stages: nucleation and crystal growth. The initial chemical reaction stage is known as induction period, which depends on saturation index and is usually completed within a couple of minutes (He et al., 1995; Fan et al., 2010). However, the equilibrium will take much longer and the precipitation rate normally follows a second order reaction rate (Yeboah et al, 1994; Shen et al, 2008). Further study by Shen et al., (2008) found that the barite precipitation rate is also reaction-direction-dependent, which means that equilibrium is normally reached rapidly when the reaction goes from under-saturation to saturation while it becomes relatively slow if the direction is from supersaturation to saturation. The focus of this study was on the latter one because the reacting ions always initially exceed the saturation levels in practice.

The induction period was not an important concern in this study and was not evaluated. Based on the visual observations in most of tests conducted in this study, turbidity of all solutions developed within a few seconds of sulfate addition, which indicates rapid barium sulfate nucleation. This is much faster than the nucleation rates found in other studies (He et al, 1995; Fan et al, 2010). A summary of experimental conditions, including the initial ion concentrations, ionic strength of the solution, ion activities calculated using Pitzer equation, and saturation indices, is given in Table 4.4.

**Table 4.4** Initial Ba<sup>2+</sup>, Sr<sup>2+</sup> and SO<sub>4</sub><sup>2-</sup> concentrations in synthetic flowback waters and corresponding ionic strength, activities and saturation indices with respect to barite and celestite

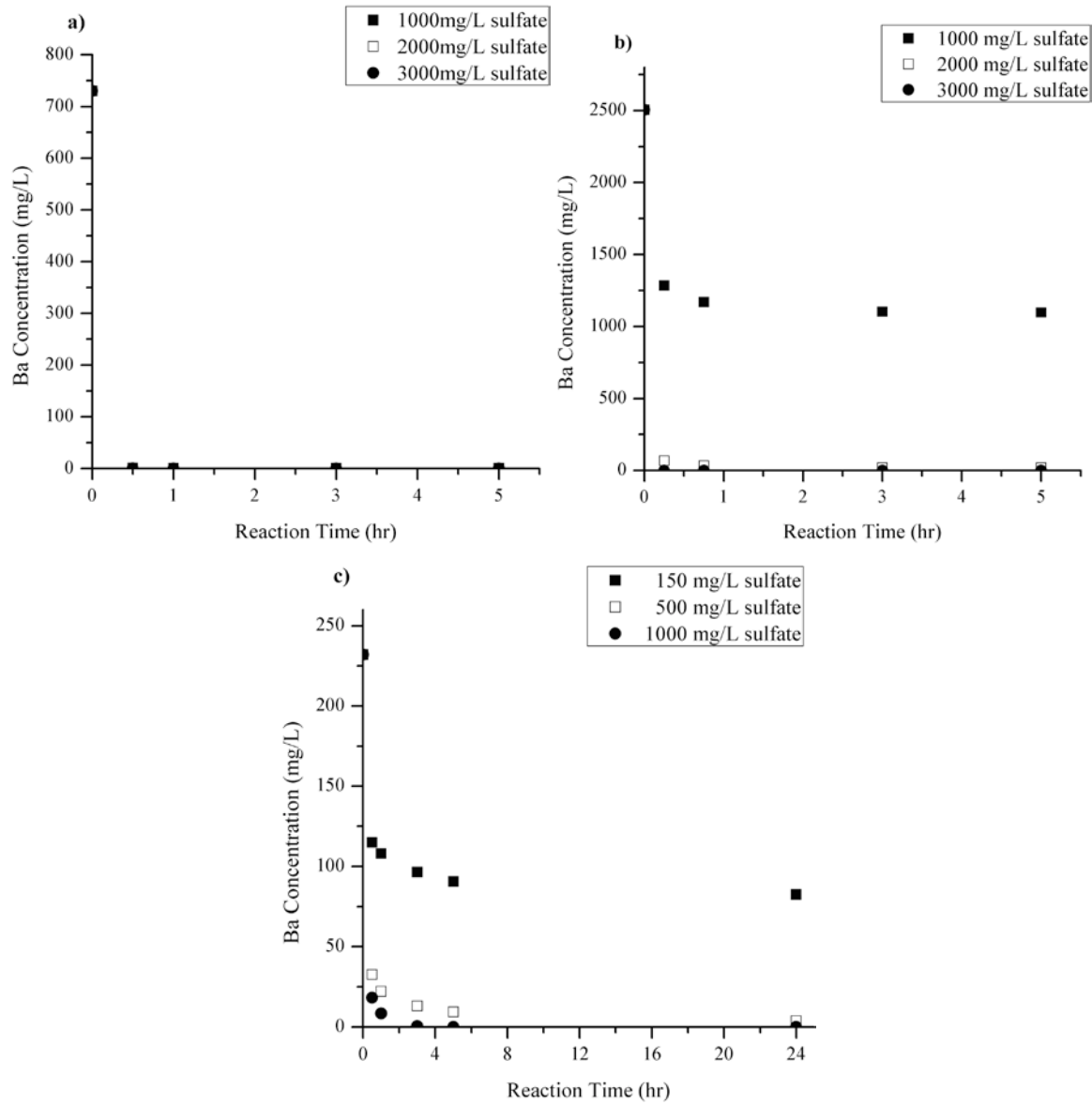
Flowback Water	[SO <sub>4</sub> <sup>2-</sup> ]	[Ba <sup>2+</sup> ]	[Sr <sup>2+</sup> ]	Ionic Strength	a <sub>SO4</sub>	a <sub>Ba</sub>	a <sub>Sr</sub>	SI <sub>BaSO4</sub>	SI <sub>SrSO4</sub>
	[mg/L]			[mol]	[mol/L]x10 <sup>3</sup>				
Site A	1000	730	367	0.95	0.781	1.115	1.051	3.91	0.55
	2000	730	367	0.98	1.542	1.126	1.106	4.21	0.83
	3000	730	367	1.02	2.284	1.139	0.985	4.39	0.98
Site B	1000	2530	1387	1.64	0.559	3.763	4.396	4.29	1.03
	2000	2530	1387	1.68	1.104	3.830	4.309	4.60	1.31
	3000	2530	1387	1.71	1.637	3.898	4.227	4.78	1.48
Site C	150	236	1817	3.62	0.029	0.568	11.65	2.20	0.18
	500	236	1817	3.63	0.098	0.572	11.63	2.72	0.70
	1000	236	1817	3.65	0.197	0.577	11.59	3.03	1.00

IS: Ionic Strength  
SI: Saturation Index is the logarithm of  $\Omega$  ( $\Omega$  is the ratio of IAP/ $K_{sp}$ , where IAP = Ion Activity Product;  
 $K_{sp,BaSO4} = 1.072 \times 10^{-10}$ ,  $K_{sp,SrSO4} = 2.291 \times 10^{-7}$ )

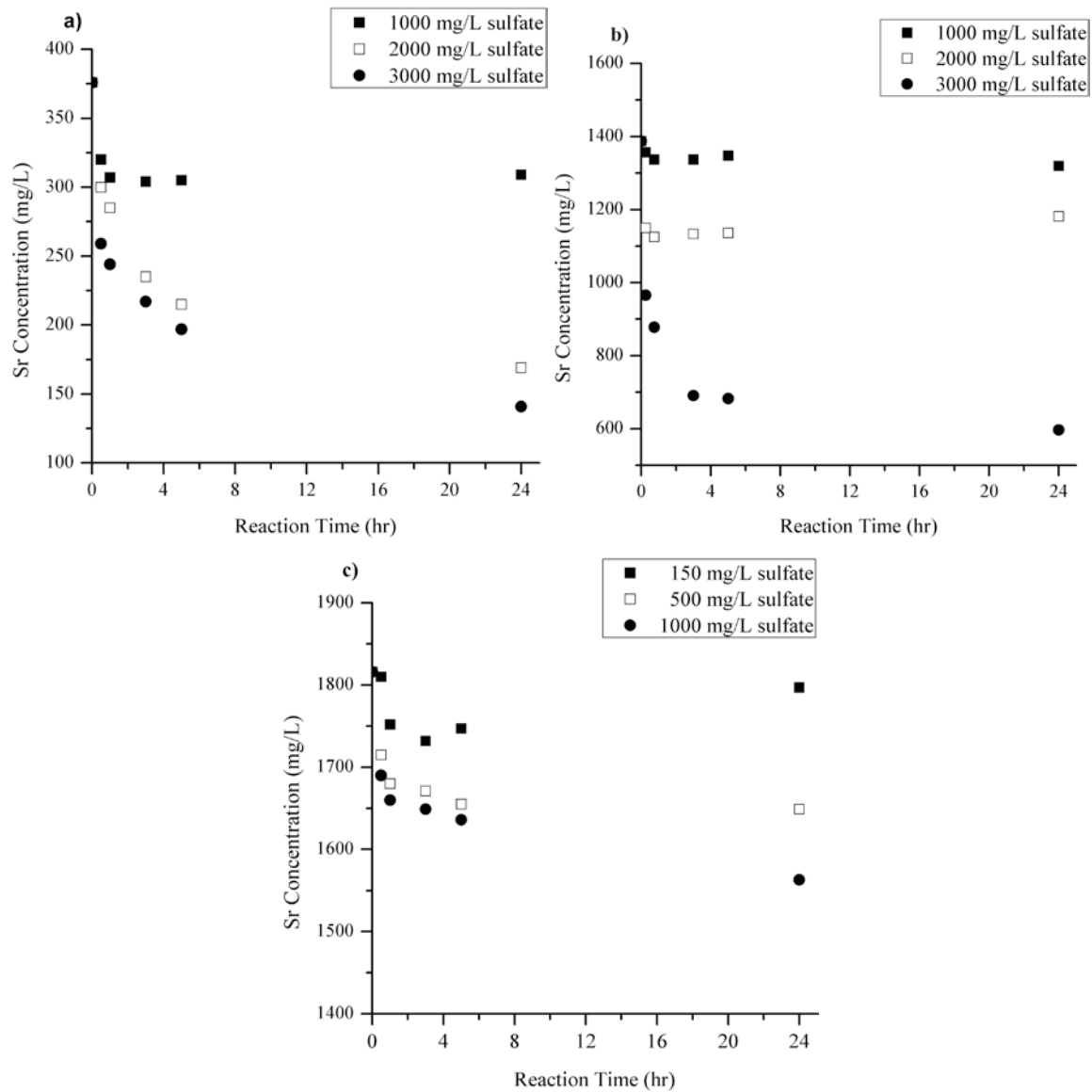
Figures 4.1 and 4.2 depict the variations of Ba and Sr in the solution for different NaSO<sub>4</sub> doses, respectively. As evidenced from these figures, barite precipitation was much faster than celestite in all cases. The differences in time to reach equilibrium for Ba and Sr was very significant for Site A and B flowback waters as Ba precipitation was essentially complete within half an hour while Sr concentration did not stabilize even after 24 hours.

Figure 4.3 indicates that strontium precipitation is such a slow process that weeks may be needed to achieve equilibrium under the experimental conditions used in this study. As shown in Table 4.4, Saturation Index (SI) for barite (2.2~4.8) was much higher than for celestite (0.18~1.48). Jones et al. (2004) suggested that the concentrations of other divalent ions, especially Ca, may impact barite and celestite precipitation kinetics by lattice poisoning. However, inhibition of barite precipitation was only observed in the case of Flowback Water C with 150 mg/L SO<sub>4</sub> addition (Figure 4.1c and 4.4), which suggests that the inhibition of barite precipitation by Na and Ca ions only occurs when barite saturation index is low. Therefore, for

the cases when flowback water has low Ba concentration, it is necessary to increase  $\text{SO}_4$  dosage to ensure rapid barite precipitation.



**Figure 4.1** Variation of Ba concentration in flowback water from: (a) Site A, (b) Site B and (c) Site C



**Figure 4.2** Variation of Sr concentration in flowback water from: (a) Site A, (b) Site B and (c) Site C

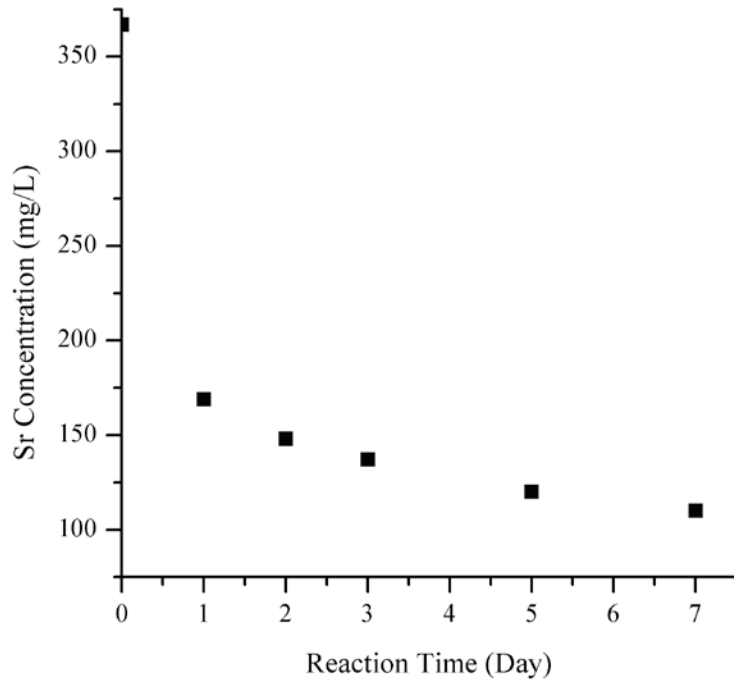


**Figure 4.3** Variation of Sr concentration in flowback water from Site A with 2000 mg/L initial sulfate concentration

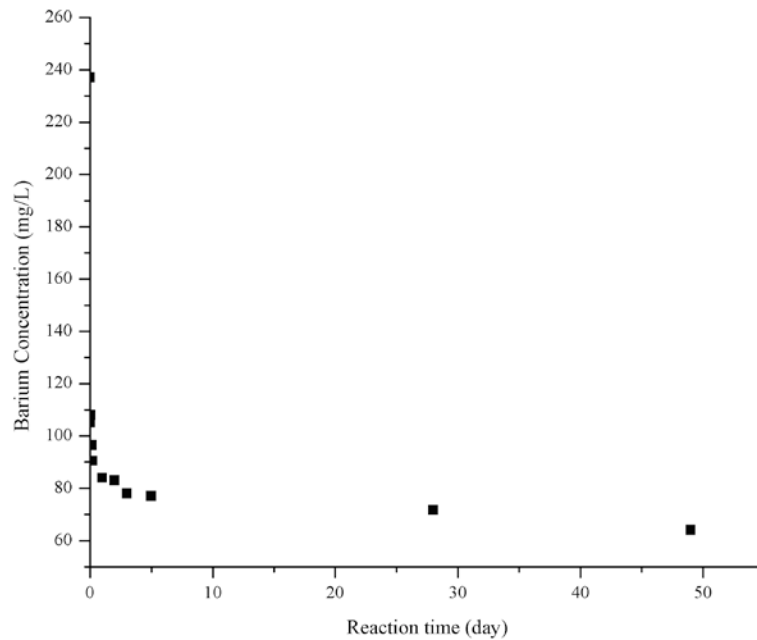


**Figure 4.4** Variation of Ba concentration in flowback water from Site C with 150 mg/L initial sulfate concentration

It is important to note that Sr concentration in the presence of very low initial sulfate concentration shown in Figure 4.2(c) initially decreased and then increased with time. Such behavior can be explained by the nucleation kinetics model for a binary system (i.e.  $(\text{Ba},\text{Sr})\text{SO}_4$ ) suggested by Pina and Putnis (2002). Sr and Ba are initially coprecipitated in the form of  $\text{Ba}_x\text{Sr}_{1-x}\text{SO}_4$  and this initial co-precipitation process proceeds based on the kinetically favored pattern, which can be described by the molar fraction of Ba in the co-precipitated solid (i.e., x in  $\text{Ba}_x\text{Sr}_{1-x}\text{SO}_4$ ). When the ratio of strontium to barium in solution is high, as is the case in flowback water from Site C, relatively Sr-rich solid composition can be expected initially as large fraction of sulfate is initially consumed for celestite formation. However, Sr is then replaced with Ba through isomorphic substitution because the equilibrium is ultimately driven by supersaturation, which is much higher for barite than for celestite. As can be seen in Figure 4.4, isomorphic substitution is a fairly slow process and Ba did not reach equilibrium even after 30 days.

As can be seen in Table 4.5, removal efficiency for Ba would be much higher than that for Sr under typical process conditions in centralized waste treatment facilities (e.g., reaction time of 1 hr). Sulfate is an excellent removal reagent for Ba but not as good for Sr because barite solubility is nearly three orders of magnitude lower than that of celestite and very high initial sulfate concentrations would be required to achieve significant Sr removal. However, this approach would lead to substantial increase in sulfate concentration in the finished water, which may prevent the reuse of this water for hydraulic fracturing because of concerns that sulfate precipitation downhole may reduce well productivity. If high Sr removal is needed, it may be better to precipitate it as strontium carbonate (strontianite), which has much lower solubility ( $K_{\text{sp, SrCO}_3} = 10^{-9.25}$ ) than celestite (Miller, 1983).



**Table 4.5** Measured Ba<sup>2+</sup> and Sr<sup>2+</sup> removal efficiency in synthetic flowback waters after 1 hr reaction for different initial sulfate concentrations

Mixtures	Ba removal efficiency	Sr removal efficiency
Site A+1000mg/L SO <sub>4</sub>	100.0%	18.4%
Site A+2000mg/L SO <sub>4</sub>	100.0%	24.2%
Site A+3000mg/L SO <sub>4</sub>	100.0%	35.1%
Site B+1000mg/L SO <sub>4</sub>	53.3%	3.6%
Site B+2000mg/L SO <sub>4</sub>	98.6%	18.3%
Site B+3000mg/L SO <sub>4</sub>	100.0%	36.7%
Site C+150mg/L SO <sub>4</sub>	55.6%	3.5%
Site C+500mg/L SO <sub>4</sub>	90.5%	8.6%
Site C+1000mg/L SO <sub>4</sub>	96.4%	10.1%

#### 4.1.2.2 Equilibrium Predictions for Synthetic Flowback Waters

Experimental data collected using synthetic flowback water from Site A (IS = 0.91 M), Site B (IS = 1.55 M) and Site C (IS = 3.41M) are compared to chemical equilibrium predictions for different initial sulfate concentrations in Figures 4.5, 4.6 and 4.7, respectively. As can be seen from these figures, theoretical calculations are in good agreement with experimental results for Ba, with Pitzer equation offering the best predictions. One exception was in the case of Ba concentration in flowback water from Site C with the initial sulfate concentration of 150 mg/L (Figure 4.5a). The deviation between measured values and model predictions based on Pitzer equation in this case is expected and can be explained by kinetic limitation (i.e., low SI for barite), lattice poisoning by high concentrations of cations in solution (I = 3.41) and slow isomorphic substitution (i.e., high initial [Sr<sup>2+</sup>]/[Ba<sup>2+</sup>] ratio) as described earlier.

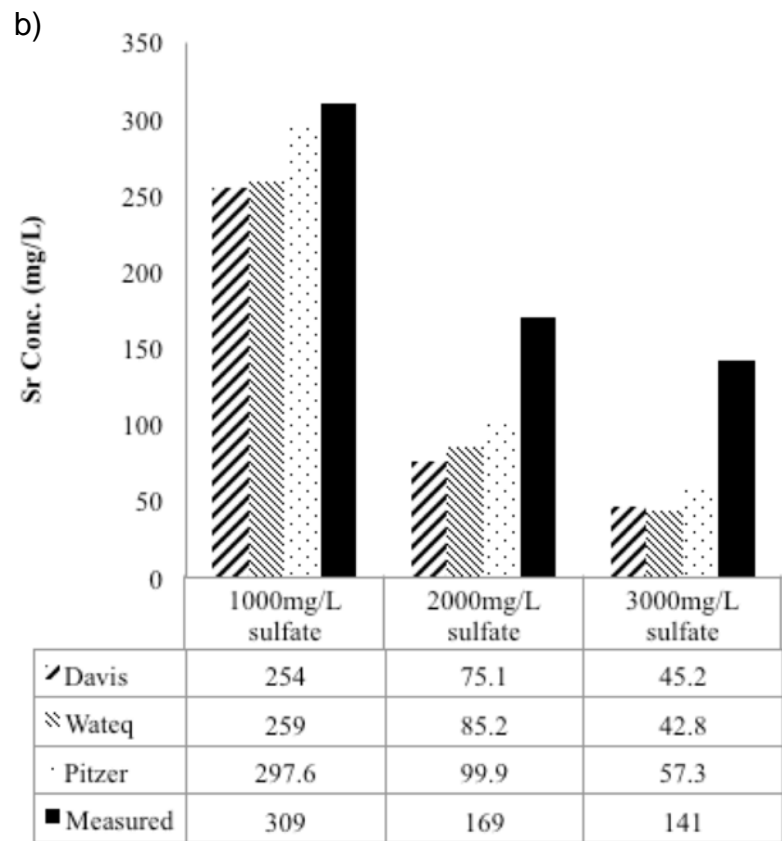
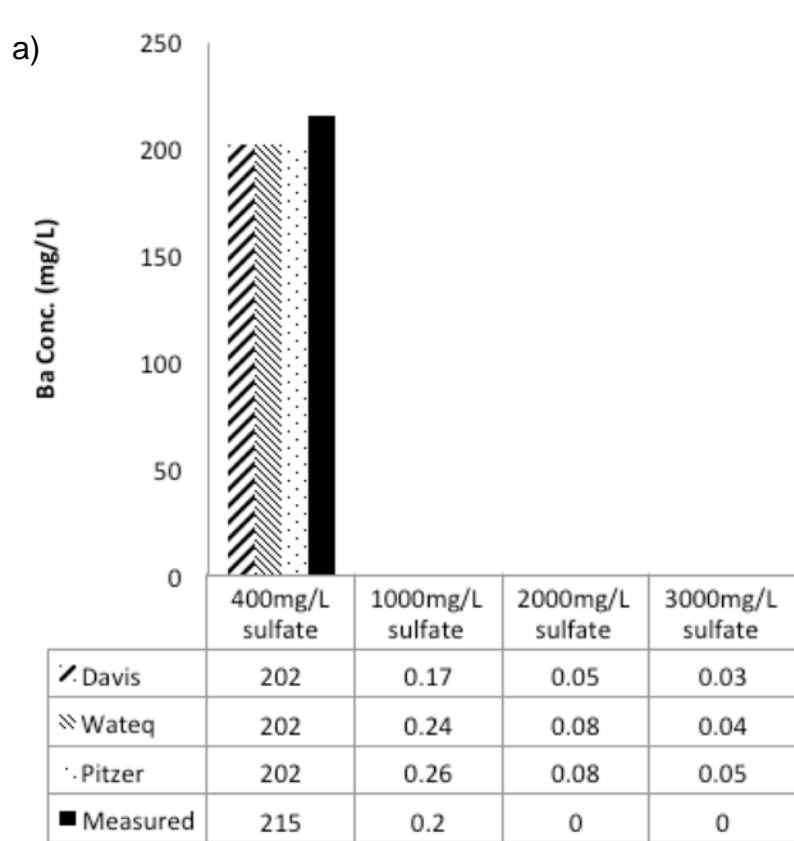


**Figure 4.5** Comparison between equilibrium predictions and experimental results after 48 hours in synthetic flowback water from Site A: (a) Ba and (b) Sr

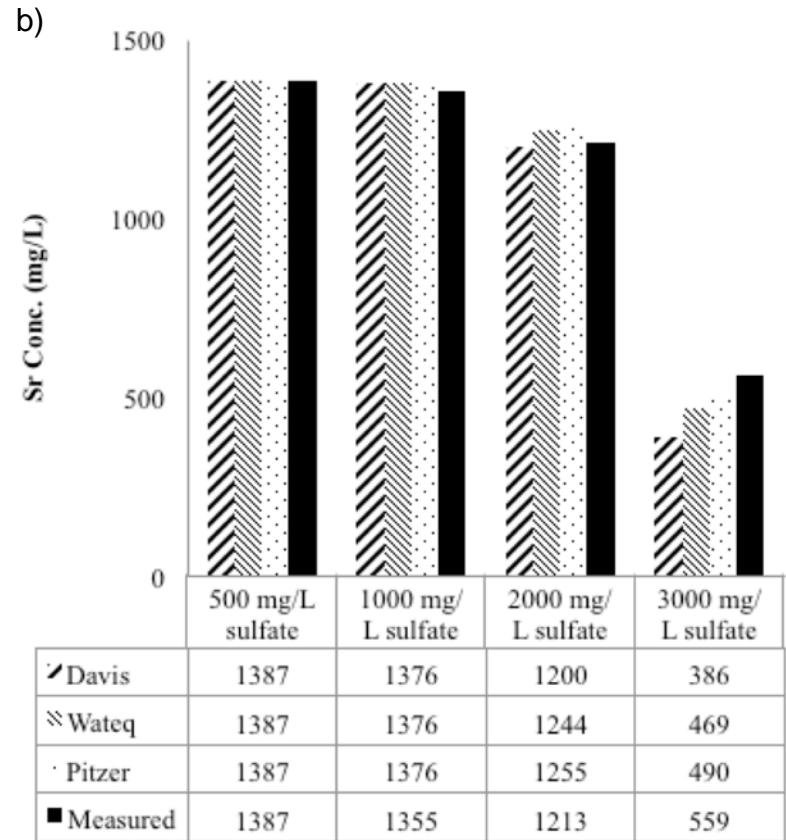
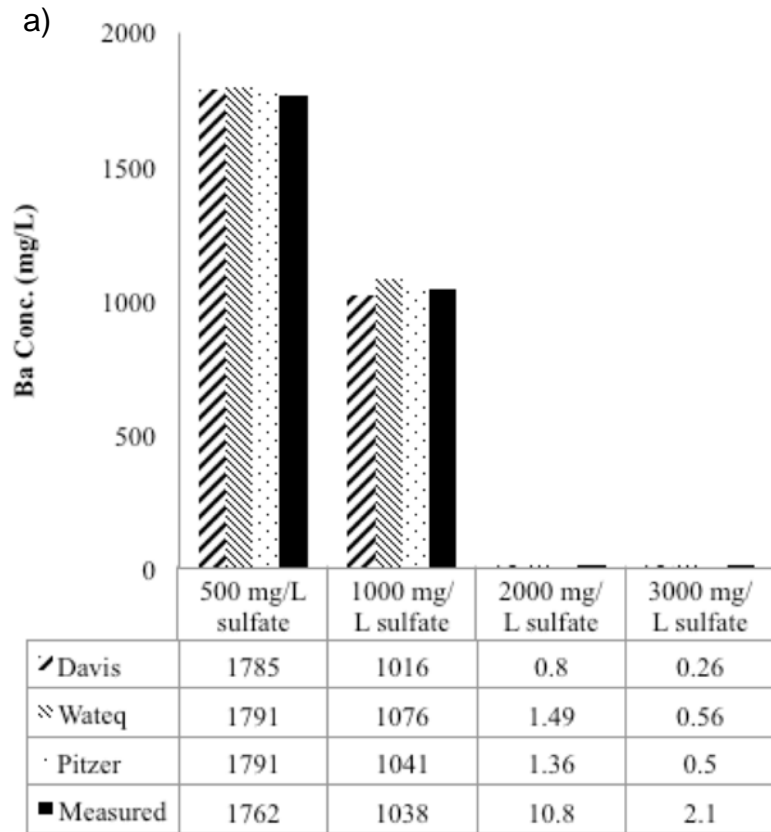


**Figure 4.6** Comparison between equilibrium predictions and experimental results after 48 hours in synthetic flowback water from Site B: (a) Ba and (b) Sr

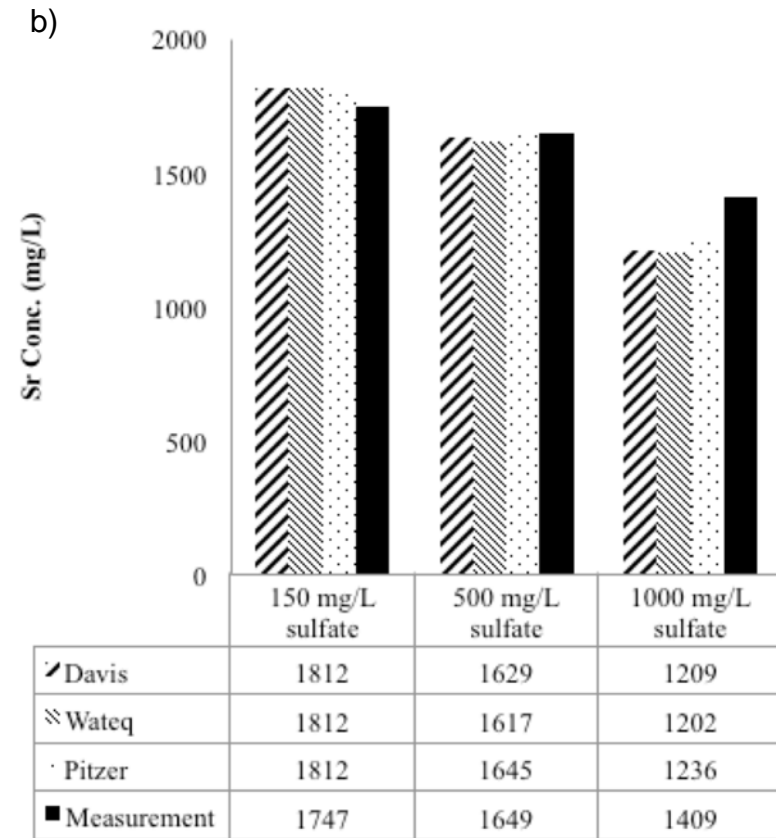
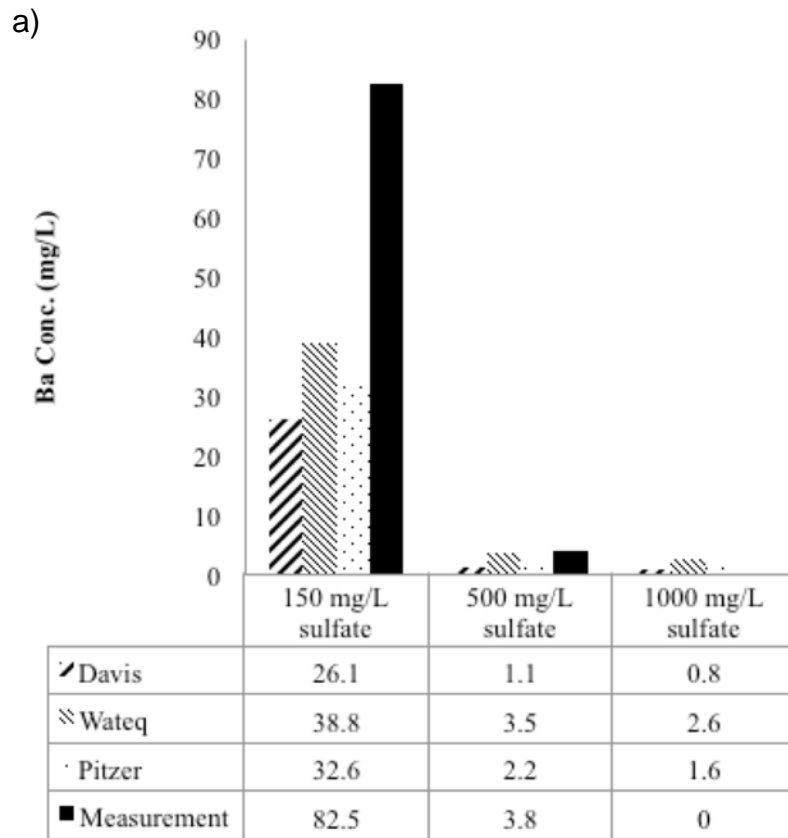


**Figure 4.7** Comparison between equilibrium predictions and experimental results after 24 hours in synthetic flowback water from Site C: (a) Ba and (b) Sr

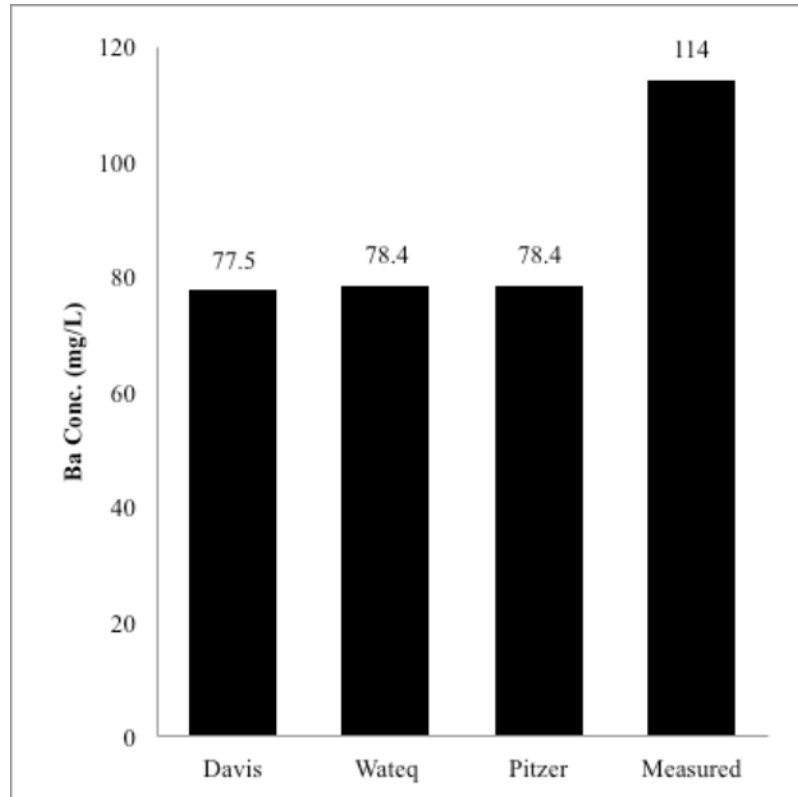
In general, chemical equilibrium model using Pitzer equation also offered the best match with experimental data for Sr collected in this study. The only significant deviation between measured and predicted Sr concentration was observed in the case when the initial Sr concentration is low (e.g., flowback water from Site A). Such behavior (Figure 4.3b) can be explained by the fact that it can take several weeks to reach equilibrium with respect to celestite precipitation (data not shown). When Sr concentration is relatively high (e.g., flowback water from Sites B and C), prediction accuracy is improved and it decreases with an increase in the initial sulfate concentration.

#### *4.1.2.3 Comparison of Barite and Celestite Precipitation in Synthetic and Real Flowback Waters*

The actual flowback water is much more complex solution compared with the synthetic water that contains only salts. Presence of organic matter from either the rock formation or from the chemical additives injected in the fracturing fluid may have an impact on precipitation kinetics, equilibrium and size and morphology of crystals that are formed. Whether the organic substances can inhibit or accelerate precipitation of inorganic compounds is still a matter of debate (Hennesy and Graham, 2002; Jones et al., 2004 and 2008; Smith et al., 2004; Hamdona and Hamza, 2010). Most studies suggest that organics, such as commercial antiscalants and polyphosphonates, could retard precipitation reactions even if present at very low concentrations (Van der Leeden, 1991). However, some other organics like methanol could promote the precipitation reactions (Jones et al., 2008).

The kinetics and equilibrium of barite and celestite precipitation in actual flowback water was evaluated using actual flowback water from Site A. The main difference between actual and synthetic flowback water is that the actual flowback water contains organic matter with total organic carbon concentration of 52 mg/L. It was found that Ba concentration reached equilibrium after 30 min reaction in actual flowback water for all sulfate doses evaluated in this study (data not shown), which is identical to the behavior observed in the synthetic flowback water. As shown on Figure 4.8, measured Ba concentration at equilibrium deviated from model predictions for the initial sulfate dose of 400 mg/L. Higher Ba concentration in solution at equilibrium is likely due to an increase in barite solubility in the presence of organic matter (Church, 1972). This study revealed that the organic matter does not have any observable

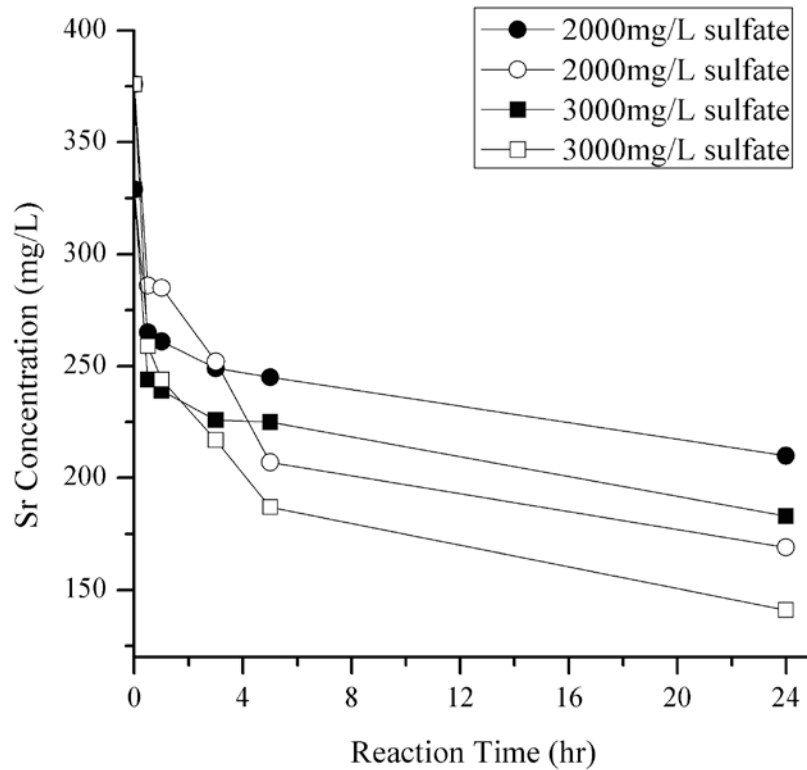
impact on barite precipitation kinetics (data not shown) but that chemical equilibrium models tend to overestimate Ba removal in actual flowback water since the impact of organic matter cannot be adequately incorporated in thermodynamic calculations.



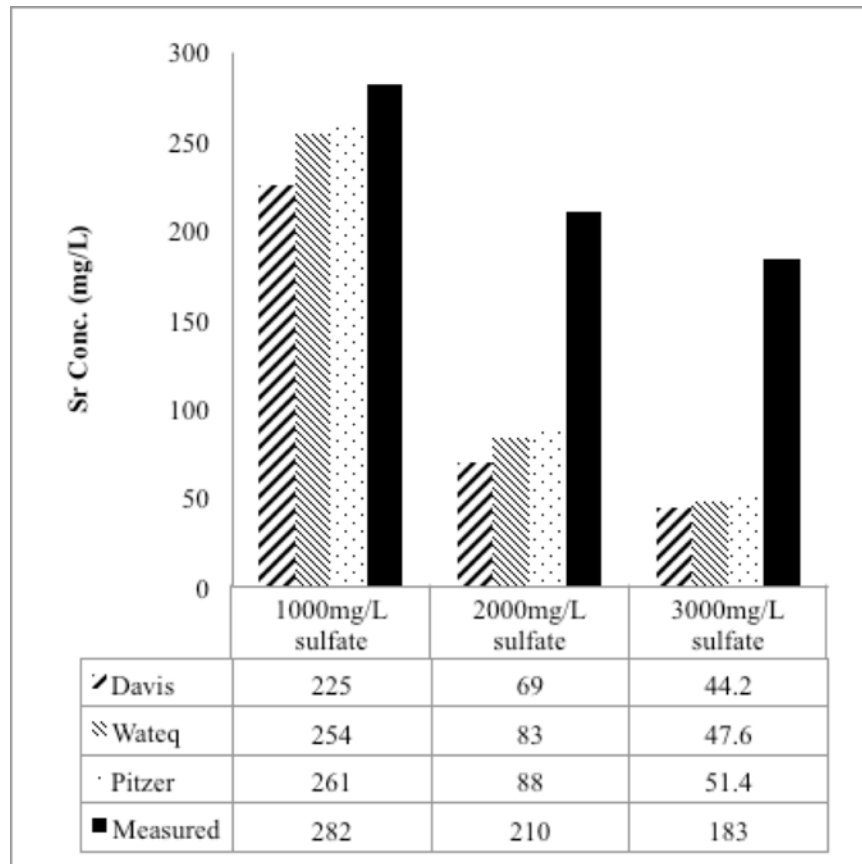
**Figure 4.8** Comparison between equilibrium predictions and measured residual Ba concentration after 24 hours of reaction in actual flowback water from Site A with 400 mg/L initial sulfate concentration

Figure 4.9 illustrates the difference in celestite precipitation kinetics in actual and synthetic flowback water from Site A. As can be seen from this figure, celestite precipitation is slower in actual flowback water compared with synthetic flowback water, which is due to inhibition by organic matter present in actual flowback water. Adsorption of organic matter on active sites on the crystal surface could block the crystal growth and decrease the kinetics of precipitation reactions (Hamdona et al., 2010). This effect was previously identified for barium sulfate precipitation at low supersaturation ratios (Van der Leeden, 1991). However, inhibition of barite precipitation by organic matter was not observed under the experimental conditions evaluated in this study (i.e., high ionic strength and high supersaturation ratio for barite) since

the reaction was essentially complete in 30 min. In comparison, celestite precipitation is much slower and further reduction in celestite precipitation kinetics caused by the organic matter present in the actual flowback water additionally exacerbated the difference between measured and predicted Sr concentrations (Figure 4.10). Therefore, equilibrium models may not be reliable in predicting Sr concentration in centralized wastewater treatment plants due to kinetic limitations.



**Figure 4.9** Strontium concentration in synthetic (open symbols) and actual flowback water (solid symbols) from Site A during sulfate precipitation



**Figure 4.10** Comparison between equilibrium predictions and experimental results for Sr after 24 hours in actual flowback water from Site A

### 4.1.3 Conclusions

Laboratory experiments were conducted to evaluate kinetics of barite and celestite precipitation and associated Ba and Sr removal from flowback water through sulfate precipitation. It was found that barium reacted rapidly with sulfate and essentially reached equilibrium within 30 min. One exception was in the case of low initial Ba (236 mg/L) and sulfate (150 mg/L) concentration but moderate strontium concentration (1,817 mg/L). Reduction in barium removal rate in this case is due to initial Ba and Sr coprecipitation with sulfate followed by slow substitution of Sr with Ba. Furthermore, barite precipitation may be inhibited in high ionic strength solutions and low barite saturation index.

Comparison between measured and predicted concentrations in synthetic flowback water solutions revealed that chemical equilibrium model based on Pitzer equation for activity corrections was superior in predicting both Ba and Sr concentration because of very high ionic



strength that characterizes most flowback waters from unconventional gas extraction. Discrepancy between measured and predicted results, especially in the case of Sr, can be significant because of slow celestite precipitation rate. In that case, chemical equilibrium models cannot reliably predict the quality of the effluent from central waste treatment plants utilizing sulfate precipitation for the control of Ba and Sr. This study also suggests that sulfate may not be the best agent for Sr removal from flowback water and that other anions (e.g., carbonate) may be better suited to accomplish high levels of Sr removal.

Barite and celestite precipitation in actual flowback water may be influenced by the presence of natural and synthetic organic matter in this water. While the organic matter had no observable impact on barite precipitation kinetics, the rate of celestite precipitation was significantly reduced. Deviation between measured and predicted Ba concentrations was influenced by the increase in barite solubility in the presence of organic matter. As the rate of celestite precipitation is further reduced in the actual flowback water, it would take even longer for Sr concentration to reach equilibrium compared to results in synthetic flowback water. Therefore, chemical equilibrium models may not be able to accurately predict the composition of effluent from centralized wastewater treatment plants treating flowback water from unconventional gas production. Due to the complexity of organics that are present in flowback water, no specific compound can be singled out for its influence on kinetics and equilibrium of barite and celestite precipitation.

#### 4.1.4 References

Aniceto, J. P., Cardoso, S. P., Faria, T. L., Lito, P. F. and Silva, C. M. (2012). Modeling ion exchange equilibrium: analysis of exchanger phase non-ideality. *Desalination*, 290(30), 43-53.

Agilent Technologies (2010). Flame atomic absorption spectrometry: Analytical method.

Barbot, E., Vidic, N. S., Gregory, K. B. and Vidic, R. D. (2013). Spatial and temporal correlation of water quality parameters of produced waters from devonian-age shale following hydraulic fracturing. *Environmental science & technology*, 47(6), 2562-2569.

Burkin, A.R. (2001). *Chemical hydrometallurgy: Theory and principles*. Imperial College, UK.

Church, T.M. and Wolgemuth, K. (1972). Marine barite saturation. *Earth and Planet. Sci. Lett.*, 15(1), 35-44.

Davis, C. W. (1962). *Ion association*. Butterworths, London.

de Witt, W. (1993). Principal oil and gas plays in the Appalachian basin (Province 131). U.S. Geological Survey Bulletin 1839-I.

Economides, M.J., Watters, L.T. and Dunn-Norman, S. (1998). Petroleum well construction, John Wiley & Sons Ltd, England.

Engelder, T., and Lash, G. G. (2008). Marcellus Shale play's vast resource potential creating stir in Appalachia. American Oil and Gas Reporter, 51(6), 76-87.

EPA (1974). Methods for the chemical analysis of water and wastes. EPA/600/4-79/020.

Fan, C., Kan, A.T., Zhang, P. and Tomson, M.B. (2010). Barite nucleation and inhibition at 0 to 200°C with and without thermodynamic hydrate inhibitors. SPE Journal, 16(2), 440-450.

Greenbergh, J.P. and Moller, N. (1989). The prediction of mineral solubilities in natural water: a chemical equilibrium model for the Na-K-SO<sub>4</sub>-H<sub>2</sub>O system to high concentrations from 0 to 250°C. Geochimica et Cosmochimica Acta, 53(10), 2503-2518.

Hamdona, S. K., Hamza, S. M. and Mangood, A. H. (2010). The influence of polyphosphonates on the precipitation of strontium sulfate (celestite) from aqueous solutions. Desalination and Water Treatment, 24(1-3), 55-60.

Harper, J.A. (2008). The Marcellus Shale: An old new gas reservoir in Pennsylvania. Pennsylvania Geology (special issue), 38(1).

Harvie, C.E., Moller, N. and Weare, J.H. (1984). The prediction of mineral solubilities in natural waters: The Na-K-Mg-Ca-H-Cl-SO<sub>4</sub>-OH-HCO<sub>3</sub>-CO<sub>3</sub>-CO<sub>2</sub>-H<sub>2</sub>O system to high ionic strength at 25°C. Geochimica et Cosmochimica Acta, 48(4), 723-751.

He, S., Oddo, J.E., and Tomson, M.B. (1995). The nucleation kinetics of barium sulfate in NaCl solutions up to 6M and 90°C. Journal of Colloid and Interface Science, 174(2), 319-326.

He, S., Oddo, J.E., and Tomson, M.B. (1995). The nucleation kinetics of strontium sulfate in NaCl Solutions up to 6 m and 90°C with or without Inhibitors. Journal of Colloid and Interface Science, 174(2), 327-335

Hennesy, A.J.B. and Graham, G.M. (2002). The effect of additives on the co-crystallisation of calcium with barium sulfate. Journal of Crystal Growth, 237-239(3), 2153-2159.

Hill, D.G., Lombardi, T.E. and Martin, J.P. (2004). Fractured shale gas potential in New York. Northeastern Geology And Environmental Sciences, 26(1/2), 57-78.

Holmes, H.F., Baes, C.F.B. Jr. and Mesmer, R.E. (1987). The enthalpy of dilution of HCl(aq) to 648 K and 40 MPa: Thermodynamic properties. The Journal of Chemical Thermodynamics, 19(8), 863-890.

Jones, F., Oliviera, A., Parkinson, G.M., Rohl, A.L., Stanley, A. and Upson, T. (2004). The effect of calcium ions on the precipitation of barium sulfate 1: calcium ions in the absence of organic additives. Journal of Crystal Growth, 262(1-4), 572-580.

Jones, F., Piana, S. and Gale, J.D. (2008). Understanding the kinetics of barium sulfate precipitation from water and water-methanol solutions. *Crystal Growth Design*, 8(3), 817-822.

Van der Leeden, M.C. (1991). The role of polyelectrolytes in barium sulfate precipitation. Ph.D. Dissertation, Technical University of Delft, Delft, Holland.

Merkel, B. J. and Planer-Friedrich, B. (2008). *Groundwater geochemistry: A practical guide to modeling of natural and contaminated aquatic systems*. 2nd Edition, Springer-Verlag Berlin Heidelberg.

Milici, R.C. and Swezey, C.S. (2006). Assessment of appalachian basin oil and gas resources: Devonian Shale–middle and upper Paleozoic total petroleum system. Reston, VA: U.S. Department of the Interior, U.S. Geological Survey.

Miller, C.W. and Benson, L.V. (1983). Simulation of solute transport chemically reactive heterogeneous system: Model development and application. *Water Resources Research*, 19(2), 381-391.

Monnin, C., and Galinier, C. (1988). The solubility of celestite and barite in electrolyte solutions and natural waters at 25 C: A thermodynamic study. *Chemical Geology*, 71(4), 283-296.

Monnin, C. (1999). A thermodynamic model for the solubility of barite and celestite in electrolyte solutions and seawater to 200 C and to 1 kbar. *Chemical Geology*, 153(1), 187-209.

Pabalan, R.T., and Pitzer, K. S. (1987). Thermodynamics of concentrated electrolyte mixtures and the prediction of mineral solubilities to high temperatures for mixtures in the system Na-K-Mg-Cl-SO<sub>4</sub>-OH-H<sub>2</sub>O. *Geochimica et Cosmochimica Acta*, 51(9), 2429-2443.

Parkhurst, D.L., Thorstenson, D.C., and Plummer, L.N. (1980). PHREEQE: A computer program for geochemical calculations. U.S. Geological Survey, Water Resources Investigations Report, 80-96

Parkhurst, D.L. and Appelo, C.A.J. (1999). User's guide to phreeqc (version 2): A computer program for speciation, batch-reaction, one-dimensional transport, and inverse geochemical calculations. U.S. Geological Survey, Water Resources Investigations Report, 99-4259.

Pina, C. M., and Putnis, A. (2002). The kinetics of nucleation of solid solutions from aqueous solutions: A new model for calculating non-equilibrium distribution coefficients. *Geochimica et Cosmochimica Acta*, 66(2), 185-192.

Pitzer K.S. (1973). Thermodynamics of electrolytes. I Theoretical basis and general equations. *The Journal of Physical Chemistry*, 77(2), 268-277.

Pitzer, K.S. and Mayorga G. (1973). Thermodynamics of electrolytes. II. Activity and osmotic coefficients for strong electrolytes with one or both ions univalent. *The Journal of Physical Chemistry*, 77(19), 2300-2308.

Pitzer K.S. and Kim, J.J. (1974). Thermodynamics of electrolytes. IV. Activity and osmosis coefficients for mixed electrolytes. *Journal of American Chemical Society*, 96(18), 5701-5707.

Pitzer K.S. (1975). Thermodynamics of electrolytes. V. Effects of higher-order electrostatic terms. *Journal of Solution Chemistry*, 4(3), 249-265.

Pitzer, K.S. (1991). *Activity coefficients in electrolyte solutions*, 2nd Ed., CRC, Boca Raton, FL.

Pletcher, J. (2008). Drillers access mile-deep gas deposits in what may be new “gold rush”. *Herald Standard*, May 18.

Risthaus, P., Bosbach, D., Becker, U. and Putnis, A. (2001). Barite scale formation and dissolution at high ionic strength studied with atomic force microscopy. *Colloids and Surface A: Physicochemical and Engineering Aspects*, 191(3), 201-214

Rodger, M., Fogel, N., Kelsey, T., Lembeck, S., Pifer, R., Whitmer, W. and Wulhorst, P. (2008). Marcellus Shale: What local government officials need to know. Penn State Extension, College of Agricultural Sciences, Marcellus Education.

Shen, D., Fu, G., Al-Saiari, H.A., Kan, A.T. and Tomson, M.B. (2009). Barite dissolution/precipitation kinetics in porous media and in the presence and absence of a common scale inhibitor. *SPE Journal*, 14(3), 462-471.

Shen, D., Fu, G., Kan, A.T. and Tomson, M.B. (2008). Seawater injection, inhibitor transport, rock-brine interactions, and BaSO<sub>4</sub> scale control during seawater injection. *SPE International Oilfield Scale Conference*.

Smith, E., Hamilton-Taylor, J., William, D., Fullwood, N.J. and McGrath, M. (2004). The effect of humic substances on barite precipitation-dissolution behaviour in natural and synthetic lake waters. *Chemical Geology*, 207 (1-2), 81-89.

Truesdell, A.H. and Jones, B.F. (1974). WATEQ, a computer program for calculating chemical equilibria of natural waters. *Journal of Research of the U.S. Geological Survey*, 2(2), 233-274.

Vidic, R.D., Brantley, S.L., Vandenbossche, J.M., Yoxheimer, D. and Abad, J.D. (2013). Impact of shale gas development on regional water quality. *Science*, 340:6134 DOI 10.1126/science.1235009

Westall, J.C, Zachary, J.L. and Morei, F.M. (1976). MINEQL: A computer program for the calculation of chemical equilibrium composition of aqueous systems. Technical Note No.18, Ralph M. Parsons Laboratory, Massachusetts Institute of Technology: Cambridge, MA.

Yeboah, Y. D., Saeed, M. R. and Lee, A. K. (1994). Kinetics of strontium sulfate precipitation from aqueous electrolyte solutions. *Journal of Crystal Growth*, 135(1), 323-330.

## 4.2 Precipitation of Ba and Sr with AMD

### 4.2.1 Materials and Methods

#### 4.2.1.1 Flowback Water and AMD Sampling

Flowback water (FW) samples were collected from two wells (Well A and Well B) in southwestern PA and one well site (Well C) in northeastern PA. Well A was fractured with reused flowback water, while Well B was fractured with tap water. Flowback water samples from these two wells were collected at various times during the flowback period from Day 1 to Day 16, and were individually stored in clean buckets and covered with lids. Composite flowback water samples for these two wells were prepared based on the proportion of flow rate on each day (i.e., flow composite sample). Flowback Water C was sampled from a storage tank.

Five AMD sites located near the gas wells were selected for this study. AMD 1 and AMD 2 are located near Well Site A; AMD 3 and AMD 4 are available in the vicinity of Well Site B, and AMD 5 is located near Well Site C. AMD 1, 3 and 4 are untreated, while AMD 2 and 5 underwent a passive treatment process to precipitate iron and raise the pH. Characteristics of AMD and flowback water samples are summarized in Table 4.6.

**Table 4.6** Characteristics of flowback water and AMD

Parameter	Flowback Water			AMD				
	FW A	FW B	FW C	AMD 1	AMD 2	AMD 3	AMD 4	AMD 5
Na <sup>+</sup> (mg/L)	27946	14913	28643	281	687	104	145	1899
Ca <sup>2+</sup> (mg/L)	15021	2973	28249	353	245	76	77	50
Mg <sup>2+</sup> (mg/L)	1720	531	3513	53	33	49	38	104
Ba <sup>2+</sup> (mg/L)	236	850	5887	-	-	-	-	-
Sr <sup>2+</sup> (mg/L)	1799	874	9000	-	3	1.5	0.7	-
Cl <sup>-</sup> (mg/L)	104300	35380	119320	101	373	71	252	-
SO <sub>4</sub> <sup>2-</sup> (mg/L)	15	0	0	696	243	709	309	560
pH	6.43	7.38	3.86	5.97	7.03	6.14	6.12	2.82

#### 4.2.1.2 *Mixing Experiments and Analytical Method*

Flowback water (FW) was mixed with AMD at ratios ranging from 10% to 70% in a 200-mL beaker covered with plastic film. Samples were collected at pre-determined time points, filtered through 0.45 µm membrane and immediately diluted to inactivate the subsequent chemical reaction. Atomic absorption spectroscopy (AAS) was used to analyze Ba and Sr ions while ion chromatography (IC) was used to analyze the dissolved sulfate. Samples for AAS analysis were diluted with 2% HNO<sub>3</sub> and 0.15% KCl solutions, while samples for IC analyses were diluted with DI water. Analysis of each ion was conducted 3 times and the average value is reported.

#### 4.2.1.3 *Radium Leaching Test*

Toxicity characteristic leaching procedure (TCLP) test was conducted following the standard procedure (EPA, 1992) to evaluate the radium leaching from solid precipitates. Solid samples were collected by filtering the suspension through 0.45 µm nylon membrane. The retained particles were completely dried and placed into the extraction liquid using 1:20 weight ratio of liquid the solids. As the pH of mixtures was above 5, CH<sub>3</sub>COOH (pH=2.88) solution was used as the extraction fluid. Sealed samples were placed on a rotary shaker and allowed to rotate for 18 hours. Liquid sample from each bottle was collected for Ra measurement. Ra-226 activity was quantified by a Canberra gamma spectrometry system with a broad energy Germanium (BeGe) detector (Be 2020).

## 4.2.2 **Results and Discussion**

#### 4.2.2.1 *Mixing Experiments and Equilibrium Prediction*

The AMD samples paired with FW A and FW B can be categorized into two groups. AMD 1 and 3 have relatively high sulfate concentration, while AMD 2 and 4 have lower sulfate concentration. As depicted in Figure 4.11, the mixtures obtained using low-sulfate AMD samples require lower percentage of flowback water to achieve the required final sulfate concentration. As the sulfate concentration in AMD increases, so does the percentage of flowback water required to achieve the acceptable equilibrium sulfate concentration. These results clearly illustrate that the variation in the mixing ratio has a strong impact on the remaining sulfate concentration in the finished water (Figure 4.11) because the increase in the percentage of

flowback water in the mixture can result in more dilution of sulfate from AMD and higher barium concentration in the mixture simultaneously. Therefore, for the flowback waters that have lower Ba concentration (e.g., FW B), the acceptable sulfate concentration in the finished water can only be obtained by using fairly lower percentage of AMD (i.e., around 20%).

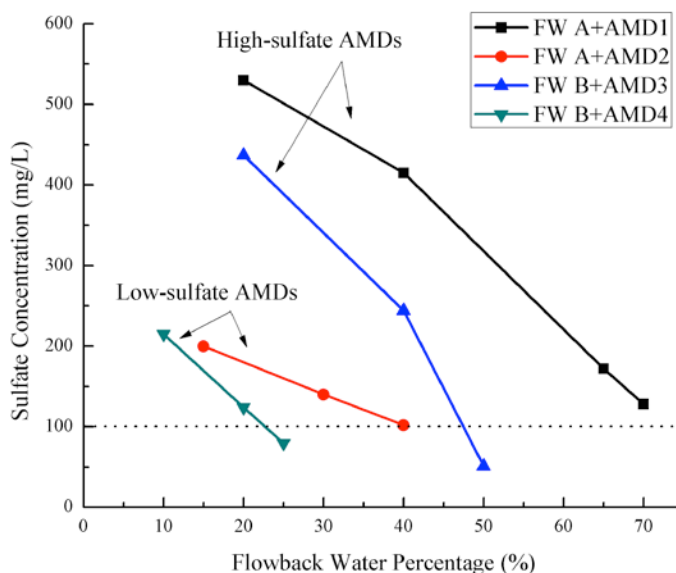


**Figure 4.11** Measured sulfate concentrations as a function of mixing ratio and mixing components.

The AMD samples used in this study have moderate sulfate concentrations ranging from 243 mg/L up to 709 mg/L. Calcium, strontium and barium concentrations in flowback water can all potentially react with dissolved sulfate to form solid precipitates. The saturation indices (SI) for  $\text{CaSO}_4$ ,  $\text{SrSO}_4$  and  $\text{BaSO}_4$  were calculated for all FW-AMD mixtures, using PHREEQC software with the Pitzer database. As listed in Table 4.7, gypsum ( $\text{CaSO}_4$ ) is undersaturated for all mixtures, even for the mixture with FW A that contains around 15,000 mg/L dissolved calcium. This is due to the fact that the solubility product for gypsum is five and two orders higher than for barite and celestite, respectively.

**Table 4.7** Mixtures of flowback water and AMD and the associated saturation indices for barite, celestite and gypsum

Mixture	Composition	SI(BaSO <sub>4</sub> )	SI(SrSO <sub>4</sub> )	SI(CaSO <sub>4</sub> )
1	15%FW A+85%AMD1	2.58	0.12	-0.45
2	40%FW A+60%AMD1	2.49	0.07	-0.52
3	65%FW A+35%AMD1	2.3	-0.06	-0.65
4	70%FW A+30%AMD1	2.25	-0.09	-0.69
5	15%FW A+85%AMD2	2.16	-0.33	-0.9
6	30%FW A+70%AMD2	2.1	-0.35	-0.94
7	40%FW A+60%AMD2	2.04	-0.38	-0.97
8	20%FW B+80%AMD3	3.61	0.23	-0.73
9	35%FW B+65%AMD3	3.56	0.2	-0.78
10	50%FW B+50%AMD3	3.46	0.11	-0.87
11	10%FW B+90%AMD4	3.23	-0.16	-1.07
12	20%FW B+80%AMD4	3.26	-0.12	-1.07
13	25%FW B+75%AMD4	3.25	-0.12	-1.09
14	70%FW B+30%AMD4	2.89	-0.44	-1.43
15	10%FW C+90%AMD5	3.79	0.6	-0.44

Although celestite is supersaturated for some mixtures (e.g., Mixtures 9 and 10) based on the thermodynamic data provided in PHREEQC, only Mixtures 1 and 7 will result in precipitation of SrSO<sub>4</sub>. This is due to the fact that standard mode of PHREEQC would not account for Sr co-precipitation with BaSO<sub>4</sub> and thermodynamically BaSO<sub>4</sub> precipitation is more favorable. Therefore, initial barium sulfate precipitation results in the consumption of dissolved sulfate, which in turn leads to the undersaturation with respect to celestite for Mixtures 9 and 10.

Although Sr co-precipitation with barite will occur, barite precipitation is the dominant reaction in the experimental system used in this study and governs the overall reaction rate. The measured SO<sub>4</sub><sup>2-</sup> concentrations after 60 min of reaction and the predicted values using PHREEQC software are compared in Figure 4.12. As illustrated in this figure, the PHREEQC offers accurate prediction of sulfate concentration at equilibrium. It is worth noting that excellent agreement between measured and predicted values indicates that the main reaction (i.e., barite precipitation) is essentially equilibrated within 60 min of reaction.



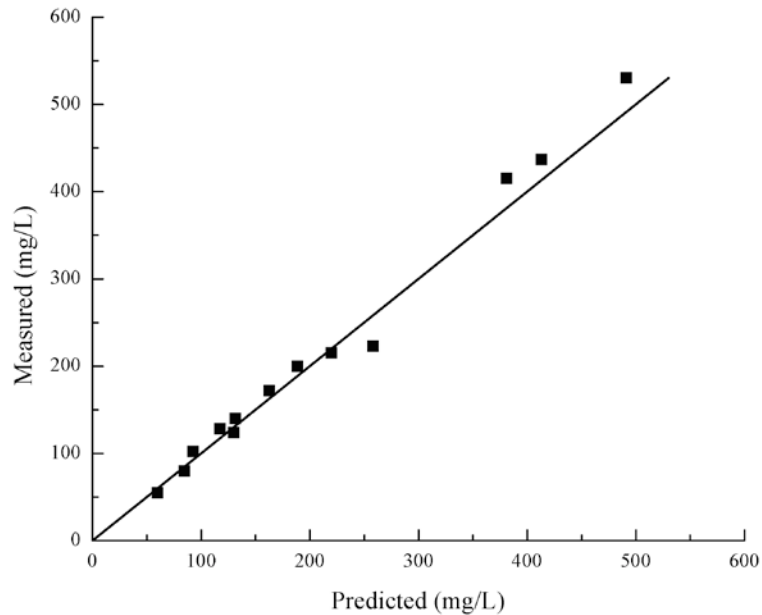


**Figure 4.12** Comparison between measured sulfate concentrations after 60 min and those predicted by PHREEQC software

#### 4.2.2.2 Celestite Precipitation

Because of the under-saturation or very low saturation state of celestite used in this study, the pure celestite precipitation would either not occur or will have minimal contribution to the sulfate removal. The barite precipitation essentially reached equilibrium after 60 min of reaction, while the slight Sr reduction was only observed for the first 20 min of reaction, which corresponds to co-precipitation of barium-strontium sulfate (Figure 4.13). Once Ba concentration in solution reached equilibrium, further decline in Sr concentration was not observed as the mixture became undersaturated with respect to celestite.

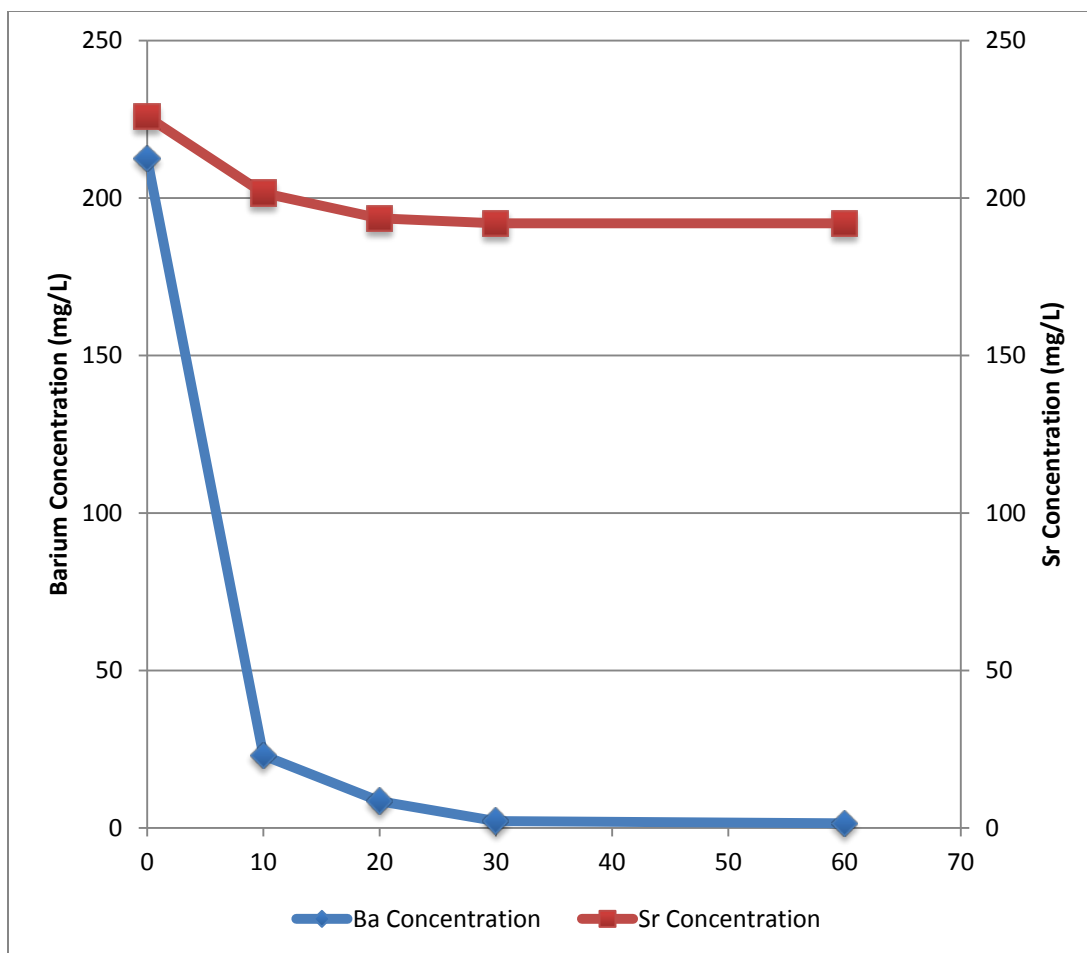


**Figure 4.13** Changes in Ba and Sr concentrations with time for Mixture 13.

In the mixing experiments conducted in this study, the pure celestite precipitation was not a concern because both sulfate and strontium concentrations were relatively low. However, if the saturation index of celestite were high after initial  $\text{BaSO}_4$  precipitation reached equilibrium, subsequent pure celestite precipitation would occur, resulting in additional sulfate removal. Kondash et al. (2013) studied the kinetics of solid precipitation for AMD-FW mixture where pure celestite precipitation was inevitable after all barium was consumed. By monitoring conductivity, Kondash et al. found that 10 hr was needed for the reaction to reach equilibrium. It was very likely that the continuous decline in conductivity observed for 10 hr was due to the pure celestite precipitation after the barite precipitation reached equilibrium.

In order to evaluate the effect of pure celestite precipitation on the overall reaction kinetics, the initial Sr concentration of Mixture 8 was adjusted to 1,200 mg/L by the addition of  $\text{SrCl}_2$ . As can be seen in Figure 4.14, rapid sulfate decline was observed during the first 10 min

of reaction followed by very slow sulfate reduction during the next 9 hr. The initial sulfate decline corresponded to the barium-strontium sulfate co-precipitation. After barium concentration essentially reached equilibrium within 60 min, the second phase of sulfate concentration decline that corresponds to pure celestite precipitation was very slow. Even after 9 hr of reaction, sulfate concentration was still far from equilibrium state (dotted line) predicted by PHREEQC. Slow celestite precipitation is consistent with previous study of the removal of barium and strontium from flowback water by the addition of  $\text{Na}_2\text{SO}_4$ , which showed that over 24 hours is needed for Sr concentration to reach equilibrium (He et al., 2014).

The slow celestite precipitation is not likely to occur in an actual wastewater treatment plant with typical detention time of 1 hr. However, the slow celestite precipitation can be avoided by selecting flowback waters that have lower Sr concentration. Alternatively, mixing ratio can be adjusted to obtain close barium and sulfate molar concentrations in the mixture. As a result, dissolved sulfate will be entirely consumed by barite precipitation (Sr coprecipitation will also occur) and the mixture will become under-saturated with respect to celestite.

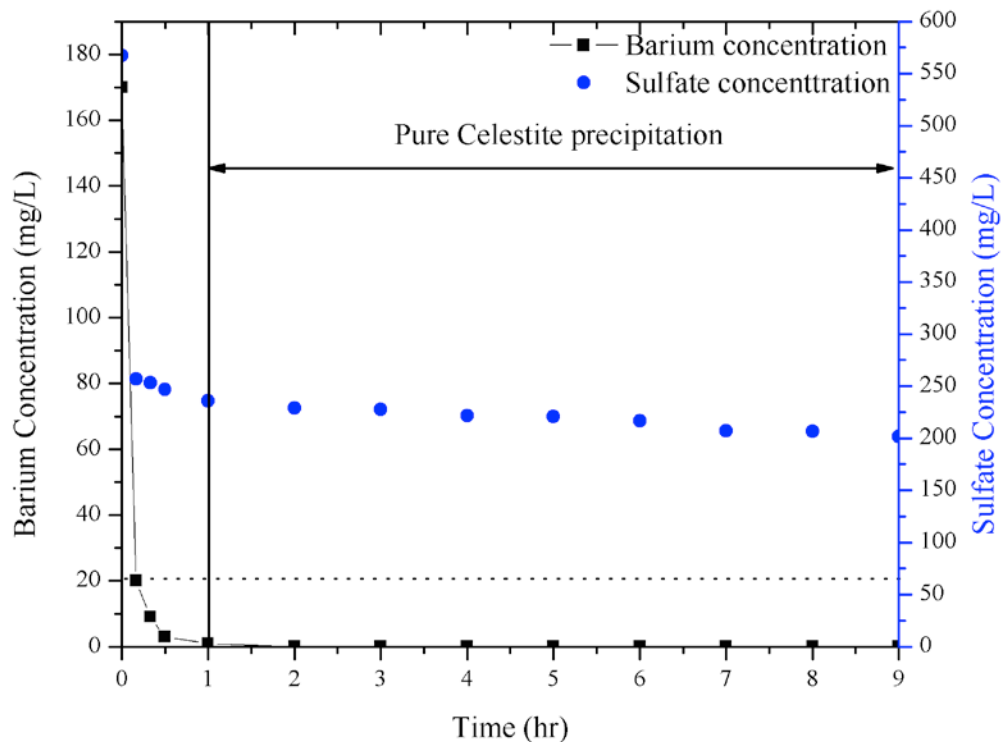


**Figure. 4.14** Precipitation kinetics of the mixture with adjustment of Sr concentration. The dotted line is the sulfate concentration at equilibrium as predicted by PHREEQC software

#### 4.2.2.3 Empirical Kinetic Model for BaSO<sub>4</sub> Precipitation

Although fundamental studies on the nucleation and crystal growth kinetics for barite precipitation have been widely reported, it is difficult to apply them to predict the barium concentration as a function time. The homogeneous nucleation model predicts rate of nuclei formation (number nuclei formed per volume per time), while the crystal growth model is used to predict the growth rate of seeded particles (length/time). Several kinetic models were developed to describe the crystal growth in the seeded experiments (Davies and Jones 1955; Nancollas and Reddy, 1971). However, the seeded growth model is applicable only at very low supersaturation conditions when homogeneous nucleation is negligible. This study used the precipitation experiments to develop an empirical process model for barium sulfate precipitation. The rate equation of BaSO<sub>4</sub> precipitation was expressed in the general form as Equation 4-5.

$$r = \frac{d[Ba^{2+}]}{dt} = \frac{d[SO_4^{2-}]}{dt} = -k[Ba^{2+}]^\alpha [SO_4^{2-}]^\beta \quad (4-5)$$

where,  $r$  is the reaction rate,  $[Ba^{2+}]$  and  $[SO_4^{2-}]$  are the molar concentrations of barium and sulfate at time  $t$ ,  $\alpha$  and  $\beta$  are the reaction order with respect to barium and sulfate, respectively.

The precipitation experiments for Mixture 1 is characterized by low barium concentration and high sulfate concentration, while Mixture 14 has barium concentration in excess compared with sulfate. Under such circumstances, either the sulfate concentration or barium is in excess and can be considered constant throughout the experiment. Therefore, for these mixtures the rate equation with respect to barium and sulfate can be rewritten as Equations 4-6 and 4-7.

$$r = \frac{d[Ba^{2+}]}{dt} = -k'[Ba^{2+}]^\alpha \quad (4-6)$$

$$r = \frac{d[SO_4^{2-}]}{dt} = -k''[SO_4^{2-}]^\beta \quad (4-7)$$

where  $k'$  is the product of  $k$  and  $[SO_4^{2-}]^\beta$ ,  $k''$  is the product of  $k$  and  $[Ba^{2+}]^\alpha$ .

The reaction order with respect to barium or sulfate was determined by fitting the experimental data with integrated rate equations (i.e., first, second, and third order). For Mixture 1, a linear relationship between  $1/[Ba]$  and time was obtained, indicating that the reaction follows the second order with respect to barium (data not shown). For mixture 14, a good linear relationship was also obtained by plotting  $1/[SO_4]$  as a function of time suggesting that the sulfate reduction rate followed the second-order reaction (data not shown). Therefore, the

overall rate law can be expressed by Equation (4-8) and the overall reaction is a fourth-order reaction.

$$r = -\frac{d[Ba^{2+}]}{dt} = -\frac{d[SO_4^{2-}]}{dt} = k[Ba^{2+}]^2[SO_4^{2-}]^2 \quad (4-8)$$

$$f([Ba^{2+}], [SO_4^{2-}]) = \left( \frac{1}{[Ba^{2+}]_0 - [SO_4^{2-}]_0} \right)^3 \left( \frac{[Ba^{2+}]_0 - [SO_4^{2-}]_0}{[Ba^{2+}]} + \frac{[Ba^{2+}]_0 - [SO_4^{2-}]_0}{[SO_4^{2-}]} + 2 \ln \left( \frac{[SO_4^{2-}]}{[Ba^{2+}]} \right) - C \right) = kt \quad (4-9)$$

where,  $[Ba^{2+}]_0$  and  $[SO_4^{2-}]_0$  are initial barium and sulfate concentrations, respectively,

$$C = \frac{[Ba^{2+}]_0 - [SO_4^{2-}]_0}{[Ba^{2+}]_0} + \frac{[Ba^{2+}]_0 - [SO_4^{2-}]_0}{[SO_4^{2-}]_0} + 2 \ln \left( \frac{[SO_4^{2-}]_0}{[Ba^{2+}]_0} \right)$$

By integration of Equation (4-8), the relationship between barium and sulfate concentration with time can be expressed as Equation (4-9). Examples of fitting the experimental data with the integrated rate equation are shown in Figure 4.15.

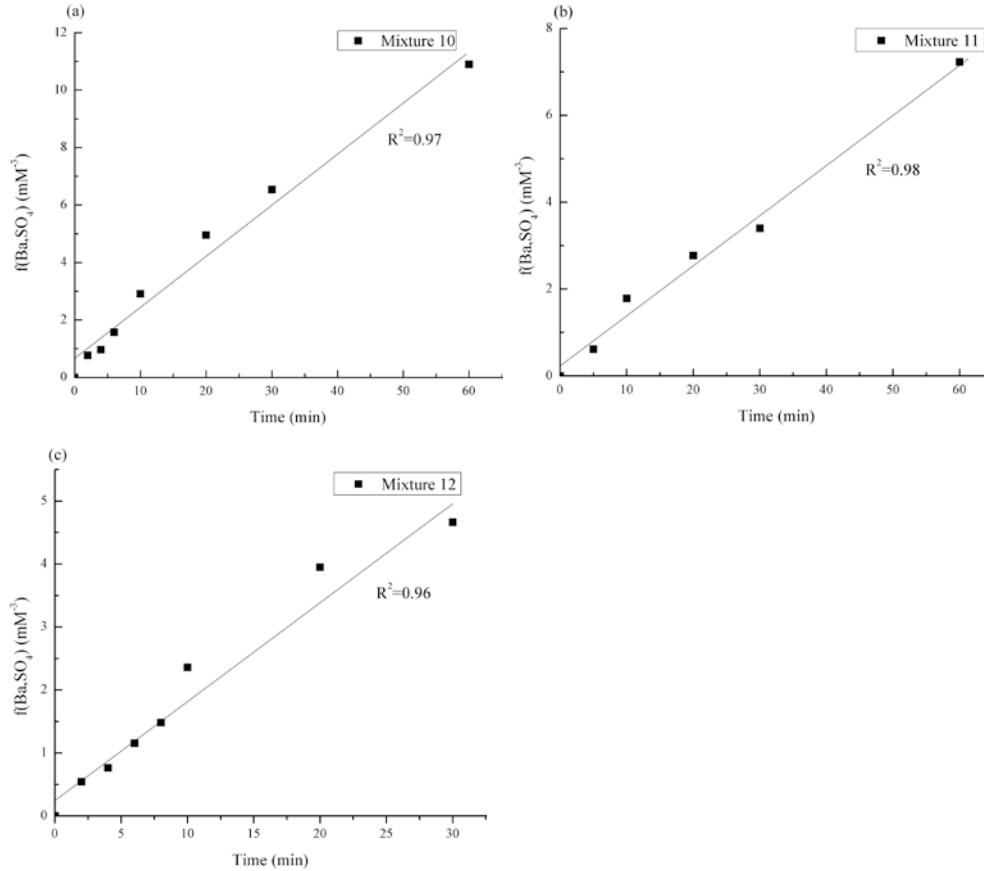


**Figure 4.15** Fitting the experimental data with (a) Mixture 10, (b) Mixture 11 and (c) Mixture 12 with Equation 5

Based on the fitting of experimental data, the rate constant varies with initial saturation index, which is as expected due to the saturation level has a great influence on the nucleation rate (Equation 4-10).

$$J(SI) = A * Exp \left[ -\frac{f(\theta)B\sigma^3\Omega^2}{b^3T^3(2.3SI)^2} \right] \quad (4-10)$$

where, B is the shape factor,  $f(\theta)$  is a factor that accounts for the impurities,  $\sigma$  is the interfacial tension, b is Boltzmann constant,  $\Omega$  is molecular volume and T is the absolute temperature (25 °C for this study).

In this study, the reaction rate constants obtained from fitting the experimental data was correlated with nucleation rate by linear regression. Except for saturation index, the variables in Equation (4-10) were assumed to be constant and their values were obtained from the literature

(Pina and Putnis, 2002; Boerlage et al., 2000; He et al., 1995). Equation (4-10) was rewritten as Equation (4-11) with “A” excluded since it will not affect the linearity of the regression. As shown in Figure 4.16, a good linearity was obtained between rate constant  $k$  and  $J(SI)$  and the regressed linear function can be used to predict the rate constant as shown in Equation (4-12).

$$J(SI) = \text{Exp} \left[ -\frac{207}{(2.3SI)^2} \right] \quad (4-11)$$

$$k = -0.00255 + 5.75 \text{Exp} \left[ -\frac{207}{(2.3SI)^2} \right] \quad (4-12)$$

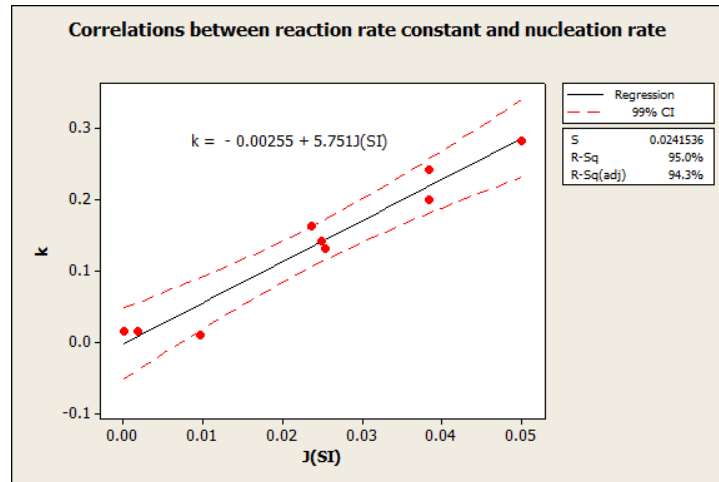


**Figure 4.16** Linear regression of reaction rate constant  $k$  and  $J(SI)$

Mixture 15 was used to test the accuracy of the empirical model. For Mixture 15, because of the comparable concentrations of Ba and  $SO_4$ , none of them can be treated as constant to simplify the rate law expression. Since Equation (4-9) is difficult to solve, for the cases where Ba and  $SO_4$  concentrations are close, it can be approximated with Equation (4-13) by ignoring the logarithmic components.

$$\left( \frac{1}{[Ba]_0 - [SO_4]_0} \right)^3 \left( \frac{[Ba]_0 - [SO_4]_0}{[Ba]} + \frac{[Ba]_0 - [SO_4]_0}{[SO_4]} - \frac{[Ba]_0 - [SO_4]_0}{[Ba]_0} - \frac{[Ba]_0 - [SO_4]_0}{[SO_4]_0} \right) = kt \quad (4-13)$$

With the predicted rate constant, the measured and predicted sulfate concentrations were compared for Mixture 15. As illustrated in Figure 4.17, this kinetic model gives a good prediction of remaining  $SO_4$  concentration as a function of time for Mixture 15.

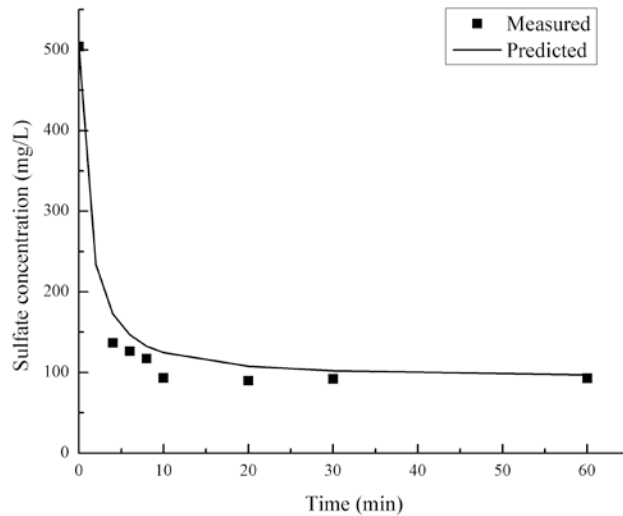


**Figure 4.17** Measured and predicted sulfate concentrations as a function of time for the Mixture

15

As discussed above, the application of this model is limited to the scenarios where initial barium or sulfate concentration is in excess or their concentrations are close. However, the initial molar concentrations of barium and sulfate are close for most practical cases in order to achieve the finished water with low sulfate concentration and control the pure celestite precipitation.

#### 4.2.2.4 Radium Leaching Test

According to current regulations, radioactive solid wastes could be disposed into landfills without exceeding the annually allowed source term loading (Smith et al., 2003). However, one key concern for this approach is the potential leaching of Ra from the solid waste, which may cause contamination of groundwater.

Previous studies have demonstrated that the leaching of Ra from barite, which was formed by mixing flowback water and  $\text{NaSO}_4$  solution, was within 2% at  $\text{pH}=0.5$  (Zhang et al., 2014). The potential for Ra leaching when the solids created in these experiments are disposed in a landfill was evaluated using the TCLP tests. Based on the results of TCLP tests, the leached Ra was below the detection limit, which indicated that the migration of Ra from solid sludge to groundwater is likely not to be significant.



### 4.2.3 Conclusion

Laboratory experiments conducted in this study demonstrated that mixing ratio of flowback water and AMD had strong impact on the final sulfate concentration in the finished water. The acceptable sulfate concentration can be achieved by increasing the percentage of flowback water in the mixture. Barite precipitation controls the fate of sulfate in these mixtures because celestite precipitation occurs at a very slow rate. When the mixture of flowback and AMD is supersaturated with respect to celestite after barite precipitation reaches equilibrium, pure celestite precipitation will take place. Although the subsequent celestite precipitation could result in additional sulfate removal, the slow reaction would require a long time to affect the change in sulfate concentration and it is not cost-effective for treatment operations. Therefore, the potential pure celestite precipitation could be neglected for practical operation.

The TCLP tests suggest that the Ra will be fixed in the barite particles and the Ra leaching from the solid wastes is negligible.

### 4.2.4 References

- Boerlage, S. F., Kennedy, M. D., Bremere, I., Witkamp, G. J., van der Hoek, J. P. and Schippers, J. C. (2000). Stable barium sulphate supersaturation in reverse osmosis. *Journal of Membrane Science*, 179(1), 53-68.
- Davies, C. W. and Jones, A. L. (1955). The precipitation of silver chloride from aqueous solutions. Part 2.—Kinetics of growth of seed crystals. *Trans. Faraday Soc.*, 51, 812-817.
- Reddy, M. M., & Nancollas, G. H. (1971). The crystallization of calcium carbonate: I. Isotopic exchange and kinetics. *Journal of Colloid and Interface Science*, 36(2), 166-172.
- He, C., Li, M., Liu, W., Barbot, E. and Vidic, R. D. (2014). Kinetics and Equilibrium of Barium and Strontium Sulfate Formation in Marcellus Shale Flowback Water. *Journal of Environmental Engineering*.
- He, S., Oddo, J. E., & Tomson, M. B. (1995). The nucleation kinetics of barium sulfate in NaCl solutions up to 6 m and 90 C. *Journal of colloid and interface science*, 174(2), 319-326.
- Kondash, A. J., Warner, N. R., Lahav, O., & Vengosh, A. (2014). Radium and barium removal through blending hydraulic fracturing fluids with acid mine drainage. *Environmental science & technology*.
- Pina, C. M. and Putnis, A. (2002). The kinetics of nucleation of solid solutions from aqueous solutions: A new model for calculating non-equilibrium distribution coefficients. *Geochimica et cosmochimica acta*, 66(2), 185-192.

Smith, K. P., Arnish, J. J., Williams, G. P., & Blunt, D. L. (2003). Assessment of the disposal of radioactive petroleum industry waste in nonhazardous landfills using risk-based modeling. *Environmental science & technology*, 37(10), 2060-2066.

Zhang, T., Gregory, K. B., Hammack, R. W., & Vidic, R. D. (2014). Co-precipitation of Radium with Barium and Strontium Sulfate and its Impact on the Fate of Radium during Treatment of Produced Water from Unconventional Gas Extraction. *Environmental Science & Technology*.

### 4.3 Evaluation of Membrane Microfiltration for Solids Separation

Flowback water generated during unconventional gas extraction is of great concern due to its high total dissolved solids (TDS), radioactive elements and organic matter. Abandoned mine drainage (AMD) is a water source that is often located in the vicinity of gas wells and can be mixed with flowback water to reduce fresh water usage for hydraulic fracturing. The feasibility of microfiltration to separate solids created by mixing actual flowback water and AMD was evaluated using a bench-scale setup. Hydrophilic polyvinylidene fluoride (PVDF) membrane with a pore size of 0.22  $\mu\text{m}$  was used as a model polymeric microfiltration membrane.

Severe membrane fouling occurred during the first 5 minutes of filtration with one flowback/AMD mixture while no significant fouling was observed for a different mixture. It was found that the flowback water that caused membrane fouling contained stable iron-based colloids with an average particles size of 0.2  $\mu\text{m}$ , especially in the samples collected early in the flowback period. These colloids were not formed by mixing flowback water containing high barium concentration with AMD rich in sulfate but were originally present in the flowback water. Stability of these sub-micron colloidal particles at high ionic strength of the flowback water is attributed to organic coating on the particle surface.

#### 4.3.1 Materials and Methods

##### 4.3.1.1 Feed Water

Samples of Marcellus Shale flowback and produced waters were collected from three separate well sites located in southwestern Pennsylvania. All samples were individually stored in clean buckets and covered with lids. Water quality characteristics of flowback water samples used in this study are listed in Table 4.8. High TDS concentration in Flowback Water B is due to the fact that this well was fractured with reused flowback water, while the wells at Sites A and C were fractured with municipal water. Samples collected at different days from Sites A and B were stored individually and were used to prepare flow composite samples for each site (i.e., samples of the flowback water collected at different days were added to the composite sample in proportion to the flow rate on each day). As the flow rate of Flowback Water C was not available for each day when the samples were collected, its composite water sample was not studied.

**Table 4.8** Flowback and AMD water characteristics

	Flowback Water A	AMD 1	Flowback Water B	AMD 2
Na (mg/L)	11,860	104.1	27,946	687.31
Ca (mg/L)	2,170	76.2	15,021	244.65
Mg (mg/L)	249	49.1	1,720	33.25
Fe (total) (mg/L)	-	32.1	-	ND
Ba (mg/L)	730.5	ND	236	ND
Sr (mg/L)	362	1.5	1,799	3
Cl <sup>-</sup> (mg/L)	29,000	70.8	104,300	373.4
SO <sub>4</sub> <sup>2-</sup> (mg/L)	-	708.7	14.8	242.5
TSS (mg/L)	98 (312 <sup>*</sup> )	118	776 (593 <sup>*</sup> )	1
TDS (mg/L)	38,000 (37,000 <sup>*</sup> )	1,328	166,484 (148,400 <sup>*</sup> )	1574
Turbidity (NTU)	60	7.4	18	0.5
TOC (mg/L)	52	-	132.7	-
Alkalinity (mg CaCO <sub>3</sub> /L)	-	40.5	44	393.8
pH	7.42	6.14	6.40	7.03

<sup>\*</sup> The TSS and TDS determined after filtration through 0.05 µm membrane.

AMD 1 represents untreated discharge in the vicinity of Well A and AMD 2 represents a discharge in the vicinity of Well B that was treated in a passive water treatment system comprised of lime addition followed by aeration and sedimentation. Water quality characteristics of AMD and composite flowback water samples are shown in Table 4.8. Mixture 1 was prepared using 10% Flowback water A and 90% AMD 1, while Mixture 2 was prepared using 15% Flowback water B and 85% AMD 2. Mixing ratios were determined based on water recovery from these wells during the flowback period. Each mixture was allowed to react for at least 12 hours before filtration experiments to ensure chemical equilibrium during the filtration tests. Diluted flowback water and AMD samples were prepared by mixing them with DI water based on the mixing ratios listed above (e.g., diluted Flowback water A sample contained 10% Flowback Water A and 90% DI water). Flowback Water A and B, were allowed to settle for 12 hours and the supernatant from each sample was diluted based on the flowback water recovery and used in membrane filtration experiment to investigate the extent of membrane fouling by

colloidal particles remaining in each sample. Additional filtration tests were conducted with diluted flowback water samples that were collected on different days and different well sites.

#### 4.3.1.2 *Fouling Mechanism Theory*

Experimental data can be used to better understand which of the four fouling mechanisms (Grace, 1956) control the permeate flux: 1) Cake filtration, 2) Intermediate blocking, 3) Standard blocking, and 4) Complete blocking. Duclos-Orsello et al. (2006) described the sequence of fouling mechanisms occurring during the filtration process, which was initially pore constriction (standard blocking) followed by pore blocking (complete blocking) and then cake filtration. Standard blocking is due to particles that are smaller than membrane pore size getting into the pores and constricting pore channels. Complete blocking is caused by the particles whose size is similar to the size of membrane pores block the entrance to pore channels. Once the membrane pores are blocked, particles will accumulate on the surface and form a cake layer, which further contributes to membrane fouling. Hermia (1982) formulated the flux decline during filtration under constant pressure as follows:

$$\frac{d^2t}{dV^2} = k \left( \frac{dt}{dV} \right)^n \quad (4-14)$$

where:

t = time (s)

V = volume of permeate (L)

n = an exponent whose value characterizes the fouling mechanism (Table 4.9),

Grenier et al. (2008) simplified Equation (4-14) and applied it to characterize the fouling of various suspensions. The four corresponding linear equations related to the fouling mechanisms described above are presented in Table 4.9 and discussed below. The fouling mechanism can be identified by plotting the filtration data using the corresponding linear form model (Table 4.9). A linear relationship characterized by the linear regression factor can be used to evaluate how well the model fits the data and decide on the existence of a specific type of fouling in the filtration process.

**Table 4.9** Fouling mechanisms and their corresponding physical basis (Grenier et. al., 2008)

Fouling mechanism	n	Corresponding linear form	Physical concept
Cake filtration	0	$\frac{dt}{dV} = \frac{1}{Q} = f(V)$	Formation of a surface deposit
Intermediate blocking	1	$\frac{dt}{dV} = \frac{1}{Q} = f(t)$	Pore blocking + surface deposit
Standard blocking	1.5	$(\frac{dV}{dt})^{1/2} = Q^{1/2} = f(V)$	Pore constriction
Complete blocking	2	$\frac{dV}{dt} = Q = f(V)$	Pore blocking

#### 4.3.1.3 Particle Size Distribution Analysis

Particle size distribution of suspended solids in composite flowback water samples A and B and in mixtures of flowback water and AMD was measured by Microtrac S3500 (Microtac, Inc., PA) and is shown in Figure 4.18 and 4.19. The dominant particle sizes for Flowback Water A and B samples were 30 and 23  $\mu\text{m}$ , respectively, while the dominant particle sizes for Mixtures 1 and 2 were 10 and 20  $\mu\text{m}$ , respectively.

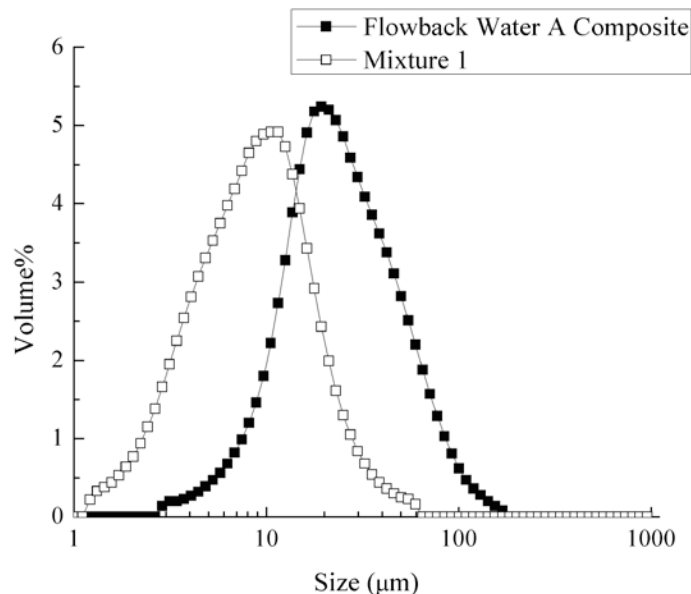


**Figure 4.18** Particle size distribution measured using Microtrac S3500: Flowback water A Composite and Mixture 1

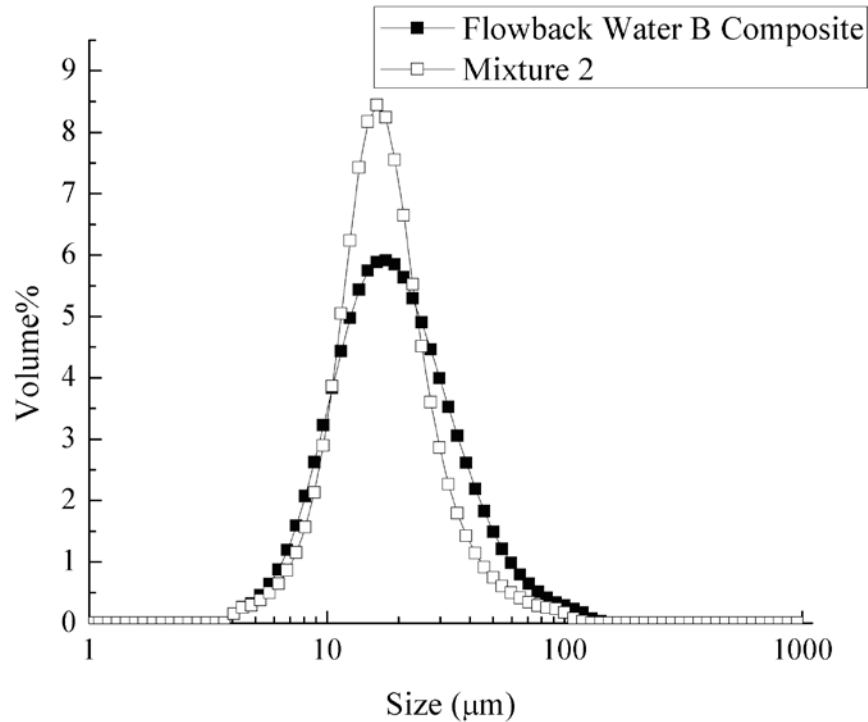


**Figure 4.19** Particle size distribution measured using Microtrac S3500: Flowback water B Composite and Mixture 2

Based on particle size distribution shown above, it was expected that a microfiltration membrane with a pore size of 0.22 µm would be efficient for removing these particles from the solution, since its pore size was an order of magnitude lower than the particle size.

Analysis of submicron particles was performed by first filtering the actual sample through 0.45 µm nylon membrane so that the permeate could be analyzed using dynamic light scattering (ALV/CGS-3 compact goniometer system, ALV-GmbH, Germany) at 90 degree angle. Several tests were performed and the one with the best correlation function was selected to determine size distribution of submicron particles using a built-in software package. The results of particle size distribution analysis for the sub-micron particles were discussed in detail in the following section.

#### 4.3.1.4 Membrane Filtration Experiment

Membrane filtration experiments were conducted using magnetically stirred dead-end cell with 340 mL volume operated in a constant pressure mode (Figure 4.20). A 2.5 L feed tank was connected to the dead-end cell and was pressurized with compressed nitrogen to allow

filtration of a larger suspension volume. The membrane filtration experiments were conducted using hydrophilic PVDF 0.22  $\mu\text{m}$  microfiltration membranes with porosity of 70% (Durapore<sup>®</sup> Millipore, Billerica, MA). The membrane was cut into a circle with a diameter of 7.5cm and was supported by a porous metal plate located at the bottom of the dead-end cell. Permeate was collected and weighed throughout the filtration test. For each membrane filtration experiment, new membrane was used after filtering 1L of deionized water to wet the membrane. All experiments were performed at room temperature (20 - 22°C) with a constant pressure of 0.5 bar (7.2psi). The morphology of the membrane surface was inspected using Scanning Electron Microscopy (SEM, Philips XL30, FEI Co., Hillsboro, OR) and the elemental composition of selected samples was determined using Energy Dispersive X-ray Spectroscopy (EDX, EDAX Inc., Mahwah, NJ). Membrane samples were carefully removed from filtration unit and gently washed with DI water prior to EDX analysis.

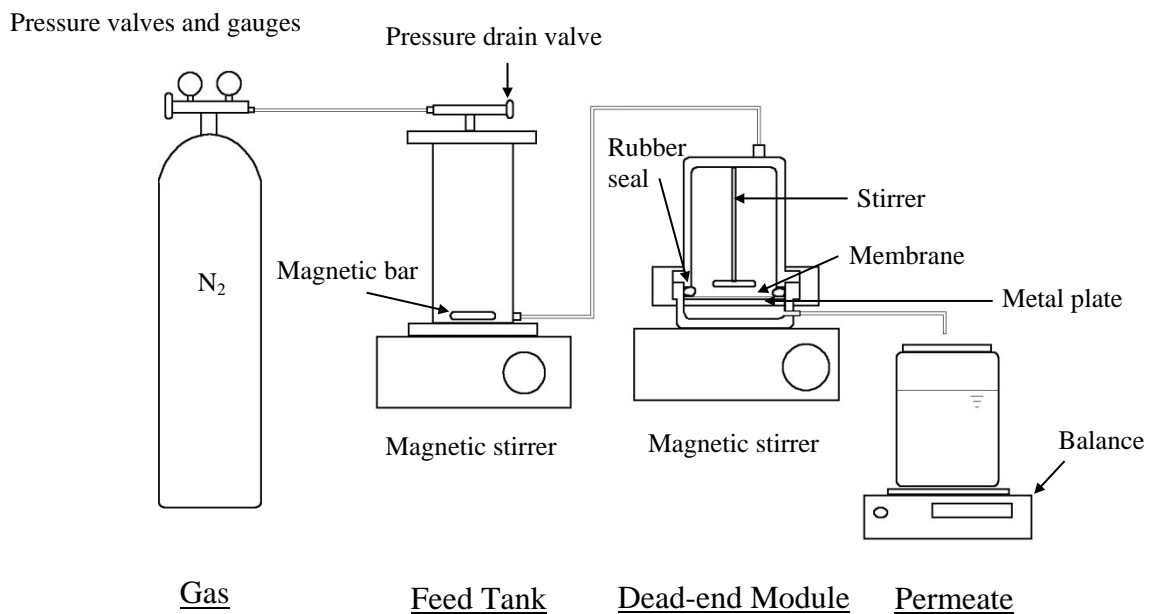


**Figure 4.20** Experimental dead-end membrane filtration apparatus

#### 4.3.1.5 Stability Evaluation

Stability of colloidal particles remaining in Day 1 samples of Flowback Water A and C after settling for 12 hours was evaluated as a function of ionic strength and oxidant addition. Ionic strength was adjusted to be identical to Day 1 sample of Flowback Water B (i.e., TDS



around 120,000 mg/L) by the addition of NaCl and CaCl<sub>2</sub> and sample turbidity was measured every 12 hours for 7 days. In order to test the hypothesis that organic coating on the surface of submicron particles affects the stability of these particles, hydrogen peroxide (Fisher Scientific, PA) was added to Day 1 sample of Flowback Water A to oxidize organic coating and its turbidity was measured every 12 hours for 5 days.

## 4.3.2 Results and Discussion

### 4.3.2.1 Membrane Filtration of the Mixture of AMD and Flowback Water

Mixtures 1 and 2 were filtered using 0.22 µm PVDF membrane to evaluate the membrane fouling caused by the particles that would form after mixing AMD and flowback water. Variations in relative flux ( $J/J_0$ ) with permeate volume for Mixtures 1 and 2 are compared with the variations in relative flux for diluted flowback water and AMD samples on Figures 4.21 and 4.22. As can be seen from these two figures, Mixture 1 caused severe membrane fouling while Mixture 2 did not. Both AMD samples collected for this study exhibited limited membrane fouling, which suggests that flowback water itself and/or barite particles formed after mixing of AMD and flowback water may be responsible for severe flux decline caused by Mixture 1.

The extent of membrane fouling caused by barite particles was evaluated by mixing AMD 1 samples with BaCl<sub>2</sub> solution (concentration of Ba was identical to that in the Flowback Water A). The flux decline was nearly identical to that observed when filtering AMD A alone, which suggests that barite particles created in the mixture had no impact on membrane fouling that occurred when filtering Mixture 1. Because the average particle size of barite formed after the addition of BaCl<sub>2</sub> to AMD is larger than 2-3 µm (Jones, 2004), this result is consistent with previous conclusion that particulate matter larger than 0.45 µm is relatively unimportant in fouling of microfiltration membranes (Howe et al., 2002). Therefore, it is hypothesized that submicron particles contained in flowback water are the main reason for membrane fouling, since the overall particle size distribution of Mixture 1 and 2 were not that different as indicated in Figures 4.18 and 4.19. It can be seen from Figure 4.21 that the flux decline during filtration of diluted Flowback Water A was more severe compared with Mixture 1. Such behavior is likely due to removal of submicron particles by adsorption or co-precipitation with barite particles that were created by mixing Flowback Water A and AMD 1.

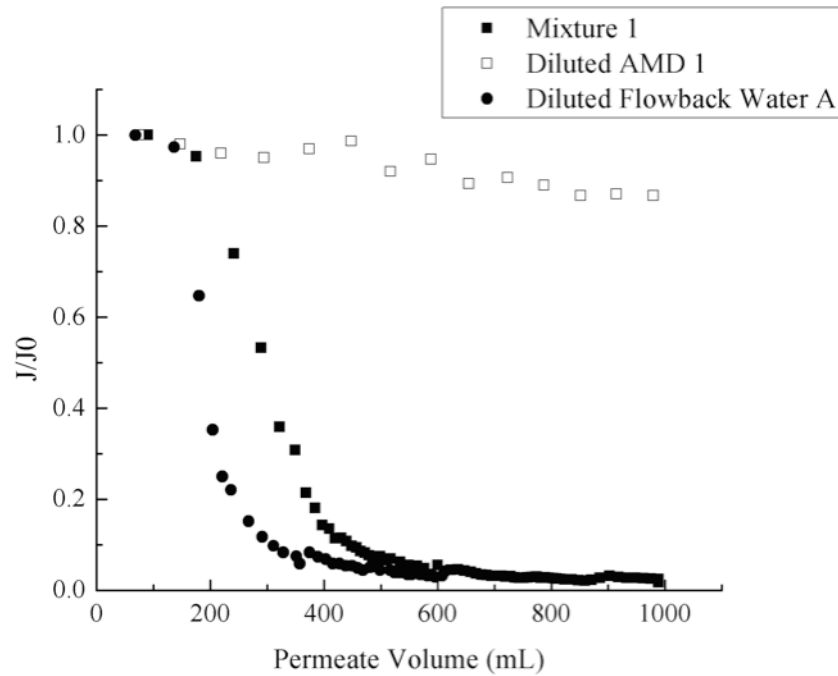


**Figure 4.20** Relative flux as a function of permeate volume for filtration of Mixture 1, diluted Flowback water A and diluted AMD 1

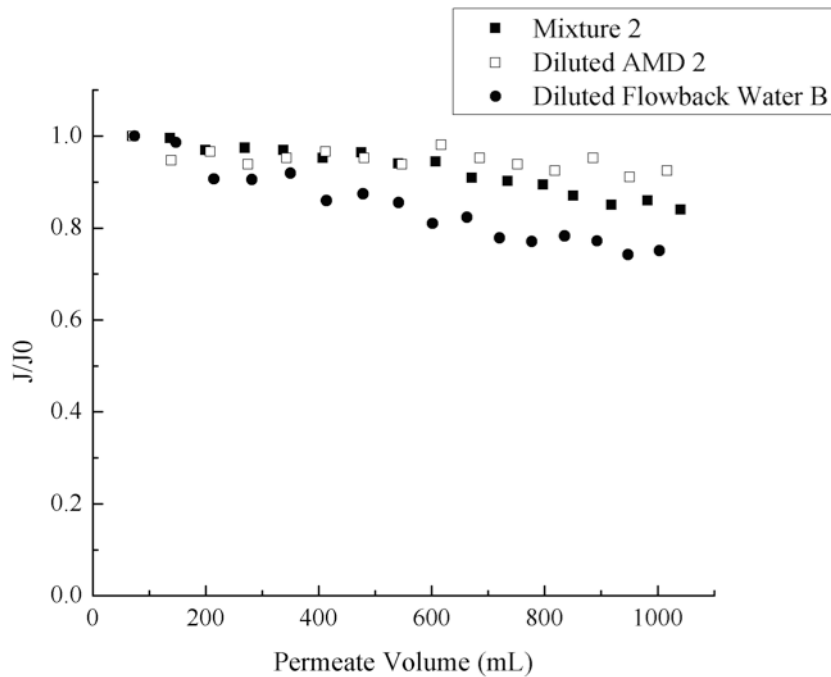


**Figure 4.21** Relative flux as a function of permeate volume for filtration of Mixture 2, diluted Flowback water B and diluted AMD 2

#### 4.3.2.2 Fouling Mechanism Identification

Grenier et al.'s (2008) fouling mechanism models were applied to determine the type of fouling in each filtration experiment. Fouling mechanisms were identified by analyzing permeate flux data to better understand the membrane fouling phenomena. In this study, the fouling mechanism models were used to find out what caused the fouling and how the fouling formed during the membrane filtration.

The results of fouling mechanism analysis for Mixture 1 are included in Figures 4.22 to 4.29. In the early stages of filtration, standard blocking and complete blocking are indicated by the linear relationship of data shown in Figure 4.22 and 4.23, respectively.

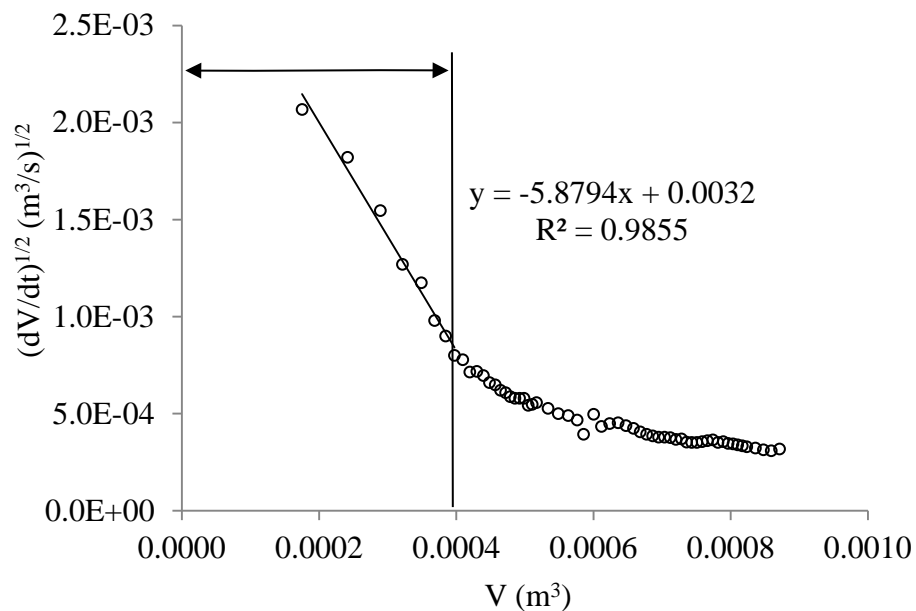


**Figure 4.22** Fouling mechanism identification for the Mixture 1: Standard blocking

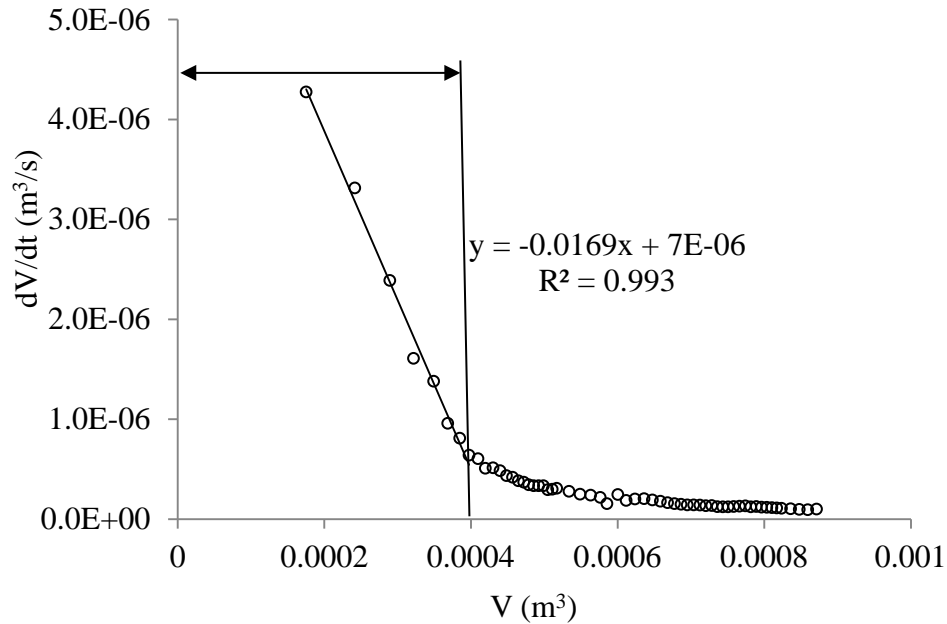


**Figure 4.23** Fouling mechanism identification for the Mixture 1: Complete blocking

In the later stages of filtration experiments with Mixture 1, cake filtration and intermediate blocking were the main fouling mechanisms as shown in Figure 4.24 and 4.25, respectively. When comparing the regression fits in Figures 4.24 and 4.25, membrane fouling due to cake filtration offered a better fit for the fouling model. Thus, for the complete filtration process of Mixture 1, the cake filtration was the dominant fouling mechanism after standard blocking and complete blocking occurred during the early stages of the test. In conclusion, standard blocking and complete blocking caused by the particles in the sub-micron range were the dominant fouling mechanisms during the first few minutes of filtration based on the rapid flux decline. After that, cake filtration and intermediate blocking occurred by a formation of a cake deposit on the surface of membrane.

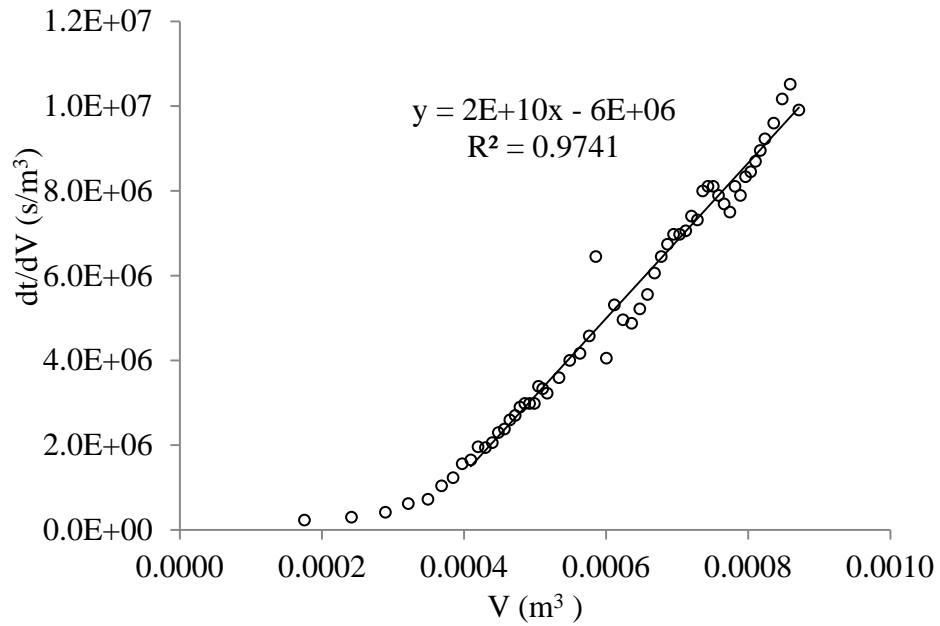


**Figure 4.24** Fouling mechanism identification for the Mixture 1: Cake filtration

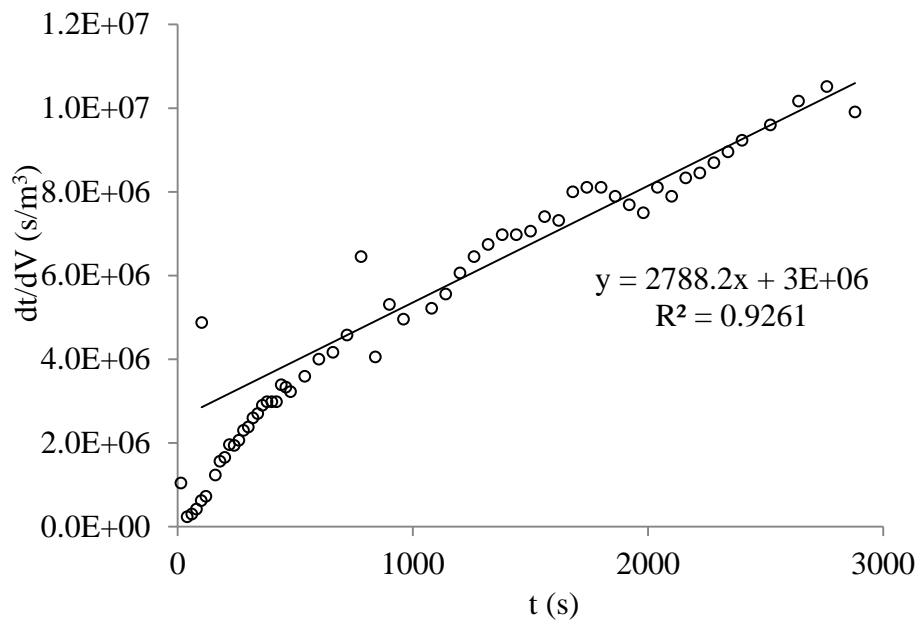


**Figure 4.25** Fouling mechanism identification for the Mixture 1: Intermediate blocking

Identifications of the four fouling mechanisms for the Mixture 2 are included in Figures 4.26 to 4.28. The linear regressions in Figure 4.26 and 4.27 indicate that standard blocking (pore blocking) and complete blocking (pore constriction) occurred during the filtration experiment with Mixture 2 at a fairly low rates. Furthermore, the slope of these fouling mechanism linear forms identified for Mixture 2 were about 4% of that for Mixture 1, which indicated that no standard blocking and complete blocking happened during filtration of Mixture 2.

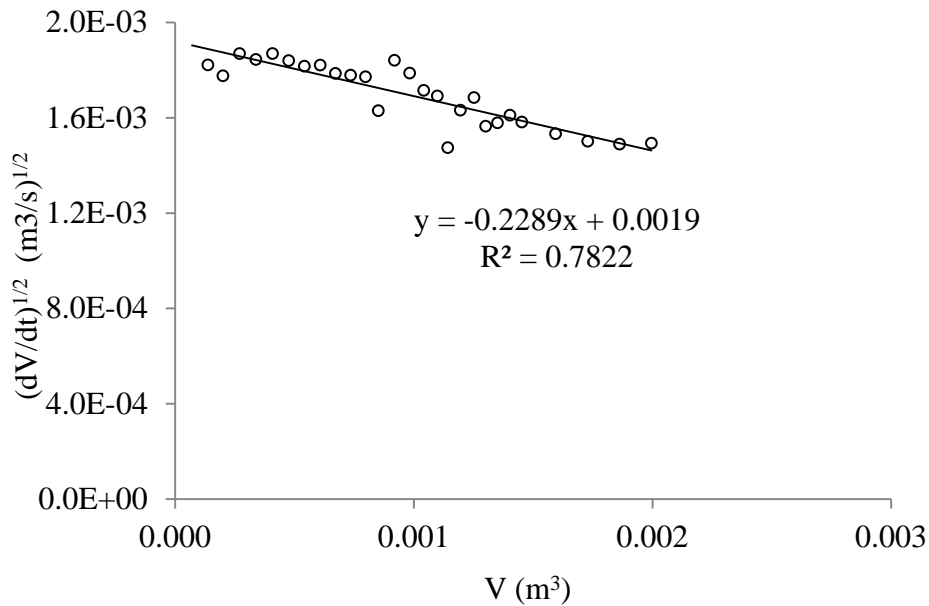


**Figure 4.26** Fouling mechanism identification for the Mixture 2: Standard blocking

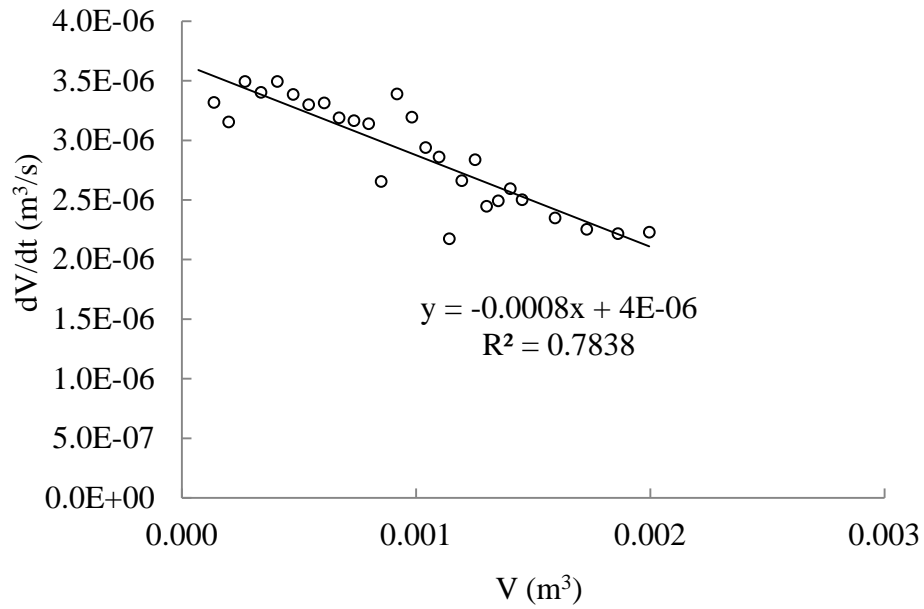


**Figure 4.27** Fouling mechanism identification for the Mixture 2: Complete blocking

In the later stages of filtration for Mixture 2, cake filtration was detected, but the impact was not as significant as in the case of Mixture 1 due to the lower slope of the regression fit and scatter in the data (Figure 4.28). The intermediate blocking occurred throughout the filtration test but its impact was quite limited, because the regression fit was as low as 0.6 (Figure 4.29). The slope of intermediate blocking linear form showed continuous increase from the beginning, which indicates built up and aggregation of a cake layer. Thus, cake filtration was the dominant fouling mechanism for Mixture 2.

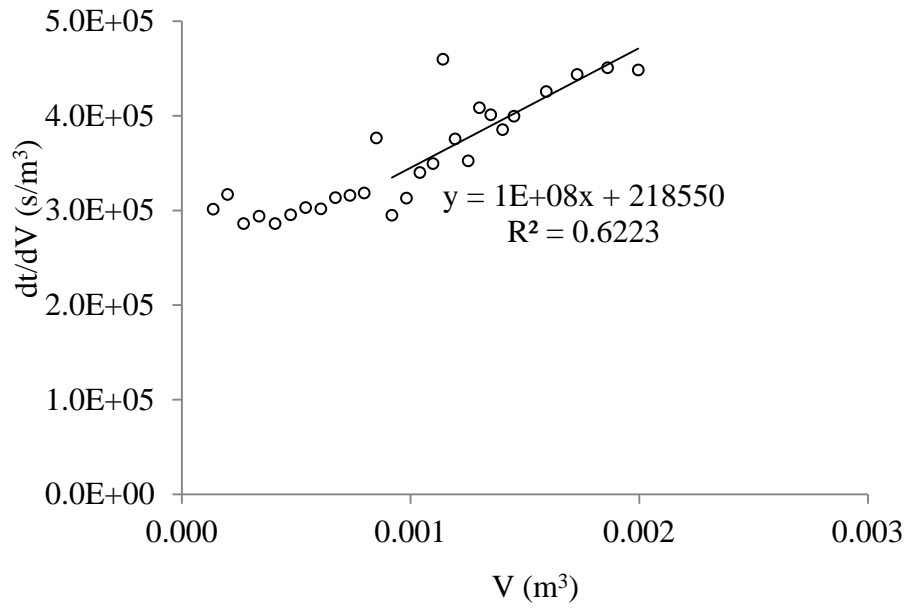


**Figure 4.28** Fouling mechanism identification for the Mixture 2: Cake filtration

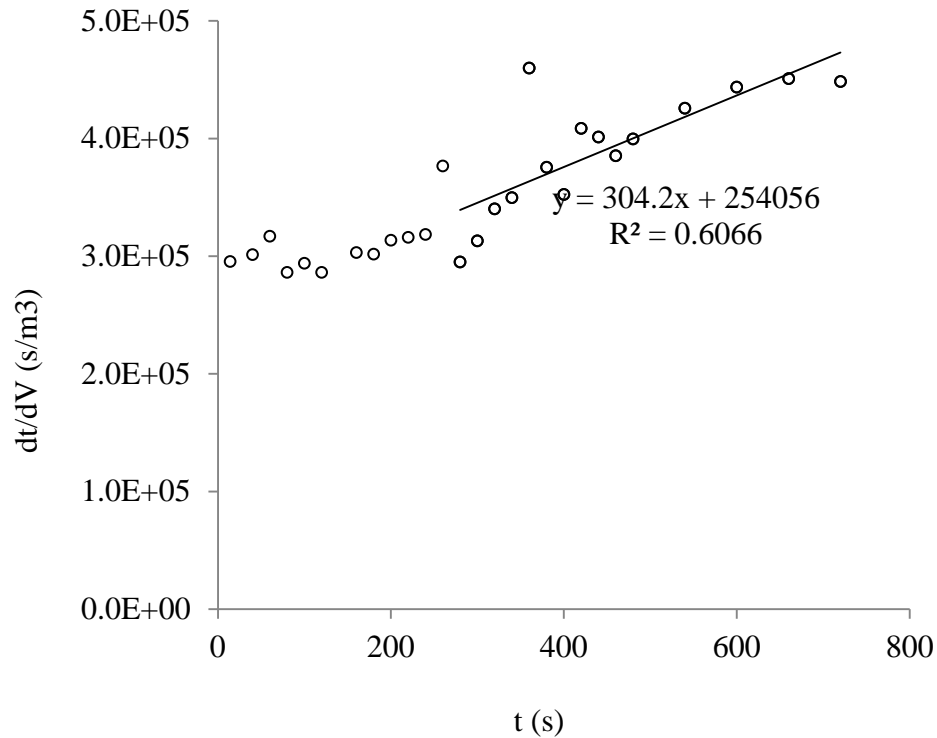


**Figure 4.29** Fouling mechanism identification for the Mixture 2: Intermediate blocking



Filtration test analyses for diluted flowback water and diluted AMDs are summarized in Table 4.10. The regression coefficients ( $R^2$ ) for different fouling mechanisms as well as the ranges of filtrate volume (L) for which the regression have been performed are also included in Table 4.10.

For the diluted Flowback water A, the fouling mechanisms were found to be similar to those detected for Mixture 1. Standard blocking and complete blocking were identified at the beginning of the filtration experiment, followed by the cake filtration in the later stages. This behavior is due to the presence of sub-micron particles in Flowback water A.

For the diluted AMD 1, no dominant fouling mechanism was found and the linear regression coefficients were fairly low for all fouling mechanisms, no significant fouling was observed when compared with Mixture 1 or Flowback water A.

No dominant fouling mechanism was identified for the diluted Flowback water B, which was similar to the results observed for Mixture 2. In the early stages of filtration, no significant standard blocking or complete blocking could be identified. Because the particles in the Flowback water B were larger than the membrane pore size, they were not able to cause pore constriction or pore blocking. Moreover, no sub-micro particles were detected in Flowback water B.

As shown in Table 4.10, there was no standard blocking (pore constriction) happened during the filtration of diluted AMD 2. This was expected because the AMD 2 contains particulate matter of larger size than the membrane pores and virtually no organic matter. Complete blocking, intermediate fouling and cake formation were observed with AMD 2 only after filtering half of feed solution.

**Table 4.10** Fouling mechanism identification data summary for flowback water and AMD

		Mixture 1	Diluted Flowback Water A	Diluted AMD 1	Mixture 2	Diluted Flowback water B	Diluted AMD 2	
Fouling Mechanism	Cake filtration	R <sup>2</sup> V (L)	0.9741, 0.40~0.90	0.9514, 0.37~0.72	0.67967 Total volume	0.6223, 0.92~2.0	0.9618, Total volume	0.95094, 0.84~end
	Intermediate blocking	R <sup>2</sup> V (L)	0.9477, 0.49~0.87	0.9122, 0.37~0.72	0.6736 Total volume	0.6066, 0.92~2.0	0.9691, Total volume	0.9569, 0.91~end
	Standard blocking	R <sup>2</sup> V (L)	0.9855, 0.18~0.40	0.9780 0~0.24	0.708 Total volume	0.7822, Total volume	0.9746, Total volume	N/A
	Complete blocking	R <sup>2</sup> V (L)	0.9930, 0.18~0.40	0.9907 0~0.22	0.7149 Total volume	0.7838, Total volume	0.9713, Total volume	0.94067, 0.84~end
V indicated the volume range for which the regression has been determined.								

To compare the severity of the fouling for membrane filtration experiments of all feed waters, cake volumic specific resistance and complete blocking parameters were calculated and summarized in Table 4.11. The cake volumic specific resistance  $\eta_C$  ( $m^{-2}$ ) was calculated based on the following equation (Grenier et al., 2008):

$$\eta_C = \frac{KAP}{\mu} \quad (4-15)$$

where:

$\eta_C$  = cake volumic specific resistance ( $m^{-2}$ )

K = slope of the  $dt/dV = f(t)$  line

A = membrane surface area ( $m^2$ )

P = applied pressure (Pa)

$\mu$  = dynamic viscosity of the permeate (Pa·s)

The complete blocking parameter represents the ratio of the blocked surface area and total membrane surface area  $\eta_B$  ( $m^{-1}$ ), and is related to the fouling by pore blocking. The complete blocking parameter is expressed by (Grenier et al., 2008):

$$\eta_B = \frac{k_B}{J_0} \quad (4-16)$$

where:

$\eta_B$  = blocking parameter ( $m^{-1}$ )

$k_B$  = slope of the  $dV/dt = f(V)$  line

$J_0$  = initial flux ( $L h^{-1} m^{-2}$ )

The severity of the membrane fouling is related to the value of the cake volumic specific resistance and the blocked surface area (Grenier et al., 2008).

In Table 4.11, the cake resistance and blocked surface area were significantly (1-2 orders of magnitude) greater for Flowback water A and Mixture 1 than for Flowback water B and Mixture 2. The high cake resistance for Mixture 1 and Flowback water A may be due to a thick and dense cake that formed on the membrane surface. The higher turbidity in the Flowback water A has the potential to cause the thicker cake deposit than in the Flowback water B. The existence of sub-micron particles in Flowback water A could easily cause membrane pore blocking or constriction in the early stages of filtration process, which explains much faster

decrease of permeate flux in Flowback water A than in Flowback water B. Therefore, it was expected that higher cake volumic specific resistances and blocked surface area would be obtained in the filtration process involving Flowback water A than Flowback water B.

Both AMDs and Flowback water B created fairly low cake resistances and very limited pore blocking compared to Flowback water A and AMD 1 (Table 4.11). These results further prove that sub-micro particles in Flowback water A caused pore constriction and pore blocking at the early stages of filtration, which was the main reason for severe membrane fouling by Mixture 1 or diluted Flowback water A. To understand the membrane fouling caused by these sub-micron particles, detailed membrane fouling analysis was conducted and discussed in the following section.

**Table 4.11** Cake volumic specific resistance and blocking parameter for flowback water and AMD

	Cake volumic specific resistance ( $m^{-2}$ )	Blocking parameter ( $m^{-1}$ )
Flowback water A	$5.12 \times 10^{15}$	(88.9)*
AMD 1	$1.36 \times 10^{13}$	0.803
Mixture 1	$4.05 \times 10^{15}$	16.64
Flowback water B	$2.49 \times 10^{13}$	0.959
AMD 2	$9.99 \times 10^{12}$	1.504
Mixture 2	$2.20 \times 10^{13}$	0.916

\* Regression was performed on a very limited set of data.

Based on Grenier's approach, the fouling mechanism is identified by fitting the experimental data with the equations corresponding to different fouling mechanisms. In order to identify the transition of membrane fouling from pore blockage to cake layer formation when filtering Flowback Water A, the approach proposed by Ho and Zydney (Ho and Zydney, 2000) was used.

The results shown in Figure 4.30 indicate a linear relationship during the early stage of the filtration experiment (i.e., low  $dt/dV$ ) with the slope of 1.88 ( $R^2=0.995$ ). Such behavior clearly indicates pore blockage as the dominant membrane fouling mechanism. During the later stage of the filtration experiment, the data on Figure 4.30 exhibit a plateau (i.e., the  $d^2t/dV^2$

becomes constant as its slope equals zero), which indicates that the membrane fouling is governed by cake formation.

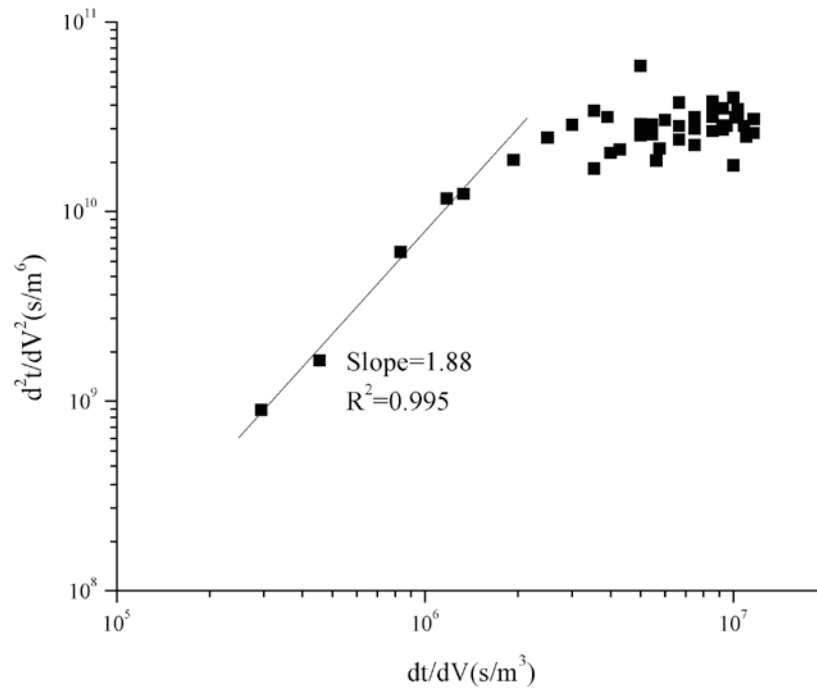


**Figure 4.30** Fouling mechanism identification according to the approach developed by Ho and Zydney

#### 4.3.2.3 Membrane Fouling Analysis

Flowback water samples collected on different days and at different well sites, as well as composite Flowback Water A and B, were allowed to settle for 12 hours and the supernatant from each sample was diluted based on the flowback water recovery and used in membrane filtration experiment to investigate the extent of membrane fouling by colloidal particles remaining in each sample. Variation in relative permeate flux with permeate volume during the filtration of Flowback Water A, B and C shown in Figure 4.31 revealed that composite Flowback Water A caused much more severe fouling compared with composite Flowback Water B. In addition, water samples that were collected on the first day of the flowback period caused more severe membrane fouling compared with samples collected on later days. Filtration experiments with Flowback Waters A and C exhibited very fast permeate flux decline, while Flowback Water B that was collected from another county had a gradual permeate flux decline. Therefore, the potential of flowback water to foul 0.22  $\mu\text{m}$  PVDF membrane is likely dependent on the location of the unconventional gas well.

SEM image of membrane surface after filtration of diluted composite Flowback Water A is shown in Figure 4.32. As can be seen from this figure, a cluster of densely packed small particles formed a cake layer on the membrane surface. Membrane drying in preparation for SEM analysis resulted in the crack in Figure 4.32 (Schäfer et al., 2000). Densely packed cake layer with low porosity is the result of high ionic strength of the flowback water that leads to a decrease in Debye length of the charged particles and enables close packing of these particles (Faibish et al., 1998; Koo et al., 2011; Yiantsios and Karabelas, 1998).

In order to identify the elemental composition of the submicron particles contained in Flowback Water A, Day 1 sample of this water was first filtered through 0.45  $\mu\text{m}$  nylon membrane. The permeate was then filtered through 0.05  $\mu\text{m}$  membrane and the elemental composition of submicron particles collected on 0.05  $\mu\text{m}$  membrane was analyzed using EDX. Typical EDX spectrum of these submicron particles is shown in Figure 4.33. High carbon peak is due to 0.05  $\mu\text{m}$  membrane that is made of polyacrylonitrile. Based on the EDX measurement at three different locations on the membrane, final elemental composition (excluding carbon) is shown in Figure 4.34. These results indicate that the submicron particles are mainly comprised of iron oxide.

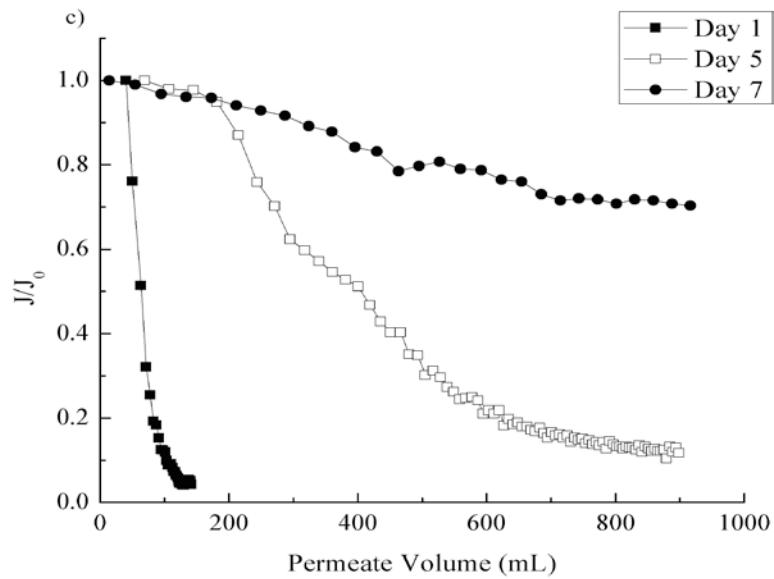
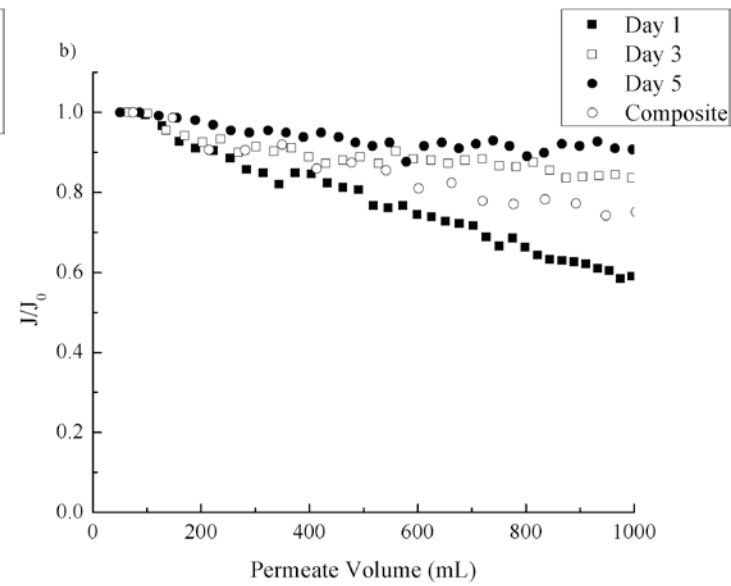
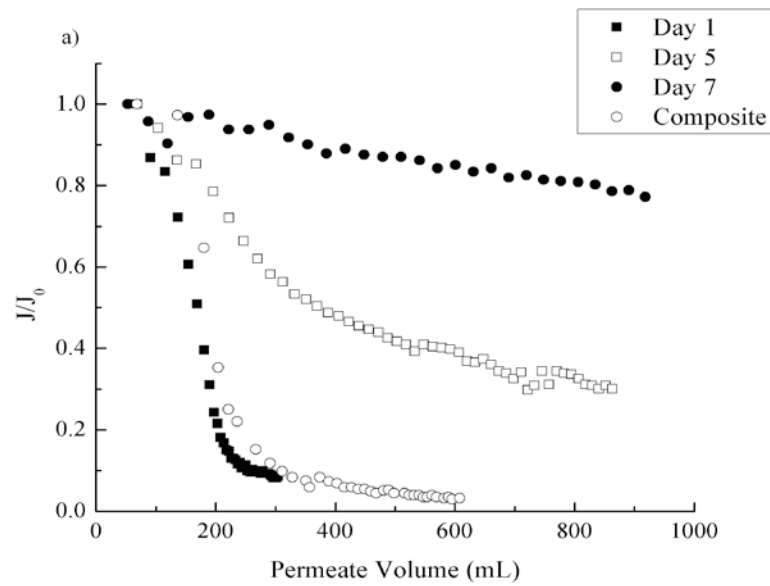


**Figure 4.31** Variation of permeate flux with permeate volume for flowback water samples collected on different days as well as flow composite sample after settling for 12 hours: (a) Flowback water A; (b) Flowback water B; and (c) Flowback Water C.

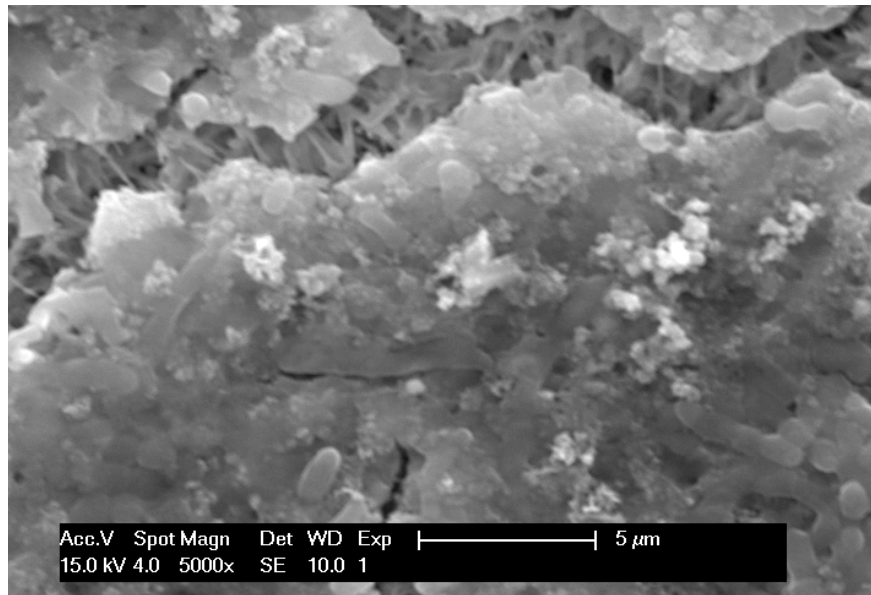


**Figure 4.32** SEM image of the cake layer on PVDF membrane after filtration of composite Flowback Water A

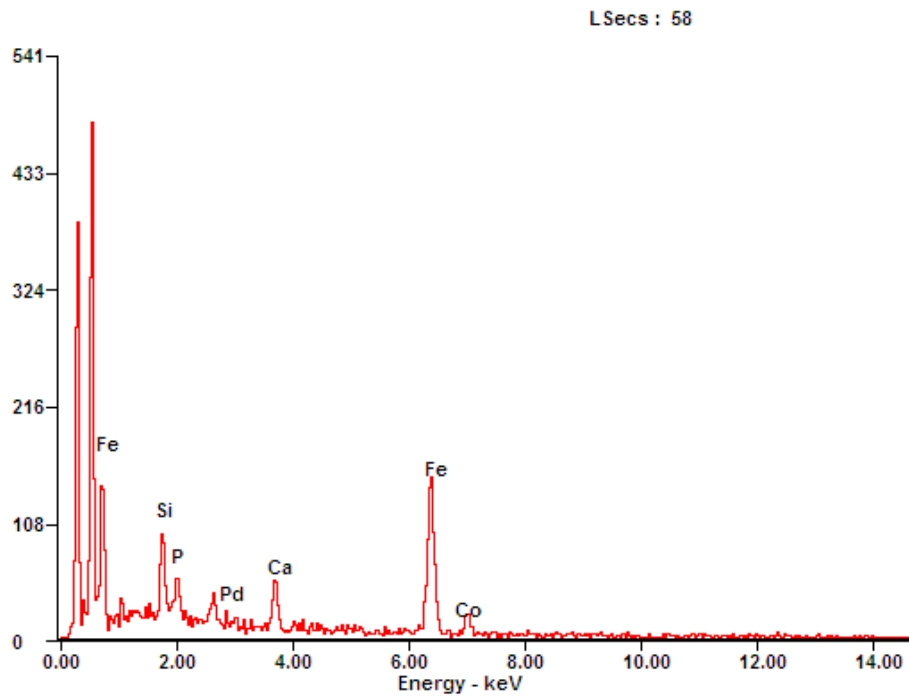


**Figure 4.33** EDX spectra of submicron particles collected on the surface 0.05 $\mu$ m membrane from Flowback Water A collected on Day 1 (raw sample was first filtered using 0.45 $\mu$ m membrane).



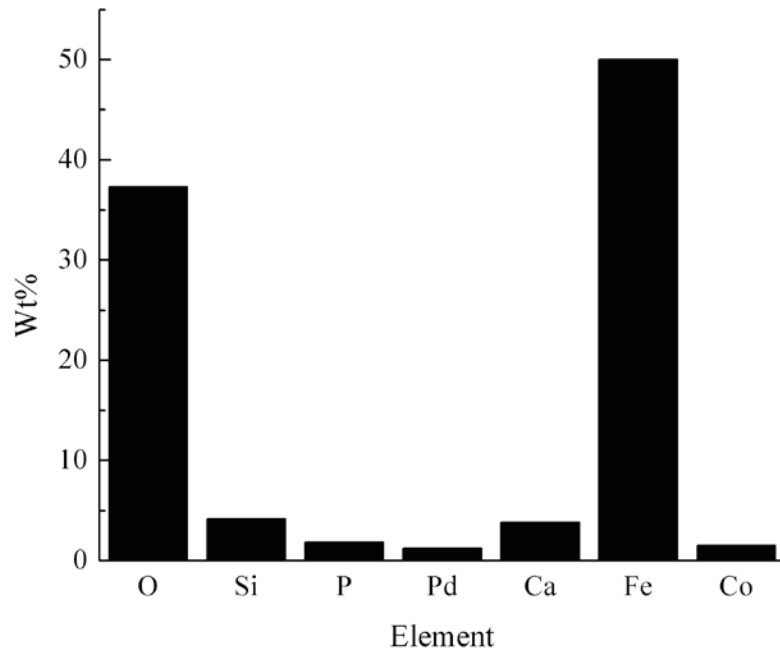


**Figure 4.34** Average elemental composition of submicron particles excluding carbon.

Particle size distribution of colloids remaining in the supernatant of the Flowback Water A collected on Day 1 and Day 5 after settling for 12 hours was measured using the ALV dynamic light scattering (DLS) instrument. The results shown in Figure 4.35 indicate that the particles in Day 1 sample of Flowback Water A had a mean particle size of 0.22 $\mu$ m, which is close to membrane pore size. On the other hand, Day 5 sample of Flowback Water A contained particles that were much larger in size with a mean particle size of about 2  $\mu$ m. Similar results were observed for Flowback Water C. Particle size distribution results shown in Figure 4.35 are consistent with the fact that the Day 1 sample of Flowback Water A caused severe membrane fouling, while Day 5 sample caused much less fouling (Figure 4.31a). These results support the hypothesis that the existence of submicron particles in the samples collected during the initial flowback period is the main reason for membrane fouling. Submicron particles in Flowback Water B were below the DLS detection limit, which is consistent with the observation of limited membrane fouling with composite Flowback Water B sample.

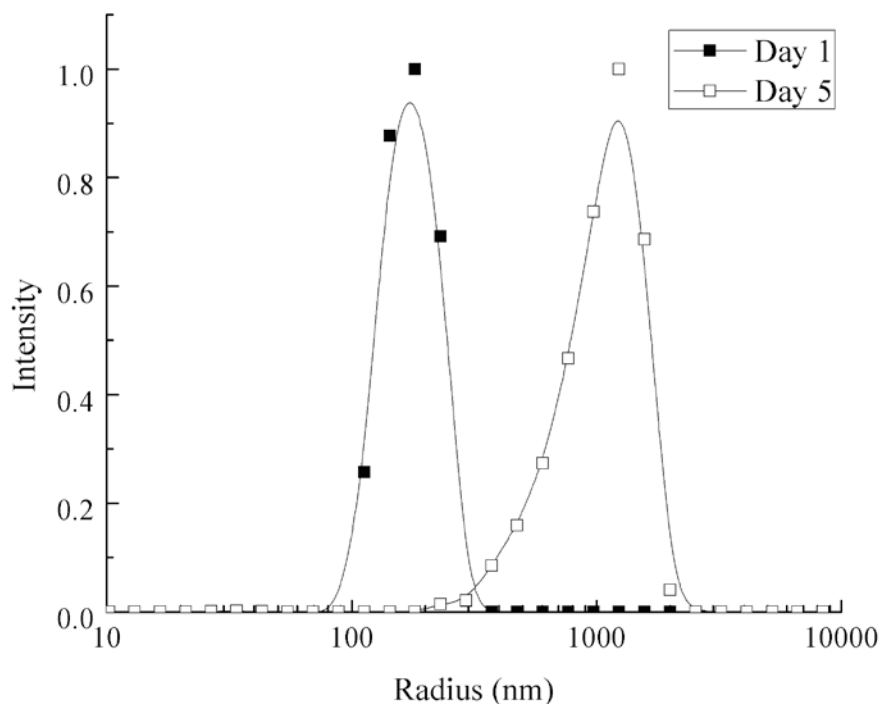


**Figure 4.35** Submicron Particle Size Distribution of Flowback Water A. Flowback water samples were allowed to settle for 12 hours to remove large particles

It is known that organic matter may contribute to membrane fouling (Park et al., 2006). Although the TOC in Flowback Water B was three times that in Flowback Water A, it caused significantly less fouling compared with Flowback Water A. In addition, salinity and TSS of Flowback Water B are 4 and 8 times that of Flowback Water A but membrane fouling by Flowback Water A was much more severe than by Flowback Water B. Thus, it can be concluded that sub-micron particles in Flowback Water A play a much more important role in membrane fouling when compared to other water quality parameters.

#### 4.3.2.4 Stability of Colloidal Suspension

Because stable submicron particles exhibited profound influence on membrane fouling, it is very important to understand the cause of stability of these colloidal suspensions, particularly considering that high ionic strength would normally lead to rapid particle aggregation (Hotze et al., 2010; Huynh and Chen, 2011). Submicron particles that caused severe membrane fouling were only found to be stable in the early samples of Flowback Water A and C, while the later samples did not contain such stable particles. In addition, Flowback Water B samples, which

had much higher ionic strength, did not contain measurable concentration of submicron colloidal particles.

Day 1 samples of Flowback Water A and C were selected to investigate the colloid stability under high ionic strength by adjusting  $\text{Na}^+$  and  $\text{Ca}^{2+}$  to the level found in Day 1 sample of Flowback Water B (i.e., TDS of around 120,000 mg/L). In essence, TDS in Day 1 sample of Flowback Water A and C were elevated more than 7 times compared to their original values. Increase in the ionic strength of solution typically results in lower electrostatic force between particles and should lead to aggregation of small particles. As the aggregates are allowed to settle, a decrease in supernatant turbidity should be observed.

Analysis of turbidity and particle size distribution in Day 1 samples of Flowback Waters A and C every 12 hours for seven days after ionic strength adjustment revealed that destabilization of the colloidal suspension did not occur (data not shown). It is hypothesized that the stability of these submicron particles is due to organic matter coating on the particle surface. Based on extended DLVO theory, which takes steric repulsion forces into consideration for particle-particle interactions, once polymer or NOM is coated on particle surface, repulsion forces between particles are largely increased, thereby increasing the stability of coated colloidal or nano-sized particles (Hotze et al., 2011; Saleh et al., 2008; Pincus, 1991). Scaling inhibitors and friction reducers, which are injected together with hydrofracturing water (Edwards et al., 2011; Paktinat et al., 2011; EPA, 2011), as well as natural organic matter from the shale matrix could be responsible for such behavior (Groundwater Protection Council, 2009).

To test this hypothesis, treatment with hydrogen peroxide was performed to oxidize organic coating on particle surfaces. After adding 1% hydrogen peroxide to Day 1 sample of Flowback Water A, turbidity of the solution was measured every 12 hours for 5 days. The results in Figure 4.36 compare the turbidity of hydrogen peroxide treated solution with the turbidity in the control sample that did not receive hydrogen peroxide treatment. The turbidity of the treated sample initially increased to 81 NTU, followed by destabilization of the dispersion as indicated by visual observation of large aggregates in the reactor. Aggregation of submicron particles resulted in relatively rapid settling and reduction in sample turbidity to 2 NTU. The results of filtration experiment with  $\text{H}_2\text{O}_2$  treated Day 1 sample of Flowback Water A are compared to the results of the filtration experiment with untreated Day 1 sample of Flowback Water A in Figure 4.37. The data shown on Figure 4.37 confirm that the submicron particles are responsible for the severe flux decline for Flowback Water samples and that the stability of these submicron particles at very high ionic strength is due to the organic coatings.

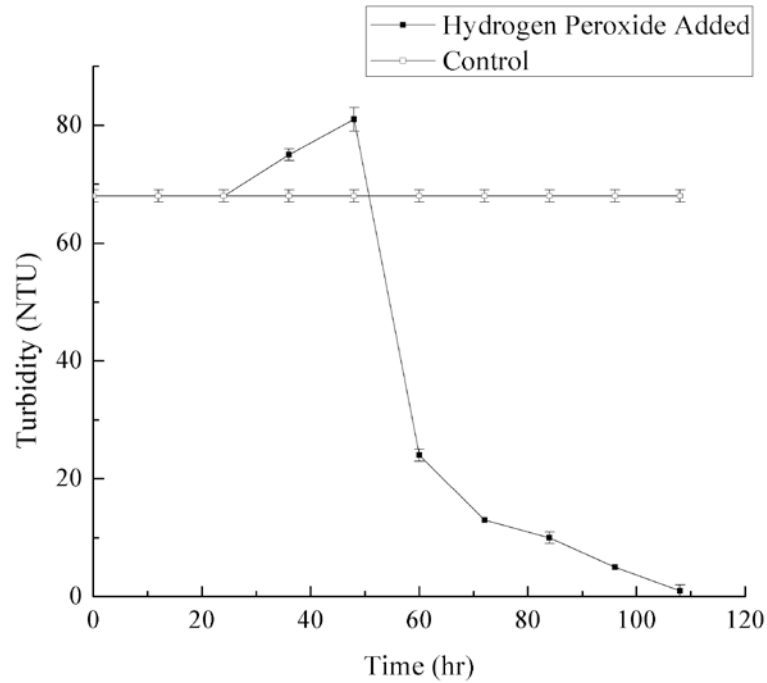


**Figure 4.36** Turbidity variation of Day 1 Flowback Water A sample after adding 1% hydrogen peroxide

Removal of the organic coating by oxidation leads to rapid agglomeration of these submicron particles and eliminates severe membrane fouling observed for some flowback water samples. Future studies should focus on the origin and characteristics of this organic coating and optimal treatment approaches for its removal.

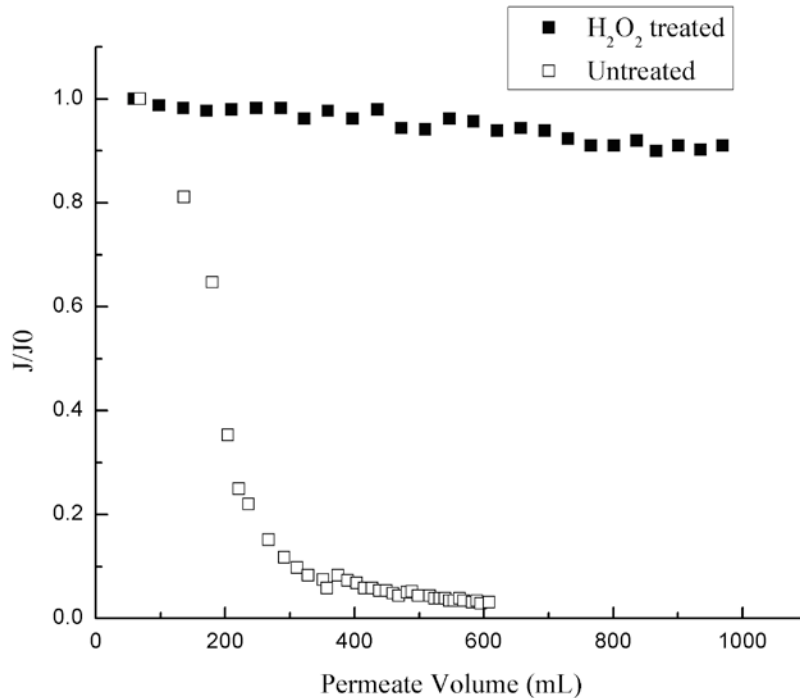


**Figure 4.37** Flux decline for H<sub>2</sub>O<sub>2</sub> treated and untreated Day 1 sample of Flowback Water A

### 4.3.3 Conclusions

A bench-scale dead-end microfiltration unit was used in this study to evaluate microfiltration for treatment of Marcellus shale flowback water to enable its reuse for hydraulic fracturing. In addition, AMD that is located in the vicinity of gas wells was evaluated as a potential make-up water source to reduce the fresh water use for hydraulic fracturing.

Mixing of AMD and flowback water results in the formation of barite solids that need to be removed prior to injection of this solution in the gas well to minimize the potential for well plugging. This study revealed that neither AMD nor barite formed in solution after mixing these two waters caused membrane fouling but that submicron particles present in some flowback waters can cause severe fouling of 0.22  $\mu\text{m}$  PVDF membrane. Severe microfiltration membrane fouling was observed for two out of three flowback water samples evaluated in this study. Both flowback water samples that caused severe membrane fouling contained submicron particles with a peak particle size close to the average membrane pore size. Analysis of filtration results revealed that complete blocking is the dominant fouling mechanism during the initial stages of filtration with subsequent cake layer formation contributing to the flux decline in the later stages of filtration.

Stable colloids that contributed to severe membrane fouling were only found in water samples collected in the first few days of the flowback period. EDX analysis revealed that these submicron particles are mainly comprised of iron oxide. The stability of submicron particles at very high ionic strength is due to organic coating of these particles. Removal of this organic layer by oxidation leads to particle aggregation and reduction in membrane fouling.

#### 4.3.4 References

Duclos-Orsello, C., Li, W. and Ho, C.C. (2006). A three mechanism model to describe fouling of microfiltration membranes. *Journal of Membrane Science*, 280, 856-866.

Edwards, P. J., Tracy, L. L. and Wilson, W. K. (2011). Chloride concentration gradients in tank-stored hydraulic fracturing fluids following flowback, US Department of Agriculture, Forest Service, Northern Research Station, Newtown Square, PA.

EPA (2011). Proceedings of the technical workshops for the hydraulic fracturing study: Chemical and analytical methods, Office of Research and Development, U.S. Environmental Protection Agency, Washington, DC.

Faibish, R.S., Elimelech, M. and Cohen, Y. (1998). Effect of interparticle electrostatic double layer interactions on permeate flux decline in crossflow membrane filtration of colloidal suspensions: an experimental investigation, *Journal of Colloid and Interface Science*, 204(1), 77-86.

Grace, H.P. (1956). Structure and performance of filter media. I. The internal structure of filter media. *AIChE J.*, 2: 307-315.

Grenier, A., Meireles, M., Aimar, M. and Carvin, P. (2008). Analysing flux decline in dead-end filtration. *Chemical Engineering Research and Design*, 86, 1281-1293.

Groundwater Protection Council, All Consulting (2009). Modern shale gas development in the United States: a primer, National Energy Technology Laboratory U.S. Department of Energy, Washington, DC.

Hermia, J. (1982). Constant pressure blocking filtration laws. Application to power-law non-Newtonian fluids. *Trans. I. Chem. E*, 60: 183-187.

Ho, C. C. and Zydney, A. L. (2000). A combined pore blockage and cake filtration model for protein fouling during microfiltration. *Journal of Colloid and Interface Science*, 232(2), 389-399.

Hotze, E. M., Phenrat, T. and Lowry, G. V. (2010). Nanoparticle aggregation: challenges to understanding transport and reactivity in the environment. *Journal of Environmental Quality*, 39(6), 1909-1924.

Howe, K.J. and Clark, M. M. (2002). Fouling of microfiltration and ultrafiltration membranes by natural waters, *Environmental Science & Technology*, 36(16), 3571-3576.

Huynh, K.A. and Chen, K.L. (2011). Aggregation kinetics of citrate and polyvinylpyrrolidone coated silver nanoparticles in monovalent and divalent electrolyte solutions, *Environmental Science & Technology*, 45(13), 5564-5571.

Jones, F., Oliviera, A., Parkinson, G. M., Rohl, A. L., Stanley, A. and Upson, T. (2004). The effect of calcium cations on the precipitation of barium sulfate 2: calcium ions in the presence of organic additives. *Journal of Crystal Growth*, 270(3-4), 593–603.

Koo, C.H., Mohammad, A.W., Suja, F. and Talib, M.Z.M. (2011). Review of the effect of selected physicochemical factors on membrane fouling propensity based on fouling indices, *Desalination*, 287, 167-177.

Paktinat, J., O'Neil, B., Aften C. and Hurd, M. (2011). Critical evaluation of high brine tolerant additives used in shale slickwater fracs, In *SPE Production and Operations Symposium*, Oklahoma City, OK.

Park, C., Kim, H. and Choi, S. (2006). Variation and prediction of membrane fouling index under various feed water characteristics, *Journal of Membrane Science* 284(1) (2006), 248-254.

Pincus, P. (1991). Colloid stabilization with grafted polyelectrolytes, *Macromolecules*, 24(10), 2912-2919.

Saleh, N., Kim, H.J., Phenrat, T., Matyjaszewski, K., Tilton, R.D., and Lowry, G.V. (2008). Ionic strength and composition affect the mobility of surface-modified FeO nanoparticles in water-saturated sand columns, *Environmental Science & Technology*, 42(9), 3349-3355.

Schäfer, A.I., Schwicker, U., Fischer, M.M., Fane, A.G. and Waite, T.D. (2000). Microfiltration of colloids and natural organic matter, *Journal of Membrane Science*, 171(2), 151-172.

Singh, G. and Song, L. (2008). Impact of feed water acidification with weak and strong acids on colloidal silica fouling in ultrafiltration membrane processes, *Water Research*, 42(3), 707-713.

Yiantsios, S. G. and Karabelas, A. J. (1998). The effect of colloid stability on membrane fouling, *Desalination*, 118(1), 143-152.

## **4.4 Evaluation of Coagulation/Flocculation for Solids Removal**

As membrane microfiltration is not always reliable to separate the suspended solids from the mixture of flowback water and AMD, the effectiveness of coagulation/flocculation for solids separation was studied. In this study, conventional coagulation/flocculation process was optimized with respect to mixing/settling time, pH and coagulant dosage. In addition, the conventional process is compared with ballasted flocculation that has smaller footprint and may be more suitable as a mobile treatment system.

The treated water quality from the conventional and ballasted flocculation processes are comparable with turbidity below 5 NTU despite the fact that the contact time required for the ballasted flocculation is just 10 min compared to 1 hour required for conventional treatment process.

### **4.4.1 Materials and Methods**

#### *4.4.1.1 Feed Water Characteristics*

Flowback Waters A, B and C, as well as AMD 1 to 5, are the same as the samples described in Chapter 4.3. Flowback Water D and AMD 6 were sampled from northeast Pennsylvania and were also used to evaluate the coagulation/flocculation process for solid removal. The flowback and AMD water pairs are summarized in Table 4.12. The main characteristics of the composite flowback water and AMD samples are listed in Table 4.13.

AMD 1 and 2 are nearby Site A, while AMD 3 and 4 are available in the vicinity of Site B. AMD 5 was taken from the vicinity of Site C while AMD 6 was located close to Site D. The AMD 1, 3 and 4 are untreated abandoned mine drainage, while AMD 2, 5 and 6 are treated mine drainage.



**Table 4.12** Flowback Water and AMD Pair Summary

Mixture No.	Flowback Water	AMD
1	20% FB A (composite)	80% AMD 1 (untreated)
2	30% FB A (composite)	70% AMD 2 (treated)
3	40% FB B (composite)	60% AMD 3 (untreated)
4	25% FB B (composite)	75% AMD 4 (untreated)
5	12% FB C	88% AMD 5 (treated)
6	25% FB D	75% AMD 6 (treated)

#### 4.4.1.2 Conventional Coagulation/Flocculation Process

Conventional coagulation/flocculation process was evaluated using six different combinations of actual Marcellus Shale flowback waters and AMDs that are available in their vicinity. Jar tests were conducted using PB-700 six-paddle jar tester (Figure 4.38). Each 1,000 mL beaker was filled with 500 mL of flowback and AMD mixture. The pH was monitored by a digital pH-meter that was calibrated daily with buffer solutions. Settled water samples were analyzed for turbidity.



**Figure 4.38** Six Paddle Jar Testers: PB-700 (Phipps & Bird, Richmond, VA)

**Table 4.13** Flowback and AMD water characteristics

Constitutes	Flowback Water				Acid Mine Drainage (AMD)					
	A	B	C	D	1	2	3	4	5	6
Na (mg/L)	27,946	18,766	28,643	28,368	281	687	104	145	1,899	1,424
Ca (mg/L)	15,021	3,496	28,249	34,247	353	245	76	77	50	6
Mg (mg/L)	1,720	614	3,513	5,060	53	33	49	38	104	67
Ba (mg/L)	236	1,204	5,887	2,350	0	0	0	0	0	0
Sr (mg/L)	1,799	625	9,000	7,000	0	3.0	1.5	0.7	0	0
Fe (Total) (mg/L)	ND	2.8	53.5	33.6	24.1	0	32.1	23.0	1.5	3.6
Cl (mg/L)	104,300	35,380	119,320	131,140	101	373	71	252	ND	ND
SO <sub>4</sub> (mg/L)	15	19	1	1	696	243	709	309	560	540
Alkalinity (mg CaCO <sub>3</sub> /L)	44	ND	ND	ND	62	394	41	50	ND	ND
pH	6.43	7.38	3.86	2.43	5.97	7.03	6.14	6.12	2.82	2.70
Turbidity (NTU)	42	54	0	0	1	7	2	0	0	0

G and Gt are important parameters in determining the mixing conditions for both rapid mixing reactor and flocculation reactor. Velocity gradient G is a parameter that can be used to express the power input as follows:

$$G = \left( \frac{P}{\mu V} \right)^{1/2} \quad (4-17)$$

where:

G = mean velocity gradient ( $s^{-1}$ )

P = the power dissipated in the water ( $N \cdot m \cdot s^{-1}$ )

V = volume of water to which the power is applied ( $m^3$ )

$\mu$  = absolute viscosity of the water ( $N \cdot s \cdot m^{-2}$ )

Acceptable Gt values range between  $10^4$  and  $10^5$  (Warren and Hammer, 1985). For high turbidity solutions as the ones used in this study, G typically ranges from  $30 s^{-1}$  to  $80 s^{-1}$ , while Gt is in the range of 36,000 to 96,000 (Davis and Cornell, 2008). As listed in Table 4.14, Gt values for coagulation and flocculation used in this study were 45,600 and 64,800, respectively.

**Table 4.14** The Gt values in the coagulation/flocculation process

Mixing rate (rpm)	Mixing time (min)	G value (sec <sup>-1</sup> )	Gt
300	1	760	45,600
25	30	36	64,800

Coagulation/flocculation process was optimized in terms of pH, coagulant dosage, and mixing/settling time. Optimization of pH was performed by mixing flowback water with its paired AMD at a predetermined mixing ratio. Ferric chloride was used as a coagulant at 20 mg/L as Fe and 0.1 M sodium hydroxide solution was used to adjust the pH. For Mixture 1, pH was adjusted to 5.00, 5.50, 6.00, 6.50, and 7.00; for Mixtures 2, 3 and 4, pH was adjusted to 6.25, 6.50, 6.75, and 7.00. Rapid mixing was conducted for one minute at 300 rpm ( $G = 760 sec^{-1}$ ) followed by slow mixing for 30 minutes at 25 rpm ( $G = 36 sec^{-1}$ ) and settling for 30 minutes. 50 mL of supernatant was collected from the beaker (depth of sample collection is 50 mm) and analyzed for treated water quality.

Once the optimum pH was determined, subsequent tests were carried out to determine the effect of coagulant dosage on finished water turbidity. Flowback water was mixed with its paired AMD water at a desired mixing ratio and pH was adjusted to optimized value determined in the previous step. For Mixture 1, coagulant dosage was adjusted to 20, 30, 40, 50, 60, 70 mg/L as Fe. For Mixtures 2, 3 and 4, coagulant dosage was adjusted to 15, 20, 25 and 30 mg/L as Fe. The rest of the procedure was identical to that used in the pH optimization test.

Slow mixing and settling time optimization was performed at pH and coagulant dosage at the optimum values obtained in previous steps. Slow mixing was varied between 15 or 30 minutes at 25 rpm and settling was conducted for 30 or 45 minutes. 50 mL of supernatant was collected from the beaker (depth of sample collection is 50 mm) and analyzed for treated water quality. Slow mixing and settling time optimization was only investigated for Mixture 1.

#### *4.4.1.3 Ballasted Flocculation*

Ballasted flocculation was tested using the pH and coagulant dosage at the optimum values determined from conventional coagulation/flocculation jar-tests. A total of 2.5 grams of microsand was added to a total mixture volume of 500 mL to achieve typical microsand dosage (5 g/L) for this process.

The initial mixing period of two minutes was followed by another three minutes of rapid mixing at 300 rpm. At that time, flocculant aid is added to the solution and mixing continued for another 15 seconds. Mixing intensity was reduced to 200 rpm for a period of 45 seconds followed by 4 min of settling time. 50 mL of supernatant was collected from the beaker (depth of sample collection is 50 mm) and analyzed for finished water turbidity.

#### *4.4.1.4 Settling characteristics of the sludge*

Settling properties of flocculated sludge were evaluated in a 1-L cylinder equipped with a diffuser stone. Aeration was used to suspended solids in order to obtain a more homogeneous aliquot for analysis. After mixing for two minutes, suspensions were allowed to settle and the sludge settling velocity was determined by observing the location of sludge interface with time.

## 4.4.2 Results and Discussion

### 4.4.2.1 Conventional Coagulation/Flocculation Jar Tests – Mixture 1

Coagulation is a process of aggregation of colloidal particles into large aggregates to obtain better settleability. Four mechanisms are involved in the coagulation process: double layer compression, charge neutralization, inter-particle bridging and particle enmeshment in the precipitate. It is known that pH is one of the key parameters that control the efficiency of coagulation/flocculation process for solids removal. The optimum pH for ferric ion as a coagulant typically ranges from 5 to 8. In general, primary mechanism of coagulation is charge neutralization at lower pH, while inter-particle bridging and enmeshment in the precipitate are the dominant mechanisms at higher pH. The impact of pH on the turbidity of treated Mixture 1 is shown in Figure 4.39. The result indicate that the turbidity of treated water can be reduced a desired level (5 NTU ) within a pH range of 5.5-6.5 while the optimum pH for turbidity removal in Mixture 1 is 6.0 (1 NTU).

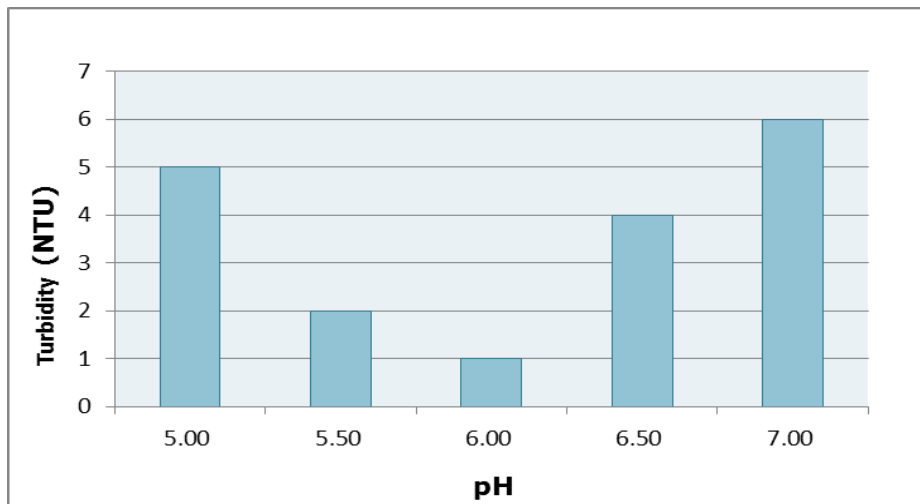


**Figure 4.39** Impact of pH on finished water turbidity in conventional flocculation process for Mixture 1

The coagulant dosage depends on the concentration of suspended solids in the mixture. Generally, the treatment efficiency in terms of turbidity removal is assumed to increase with increasing coagulant dosage. When the treatment efficiency reaches a maximum, finished water turbidity increases with the further addition of coagulant. Figure 4.40 demonstrates the results of

coagulant dosage optimization experiments using 15 and 30 minutes of slow mixing time followed by 30 minutes settling time.

When the slow mixing time was 15 minutes, the optimal coagulant dose was 50 mg/L. However, when the slow mixing time increased to 30 minutes, there were no significant differences between the coagulant dosage in the range from 20 to 70 mg/L as Fe, as the final turbidity of all samples was below 2.0 NTU (the treated turbidity decreased two to five times compared with the results obtained with the slow mixing time of 15 minutes). Therefore, the coagulant dosage of 20 mg/L and slow mixing time of 30 minutes are optimal parameters for the conventional coagulation/flocculation process.

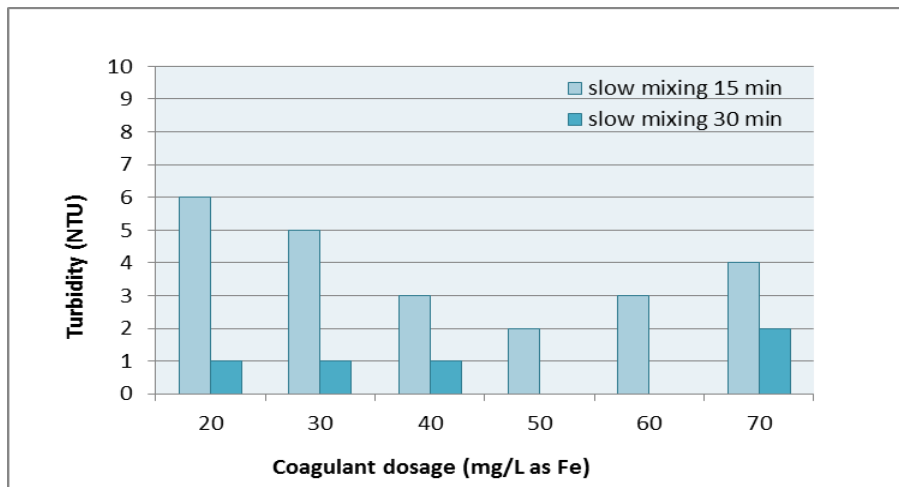


**Figure 4.40** Impact of coagulant dose and slow mixing time on finished water turbidity in conventional flocculation process for Mixture 1 with 30 min of settling

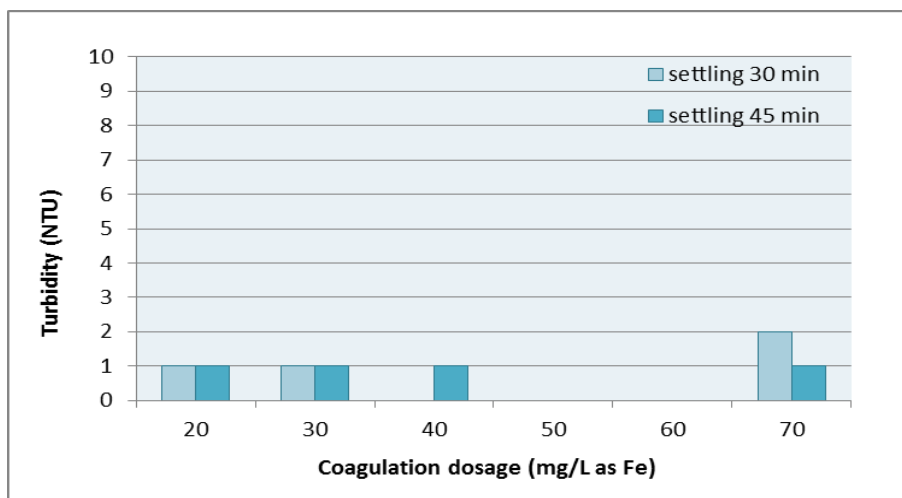


**Figure 4.41** Impact of coagulant dose and settling time on effluent turbidity in conventional flocculation process for Mixture 1 with 30 min slow mixing time

Optimization of the settling time using 30 minutes of slow mixing is shown in Figure 4.41. The variation in settling time from 30 to 45 minutes did not have significant impact on turbidity removal. Therefore, 30 min of settling is deemed sufficient for solids separation. In summary, the optimum coagulation conditions for Mixture 1 were pH 6.0, coagulant dose of 20 mg/L as Fe, 30 min of slow mixing and 30 min of settling.

#### 4.4.2.2 Conventional Coagulation/Flocculation Jar Tests – Mixtures 2, 3 and 4

Characteristics of feed water for these three mixtures are listed in Table 4.13. Mixture 2 is comprised of 30% Flowback (FB) water A and 70% AMD 2. Mixture 3 consists of 40% FB water B and 60% AMD 3. Mixture 4 contains 25% FB water B and 75% AMD 4. The initial sulfate concentration in Mixtures 2, 3 and 4 was 174 mg/L, 433 mg/L and 236 mg/L, respectively. The initial barium content of Mixtures 2, 3 and 4 was 71 mg/L, 496 mg/L and 291 mg/L, respectively. Mixture 2 had almost twice sulfate compared to barium, while Mixtures 3 and 4 had similar sulfate and barium mass ratios. The only difference between Mixtures 3 and 4 is that both sulfate and barium concentrations in Mixture 3 were nearly twice that in Mixture 4. All flocculation tests with these three mixtures were performed with one minute of rapid mixing, 30 min of slow mixing and 30 min of settling.

The optimization of solution pH for conventional coagulation/flocculation process for Mixtures 2, 3 and 4 using 30 minutes of slow mixing and 30 minutes settling is shown in Figure 4.42. As can be seen in this figure, pH variation in the range from 6.25-7.00 has significant impact on treated water turbidity. Based on these results, it can be concluded that all three mixtures achieved the lowest treated water turbidity at pH 6.50.

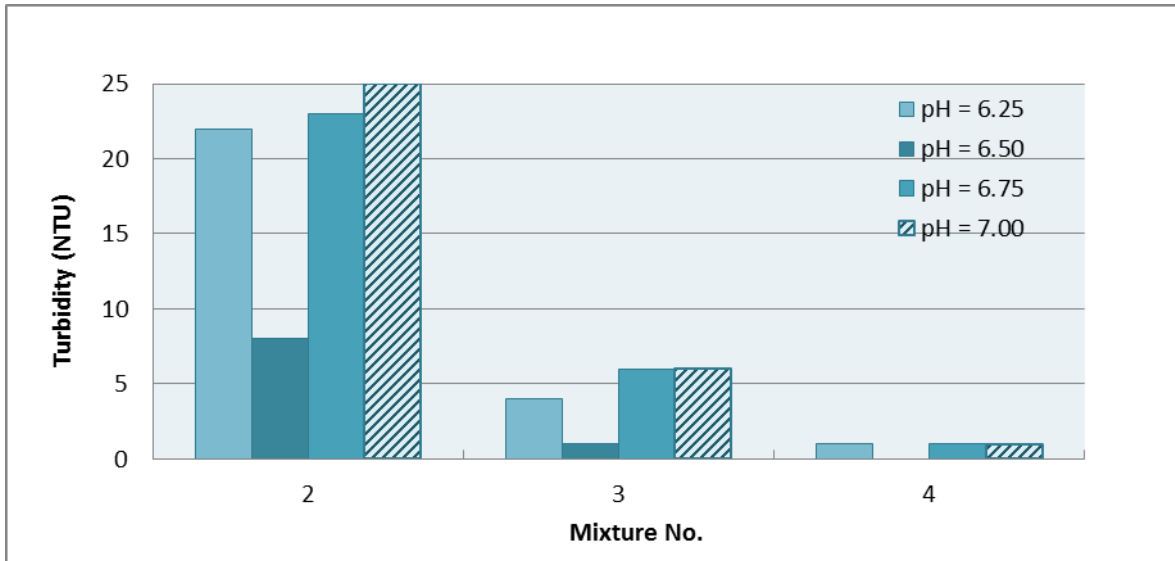
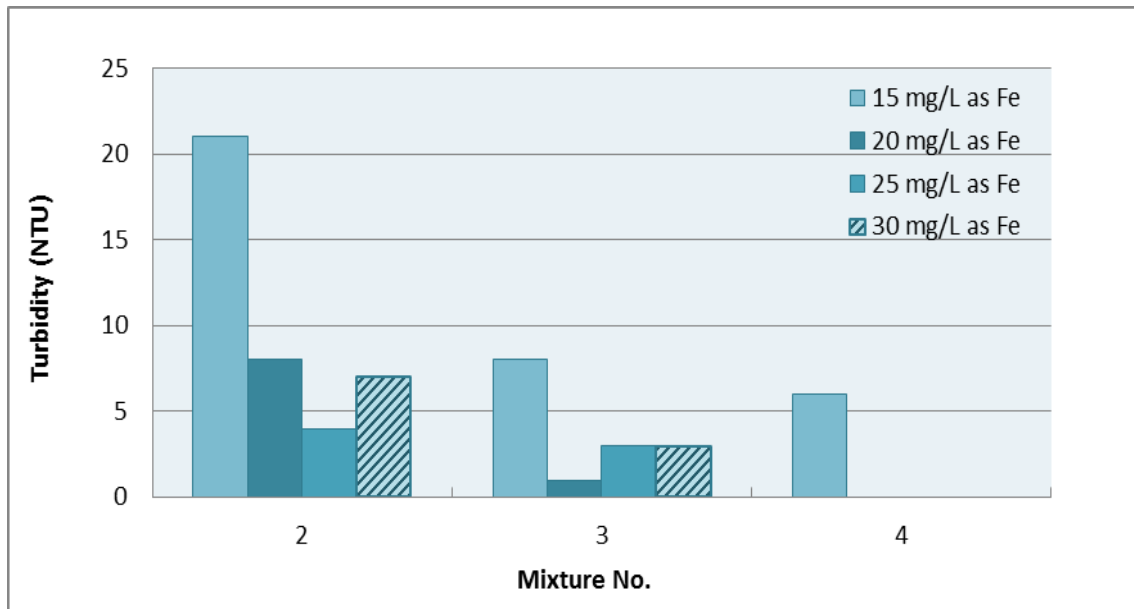


**Figure 4.42** Impact of pH on effluent turbidity for conventional flocculation process with Mixtures 2, 3 and 4 (Ferric Chloride Dosage = 20 mg/L as Fe)

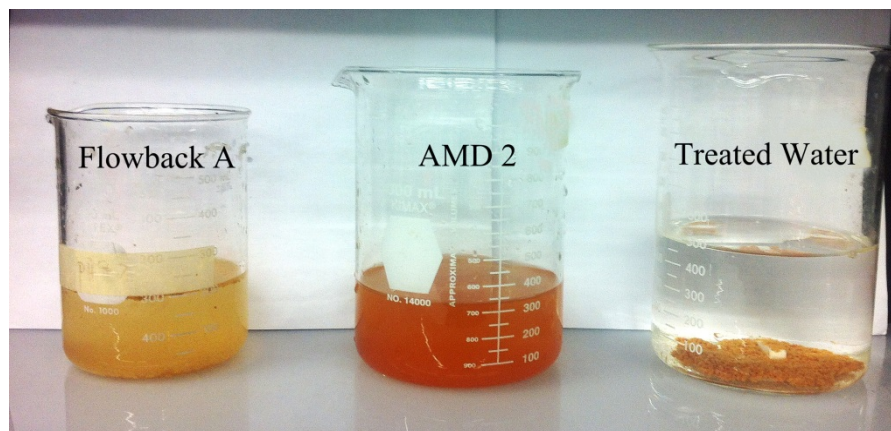
The results of coagulant dose optimization at pH 6.5 for Mixtures 2, 3 and 4 are shown in Figure 4.43. These results indicate that the optimal coagulant dose for Mixture 2 is 25 mg/L as Fe while 20 mg/L as Fe was sufficient to remove most of the turbidity for Mixtures 3 and 4. Based on the results with Mixtures 1 to 4, the optimum pH ranges turbidity removal is from 6.0 to 6.5, while the optimum coagulation dose is between 20 mg/L to 30 mg/L.

Figure 4.44 shows the appearance of Flowback Water A, AMD 2 and treated mixture from the conventional coagulation/flocculation/sedimentation process. Visible decrease in color and turbidity of treated water compared with both flowback and AMD is apparent in this figure.





**Figure 4.43** Impact of coagulant dose on effluent turbidity in conventional flocculation process with Mixtures 2, 3 and 4 at pH 6.5



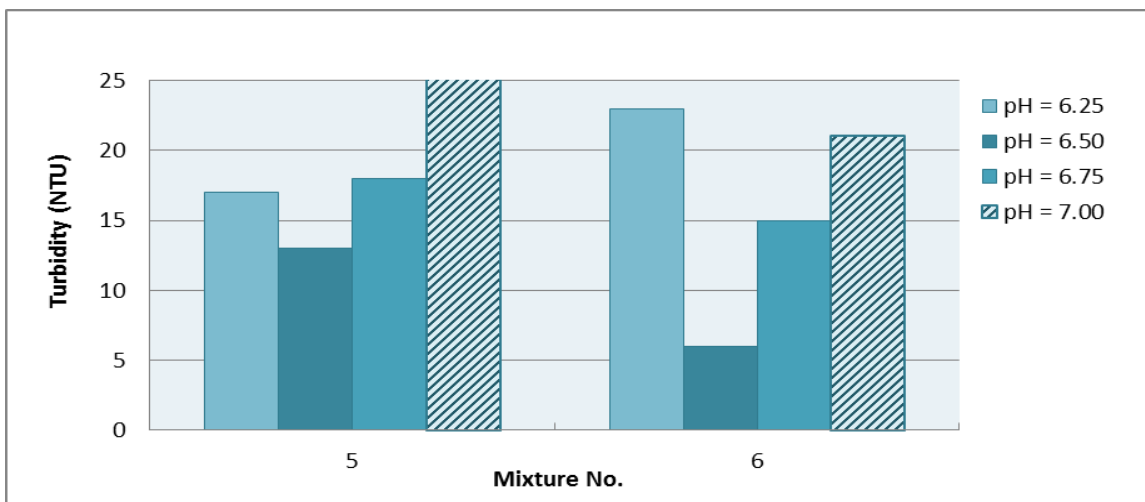
**Figure 4.44** Observation of feed water and effluent characteristics

#### 4.4.2.3 Conventional Coagulation/Flocculation Jar Tests – Mixtures 5 and 6

Characteristics of these three mixtures are listed in Table 4.13. The initial sulfate concentration in Mixtures 5 and 6 was 405 and 493 mg/L, respectively. The initial barium content of Mixtures 5 and 6 was 588 and 706 mg/L, respectively. Compared with Mixtures 1 to 4, Mixtures 5 and 6 have higher concentrations of sulfate and barium, and could produce more

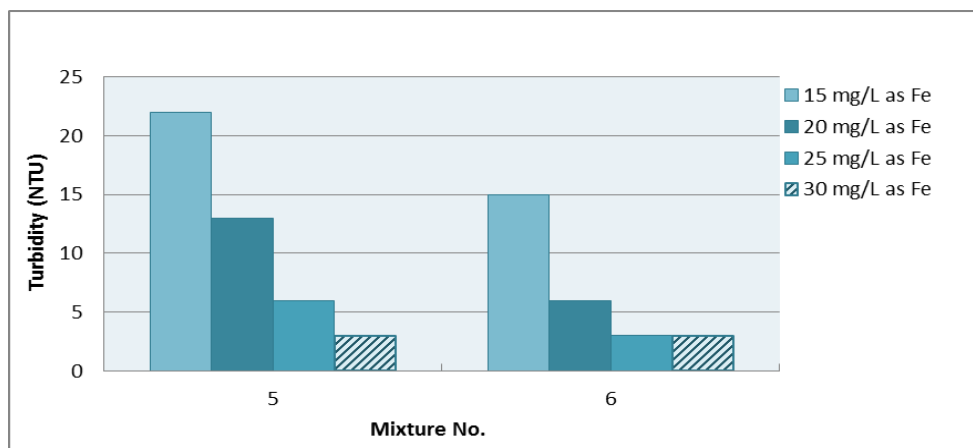
suspended solids after mixing. Since TSS of Mixture 5 and 6 is much higher, a higher coagulant dosage is expected.

Figure 4.45 indicates the impact of pH on effluent turbidity. As can be seen in this figure, variation of pH in the range from 6.25-7.0 has remarkable impact on treated water turbidity. Based on these results, it can be concluded that both mixtures achieved the lowest turbidity at pH 6.50. In addition, the coagulant dosage of 20 mg/L as Fe cannot reduce the turbidity to a desired value (5 NTU), which might be because the removal of higher solid concentration requires higher coagulant dosage.



**Figure 4.45** Impact of pH on effluent turbidity in conventional flocculation process with Mixtures 5 and 6 (Ferric Chloride Dosage = 20 mg/L as Fe)

The results of coagulant dose optimization at pH 6.5 for Mixtures 5 and 6 are shown in Figures 4.46. The treated water turbidity decreases with an increase in coagulant dosage, suggesting that higher coagulant dosage is required for the wastewater that has high TSS. The optimum coagulant dosage for Mixture 5 and 6 was 30 mg/L as Fe (Figure 4.46).



**Figure 4.46** Impact of coagulant dose on effluent turbidity in conventional flocculation process with Mixtures 5 and 6 at pH 6.5

The optimized conventional coagulation/flocculation process for the removal of suspended solids after mixing of flowback water and AMD includes rapid mixing at 300 rpm for one minutes, slow mixing at 25 rpm for 30 minutes and settling for 30 minutes. The optimal pH for this process is between 6.0 and 6.5 and the optimal coagulant dosage ranges from 20 mg/L to 30 mg/L as Fe. The treated water turbidity can be reduced to below 5 NTU for all the mixtures with conventional coagulation/flocculation process.

#### 4.4.2.4 Ballasted Flocculation – Mixture 1

Ballasted flocculation, also known as high rate clarification, features much smaller footprint compared to conventional process and is more suitable as a mobile treatment system for the co-treatment of flowback water and AMD. During ballasted flocculation process, microsand and flocculation aid are added to improve the settling properties of suspended solids by the enhancement of floc bridging. The impact of adding anionic and cationic flocculant aids was evaluated for the flowback water and AMD mixtures and their dosages were optimized to achieve lowest treated water turbidity.

The optimization of flocculant aid is shown in Figure 4.47. Four types of anionic polymers and four types of cationic polymers were tested at dosages of 1 ppm and 2ppm. In general, anionic flocculant aids performed better than most of the cationic polymers (Figure 4.47). Among the four different anionic flocculant aids tested in this study, Hydrex 6161 yielded best results with treated water turbidity below 1 NTU.

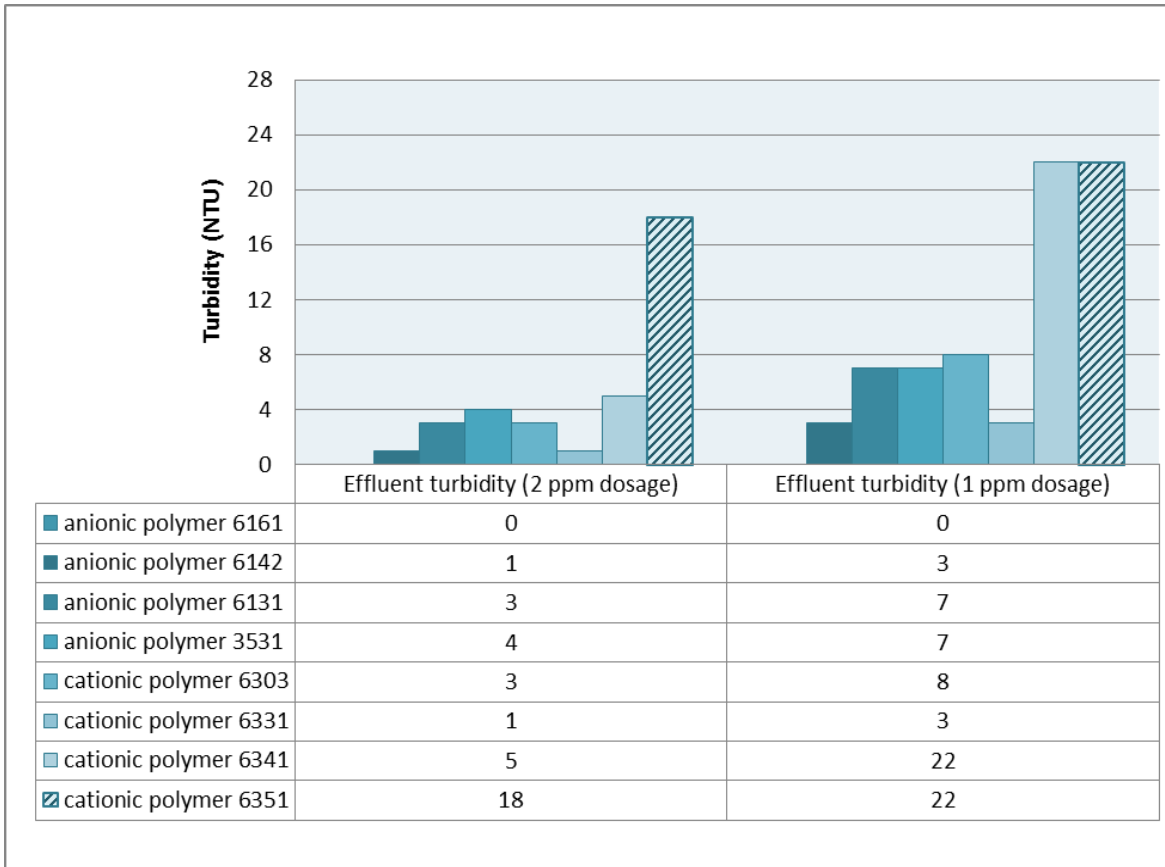


**Figure 4.47** Impact of flocculant aid type and dosage on turbidity of the treated water with ballasted flocculation for Mixture 1

The minimization of Hydrex 6161 dosage aims to reduce the operating cost of this treatment process. Adding 0.5 ppm of Hydrex 6161 resulted in treated water turbidity below 1 NTU, while further reduction to 0.2 ppm increased treated water turbidity to 4 NTU (Figure 4.48), which is still acceptable finished water quality. Consequently, the minimum dosage of anionic polymer Hydrex 6161 is 0.2 ppm.

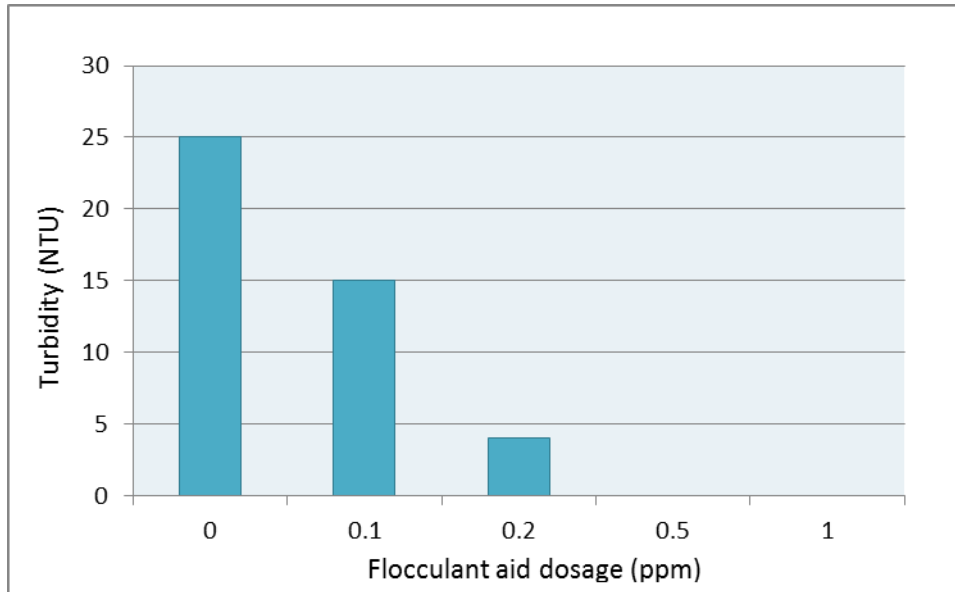


**Figure 4.48** Impact of Hydrex 6161 flocculant aid on ballasted flocculation of Mixture 1

#### 4.4.2.5 Ballasted Flocculation – Mixtures 2, 3 and 4

The results of flocculant aid optimization for Mixtures 2, 3 and 4 are shown in Figure 4.49. Four types of anionic polymers and four types of cationic polymers were tested at a dosage of 1 ppm. The results shown in Figure 4.49 indicate that anionic flocculant aids also performed better than cationic polymers for these mixtures of flowback water and AMD. Hydrex 6161 exhibited best performance as the treated water turbidity for all three mixtures was below 2 NTU. These results are very similar to those obtained with Mixture 1.

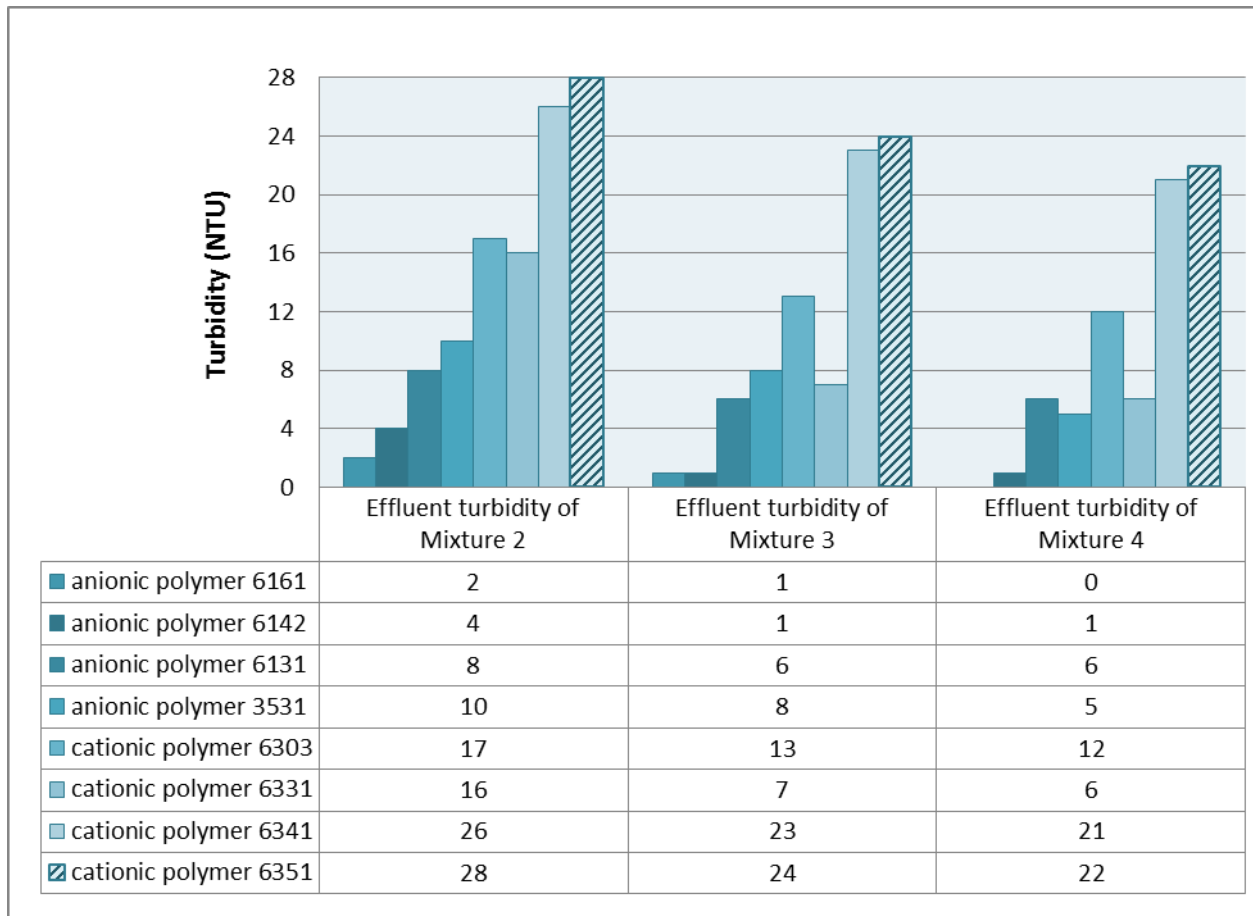


**Figure 4.49** Impact of flocculant aid type on turbidity of the effluent from ballasted flocculation with Mixtures 2, 3 and 4 at flocculant aid dosage of 1 ppm

In order to reduce the operating cost, the impact of flocculation aid dosage on finished water turbidity was evaluated in this study. Figure 4.50 indicates that adding 0.5 ppm of Hydrex 6161 to Mixture 2 could achieve treated water turbidity of 6 NTU, while 0.2 ppm was sufficient to achieve equal or better effluent turbidity for Mixtures 3 and 4. Similar to the results obtained with Mixture 1, the turbidity removal increases with an increase in polymer dosage.

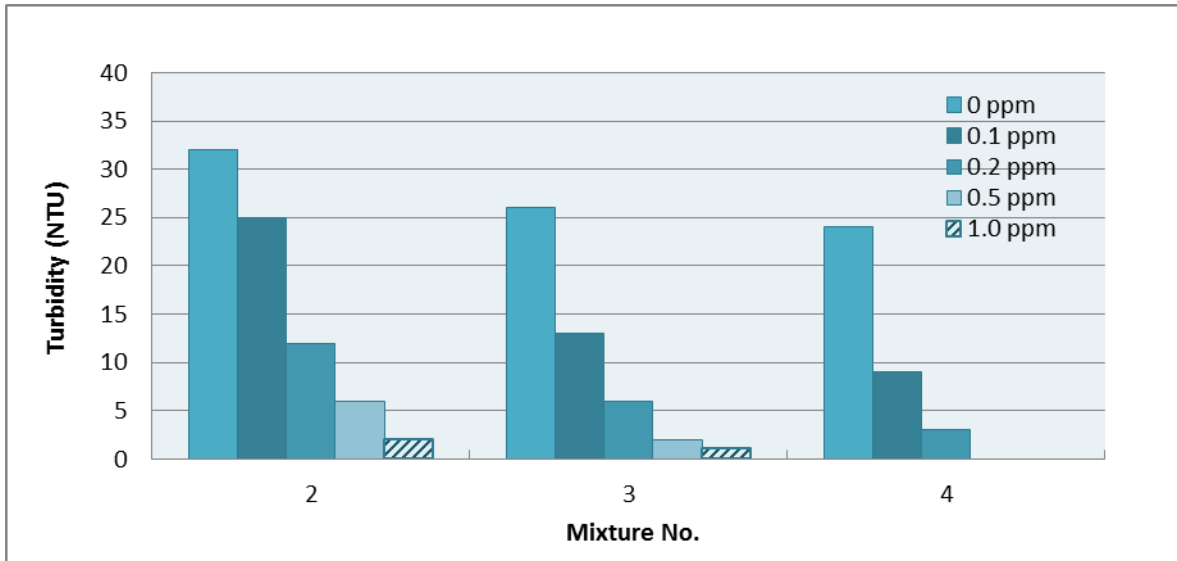


**Figure 4.50** Impact of Hydrex 6161 on ballasted flocculation with Mixtures 2, 3 and 4

#### 4.4.2.6 Ballasted Flocculation – Mixtures 5 and 6

Based on the results obtained for Mixtures 1, 2, 3 and 4, anionic flocculant aid Hydrex 6161 was used as coagulant aid for solids removal from Mixtures 5 and 6. Figure 4.51 reveals that adding 0.5 ppm of Hydrex 6161 to Mixtures 5 and 6 can reduce treated water turbidity below 5 NTU.

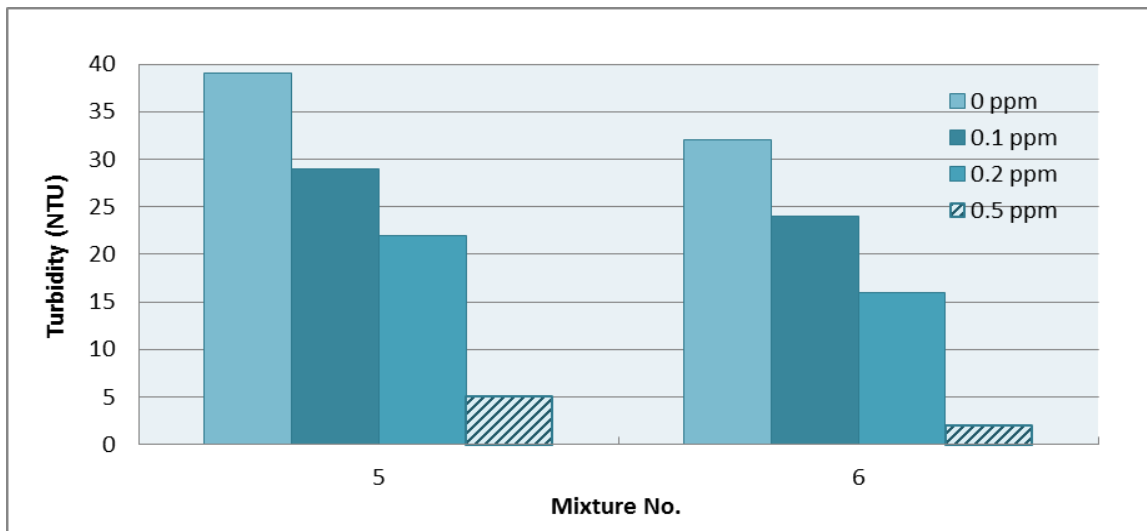


**Figure 4.51** Impact of Hydrex 6161 on ballasted flocculation with Mixtures 5 and Mixture 6

#### 4.4.2.7 Settling properties of the sludge

Sludge settling characteristics were studied for Mixture 3 with solids concentration of around 10,000 mg/L where interactions between particles are important in the overall settling behavior of the solids. Settling under these conditions is classified as Type II settling because the solid suspension tends to settle as a zone or a blanket where solids maintain the same position relative to each other. There is usually a distinct clarified zone showing a liquid-solid interface.

The settling and compaction curves are developed by plotting the height of the sludge interface versus time of settling. Figure 4.52 shows the settling curve of conventional flocculated sludge, while Figure 4.53 presents the settling curve of ballasted flocculated sludge. Comparison among these two coagulation/flocculation processes reveals that flocs generated in ballasted flocculation process have much better settling properties. Therefore, the ballasted flocculation process is more suitable for a mobile treatment, since much shorter hydraulic retention time of the overall process would be required.

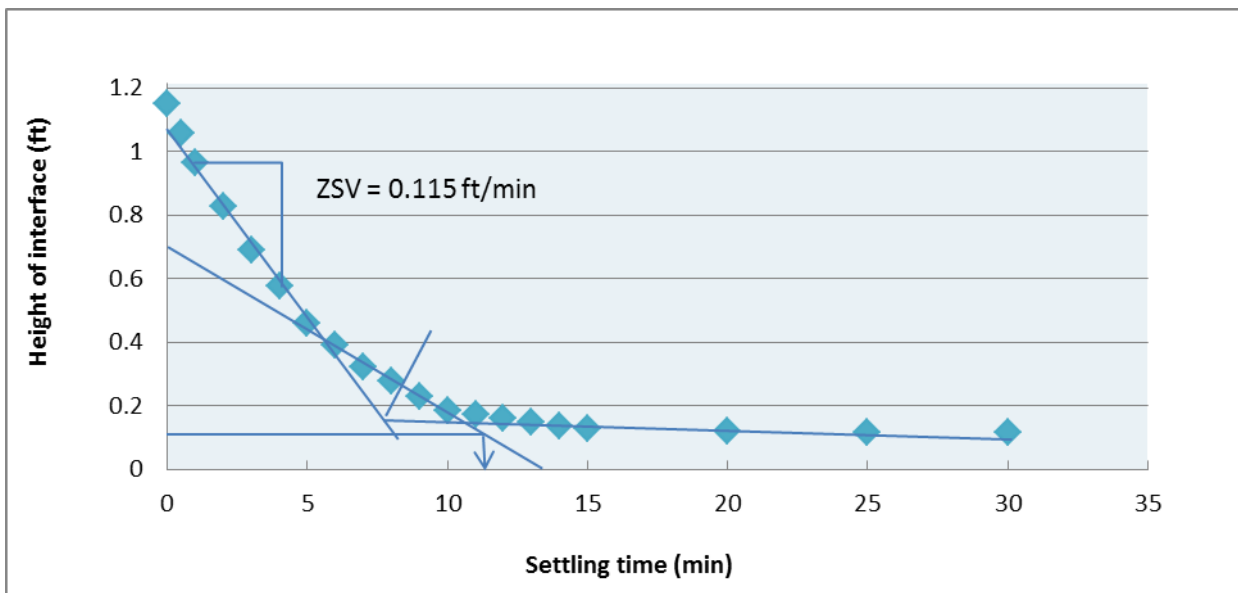


**Figure 4.52** Settling curve of conventional flocculated sludge



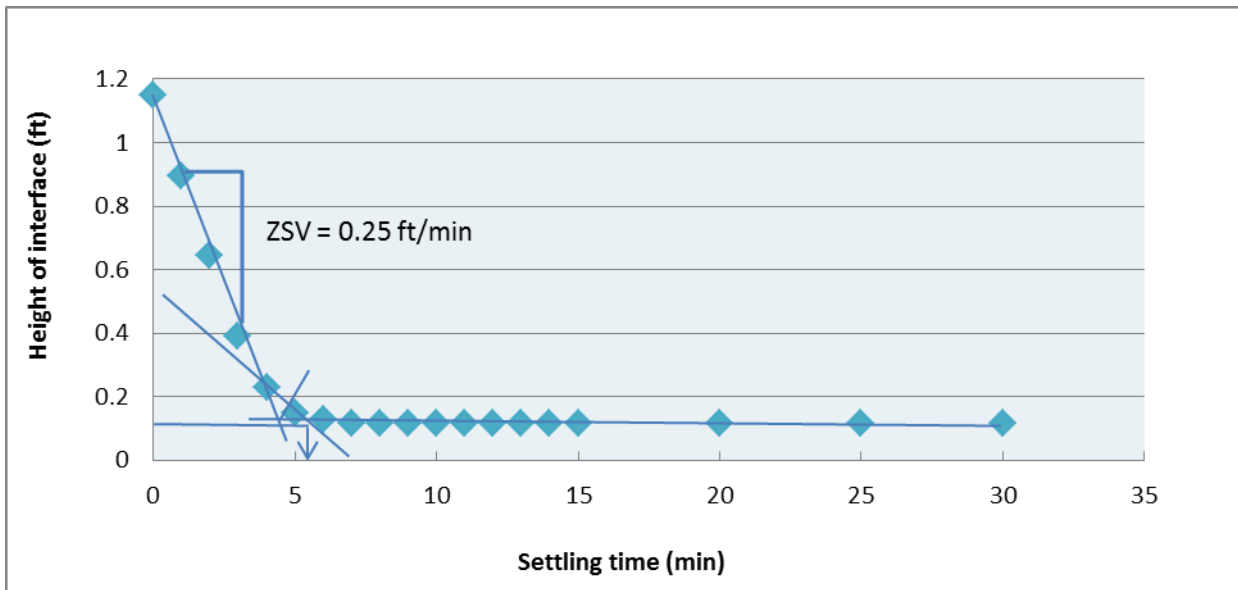


**Figure 4.53** Settling curve of ballasted sand flocculated sludge

#### 4.4.3 Conclusion

The treated water quality with respect to turbidity from the conventional and ballasted flocculation processes were comparable (i.e., below 5 NTU) despite the fact that the contact time required for the ballasted flocculation is ten minutes compared to one hour required for conventional treatment process.

For conventional coagulation/flocculation process, the optimum pH was in the range 6.0 to 6.5 and the optimum coagulant dosage was in the range from 20 to 30 mg/L as Fe. A decrease in slow mixing time from 30 min to 15 min resulted in an increase in treated water turbidity, suggesting that a relative longer flocculation time is required to achieve more complete solids removal by settling. The variation in settling time between 30 and 45 min did not have a significant impact on the finished water turbidity.

In general, anionic flocculant aids were found to work better than cationic flocculant aids for ballasted sand flocculation process. Most anionic flocculant aids helped to reduce turbidity of the finished water to a desired level. Among the anionic polymers tested in this study, Hydrex 6161 performed the best for all flowback and AMD mixtures tested in this study. The minimum flocculant aid dosage ranged from 0.2 mg/L for Mixtures 1, 3 and 4 to 0.5 mg/L for Mixtures 2, 5 and 6.

Previous chapter reveals that significant membrane fouling will potentially occur when filtering the mixture of flowback water and AMD. Therefore, coagulation/flocculation process is more suitable for the solid separation after mixing flowback water and AMD and it will be evaluated in the pilot-scale test.

#### **4.4.4 References**

Davis, M. L., & Cornwell, D. A. (2008). Introduction to environmental engineering. McGraw-Hill Companies, New York City.

Warren, Viessman, and Hammer, M.J. (2008). Water supply and pollution control. Prentice Hall, New Jersey.

## **5.0 Field Demonstration of the Treatment System**

Flowback water generated during shale gas extraction in Pennsylvania is mostly reused for hydraulic fracturing operation. Acid mine drainage (AMD), one of the most serious threats to water quality in Pennsylvania, can potentially serve as a make-up water source to enable flowback water reuse. This study demonstrates co-treatment of flowback water and AMD produced in northeastern Pennsylvania in a pilot-scale system consisting of rapid mixing reactor, flocculation tank and sedimentation tank. Sulfate concentration in the finished water can be controlled at a desired level (i.e., below 100 mg/L) by adjusting the ratio of flowback water and AMD in the influent. Ferric iron contained in the AMD can serve as a coagulant to enhance the removal of suspended solids, during which total iron is reduced to a desirable level.

### **5.1 Materials and Methods**

#### **5.1.1 Characteristics of Flowback Water and AMD**

Flowback water and AMD were collected from sites in northeastern Pennsylvania and stored in 20,000 gallon frac tanks for use in the pilot-scale study (Figure 5.1). Characteristics of these impaired waters sampled from the storage tanks are summarized in Table 5.1. The flowback water used in this study contains much higher concentrations of divalent cations compared with the flowback water from southeast PA reported previously (He et al., 2014a; He et al., 2014c; He et al., 2013; Kondash et al., 2013) and is in agreement with the water quality model developed by Barbot et al. (2013).



**Figure 5.1** Frac tanks for flowback water and AMD storage

**Table 5.1** Characteristics of flowback water and AMD

Constitutes	Flowback Water	AMD
Na <sup>+</sup> (mg/L)	31,382	37.6
Ca <sup>2+</sup> (mg/L)	31,270	66.3
Mg <sup>2+</sup> (mg/L)	1,590	82
Ba <sup>2+</sup> (mg/L)	19,763	-
Sr <sup>2+</sup> (mg/L)	16,141	-
Cl <sup>-</sup> (mg/L)	152,213	166
SO <sub>4</sub> <sup>2-</sup> (mg/L)	-	275
Fe (III) (mg/L)	-	29.7
Fe (II) (mg/L)	28.2	5.9
Ra-226 (pCi/L)	15,570	-
Ra-228 (pCi/L)	1,385	-
pH	6.2	2.6

Based on the analysis of 140 AMD samples, Cravotta demonstrated that pH of AMD varies widely from 2.7 to 7.3, with the majority being either acidic or neutral (Cravotta, 2008). AMD generally contains dissolved iron and the concentration can vary from below 0.1 mg/L to a few hundred mg/L (Cravotta, 2008). Low-pH AMD can contain both ferric and ferrous iron, and the ratio depends on geological conditions (Wei and Viadero, 2007; Druschel et al., 2004). The non-treated AMD used in this study is acidic and rich in ferric iron, which is consistent with the study that sampled AMD from the same region (Ott, 1986). Although ferric hydroxide can precipitate to form hematite, this process is limited kinetically as it will take over 4 months to accomplish the precipitation reaction considering the pH and ferric iron concentration of AMD (Cornell et al., 1989).

The sulfate concentration in the AMD collected for this study was very low compared to the barium concentration in the flowback water (Table 5.1). If the AMD percentage in the mixture corresponded to the unrecovered fraction of hydraulic fracturing fluid (i.e., 90% on average) (Vidic et al., 2013), the sulfate concentration in the effluent would be negligible because of the high molar ratio of barium to sulfate (5.6:1). Therefore, sulfate concentration in actual AMD and barium concentration in the flowback water were adjusted to represent more challenging treatment conditions by adding Na<sub>2</sub>SO<sub>4</sub> to AMD and diluting flowback water to achieve initial concentration indicated in Table 5.2.

**Table 5.2** Barium and sulfate in flowback water and AMD after adjustment

Concentration	Barium (Flowback Water)	Sulfate (AMD)	Mixing ratio (Flowback: AMD)
Low	11,474	1,172	1:9
High	19,115	2,150	1:8

The adjustment of barium and sulfate was determined in the field with turbidimetric method and validated by laboratory analysis

### 5.1.2 Pilot-scale Operation

Unit processes in the pilot-scale treatment system included rapid mixing, flocculation, sedimentation and sludge recycling (Figure 5.2). Two 25-gallon tanks equipped with variable-speed electric mixers (80-4000 RPM) were used as rapid mixing tank and AMD mixing tank. The mixing speed of rapid mixers was approximately 1600 rpm based on the conversion from power

input. A 300-gallon tank equipped with paddle mixer was used as flocculation tank with the mixing speed used for flocculation adjusted to 8 RPM. A 500-gallon cone-bottom settling tank was equipped tube settler to ensure better separation of suspended solids. The detailed designs for the paddle mixer, flocculation tank, settling tank are shown in Appendix II. The total influent flow rate of flowback water and AMD was targeted at 5 GPM, while the flow rate of the recycled sludge was targeted at 5 GPM. The TSS of the sludge was 7.5% and the diaphragm pump was used to recycle such high solids concentration back to AMD mixing reactor.

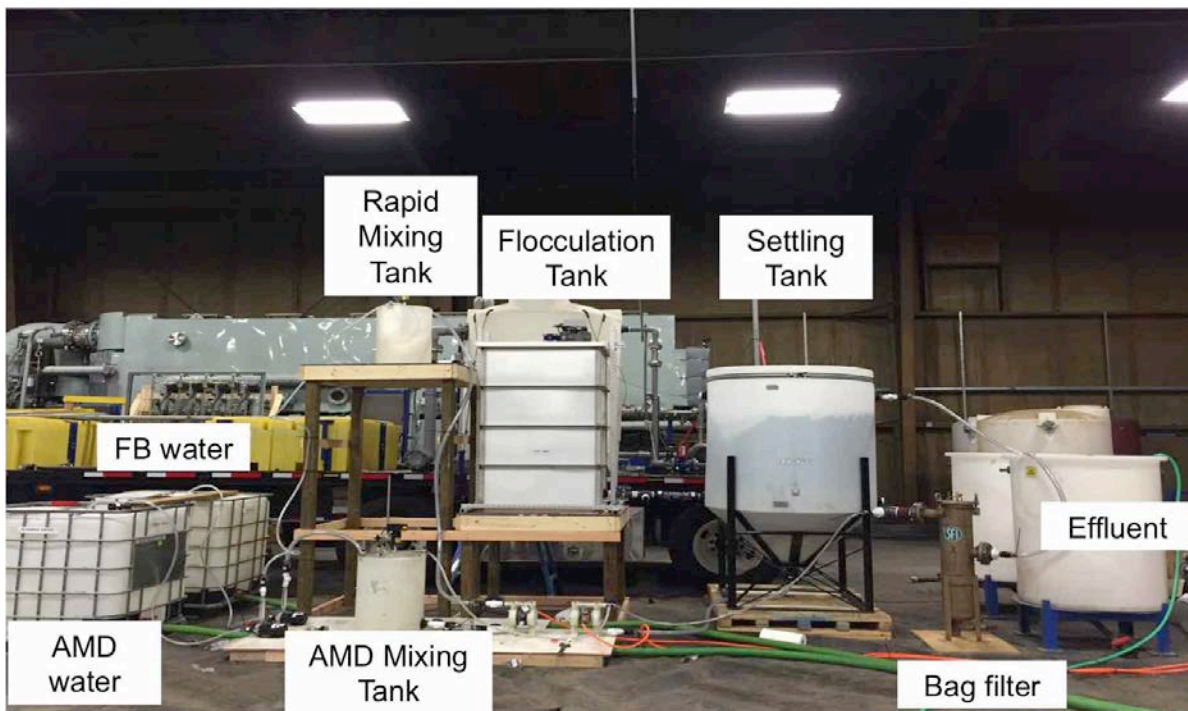


**Figure 5.2** Pilot-scale Treatment System Installed in Tioga County

Prior to pilot-scale tests, bench-scale study using a six-paddle jar tester (Phipps & Bird, Richmond, VA) was conducted to find optimal operating conditions for turbidity and iron removal. Rapid mixing in these tests was conducted for 1 min at the speed of 300 rpm followed by slow mixing for 25 min at speed of rpm and settling for 30 min.

### 5.1.3 Analytical Methods

Cation and anion analysis in the laboratory was performed using atomic absorption spectroscopy (Perkin-Elmer model 1000 AAS) and ion chromatography (Thermo Scientific, ICS-1100), respectively. Filtered samples for AAS analysis were diluted with 2% nitric acid and 0.15% KCl solution to eliminate ionization interference during AAS analysis for Ba and Sr (Barbot et al., 2013 He et al., 2014a). For dissolved iron analysis, samples were filtered with 0.22- $\mu\text{m}$  membrane to eliminate the interference of sub-micron particles with significant iron content (He et al., 2014b).

A high-resolution Apex Gamma spectrometry system (Ortec, Oak Ridge, TN) with a high-purity Germanium detector was used to quantify the activity of radionuclides. Prior to Ra analysis, samples were placed in 47 mm petri dishes, sealed by vinyl electrical tape, and kept for at least 2 days to ensure equilibrium between Ra-228 and Ac-228. Ra-226 activity was analyzed by measuring gamma ray emission at 186 KeV, while Ac-228 activity was analyzed based on multiple gamma ray emissions at 270, 338, 911, and 964 KeV. Ra-228 activity was calculated based on the activity of its equilibrium progeny Ac-228.

Figure 5.3 illustrates the analytical instruments for on-site measurement, including Hach colorimeter, pH meter, oven, vacuum pump, hot plate, filtration cell and balance. The on-site measurements for barium (Hach Method 10251) and sulfate (Hach Method 8051) were conducted using Hach turbidimetric method. Comparison between Hach method and AAS method for dissolved barium and ion chromatography for sulfate measurement was performed under the conditions that are relevant for shale gas wastewater. It was found that dissolved sulfate measurements by these two analytical methods were in good agreement (data not shown). However, for barium analysis, the turbidimetric method is reliable when strontium concentration is close to or less than barium concentration (Hach Method 10251). The total dissolved iron and ferrous iron on site analyses were conducted by FerroVer Method (Hach Method 10249) and 1,10-phenanthroline method (Hach Method 8146), respectively. The ferric ion concentration was calculated from the difference between total iron and ferrous iron concentration.



**Figure 5.3** Instruments for on-site measurement

## **5.2 Results and Discussion**

### **5.2.1 Sulfate Removal**

Presence of dissolved sulfate in the fracturing fluid is of concern because of the potential to cause mineral scaling, particularly in Marcellus Shale that is rich in Ba, Sr and Ca (He et al., 2014a; He et al., 2013). Therefore, the sulfate concentration in the hydraulic fracturing fluid is generally limited to 100 mg/L (He et al., 2013). It was previously reported that mixing of AMD and flowback water requires more than 10 hours to reach precipitation equilibrium as indicated by conductivity analysis (Kondash et al., 2013). He et al. (2014a) reported that barium sulfate precipitation is very rapid and reaches equilibrium within 30 min when excess sulfate is added to flowback water, while Sr concentration would keep declining for more than 24 hours. Because the target sulfate concentration in hydraulic fracturing fluid is below 100 mg/L and it is desirable to minimize the size of the treatment plant, slow celestite and gypsum precipitation reactions were not considered in this study for the control of sulfate in the finished water.

The flow rates of flowback water and AMD were determined based on the thermodynamic prediction of sulfate concentration in equilibrium with barite solids. Sulfate



concentration measurement in the treatment system revealed that barite precipitation reaction proceeded rapidly in the mixing reactor and reached equilibrium after the flocculation tank (Figure 5.4). Such behavior was expected because the barite saturation index ( $SI = \log \frac{Ion\ Activity\ Product}{K_{sp}}$ ) was greater than 4.0 for all experimental conditions evaluated in this study, which corresponds to rapid barite precipitation (He et al., 2014a). Another observation from results in Figure 5.4 is that the sulfate concentration in treated water is reduced to below 100 mg/L for all three experimental conditions by adjusting the mixing ratio of flowback water and AMD.

The average sulfate consumption rates in the rapid mixing reactor were 2.0 and 4.2 mM/(L•min) for low and high concentrations, respectively. This increase in sulfate consumption was due to an increase in barite SI from 4.41 to 4.72.

Experiments conducted at low concentrations with sludge recycle had SI of 4.08 because of dilution, but the TSS in the mixing reactor increased over 19 times when compared to the test without sludge recycle. Decrease in saturation index will lead to lower homogeneous nucleation rate, while the increase in seed concentration will increase the seeded growth rate (Nancollas and Purdie, 1964). The average sulfate consumption rate in the mixing reactor increased to 2.15 mM/(min L) due to sludge recycling, suggesting that the growth of existing particles in the reactor was promoted.

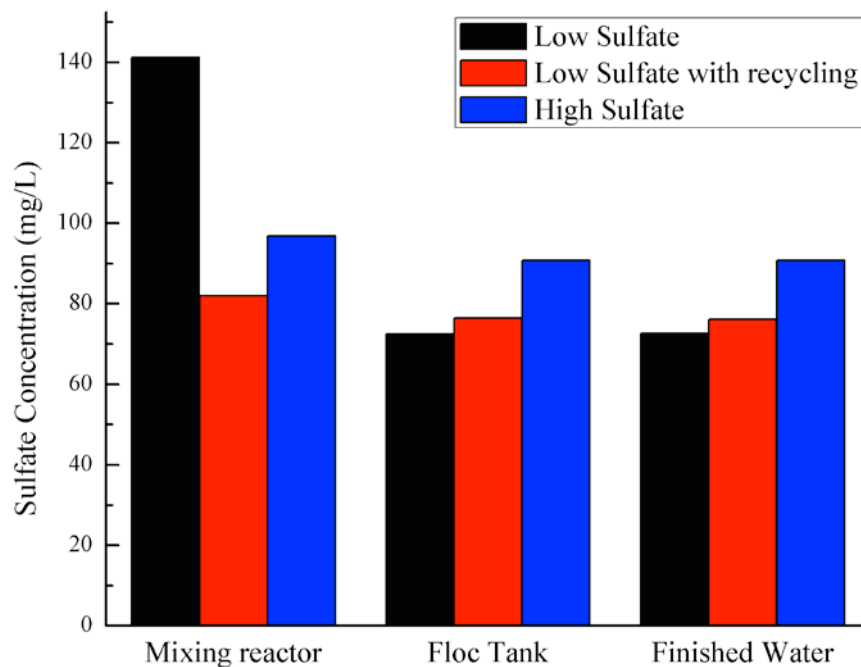


**Figure 5.4** Sulfate concentration in the treatment units in pilot-scale experiments

It was reported that barium sulfate precipitation reaction could become very slow and require over 5 hours to reach equilibrium when the initial saturation for barite is low (e.g.,  $SI < 2.20$ ) (He et al., 2014a). For such case, the sludge recycling will become very beneficial to increase barite precipitation rate by promoting the seeded growth.

## 5.2.2 AMD as a source of coagulant

Dissolved iron typically present in AMD can potentially serve as the internal coagulant for agglomeration of barite particles that precipitate in the system. Salama et al. (2015) reported that AMD was useful for coagulating microalgae biomass at pH between 7 and 9. Sun et al. (2013) studied As removal by coagulation with Fe (III) formed in situ from AMD. Previous laboratory-scale study found that coagulation with ferric chloride was an effective process for the removal of the suspended solids formed by mixing flowback water and AMD and that the treated water turbidity can be reduced to below 5 NTU with ferric chloride dosage of 20-60 mg/L as Fe at pH 6.0-7.0 (Zheng, 2013). This study evaluated the feasibility of using iron in AMD for the coagulation process to reduce the cost and total life cycle impact of the proposed use of AMD as make up water up water for hydraulic fracturing.

The AMD used in this study is rich in ferric iron, while the flowback water sample contains ferrous iron (Table 5.1). The pilot-scale experiment where pH of the solution was adjusted with NaOH was conducted at low sulfate concentration. The initial concentrations of ferric and ferrous ions in the mixture were 26.7 mg/L and 8.1 mg/L, respectively. Prior to pilot-scale experiment, laboratory studies revealed that the optimum pH for turbidity and iron removal was between 7.0 and 7.5, when the turbidity of the supernatant was reduced to 2 NTU, while the total iron was reduced to 0.1 mg/L. The coagulant dosage used in this study is in agreement with the effective range of ferric chloride dosage reported previously (Zheng, 2013).

Turbidity and total iron in the effluent from the pilot system at pH 7.5 were 3 NTU and 0.1 mg/L, respectively, indicating that iron contained in the wastewater effectively served as coagulant to promote agglomeration of barite particles and lead to their effective removal in the settling tank. Although aeration was not applied in the pilot-scale system, the total iron was reduced to a desired level (0.1 mg/L) at pH 7.5. The dissolved iron concentrations in rapid mix reactor, flocculation tank and settling tank are shown in Figure 5.5. As the difference between total dissolved iron concentration and ferrous ion concentration is below the detection limit of the analytical method used in this study (i.e., 0.1 mg/L), the ferric ion concentration was not shown in this figure.

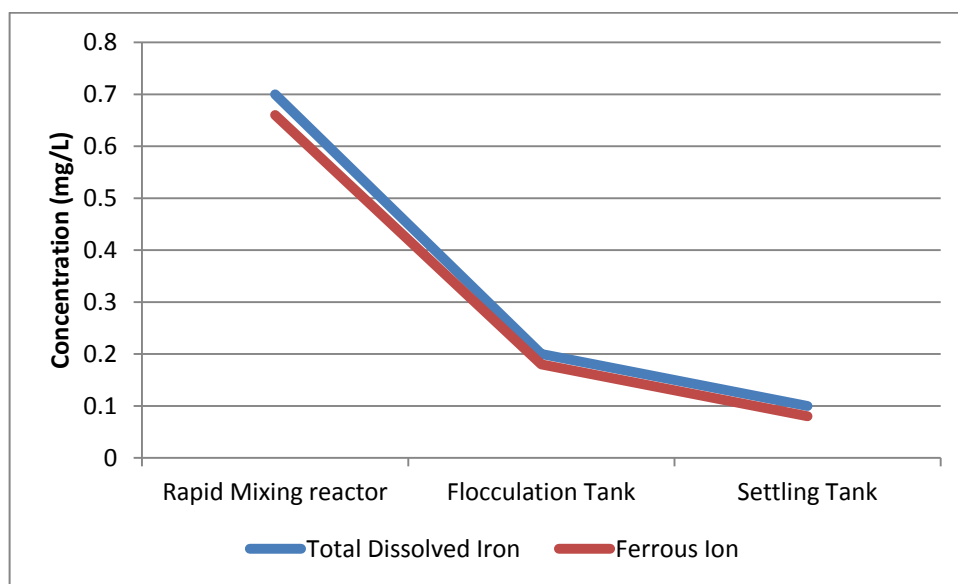


**Figure 5.5** Dissolved iron concentration in the treatment system at low concentration condition with pH adjustment

To better understand the rapid removal of ferrous iron, its concentration was predicted with the kinetic model developed by Singer and Stumm (1970). The rate equation was incorporated into PHREEQC software to account for the ion complexation and activity adjustment. The dissolved oxygen concentration was assumed to be 4 mg/L. Kinetic model prediction was that ferrous iron should be reduced from 8.1 to 5.8 mg/L after 1 min of contact time. Jar test results revealed that the ferric ion concentration rapidly decreased from 26.7 mg/L to 0.12 mg/L after rapid mixing (1 min), while the ferrous ion concentration was reduced from 8.1 mg/L to 0.78 mg/L. The difference between measured and predicted ferrous concentration suggests that the reduction of ferrous iron in the rapid mix reactor was likely due to incorporation of  $\text{Fe}^{\text{II}}$  into ferric hydroxide by coprecipitation reaction (Tronc et al., 1992 Wei and Viadero, 2007) rather than oxidation reaction. As the ferric hydroxide precipitation essentially reached equilibrium after rapid mixing reactor, the subsequent iron removal in flocculation tank and settling tank was likely attributed to the oxidation of  $\text{Fe}^{\text{II}}$  to  $\text{Fe}^{\text{III}}$ , followed by rapid precipitation as ferric hydroxide.

When sludge recycling was initiated at pH 7.5, the treated water turbidity increased to 16 NTU (Figure 5.6), which was likely due to the fact that the iron concentration in the mixture and hydraulic retention time in the flocculation tank and settling tank were halved due to flow of

sludge back to the influent of the pilot-scale system. Therefore, 1 mg/L of polymeric coagulant was added in the rapid mix reactor, which was effective in reducing the effluent turbidity to 2 NTU (Figure 5.6).

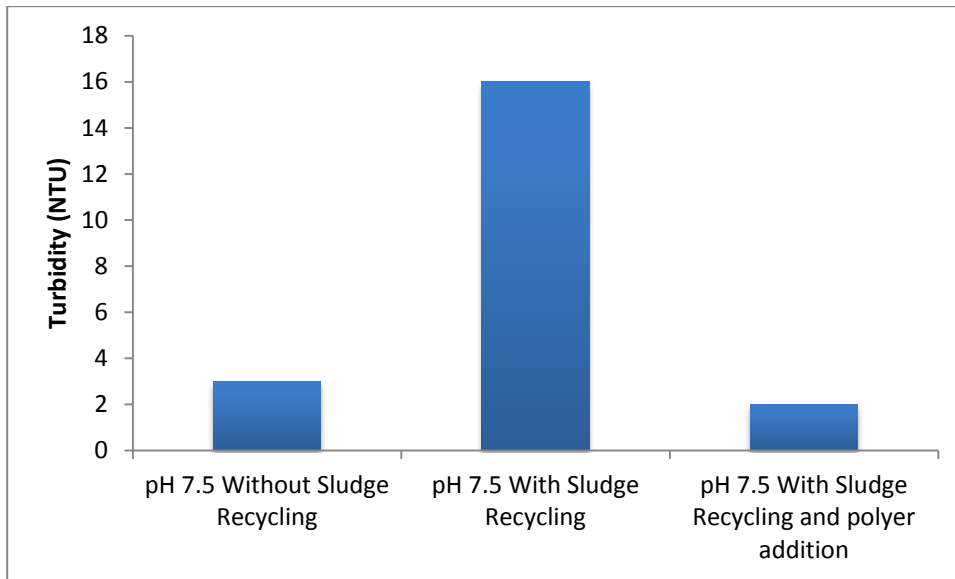


**Figure 5.6** Effluent turbidity from the pilot-scale system as a function of sludge recycle and coagulant addition

### 5.3 Conclusions

The results of the pilot-scale tests revealed that the sulfate was rapidly removed from liquid phase at high barite supersaturation levels so that the sulfate concentration in the effluent is reduced to below 100 mg/L with appropriate mixing ratio between flowback water and AMD.

This pilot-scale study revealed that a treatment system with rapid mix reactor, flocculation tank and settling tank is effective for the co-treatment of flowback water and AMD with the treated effluent quality meeting the criteria for reuse in hydraulic fracturing of unconventional wells in Marcellus Shale.

## 5.4 References

- Barbot, E., N. S. Vidic, K. B. Gregory and R. D. Vidic (2013). Spatial and temporal correlation of water quality parameters of produced waters from devonian-age shale following hydraulic fracturing. *Environmental Science & Technology*, 47(6), 2562-2569.
- Cornell, R. M., R. Giovanoli and W. Schneider (1989). Review of the hydrolysis of iron (III) and the crystallization of amorphous iron (III) hydroxide hydrate. *Journal of Chemical Technology and Biotechnology*, 46(2), 115-134.
- Cravotta, C. A. (2008). Dissolved metals and associated constituents in abandoned coal-mine discharges, pennsylvania, USA. Part 1: Constituent quantities and correlations. *Applied Geochemistry*, 23(2), 166-202.
- Druschel, G. K., B. J. Baker, T. M. Gihring and J. F. Banfield (2004). Acid mine drainage biogeochemistry at iron mountain, california. *Geochemical Transactions*, 5(2), 13-32.
- He, C., T. Zhang and R. D. Vidic (2013). Use of abandoned mine drainage for the development of unconventional gas resources. *Disruptive Science and Technology* 1(4), 169-176.
- He, C., M. Li, W. Liu, E. Barbot and R. Vidic (2014a). Kinetics and equilibrium of barium and strontium sulfate formation in marcellus shale flowback water. *Journal of Environmental Engineering*, 140(5), B4014001.
- He, C., X. Wang, W. Liu, E. Barbot and R. D. Vidic (2014b). Microfiltration in recycling of marcellus shale flowback water: Solids removal and potential fouling of polymeric microfiltration membranes. *Journal of Membrane Science*, 462, 88-95.
- He, C., T. Zhang, X. Zheng, Y. Li and R. D. Vidic (2014c). Management of marcellus shale produced water in pennsylvania: A review of current strategies and perspectives. *Energy Technology*, 2(12), 968-976.
- Kondash, A. J., N. R. Warner, O. Lahav and A. Vengosh (2013). Radium and barium removal through blending hydraulic fracturing fluids with acid mine drainage. *Environmental Science & Technology*, 48(2), 1334-1342.
- Nancollas, G. and N. Purdie (1964). The kinetics of crystal growth. *Q. Rev. Chem. Soc.* 18(1), 1-20.
- Ott, A. N. (1986). Estimating iron and aluminum content of acid mine discharge from a north-central pennsylvania coal field by use of acidity titration curves, US Geological Survey.
- Salama, E.-S., J. R. Kim, M.-K. Ji, D.-W. Cho, R. A. Abou-Shanab, A. N. Kabra and B.-H. Jeon (2015). Application of acid mine drainage for coagulation/flocculation of microalgal biomass. *Bioresource Technology*, 186, 232-237.
- Sun, Y., X. Xiong, G. Zhou, C. Li and X. Guan (2013). Removal of arsenate from water by coagulation with in situ formed versus pre-formed Fe (III). *Separation and Purification Technology* 115, 198-204.

Vidic, R. D., S. L. Brantley, J. M. Vandebossche, D. Yoxtheimer and J. D. Abad (2013). Impact of shale gas development on regional water quality. *Science*, 340(6134).

Wei, X. and R. C. Viadero (2007). Synthesis of magnetite nanoparticles with ferric iron recovered from acid mine drainage: Implications for environmental engineering. *Colloids and Surfaces A: Physicochemical and Engineering Aspects*, 294(1), 280-286.

Zheng, X. (2013). Optimization of treatment options to enable the use of abandoned mine drainage (AMD) for hydraulic fracturing in marcellus shale. Master Thesis, University of Pittsburgh.

## 6.0 Compatibility of AMD Water with Hydraulic Fracturing of Marcellus Shale

The two main concerns with the use of fluid rich in sulfate for hydraulic fracturing are: (1) potential for souring the well by microbial reduction of sulfate to hydrogen sulfide and (2) potential reduction in well permeability by the barium sulfate that will precipitate in the subsurface. Clearly, the first concern is not a valid one because of the high levels of barium in Marcellus Shale formation brine that will lead to precipitation of barite, which is virtually insoluble even in highly acidic solution (e.g., pH of 1.5). Consequently, it is highly likely that microorganisms will not be able to digest sulfate that is present in barite to produce hydrogen sulfate. The second concern may be justifiable depending on the level of sulfate that is present in the fracturing fluid. Preliminary calculations shown in Table 6.1 suggest that the volume of barite that would form downhole can range from 0.1% of the proppant volume in case the fracturing fluid contains 200 mg/L of sulfate to as much as 1.2% of the proppant volume when the fracturing fluid contains 2,000 mg/L sulfate.

**Table 6.1** Barite formation downhole

Sulfate in the frack fluid (mg/L)	Barite formed in the well (m <sup>3</sup> )	Percentage of the proppant volume (%)
200	1.2	0.1
800	4.9	0.5
2,000	9.8	1.2

Assumptions:

- volume of fracturing fluid is 3x10<sup>6</sup> gallons;
- proppant fraction is 9% by volume;
- barite density is 4500 kg/m<sup>3</sup>

When the volume of barite that could form in the subsurface is significant to potentially cause permeability reduction, it is important to understand the fate of barite in the horizontal section of the gas well. Hence, the formation of barite and its transport through porous shale core and proppant sand media was evaluated in this study. BaSO<sub>4</sub> particles formed at high ionic strength (0.5 M) have large size and very low mobility through these two media. Therefore, BaSO<sub>4</sub> formed in the subsurface will be unlikely to move back to surface during the flowback period because the shale formation brine has very high salinity.

In addition of commonly used antiscalants cannot prevent rapid formation of BaSO<sub>4</sub> at high supersaturation levels. Ethylene glycol, which is often used as a chemical additive to inhibit particle deposition, has no impact on the mobility of BaSO<sub>4</sub> through porous media. However, BaSO<sub>4</sub> particles formed in the presence of selected polymeric antiscalants have much smaller size and greater mobility through the shale core and proppant sand media. Furthermore, several antiscalants could help mitigate the attachment of barium sulfate to well casing.

## **6.1 Impact of Antiscalants on the Fate of Barite in the Unconventional Wells**

Barium sulfate is a common mineral scale found in various industrial processes, such as oil and gas production and seawater desalination with reverse osmosis. Because of its low solubility and resistance to acid, the removal of barium sulfate scale requires addition of chelating agents, such as ethylenediaminetetraacetic acid. Therefore, antiscalants are often used to prevent or mitigate the formation of barium sulfate scales. Common antiscalants used for barium sulfate include phosphonate additives (e.g., hydroxyethylenediphosphonic acid) and polyelectrolyte (e.g., polymaleic acid and polyacrylic acid). Multiple functionalities of antiscalants involve with the mechanisms of scaling mitigation. First, substoichiometric level of antiscalants is able to prevent the formation of insoluble salts when solubility product is exceeded, which is often referred to threshold inhibition and is the most common application of antiscalants. Second, negatively charged antiscalants can target the positive charges on nuclei, resulting in distorted and less adherent precipitates. Third, antiscalant molecules can stabilize the mineral particulates through electrostatic and/or steric interactions, which result in reduced tendency of sedimentation or deposition.

Antiscalants can effectively retard the nucleation and growth of barium sulfate when the saturation level is relatively low. However, once the saturation level reaches to a critical point, the antiscalants may no longer prevent or even retard the formation of barium sulfate. The objective of this study is to evaluate the potential mobility enhancement of BaSO<sub>4</sub> particles through proppant sand media and shale core media with selected antiscalants.

In this study, it was found that the presence of polymeric antiscalants could effectively limit the size of the barium sulfate precipitates under high ionic strength, which in turn resulted in greater mobility of barium sulfate particles through porous proppant sand and shale core media. The potential mechanisms involves with the enhanced mobility by the presence of



selected antiscalants includes the reduced particle size, increased electrostatic repulsion force and electrosteric repulsion force.

## 6.1.1 Materials and Methods

### 6.1.1.1 Granular Porous Media

The mobility of  $\text{BaSO}_4$  particles through porous media was evaluated using actual proppant (silica sand) and crushed shale core samples. The proppant was sieved through 20 US Mesh sieve to screen large particles and the average size of proppant particles measured by Microtrac S3500 was 0.25 mm. Sieved proppant was rinsed with DI 2-3 times before packing it into the column. The shale core sample was crushed and sieved to 30x40 US Mesh size (Figure 6.1). Sieved shale core particles were washed with DI water 5-10 times. Optical microscope observation revealed that both proppant sand and crushed core particles have irregular shape.

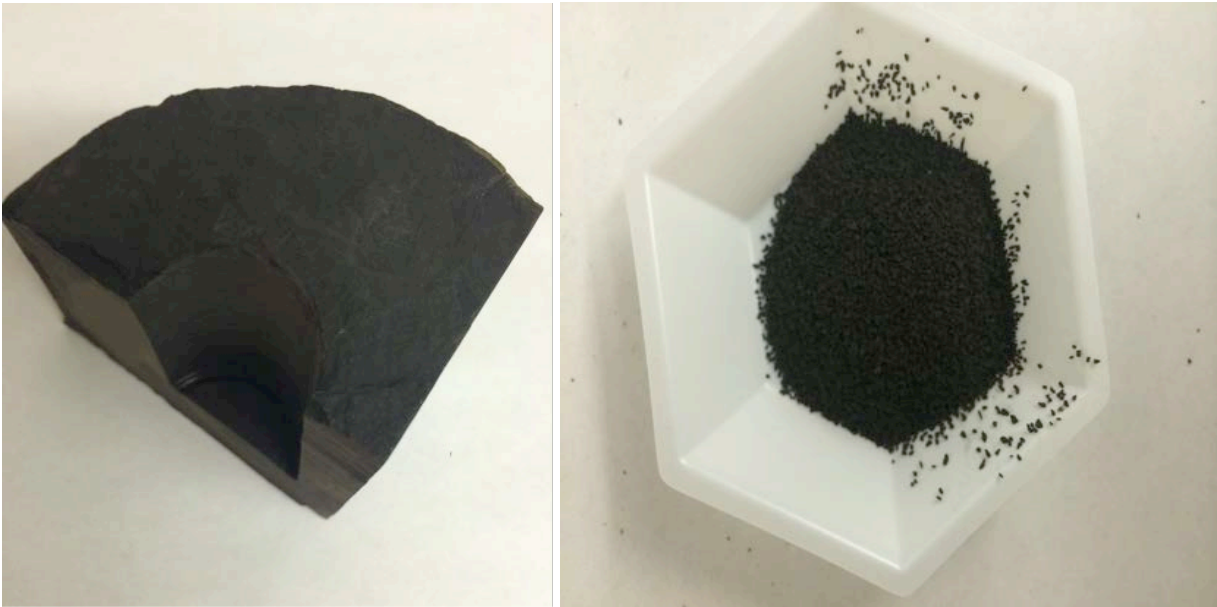


**Figure 6.1** Raw shale core sample (left) and crushed shale core particles (right)

### 6.1.1.2 Feed Solution

Effect of a sulfonated phosphino poly carboxylic acid (SPPCA), polymaleic acid (PMA), hydroxyethylenediphosphonic acid (HEDP) and ethylene glycol (EG) on  $\text{BaSO}_4$  precipitation reaction and transport through porous proppant sand and scale core media was evaluated in

this study. PMA (50 wt%) and HEDP (60 wt%) were provided by Kroff Chemical Company (Pittsburgh, PA). SPPCA is a commercial product, Bellasol S50, from BWA Water Additives (Tucker, GA) and EG was obtained from Fisher Scientific (Pittsburgh, PA).

BaSO<sub>4</sub> feed solution (1,000 mg/L) was prepared by mixing 4.29 mM BaCl<sub>2</sub> and 4.29 mM NaSO<sub>4</sub> in a 200-mL beaker. Antiscalant and concentrated NaCl were added between dosing stock solution of BaCl<sub>2</sub> and NaSO<sub>4</sub>. HCl or NaOH stock solutions were used to adjust the solution pH to a desired level. The feed solution was mixed using a magnetic stirring bar at the speed of 400 rpm throughout each column experiment.

Particle size distribution of BaSO<sub>4</sub> that was prepared fresh for each experimental condition was measured using Microtrac S3500. Scanning electron microscope (SEM) was used to analyze the morphology of BaSO<sub>4</sub> precipitates. Zeta potential of BaSO<sub>4</sub> particles was measured by Malvern Zetasizer (Malvern Instruments Ltd., UK) to quantify the microscopic long-range interactions between BaSO<sub>4</sub> particles and proppant sands collector.

#### 6.1.1.3 Column Experiment

Transport experiments with BaSO<sub>4</sub> were conducted using a glass chromatography column with inner diameter of 10 mm and length of 10 cm (Omnifit USA, Toms River, NJ). A 125- $\mu$ m nylon mesh screen was placed on each end of the column to prevent the loss of proppant sand or shale core particles during the experiment while enabling the passage of relatively small (i.e., few microns) BaSO<sub>4</sub> particles.

Prior to BaSO<sub>4</sub> transport experiments, packed column was flushed with at least 10 pore volumes (PV) of DI water to wash out the fines and until the effluent turbidity was below 1 NTU. Then PV of solution with identical ionic strength (adjusted by NaCl) and pH as the feed solution was passed through the column to precondition the proppant and shale core media. Freshly-made BaSO<sub>4</sub> feed solution was injected into the column by a peristaltic pump at a constant flow rate of 13 ml/min at room temperature (21 °C). Effluent was sampled every 30 seconds and analyzed by UV/VIS spectrophotometer at a wavelength of 500 nm to determine BaSO<sub>4</sub> concentration. Spectrophotometer calibration was performed prior to each experiment.

#### 6.1.1.4 Single Collector Efficiency Model

Overall collector removal efficiency for a single collector is given as (Tufenkji and Elimelech, 2004):

$$\eta_0 = \eta_D + \eta_I + \eta_G \quad (6-1)$$

where,  $\eta_D$  is the transport by diffusion,

$\eta_I$  is the transport by interception, and

$\eta_G$  is the transport by gravity.

The overall collector removal efficiency,  $\eta_0$ , can be further expressed as shown in Equation (6-2) with the parameters defined in Table 6.2.

$$\eta_0 = 2.4A_s^{1/3} N_R^{-0.081} N_{Pe}^{-0.715} N_{vdW}^{0.052} + 0.55A_s N_R^{1.55} N_{Pe}^{-0.125} N_{vdW}^{0.125} + 0.22N_R^{-0.24} N_G^{1.11} N_{vdW}^{0.053} \quad (6-2)$$

**Table 6.2** Summary of dimensionless parameters governing particle transport through porous media (Tufenkji and Elimelech, 2004)

Parameter	Definition	Physical Interpretation
$N_R$	$\frac{d_p}{d_c}$	Aspect ratio
$N_{Pe}$	$\frac{U d_c}{D}$	Peclet number characterizing ratio of convective transport to diffusive transport
$N_{vdW}$	$\frac{A}{kT}$	Van der Waals number characterizing ratio of van der Waals interaction energy to the particle's thermal energy
$N_{gr}$	$\frac{4 \pi a_p^4 (\rho_p - \rho_f) g}{3 kT}$	Gravitational number; ratio of particle's gravitational potential when located on particles radius from collector to particle's thermal energy
$N_A$	$\frac{A}{12 \pi \mu a_p^2 U}$	Attraction number; represents combined influence of van der Waals attraction forces and fluid velocity on particle deposition rate due to interception
$N_G$	$\frac{2 a_p^2 (\rho_p - \rho_f) g}{9 \mu U}$	Gravity number; ratio of Stokes particle settling velocity to approach velocity of the fluid
$A_s$	$\frac{2 \left[ 1 - (1 - f)^{\frac{5}{3}} \right]}{2 - 3(1 - f) + 3(1 - f)^5 - 2(1 - f)^6}$	Porosity-dependent parameter

$d_p$  is the particle diameter,  $d_c$  is the collector diameter,  $U$  is the fluid approach velocity,  $D$  is the bulk diffusion coefficient,  $A$  is the Hamaker constant,  $k$  is the Boltzmann constant,  $T$  is the fluid absolute temperature,  $a_p$  is particle radius,  $\rho_p$  is particle density,  $\rho_f$  is fluid density,  $\mu$  is the absolute fluid viscosity,  $g$  is the gravitational acceleration and  $f$  is the porosity. Note that  $N_G = 2N_{gr}N_R^{-1}N_{Pe}^{-1}$ . Thus,  $N_{gr}$  is not present in Equation 6-2.

## 6.1.2 Results and Discussion

### 6.1.2.1 Characterization of Barium Sulfate Particles

Laboratory studies have demonstrated that the presence of phosphonate and polyelectrolyte compounds can significantly inhibit the barium sulfate precipitation at low supersaturation levels (Jones et al., 2002; Jones et al., 2006; van der Leeden, 1991). The inhibition mechanism involved in these studies can be categorized as threshold inhibition, a mechanism by which a sub-stoichiometric amount of inhibitor retards precipitation by interfering with the nucleation phase. However, the impact of these antiscalants on barium sulfate precipitation at elevated supersaturation level (i.e., high SI) and subsequent deposition of these particles on different grain surfaces have not been studied previously.

Bench-scale beaker tests were conducted to evaluate PMA, SPPCA, HEDP and EG in terms of their ability to inhibit BaSO<sub>4</sub> precipitation. It was found that the selected antiscalants had minimal effect on the retardation of BaSO<sub>4</sub> precipitation under the S<sub>a</sub> condition that are relevant in oil and gas industry and at reasonable antiscalant dosages (Chapter 6.1). Induction period was always just a few seconds based on visual observation of the occurrence of turbidity and the equilibrium was achieved within 60 minutes of reaction.

At lower supersaturation level, antiscalants could interact with nuclei to prevent them from reaching the critical size, which results in their re-dissolution. However, for highly supersaturated solution used in this study, both the formation and growth of nuclei are so fast that the antiscalant fails to limit the nuclei growth. As a result, no measurable retardation in barium sulfate precipitation by selected antiscalants was observed in this study.

While the selected antiscalants did not exhibit observable impact on the inhibition of BaSO<sub>4</sub> precipitation, SEM images illustrated that the morphology and size of barium sulfate precipitates were significantly altered by the presence of antiscalants (Figure 6.2). BaSO<sub>4</sub> particles formed in the presence of 0.5M NaCl but in the absence of antiscalants have a “rugby-like” shape and are large in size. Once the selected antiscalants are added to the solution, the BaSO<sub>4</sub> particles that form are visibly smaller. The addition of 10 ppm PMA or SPPCA lead to the formation of spherical BaSO<sub>4</sub> particles that are much smaller in size compared with that formed in the presence of ethylene glycol. On the other hand, BaSO<sub>4</sub> particles formed in the presence of EG had similar shape to that formed in the absence of any antiscalants and their size was slightly smaller.

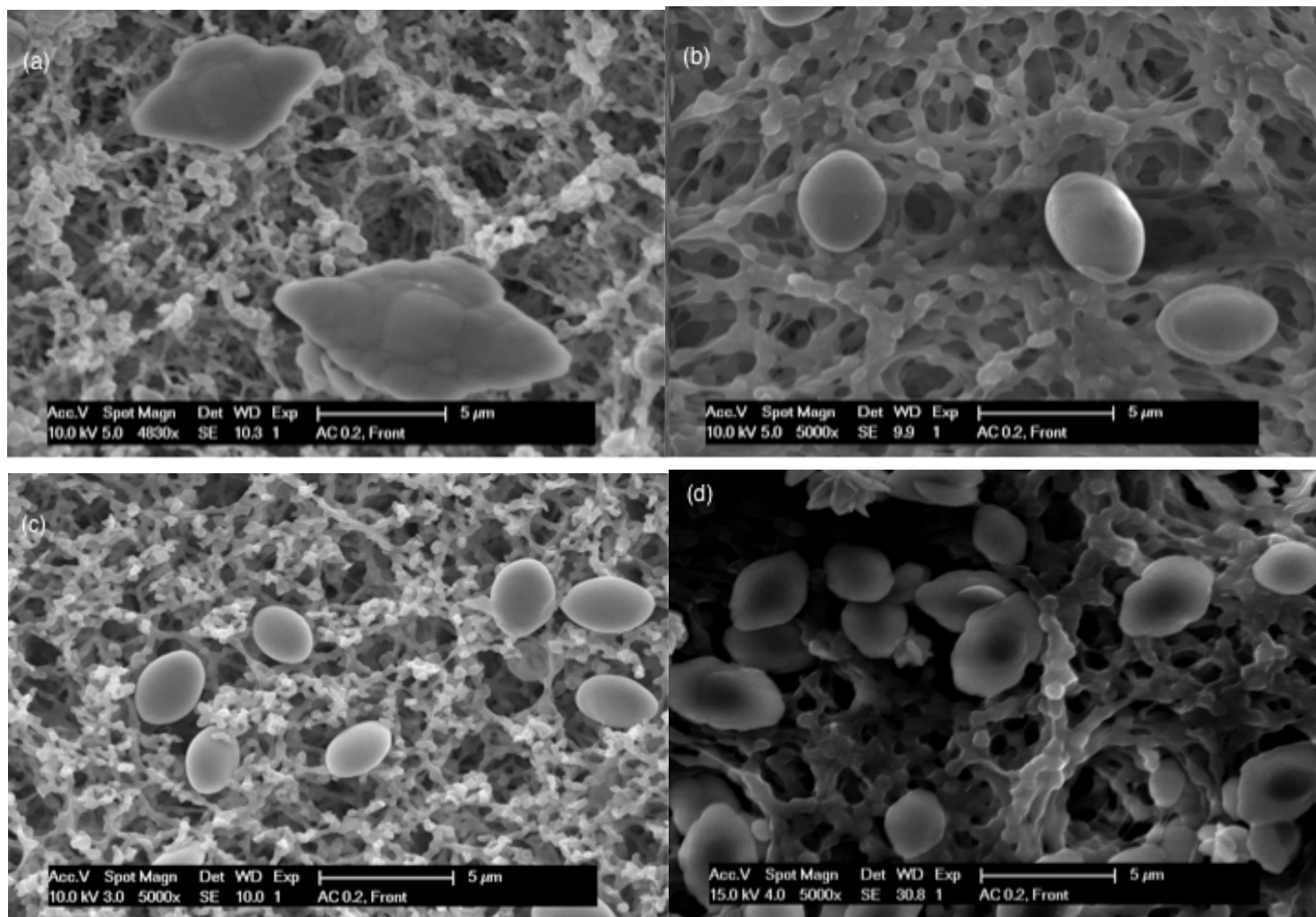


**Figure 6.2** SEM images of BaSO<sub>4</sub> particles formed with addition of 0.5M NaCl and (a) no antiscalants; (b) with addition of 10 mg/L SPPCA; (c) with addition of 10 mg/L PMA and (d) with addition of 10 mg/L ethylene glycol

The size of BaSO<sub>4</sub> particles as a function of pH, ionic strength and presence of antiscalants was analyzed using Microtrac S3500. As shown in Figure 6.3, average particle size of bare BaSO<sub>4</sub> increased with an increase in ionic strength (i.e., NaCl addition) at pH 7, which can be explained by rapid agglomeration of newly formed fine BaSO<sub>4</sub> nuclei due to electric double layer compression at high ionic strength. In addition, seeded growth will take place on initially formed BaSO<sub>4</sub> agglomerates, which further increases the particle size. The mean particle size increased significantly with the ionic strength, while the presence of SSPCA can limit the particle size even in high ionic strength solution (Figure 6.4).

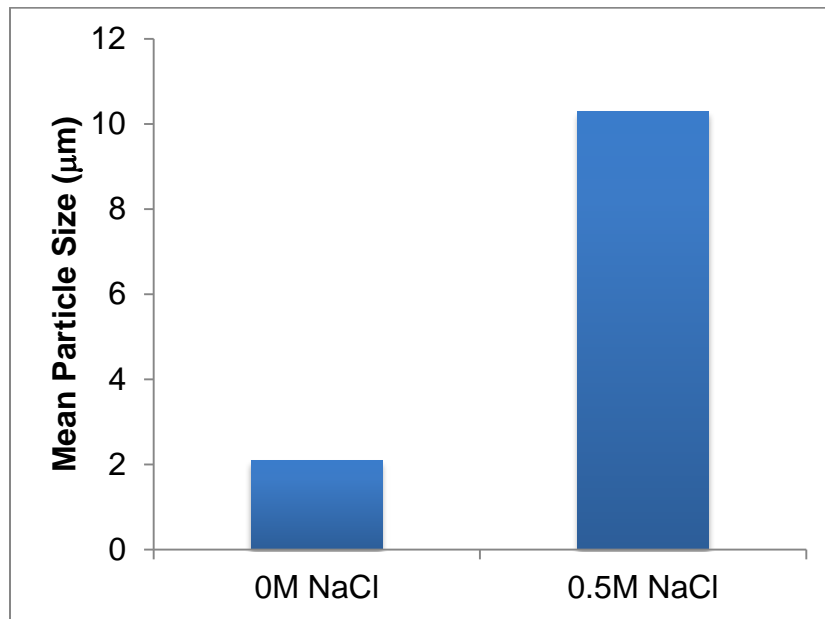


**Figure 6.3** Impact of ionic strength on mean BaSO<sub>4</sub> particle size at pH 7

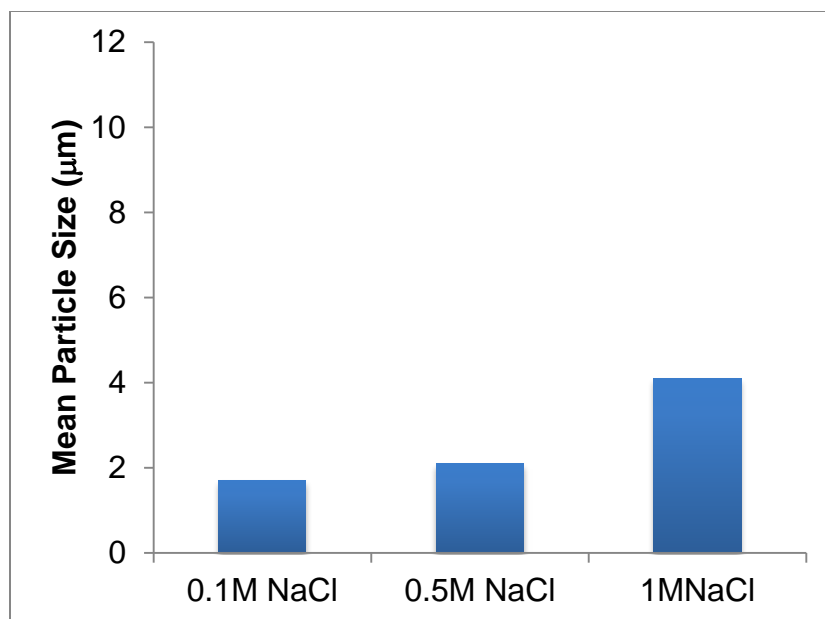


**Figure 6.4** Impact of 10 mg/L SPPCA on mean BaSO<sub>4</sub> particle size at different ionic strengths

The average particle size of BaSO<sub>4</sub> increased very slightly with ionic strength when PMA or SPPCA were added to the solution, indicating that these antiscalants were effective in preventing agglomeration under these conditions. This phenomenon may be due to adsorption of polymeric antiscalants on particle surface, which yields stronger electrostatic and electrosteric repulsion. Schematic diagram (Figure. 6.5) depicts possible mechanisms governing BaSO<sub>4</sub> precipitation in the absence and presence of polymeric antiscalants. For the case where no antiscalants were added to solution, homogeneous nucleation, seeded growth and aggregation of newly formed small BaSO<sub>4</sub> particles contribute to the formation of large BaSO<sub>4</sub> precipitates in solution. When polymeric antiscalants are present in solution, they will adsorb on the active sites on the surface of nuclei in solution so that the crystal growth of BaSO<sub>4</sub> is inhibited by strong electrostatic and steric repulsion induced by these polymers.



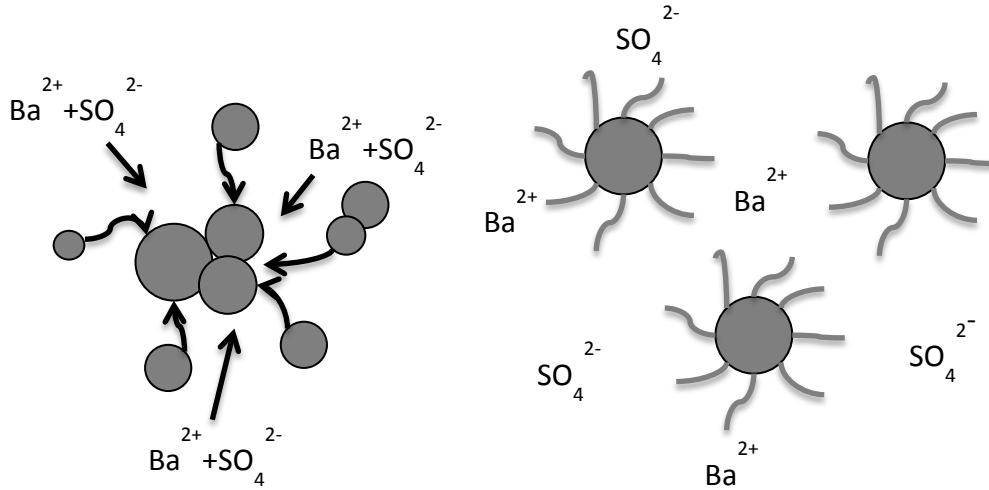


**Figure 6.5** Schematic diagram of  $\text{BaSO}_4$  formation under high ionic strength with (left) no antiscalants; (right) polymer antiscalants.

In order to evaluate the impact of particle size on the transport behavior of barite particles through porous media, theoretical single collector contact efficiency was calculated as a function of particle size using the parameters listed in Table 6.3.

**Table 6.3** Parameters for single collector contact efficiency model

Parameter	Value
Hamaker Constant	$1.7 \times 10^{-20}$ J
Gravitational acceleration	$9.8 \text{ m/s}^2$
Approach velocity	$2.7 \times 10^{-4}$ m/s
Boltzmann constant	$1.38 \times 10^{-23} \text{ m}^2 \text{ kg s}^{-2} \text{ K}^{-1}$
Temperature	293 K
Collector Diameter	$0.256 \times 10^{-3}$ m
Absolute Fluid viscosity	$10^{-3} \text{ kg/(m s)}$

As illustrated in Figure 6.6, the single collector contact efficiency increases sharply when particle size increase from 1,000 to 10,000 nm. The average barite particle size increases from about 2,000 nm to about 10,000 nm when the ionic strength of the solution increased from 0 to 0.5 M (Figure 6.3). However, the average particle size of precipitated barite increased only slightly (from 2,000 to 4,000 nm) when 10 mg/L of SPPCA was added to the solution (Figure

6.4). These results indicated that the collision between barite particles and collector surface will be significantly lower in the presence of aniscalants, which would likely lead to higher mobility of barite particles.

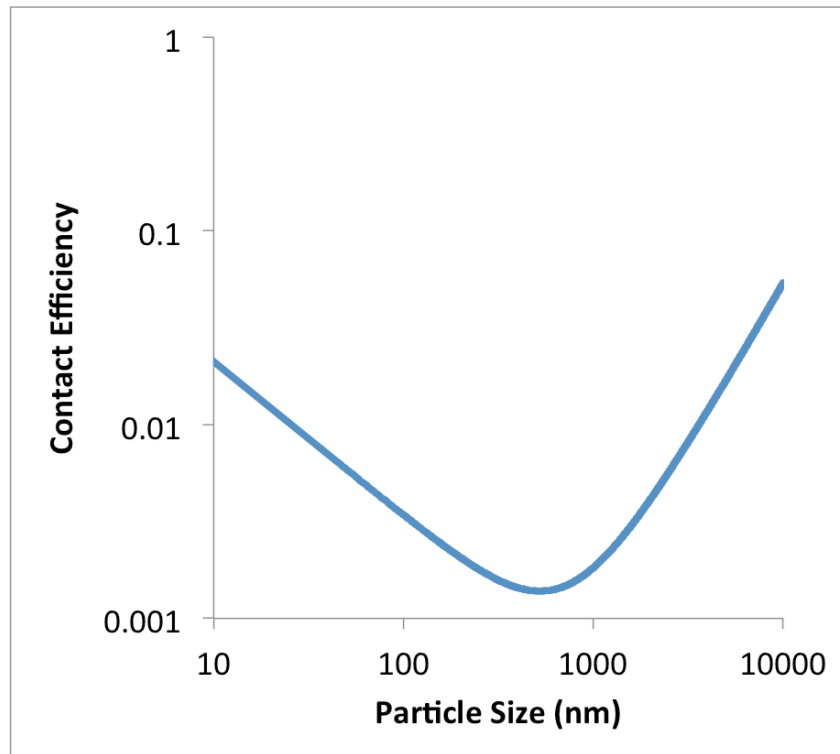


**Figure 6.6** Single collector contact efficiency as a function of  $\text{BaSO}_4$  particle size

#### 6.1.2.2 Mobility of $\text{BaSO}_4$ through Proppant

Because the shale formation brine has high salinity, it is important to investigate the influence of salt concentration on the mobility of barite particles through the proppant pack. Column experiments with  $\text{BaSO}_4$  suspension formed in the absence of antiscalants showed that the mobility of  $\text{BaSO}_4$  particles was significantly reduced when the ionic strength of the solution increased from 0 to 0.5 M (Figure 6.7). As can be seen in Figure 6.7, gradual increase in  $\text{BaSO}_4$  concentration in the effluent was observed when the ionic strength of the solution was not adjusted with NaCl while negligible breakthrough of  $\text{BaSO}_4$  particles was detected when 0.5M NaCl was added to the feed solution.

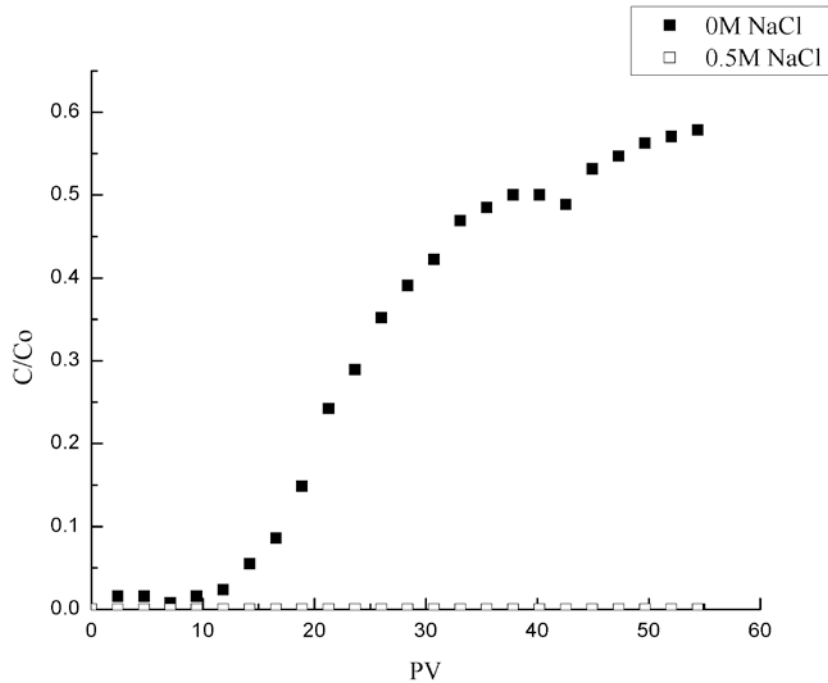


**Figure 6.7** Impact of ionic strength on BaSO<sub>4</sub> transport through proppant media

The effect of electrolyte concentration on the mobility of particles through porous sand media has been widely studied and can be explained by classical DLVO theory (Saleh et al., 2008; Liu et al., 1995, Bradford et al., 2007). The electrostatic repulsion between the particles and sand media becomes weaker with an increase in electrolyte concentration, which leads to greater particle deposition on the collector surface. However, in this study salt concentration not only reduced the electrostatic interactions between particle and collector, but also influenced the size of particles that precipitated in solution.

As illustrated in Figure 6.3, average particle size of BaSO<sub>4</sub> formed with and without addition of 0.5 M NaCl was 10.3 μm and 2.1 μm, respectively. According to theoretical analysis shown in Figure 6.6, which describes the tendency of attachment between a single particle and a single collector, single collector contact efficiency increases with an increase in particle size. Therefore, the increased probability of contact between particles and collector, and the reduced long-range electrostatic interaction are responsible for significant decrease in mobility of BaSO<sub>4</sub> particles at higher ionic strength of the solution. When the ionic strength of the feed solution is high ( $I \geq 0.5$  M), there was no detectable breakthrough of BaSO<sub>4</sub> particles from the proppant column even when the solution pH was varied in the range from 4 to 9 (data not shown).

### 6.1.2.3 Impact of Antiscalants on the Mobility of BaSO<sub>4</sub> through Proppant

The impact of selected antiscalants on BaSO<sub>4</sub> transport through proppant pack was evaluated using experiments that are designed to represent different subsurface conditions. Breakthrough curves for transport of BaSO<sub>4</sub> particles that are formed in the presence of SPPCA as a function of ionic strength are shown in Figure 6.8. As can be seen in this figure, addition of SPPCA significantly reduced attachment of BaSO<sub>4</sub> by silica sand and the mobility of BaSO<sub>4</sub> is relatively high even when 1M NaCl was added to the feed solution. Because the electrostatic repulsion is essentially non-existent at such high ionic strength (Saleh et al., 2008; Hiemenz and Rajagopalan, 1997), this result suggests that the enhanced mobility of SPPCA-modified BaSO<sub>4</sub> is likely due to steric repulsion interactions induced by the attachment of polymeric antiscalant to BaSO<sub>4</sub> surface.

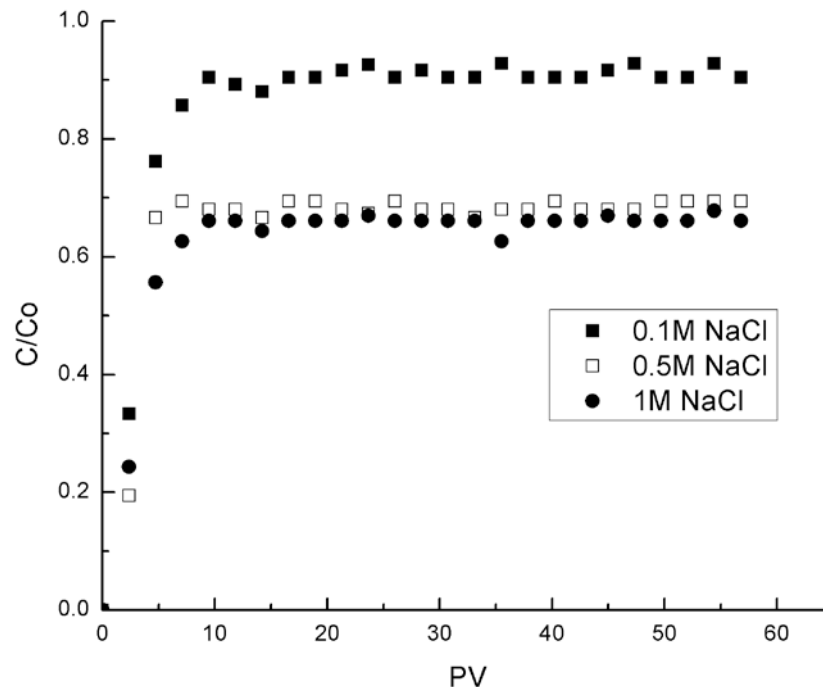


**Figure 6.8** Impact of ionic strength on transport of SPPCA modified BaSO<sub>4</sub> through proppant column at pH 7

Both PMA and SPPCA can significantly improve mobility of BaSO<sub>4</sub> at high ionic strength (0.5 M) as shown in Figure 6.9. Such behavior is mainly due to the ability of these polyelectrolytes to control barite particle size during precipitation reaction and induce stronger steric repulsion forces. In addition, BaSO<sub>4</sub> particles formed in the presence of PMA or SPPCA

are spherical (Figure 6.2), which enables the rolling of particles on collector surface as the primary mechanism of hydrodynamic detachment (Bradford et al., 2007; Bergendahl and Grasso, 2000). The results in Figure 6.9 also indicate that SPPCA is more effective at preventing attachment of barite to proppant pack than PMA because the average particle size for SPPCA and PMA modified barite particles was  $1.7\mu\text{m}$  and  $3.0\mu\text{m}$ , respectively.

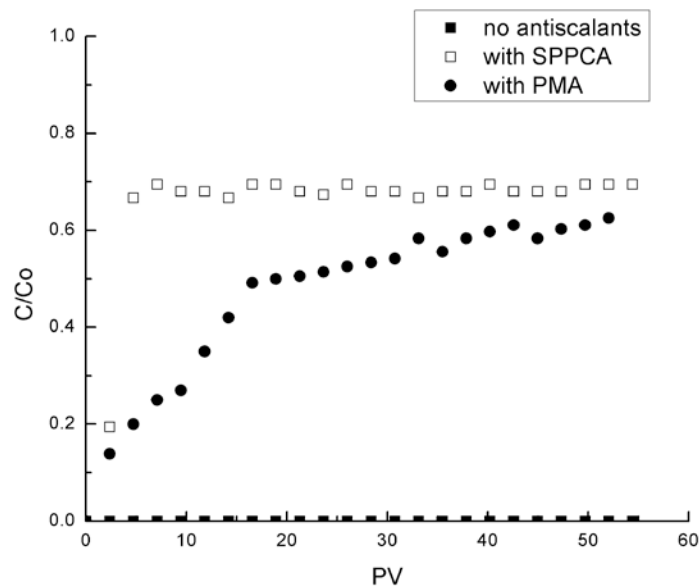


**Figure 6.9** Impact of SPPCA and PMA on  $\text{BaSO}_4$  transport through proppant column at high ionic strength (0.5 M) and pH 7

The results of the column experiment with  $\text{BaSO}_4$  formed in the presence of 10 mg/L ethylene glycol is not included in this report because no measurable  $\text{BaSO}_4$  was observed in the effluent when the ionic strength was 0.5M. This observation indicates that ethylene glycol that is commonly used in shale gas extraction has no impact on barite mobility through proppant pack. Even the EG concentration of 20 mg/L showed no measurable ability to mobilize barite. Ineffectiveness of ethylene glycol to inhibition of  $\text{BaSO}_4$  attachment to proppant sand is likely due to relatively large particle size (Figure 6.2) and the inability of EG to provide steric repulsion interactions and affect the particle size of barite formed under relevant experimental conditions.

Mobility of  $\text{BaSO}_4$  particles formed in the presence of PMA or SPPCA is very dependent on the solution pH as can be seen from the results presented in Figure 6.10. The results in this figure suggest that the mobility of  $\text{BaSO}_4$  particles increases with pH for both antiscalants tested in this study. The change is particularly dramatic in the case of PMA where no breakthrough of

BaSO<sub>4</sub> particles was observed at pH 4 and rapid breakthrough was observed at pH 8.5. The increase in pH condition could result in deprotonation of polyelectrolytes, which in turn affects the distortion of BaSO<sub>4</sub> nucleation and growth, the electrostatic properties, and potentially the conformation of polymer itself (van der Leeden, 1991, Wan et al., 2004) .

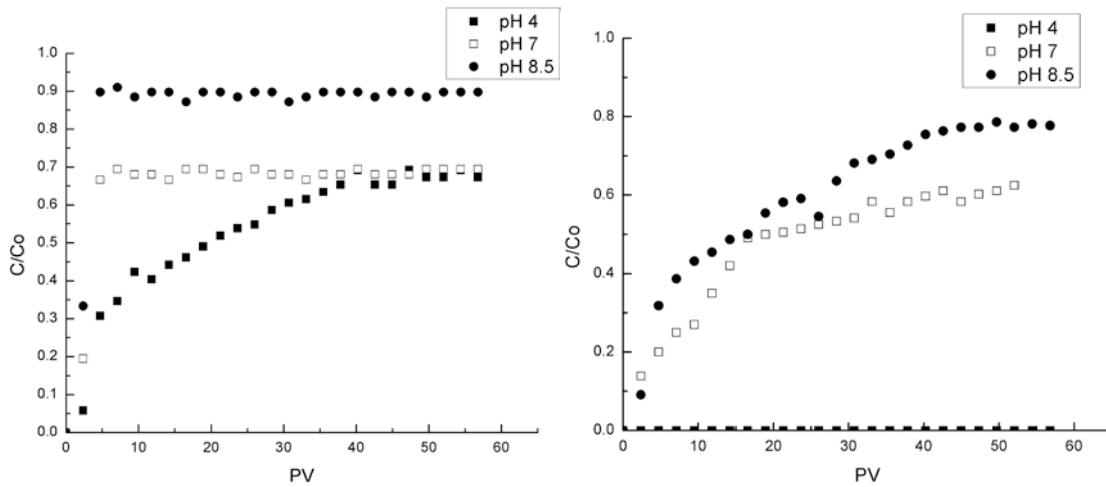


**Figure 6.10** Breakthrough of SPPCA (left) and PMA (right) modified BaSO<sub>4</sub> particles as a function of pH

Surface charge of barite particles as measured by zeta potential can influence mobility of BaSO<sub>4</sub> particles through proppant sand media as it affects electrostatic interactions between BaSO<sub>4</sub> particles and sand collector and between BaSO<sub>4</sub> particles themselves. As illustrated in Figure 6.11, presence of both SPPCA and PMA resulted in the shift of point of zero charge of freshly precipitated barite towards lower pH. It is known that zeta-potential of silica surface is negatively charged at pH between 4 and 9 (Solovitch, 2010). Therefore, BaSO<sub>4</sub> particles with negative surface charge will have greater mobility and reduced deposition in this pH range because of electrostatic repulsion with the proppant sand.

Zeta potential of PMA modified BaSO<sub>4</sub> particles varies slightly in the pH range from 7 - 8.5, which corresponds to similar transport behavior through proppant sand as observed in Figure 6.10. As the zeta potential of SPPCA modified BaSO<sub>4</sub> decreases with an increase in pH (i.e., barite particles become more negatively charged), the mobility of these particles through proppant sand should increase with pH increase. This hypothesis is confirmed by the results shown in Figure 6.10 where higher pH resulted in greater mobility of SPPCA-modified BaSO<sub>4</sub> particles. The same can be concluded about PMA-modified barite particles. It is worth noticing that the zeta potential of BaSO<sub>4</sub> particles formed in the presence of PMA at pH 4 was slightly

positive, which results in the attraction by negatively charged proppant sand and severe reduction in mobility through the proppant pack. In addition, the repulsion force between barite particles would be rather weak and result in severe agglomeration within the porous media, which would result in additional reduction in mobility due to size effects.

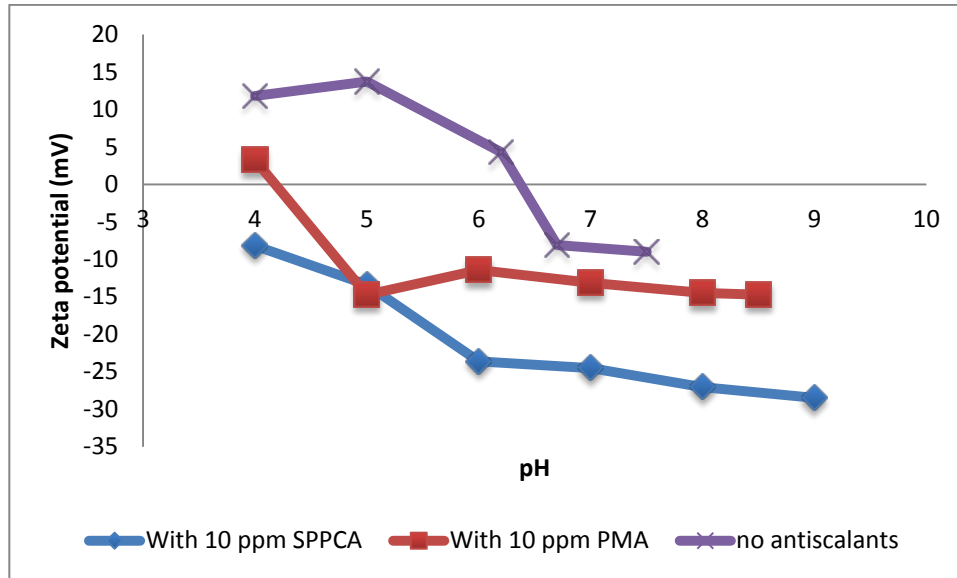


**Figure 6.11** Zeta potential of BaSO<sub>4</sub> particles formed in the presence of PMA and SPPCA.

#### 6.1.2.4 Impact of Antiscalants on the Mobility of BaSO<sub>4</sub> through Shale Core

Column tests were conducted to evaluate BaSO<sub>4</sub> transport through porous shale core. Similar to the transport behavior of BaSO<sub>4</sub> through proppant sand, the mobility of large BaSO<sub>4</sub> particles formed at high ionic strength (0.5 M NaCl) in the absence of antiscalant is very limited. As illustrated in Figure 6.12, the breakthrough of BaSO<sub>4</sub> was not observed under these conditions, while the antiscalant-modified BaSO<sub>4</sub> particles had much greater mobility.

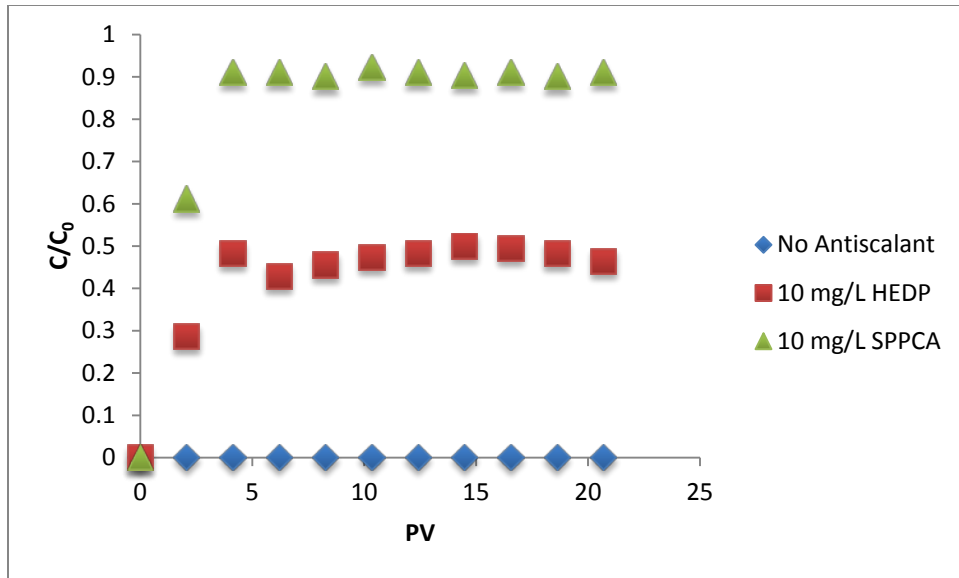


**Figure 6.12** Breakthrough of barite particles formed at 0.5 M ionic strength and pH7

Figures 6.13 and 6.14 illustrate the breakthrough of  $\text{BaSO}_4$  formed in the presence of HEDP and SPPCA at pH 7 and under various ionic strength conditions through the shale core. As can be seen in Figure 6.13, mobility of barite particles precipitate in the presence of 10 mg/L of HEDP was significantly reduced by the increase in ionic strength of the feed solution. This reduction in mobility is likely to be due to the fact that HEDP adsorbed on the barite surface cannot provide sufficient electro-steric repulsion between barite particle and the shale core. As a result, the repulsion interaction for HEDP modified  $\text{BaSO}_4$  is much weaker compared with SPPCA modified  $\text{BaSO}_4$  particles.

However, as can be seen in Figure 6.14, the increase in ionic strength did not significantly affect the mobility of SPPCA modified  $\text{BaSO}_4$  (i.e., the equilibrium particle concentration in the effluent decreased from 0.987 to 0.906 with the increase of ionic strength). Such behavior is likely due to adsorption of SPPCA on barite that can prevent aggregation of barite particles within the pores and provide strong electrostatic repulsion between the shale core surface and barite particles. The mobility SPPCA modified  $\text{BaSO}_4$  through shale core media is greater compared with proppant sand media, which is mainly because the shale core particles used in this study have larger size compared with the proppant sand particles.



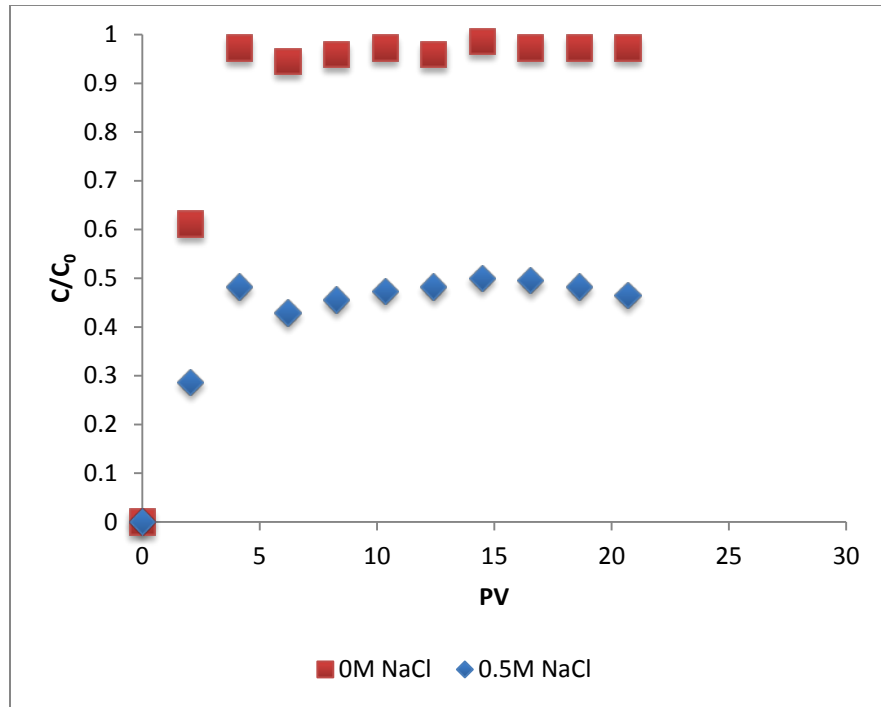


**Figure 6.13** Breakthrough of barium sulfate particles formed in the presence of 10 mg/L HEDP at pH 7

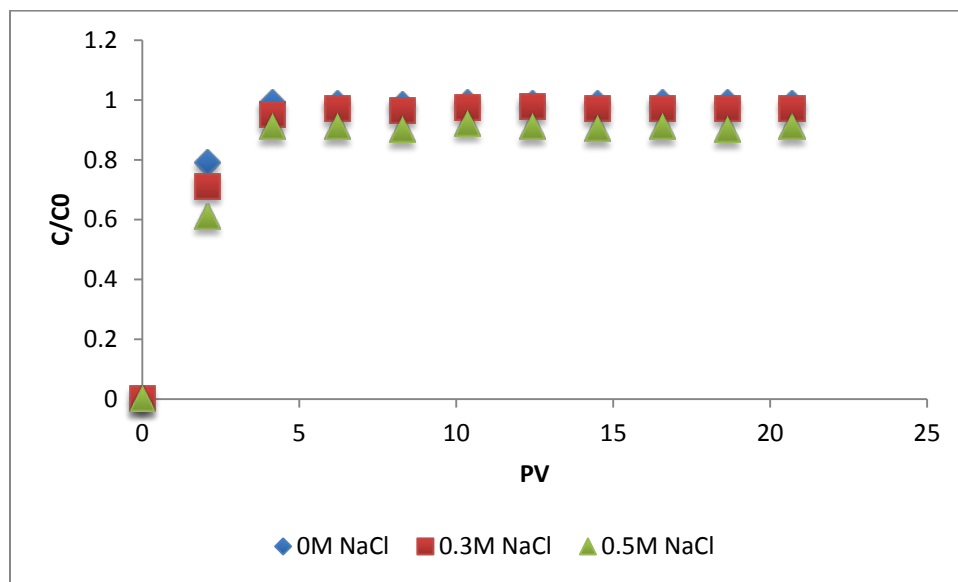


**Figure 6.14** Breakthrough of barium sulfate particles formed in the presence of 10 mg/L SPPCA at pH 7

### 6.1.3 Conclusions

The mobility of BaSO<sub>4</sub> particles in saturated porous media is important to estimate potential well plugging by barite that could form in the subsurface if there is substantial sulfate concentration in the fracturing fluid. This study provides fundamental information about barite interaction with both proppant pack and shale surface in terms its potential to cause well plugging and offers insights in the application of antiscalants to control barite transport in the subsurface.

First, ethylene glycol, which is often used in hydraulic fracturing to control scaling behavior in the subsurface, has limited impact on improving the mobility of BaSO<sub>4</sub> particles through proppant sand at high ionic strength ( $I > 0.5M$ ). Therefore, BaSO<sub>4</sub> particles are most likely to be retained in the subsurface because the salinity of shale formation brine is normally very high.

Second, polymeric antiscalants, such as PMA and SPPCA, are effective in mitigating the retention of BaSO<sub>4</sub> particles in proppant sands, which in turn reduces well plugging and potential for productivity reduction.

Finally, PMA and SPPCA that are generally considered when the goal is to inhibit the formation of mineral scales are unlikely to prevent barite formation at high supersaturation conditions that are typical for unconventional gas industry. However, they can inhibit the deposition of bulk precipitates onto the collector surface by limiting the particle size and inducing stronger repulsion interactions. The anti-deposition function of antiscalants can possibly be applied to other fields where rapid formation of mineral precipitates is inevitable despite the addition of antiscalants.

## 6.2 Affinity of Barium Sulfate for the Casing Material

Deposition of  $\text{BaSO}_4$  particles onto stainless steel surface was studied in a bench-scale recirculating system. Total force acting on the  $\text{BaSO}_4$  particles in the fluid was calculated to indicate the tendency of  $\text{BaSO}_4$  deposition as a function of particle size and flow velocity. The effectiveness of antiscalants in mitigating  $\text{BaSO}_4$  deposition on stainless steel surface was also evaluated in order to find solutions to prevent scaling of the well casing and associated accumulation of NORM on the casing.

### 6.2.1 Materials and Methods

#### 6.2.1.1 Bench-scale Recirculating System

A bench-scale recirculating system shown in Figure 6.15 was made of  $\frac{3}{4}$ " PVC pipes and equipped with removable stainless steel (SS316) circular disc specimens ( $5.61 \text{ cm}^2$ ) to track particle scaling/deposition from the recirculating water with time. The 2-L beaker contained the feed solution and was placed on a hotplate with stirring speed of 400 rpm to control the temperature of the solution. The deposition behavior of barium sulfate particles was tracked in terms of mass gain on the stainless steel coupons with time at various experimental conditions (e.g., flow rate, temperature, addition of antiscalants).

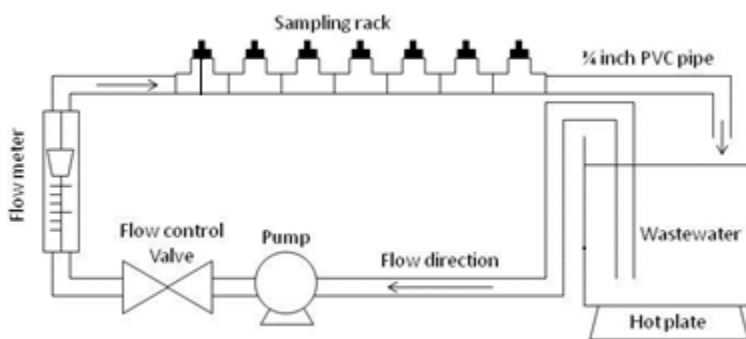


**Figure 6.15** Schematic diagram of bench-scale recirculating system

#### 6.2.1.2 Feed Solution

Experiments with freshly formed barium sulfate particles were conducted by first mixing 4.29 mM  $\text{BaCl}_2$  and 4.29 mM  $\text{NaSO}_4$  in a 2-L beaker to create a solution containing 1,000 mg/L  $\text{BaSO}_4$ . Barite precipitation was allowed to proceed for 30 min before the start of the bench-scale recirculation test. The effectiveness of polymaleic acid (PMA, Kroff Chemical Company,

Pittsburgh, PA) and sulfonated phosphino polycarboxylic acid (SPPCA, BWA Water Additives, GA) as model antiscalants on the accumulation of barite on stainless steel coupons was tested by adding them to the solution between the addition of BaCl<sub>2</sub> and Na<sub>2</sub>SO<sub>4</sub>. HCl and NaOH were used to maintain solution pH at 7 throughout the experiment.

### 6.2.1.3 Theoretical Calculation of the Forces Acting on Barite Particles

Vertical forces (gravity, buoyancy and lift force) that act on barite particle in the vicinity of the pipe wall are calculated based on theoretical analysis. Total vertical force ( $F_{\text{vertical}}$ ) can serve as an indicator of the potential for particle deposition. Positive  $F_{\text{vertical}}$  indicates the deposition of bulk precipitates while negative  $F_{\text{vertical}}$  indicates limited particle deposition on the pipe surface. Previous study has summarized the equations used to calculate vertical forces that act on barium sulfate particles (Liu, 2013).

In the vicinity of the pipe wall, when the size of a particle is smaller than the thickness of the boundary layer, the following vertical forces act on that particle: gravity force,  $F_G$ ; buoyancy force,  $F_B$ ; and lift force,  $F_L$ .

If the bulk precipitate is assumed to be spherical, the gravity force,  $F_G$  (N), is:

$$F_G = \frac{1}{6}\pi\rho_p g d_p^3 \quad (6-3)$$

where,  $\rho_p$  is the density of the particle ( $4.37 \times 10^3 \text{ kg/m}^3$  for barite particle),  $g$  is the acceleration of gravity ( $9.81 \text{ m/s}^2$ ), and  $d_p$  is the diameter of the particle (m).

The buoyancy force,  $F_B$  (N), is:

$$F_B = \frac{1}{6}\pi\rho_L g d_p^3 \quad (6-4)$$

where,  $\rho_L$  is the density of water.

The lift force  $F_L$  (N) is caused by the shear flow in the immediate vicinity of the pipe wall surface and can be calculated as follows (Altmann and Ripperger, 1997):

$$F_L = 0.761 \cdot \frac{\tau_w^{1.5} \cdot d_p^3 \cdot \rho_L^{0.5}}{\eta} \quad (6-5)$$

where,  $\tau_w$  is the shear stress at the tube wall (N/m<sup>2</sup>), and  
 $\eta$  is the dynamic fluid viscosity (1.002×10<sup>-3</sup> N·s/m<sup>2</sup> at 20 °C and 0.467×10<sup>-3</sup> N·s/m<sup>2</sup> at 60 °C).

The shear stress in a pipe can be expressed in terms of the Darcy friction factor  $f$  and the mean fluid velocity  $\bar{u}$  (Littlejohn et al., 2000):

$$\tau_w = \frac{1}{8} f \rho_L \bar{u}^2 \quad (6-6)$$

Friction factor  $f$  can be estimated by Swamee-Jain equation:

$$f = \frac{0.25}{\left[ \log_{10} \left( \frac{\varepsilon}{3.7D} + \frac{5.74}{Re^{0.9}} \right) \right]^2} \quad (6-7)$$

where,  $\varepsilon$  is roughness height (m),  
 $D$  is pipe diameter, and  
 $Re$  is Reynolds number.

To simplify the calculation, it is assumed that the surface is smooth, which means that the roughness height ( $\varepsilon$ ) equals zero. The total vertical force is then calculated as:

$$F_{vertical} = F_G - F_B - F_L = \frac{1}{6} \pi (\rho_P - \rho_L) g d_p^3 - 0.761 \cdot \frac{\tau_w^{1.5} \cdot d_p^3 \cdot \rho_L^{0.5}}{\eta} \quad (6-8)$$

The above equation indicates that the occurrence of particulate fouling is mainly determined by the particle size distribution and hydrodynamic conditions. Positive  $F_{vertical}$  indicates the deposition potential of bulk precipitates while little particulate fouling is theoretically feasible in the case of negative  $F_{vertical}$ .

## 6.2.2 Results and Discussion

### 6.2.2.1 Theoretical Calculation of the Total Force

Total vertical force calculated as a function of particle size is illustrated in Figures 6.16 and 6.17. As shown in Figure 6.16, the flow velocity plays a very important role for the particles that are larger than 3  $\mu\text{m}$  at a given temperature. In addition, the total vertical force decreases from positive to negative (corresponding to change in scaling potential from positive to negative scaling tendency) with an increase in flow velocity from 0.22 to 0.88 m/s.

Figure 6.17 illustrates the impact of temperature on total vertical force at a flow rate of 1 gpm. The total vertical force is slightly higher at 60  $^{\circ}\text{C}$  compared to 20  $^{\circ}\text{C}$ . When temperature increases, the buoyancy force and gravity force do not change while the lift force varies. The dynamic viscosity decreases when temperature increases but the shear stress force also decreases due to reduction in friction factor. The overall change in lift force is small due to simultaneous decrease in dynamic viscosity and stress force. However, this slight difference may not have great influence on the scaling tendency.

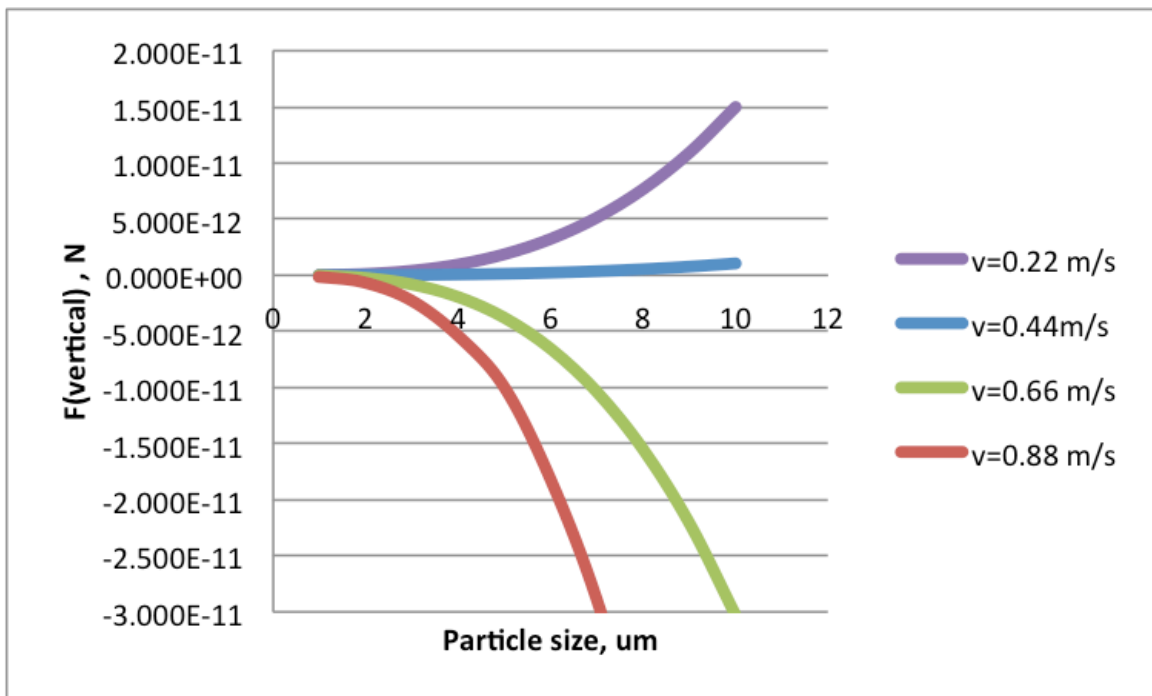
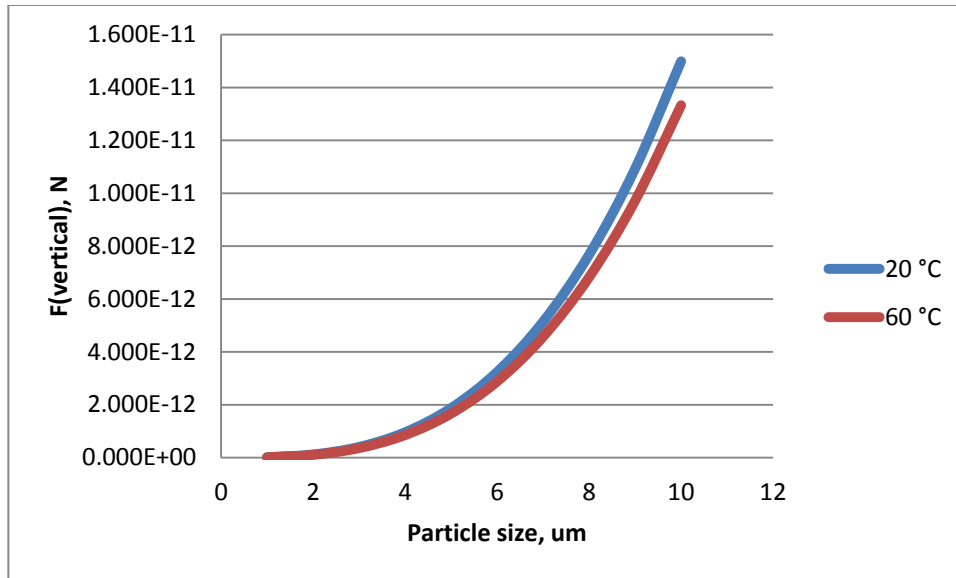


Figure 6.16 Total vertical force for different particle sizes as a function of flow velocity at 20  $^{\circ}\text{C}$



**Figure 6.17** Relationship between total vertical force and particle size at 20 and 60 °C and 1 gpm flow rate

#### 6.2.2.2 Impact of Temperature on Barite Deposition

First set of experiments was conducted using commercial barite particles at 1 and 2 gpm flowrate (average flow velocity of 0.22 and 0.44 m/s) and at two different temperatures (20 °C and 60 °C). It is important to note that commercial barite is produced by milling of the ore and has larger particle size (~7  $\mu\text{m}$ ) than freshly precipitated barite (~2  $\mu\text{m}$ ).

Mass gain on the stainless steel sampling coupons at 1 gpm flow rate (average flow velocity of 0.22 m/s) is shown in Figure 6.18, while Figure 6.19 shows the impact of flow velocity on barite deposition at 60 °C. As can be seen in Figure 6.18, barite deposition is enhanced at higher temperature. Based on theoretical calculation, the total vertical force on barite particles at flow velocity of 0.22 m/s is positive under these two conditions (20 and 60 °C). Theoretical calculation of the total vertical force (Figure 6.17) suggests that it does not change much between 20 and at 60 °C, which does not explain experimental results in Figure 6.18. The difference between the theoretical calculation and experimental result suggests that there are other reasons for the enhanced barite deposition at higher temperature. This may be due to the fact that at 60 °C the fluid is much more turbulent (i.e., higher Reynolds number at 60 °C than at 20 °C due to lower viscosity), which leads to increased collision frequency between barite particles and coupon surface. Figure 6.19 illustrates that higher flowrate (2 gpm or average flow

velocity of 0.44 m/s) results in less scaling compared to lower flowrate (1 gpm or average flow velocity of 0.22 m/s), which is consistent with theoretical calculations.

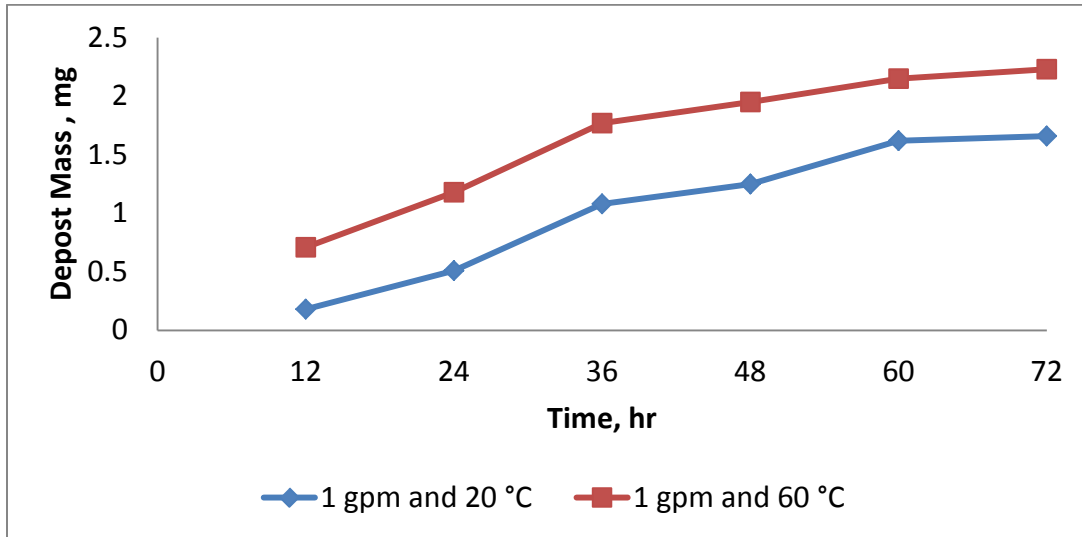


**Figure 6.18** Effect of temperature on scaling at flow rate of 1gpm

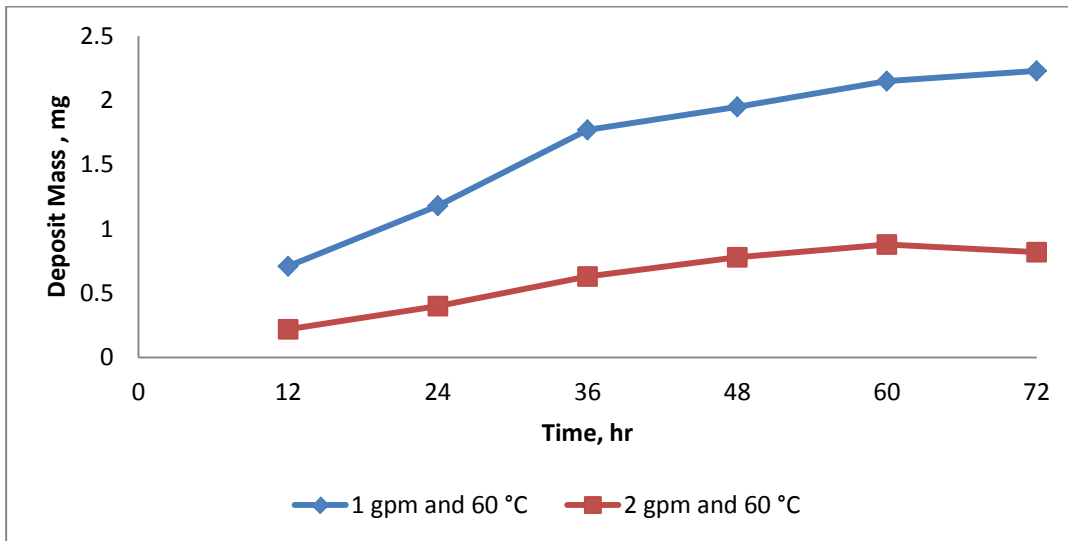


**Figure 6.19** Effect of flow rate on scaling at 60 °C

### 6.2.2.3 Deposition of Freshly Precipitated Barite in the Absence of Antiscalants

The second set of experiments was conducted by mixing sodium sulfate with barium chloride in the 2 L beaker incorporated in the system to create freshly precipitated barite prior to the initiation of the experiment. The molar ratio of Ba to  $\text{SO}_4$  was 1:1 and total chemical addition



was adjusted to achieve barite particle concentration in the system after complete reaction of 1,000 mg/L. Experiments were conducted at room temperature and at three different flow rates (i.e., 1, 2 and 4 gpm). Figure 6.20 shows that the scaling behavior at two different conditions is nearly identical at flow rates of 1 and 2 gpm. As shown in Figure 6.16 the total vertical force at average flow velocities of 0.22 and 0.44 m/s are both positive and fairly close for small barite particles (1-3  $\mu\text{m}$ ). However, when the flow rate was increased to 4 gpm, the  $\text{BaSO}_4$  deposition was reduced, which is likely due to the shift from positive to negative total vertical force acting on the small barite particles present in the system.

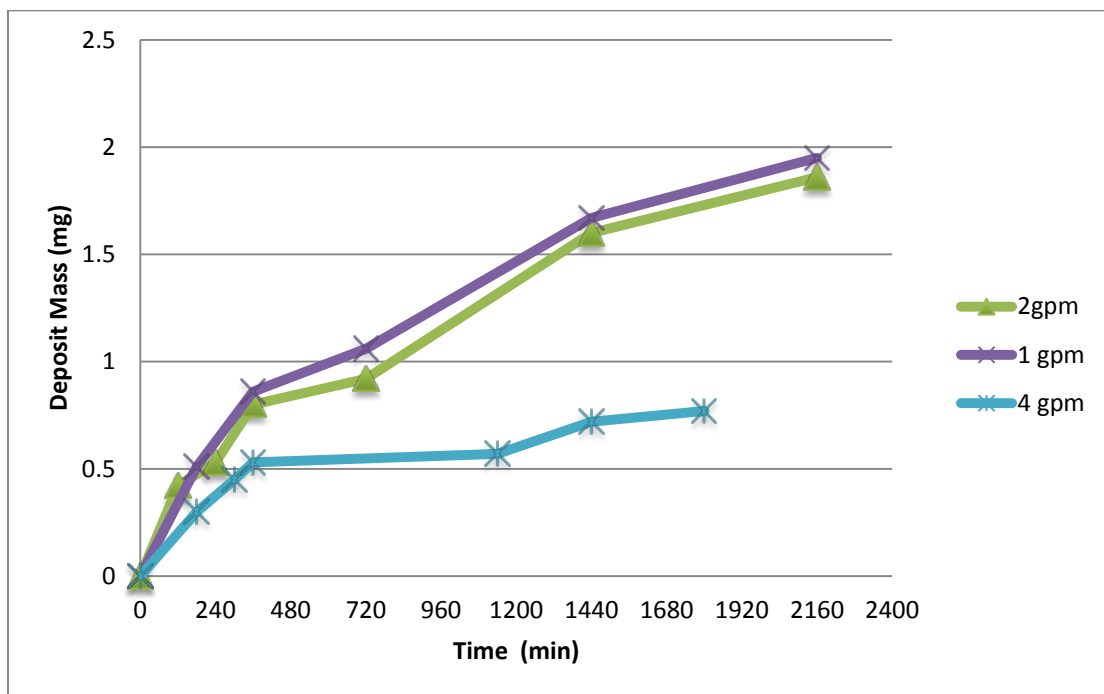


**Figure 6.20** Barite deposition at 1, 2 and 4 gpm at room temperature

#### 6.2.2.4 Deposition of Freshly Precipitated Barite in the Presence of Antiscalants

The initial experiment was conducted by adding 0.5 mL of 100 mM Ba and 0.5 mL of 100 mM  $\text{SO}_4$  to 200 mL DI water containing 20 mg/L SPPCA. During one-hour of intense mixing in the beaker, the conductivity changed very slightly, which means that all of the ions added to the solution remained dissolved and that SPPCA was successful in preventing barite precipitation. However, these experimental conditions represent very low saturation index (i.e.,  $\text{SI}=2.6$ ), which is unlikely to be encountered in flowback water reuse practice.

Since the saturation index for barite is typically higher than 3 when raw AMD is mixed with flowback water, second experiment was conducted with high barite saturation index. The second experiment was conducted by mixing 2 mM BaCl<sub>2</sub> with 2 mM Na<sub>2</sub>SO<sub>4</sub> in a 200-mL beaker. As shown in Figure 6.21, the dissolved Ba concentration was nearly identical with and without SPPCA addition (Ba concentration in solution after 5 min of mixing was slightly higher when SPPCA was added (15.3 mg/L compared with 7.1 mg/L without SPPCA)). In both cases, the reaction reached equilibrium (complete precipitation of barite) within 30 min. This result indicates that the scaling inhibitor has only limited impact on the prevention of nucleation and crystallization of barite at high saturation index.

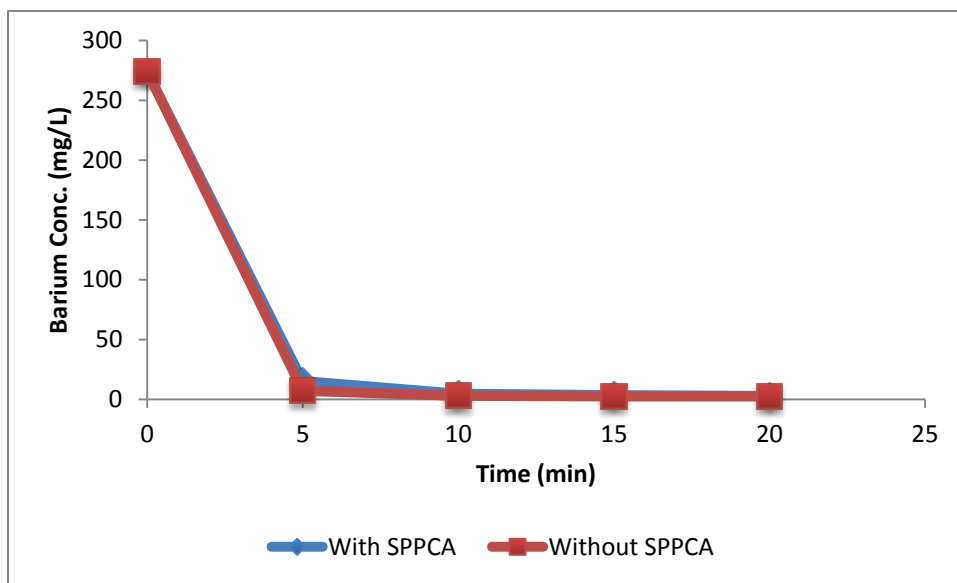


**Figure 6.21** Impact of SPPCA on Barium Precipitation

Although BaSO<sub>4</sub> precipitation cannot be inhibited by antiscalants at high supersaturation levels, it is possible that antiscalants could prevent deposition of barite particles on well casing. This possibility was studied by adding 10 mg/L of selected antiscalants to the system prior to initiating barite precipitation reactions. As shown in Figure 6.22, the BaSO<sub>4</sub> deposition on the stainless steel coupons was drastically reduced in the presence of 10 mg/L SPPCA or PMA. This result indicates that the presence of antiscalant during reaction cannot inhibit the formation of precipitates but can modify their behavior to mitigate particle attachment to stainless steel surface.

To investigate the mechanism by which these antiscalants inhibit attachment of barite to stainless steel surface, 10 mg/L of SPPCA was added to the recirculating system after the

precipitation of barite in a 2-L beaker was completed. As shown in Figure 6.23, the addition of SPPCA after the precipitation reached equilibrium does not have much impact on the  $\text{BaSO}_4$  deposition onto the stainless steel surface. This result suggests that that the main function of these antiscalants is most likely the modification of the crystals formed during precipitation reactions, which will be discussed in subsequent section.

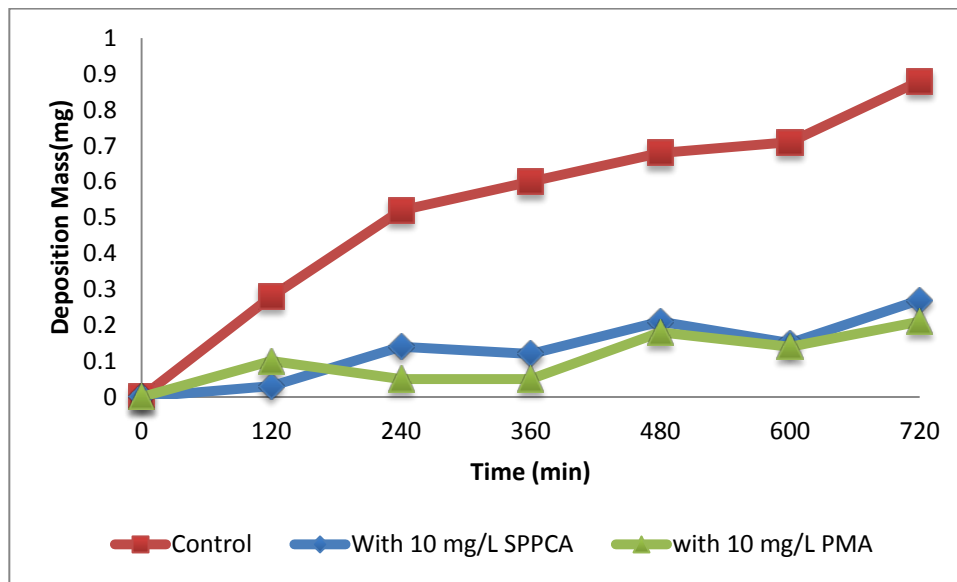


**Figure 6.22** Impact of antiscalants on the deposition of  $\text{BaSO}_4$  particles on the stainless steel surface

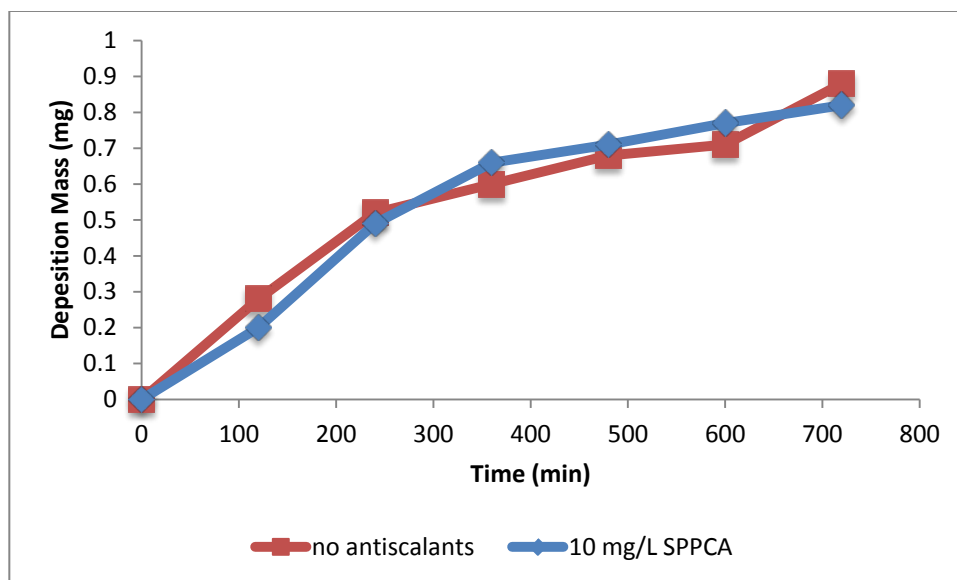


**Figure 6.23** Impact of SPPCA on the deposition of preformed BaSO<sub>4</sub> particles on the stainless steel surface

### 6.2.3 Conclusions

The affinity of BaSO<sub>4</sub> towards the attachment to well casing material was studied using a bench-scale water recirculation system. Total forces acting on the BaSO<sub>4</sub> particles were first calculated to understand the tendency of BaSO<sub>4</sub> towards deposition as a function of flow rate and particle size. It was found that the higher flow rate could partially mitigate BaSO<sub>4</sub> deposition on the stainless steel surface. Addition of antiscalants after the precipitates were formed in the system had limited impact on the scaling behavior. However, addition of antiscalants during BaSO<sub>4</sub> precipitation can significantly reduce subsequent deposition of BaSO<sub>4</sub> on stainless steel surface.

### 6.3 References

Altmann, J. and Ripperger, S. (1997) Particle deposition and layer formation at the crossflow microfiltration. *Journal of Membrane Science*, 124(1), pp.119-128.

Bergendahl, J. and Grasso, D. (2000). Prediction of colloid detachment in a model porous media: Hydrodynamics. *Chemical Engineering Science*, 55(9), 1523-1532.

Bradford, S. A., Torkzaban, S. and Walker, S. L. (2007). Coupling of physical and chemical mechanisms of colloid straining in saturated porous media. *Water Research*, 41(13), 3012-3024.

Hiemenz, P. C. and Rajagopalan, R. (1997). *Principles of Colloid and Surface Chemistry*. CRC press, 3<sup>rd</sup> edition, Boca Raton, FL.

Jones, F., Oliveira, A., Rohl, A. L., Parkinson, G. M., Ogden, M. I. and Reyhani, M. M. (2002). Investigation into the effect of phosphonate inhibitors on barium sulfate precipitation. *Journal of Crystal Growth*, 237, 424-429.

Jones, F., Richmond, W. R. and Rohl, A. L. (2006). Molecular modeling of phosphonate molecules onto barium sulfate terraced surfaces. *The Journal of Physical Chemistry B*, 110(14), 7414-7424.

Ko, C. H. and Elimelech, M. (2000). The “shadow effect” in colloid transport and deposition dynamics in granular porous media: measurements and mechanisms. *Environmental Science & Technology*, 34(17), 3681-3689.

Littlejohn, F., Grant, C.S. and Sáez, A.E. (2000) Mechanisms for the removal of calcium phosphate deposits in turbulent flow. *Industrial & Engineering Chemistry Research*, 39(4), pp.933-942.

Liu, W. (2013). Control of mineral scaling in power plant recirculating cooling systems using treated municipal wastewater (Doctoral dissertation, University of Pittsburgh).

Liu, D., Johnson, P. R. and Elimelech, M. (1995). Colloid deposition dynamics in flow-through porous media: Role of electrolyte concentration. *Environmental Science & Technology*, 29(12), 2963-2973.

Saleh, N., Kim, H. J., Phenrat, T., Matyjaszewski, K., Tilton, R. D. and Lowry, G. V. (2008). Ionic strength and composition affect the mobility of surface-modified FeO nanoparticles in water-saturated sand columns. *Environmental Science & Technology*, 42(9), 3349-3355.

Solovitch, N., Labille, J., Rose, J., Chaurand, P., Borschneck, D., Wiesner, M. R. and Bottero, J. Y. (2010). Concurrent aggregation and deposition of TiO<sub>2</sub> nanoparticles in a sandy porous media. *Environmental Science & Technology*, 44(13), 4897-4902.

Tufenkji, N. and Elimelech, E. Correlation equation for predicting single-collector efficiency in physicochemical filtration in saturated porous media. *Environmental Science & Technology* 38.2 (2004), 529-536

Van der Leeden, M. C. (1991). The role of polyelectrolytes in barium sulphate precipitation. TU Delft, Delft University of Technology.

Wan, K. W., Malgesini, B., Verpilio, I., Ferruti, P., Griffiths, P. C., Paul, A. and Duncan, R. (2004). Poly (amidoamine) salt form: effect on pH-dependent membrane activity and polymer conformation in solution. *Biomacromolecules*, 5(3), 1102-1109.

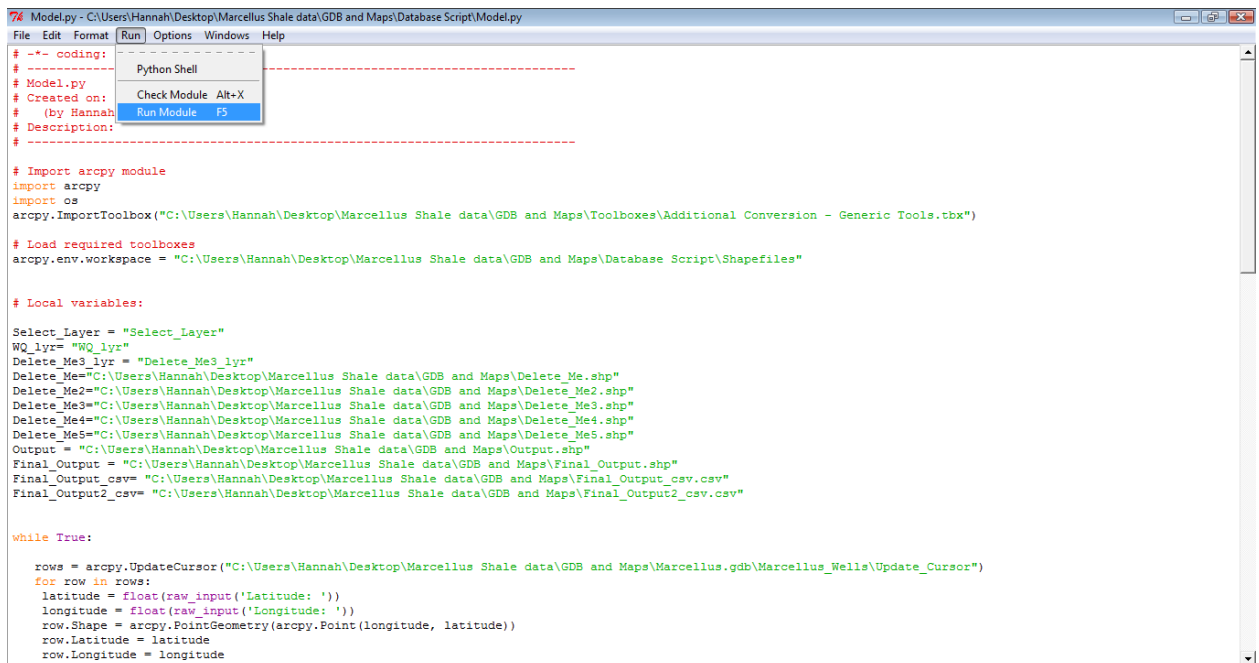
## Appendix GIS Database User Manual

### A.1 Sample Location Selection using Python Script

The following script allows the user to input a set of coordinates and find AMD sample locations from a selected database within a specified distance and with a specified flow rate. The sample locations and accompanying water quality data are exported as both an Excel file and an ArcGIS layer. ArcGIS does not need to be open to run this script.



1. Navigate to IDLE (Python GUI)
2. Once in IDLE, open Model.py at **C:\Marcellus Shale data\GDB and Maps\Database Script**
3. When Model.py has loaded, go to “Run” and select “Run Module”



```
Model.py - C:\Users\Hannah\Desktop\Marcellus Shale data\GDB and Maps\Database Script\Model.py
File Edit Format Run Options Windows Help
# -*- coding: #
# ----- Python Shell
# Model.py Check Module Alt-X
# Created on: Run Module F5
# (by Hannah)
# Description:
# -----

# Import arcpy module
import arcpy
import os
arcpy.ImportToolbox("C:\Users\Hannah\Desktop\Marcellus Shale data\GDB and Maps\Toolboxes\Additional Conversion - Generic Tools.tbx")

# Load required toolboxes
arcpy.env.workspace = "C:\Users\Hannah\Desktop\Marcellus Shale data\GDB and Maps\Database Script\Shapefiles"

# Local variables:
Select_Layer = "Select_Layer"
WQ_lyr = "WQ_lyr"
Delete_Me3_lyr = "Delete_Me3_lyr"
Delete_Me2="C:\Users\Hannah\Desktop\Marcellus Shale data\GDB and Maps\Delete_Me.shp"
Delete_Me3="C:\Users\Hannah\Desktop\Marcellus Shale data\GDB and Maps\Delete_Me2.shp"
Delete_Me4="C:\Users\Hannah\Desktop\Marcellus Shale data\GDB and Maps\Delete_Me3.shp"
Delete_Me5="C:\Users\Hannah\Desktop\Marcellus Shale data\GDB and Maps\Delete_Me4.shp"
Delete_Me6="C:\Users\Hannah\Desktop\Marcellus Shale data\GDB and Maps\Delete_Me5.shp"
Output = "C:\Users\Hannah\Desktop\Marcellus Shale data\GDB and Maps\Output.shp"
Final_Output = "C:\Users\Hannah\Desktop\Marcellus Shale data\GDB and Maps\Final_Output.shp"
Final_Output_csv= "C:\Users\Hannah\Desktop\Marcellus Shale data\GDB and Maps\Final_Output_csv.csv"
Final_Output2_csv= "C:\Users\Hannah\Desktop\Marcellus Shale data\GDB and Maps\Final_Output2_csv.csv"

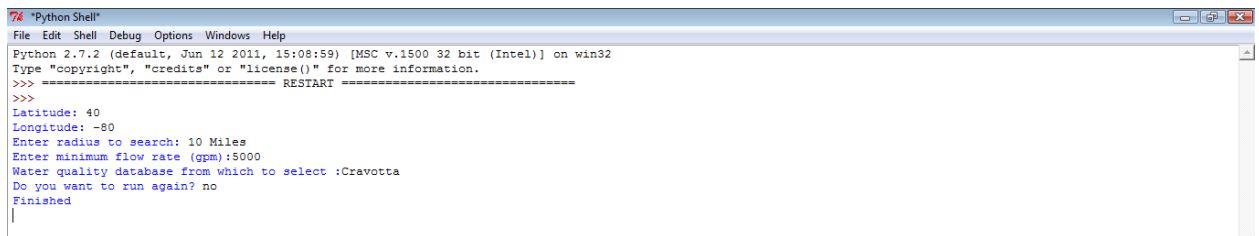
while True:

    rows = arcpy.UpdateCursor("C:\Users\Hannah\Desktop\Marcellus Shale data\GDB and Maps\Marcellus.gdb\Marcellus_Wells\Update_Cursor")
    for row in rows:
        latitude = float(raw_input('Latitude: '))
        longitude = float(raw_input('Longitude: '))
        row.Shape = arcpy.PointGeometry(arcpy.Point(longitude, latitude))
        row.Latitude = latitude
        row.Longitude = longitude
```

4. Enter latitude and longitude coordinates in decimal format (XX.XXXX), including negative signs for direction.
5. Enter the radius to search for sample locations. The distance units must also be entered, with the first letter capitalized. For example, enter 10 Miles or 1000 Meters.
6. Enter the minimum flow rate of the sample points to be returned. The function searches for flow rate in gpm, the units do not need to be entered.

7. Select water quality database:

- I. Cravotta
- II. PADEP
- III. Orphan1
- IV. Orphan2
- V. Lookenbill Iron
- VI. Lookenbill Sulfate
- VII. EPCAMR



```
Python Shell
File Edit Shell Debug Options Windows Help
Python 2.7.2 (default, Jun 12 2011, 15:08:59) [MSC v.1500 32 bit (Intel)] on win32
Type "copyright", "credits" or "license()" for more information.
>>> ----- RESTART -----
>>>
Latitude: 40
Longitude: -80
Enter radius to search: 10 Miles
Enter minimum flow rate (gpm):5000
Water quality database from which to select :Cravotta
Do you want to run again? no
Finished
|
```

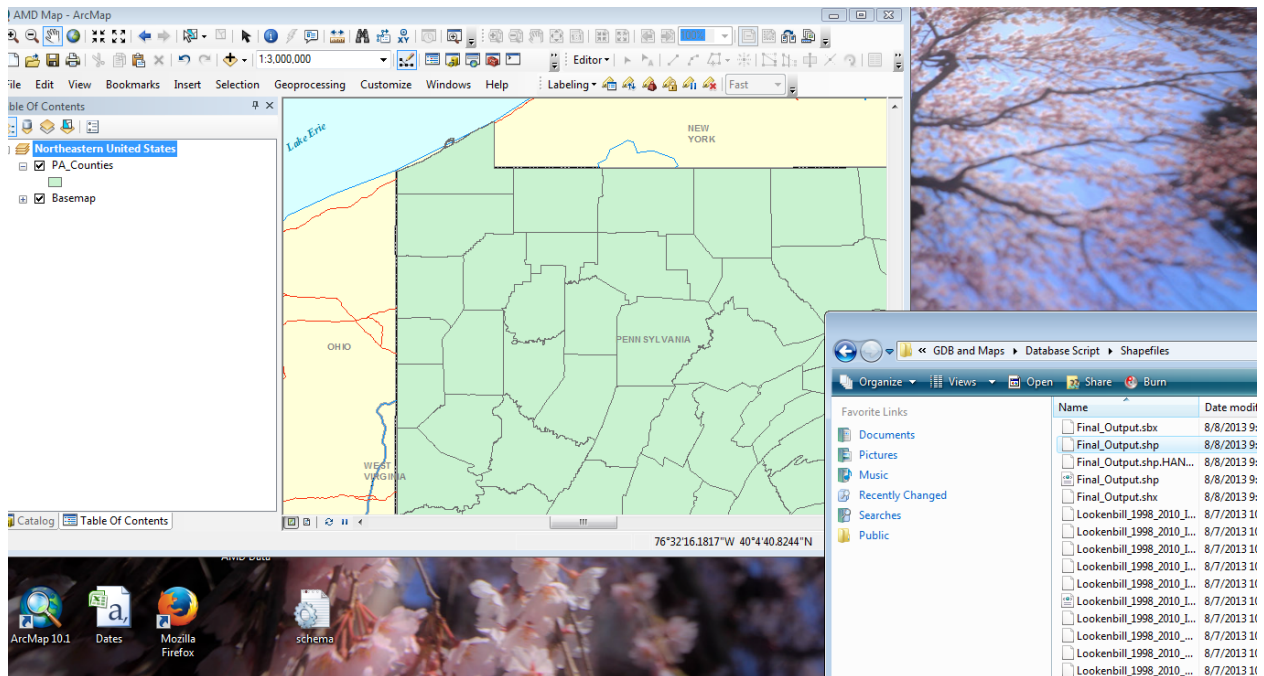
8. The resulting table is titled Final\_Output.csv and exports to C:\Marcellus Shale data\GDB and Maps\Database Script\Exports . The shapefile is called Final\_Output.shp and exports to the same location. The script runs on a loop so another database or query can be run.

## A.2 Viewing and Editing Script Export in ArcGIS

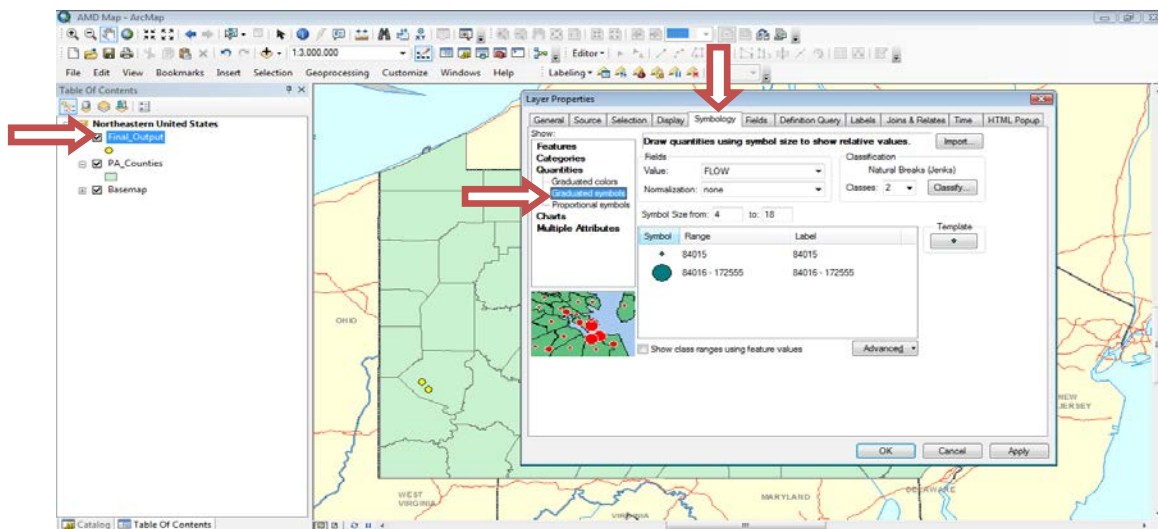
### A.2.1 Symbology

1. To view the shape file result from the script in ArcGIS, open AMD Map.mdx at C:\Marcellus Shale data\GDB and Maps and drag and drop Final\_Output.shp onto the screen.

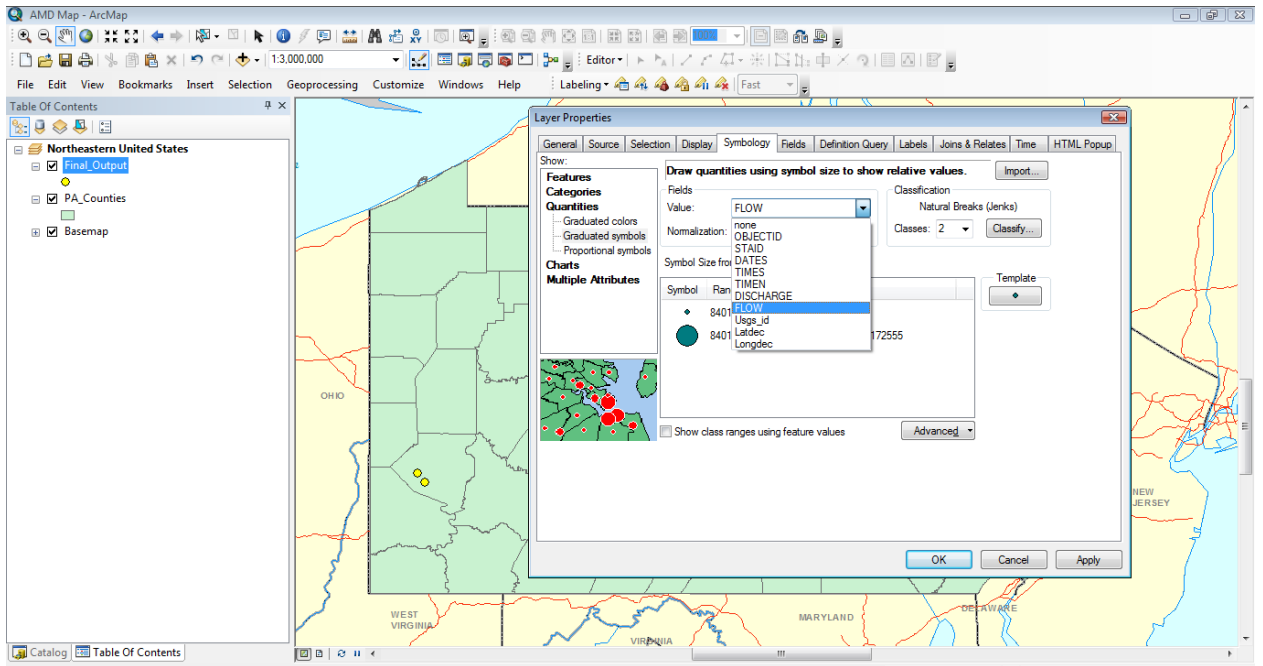




2. Right click Final\_Output in the ArcMap table of contents after dropping it onto the map. Click Properties, and go to the Symbology tab. Under “Quantities”, you can select either Graduated Colors or Graduated Symbols to change the symbology of Final\_Output based on the quantities of a particular attribute.

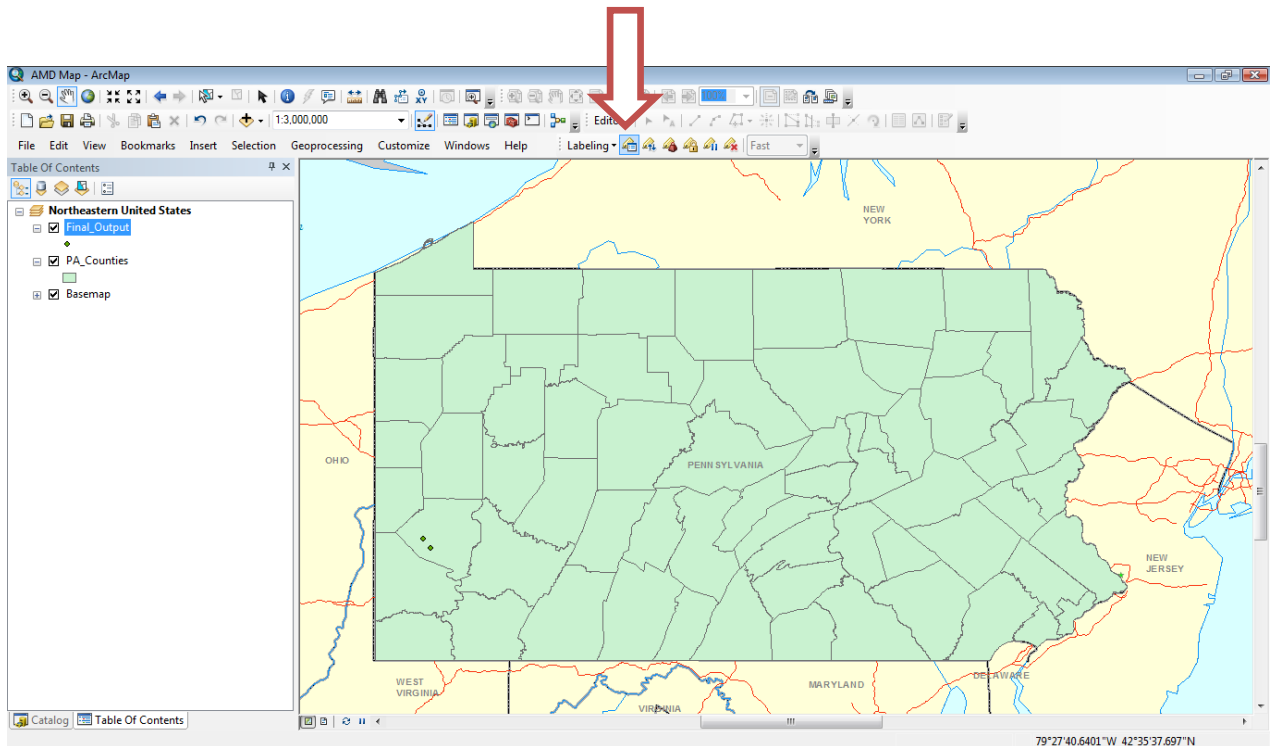


3. Next to “Value”, select the attribute to be represented on the map (flow, sulfate concentration, etc.) and hit Ok.

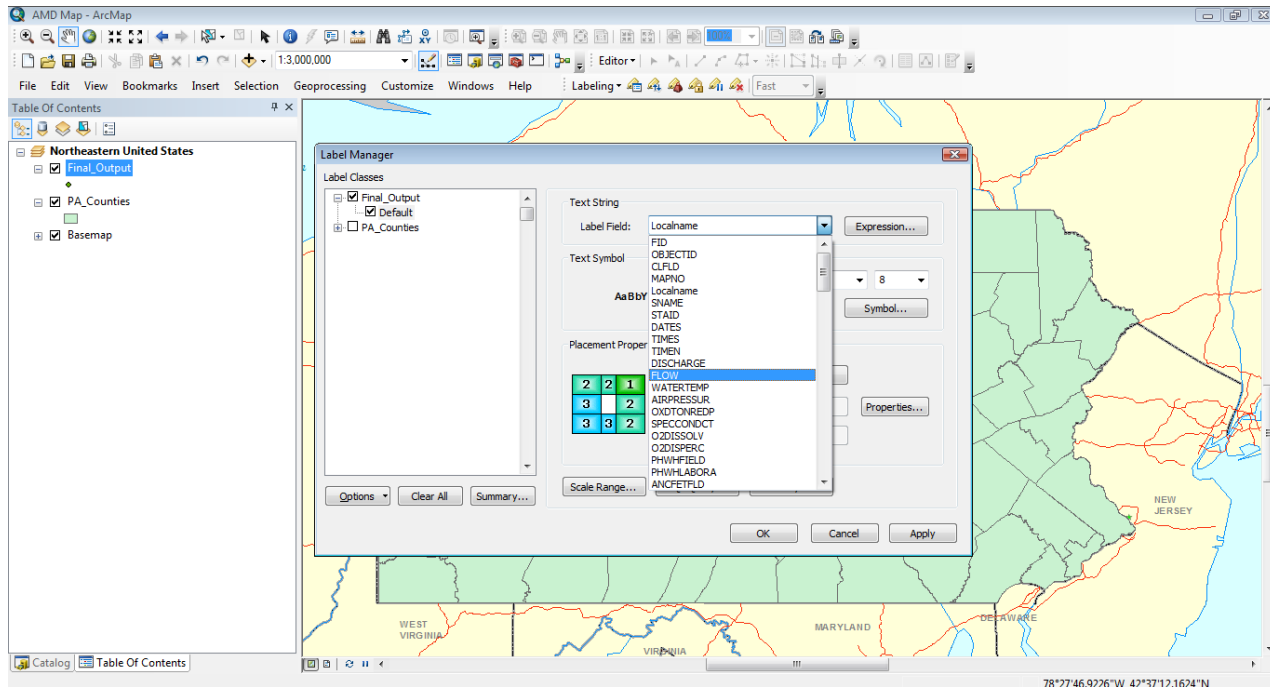


## A.2.2 Labeling

1. Select the label manager button on the toolbar



- In label manager, make sure that Final\_Output and Default are checked, and next to Label Field, select the attribute you want to label the points and hit Ok.



### A.2.3 Descriptions of Available Data

Data is organized at **C:\Marcellus Shale data\GDB and Maps\Databases (Excel Data)**. Files are saved in the format “Collector (Date)- Additional Information”. A description of how each dataset was derived or renamed from the “original” data is at **C:\Marcellus Shale data\Data Management.xls**

#### **Water Quality Databases**

##### 1. PADEP (1998-2010)- Chemical Parameters

Contains exhaustive state-wide water quality analysis of AMD sites, with 90,000+ points and 20+ collectors. Approximately one third of the data points contain information on flow rate. Acidity, Alkalinity, Aluminum, Bromide, Calcium, Carbon, Chloride, Chromium, Cobalt, Coliform, Ferrous Iron, Hardness, Lead, Total Iron, Magnesium, Manganese, Nickel, Nitrate, pH, Potassium, Sodium, Conductivity, Sulfate, TSS, and Zinc were analyzed. Data was saved in a text file rather than Excel due to the amount of data (Excel only allots 63,000 rows per sheet).

2. AMLI (XXXX)- Chemical Parameters

Only contains information on flow rate, with 3000 points and no information on date. Also indicates whether site is abandoned or reclaimed

3. Cravotta (1999)- Chemical Parameters

Contains 103 points in Western Pennsylvania, including flow rate, Aluminum, Bromide, Calcium, Chloride, Chromium, Cobalt, Iron, Hardness, Lead, Magnesium, pH, Sulfate, Conductivity, dissolve oxygen, and heavy metals

4. EPCAMR (1996)- Chemical Parameters

Contains data for Northeastern Pennsylvania with information on flow rate, pH, sulfate, and alkalinity. Layer was retrieved from Michael Hewitt (hardcoal@epcamr.org), whose contact info was found on the RAMLIS webpage. Locations were recently re-tested by a student at Lehigh University, but the data is not available yet.

5. Lookenbill (1998-2010)- Iron and Lookenbill (1998-2010)- Sulfate

Contains 9000 data points in Southwestern Pennsylvania with information on iron and sulfate concentration only

6. PADEP (2004-2006)- Orphan Mine Discharge 1

Contains 38 data points with information on flow rate, iron, sulfate, TS, and hardness.

7. PADEP (2004-2006)- Orphan Mine Discharge 2

Contains 340 data points from PADEP and USGS with information on flow rate, alkalinity, aluminum, calcium, iron, magnesium, hardness, pH, sulfate, and TSS

### ***Marcellus Shale***

1. BOGM (2008-2009)- Active Operators

Contains the location of 29 wells with fracking flowback pH, alkalinity, acidity, oil/grease, ammonia, sulfate, iron, bromide, chloride, heavy metals and hardness

2. BOGM (2008-2009)- Flowback quality, Yantko

Contains information on flowback pH, alkalinity, acidity, oil/grease, ammonia, sulfate, iron, bromide, chloride, heavy metals, and hardness, as well as inorganics, VOAs, SVOAs, GLYCOL, and RAD36.

3. Total Wells per County (2010)- BaSr, BaCl Ratios

Contains the number of drilled wells in each Pennsylvania county, along with Ba:Sr and Ba:Cl ratios and horizontal vs vertically drilled wells

4. Dan Bain (2007-2009)- Permit Status

Contains the location of all permitted wells and their status

**Miscellaneous**

1. RAMLIS (2013)- Problem Areas

Contains locations of all water sources impacted by mining with no further information

2. AMLI (2013)- AMR Funding

Contains the locations of all water sources eligible for funding under Abandoned Mine Reclamation Act, along with the funding status and funding type

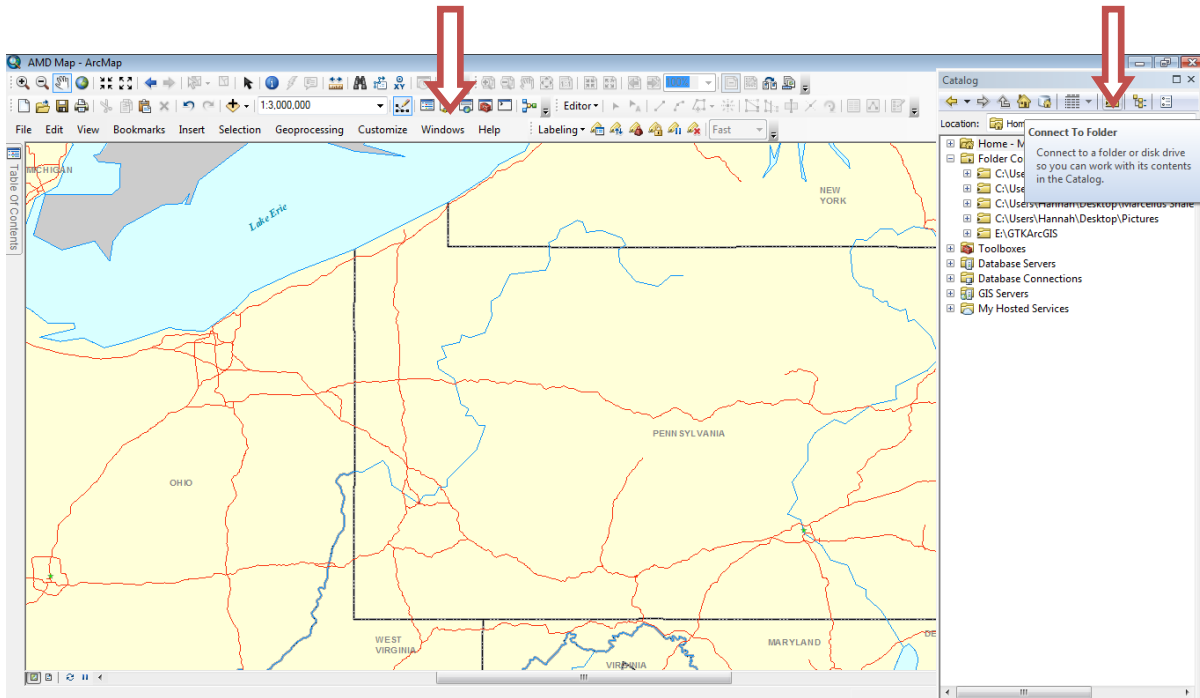
3. Coal Mining Operations (2010)

Contains the locations of all coal mining operations in Pennsylvania, as well as mine type, status, and compliance record

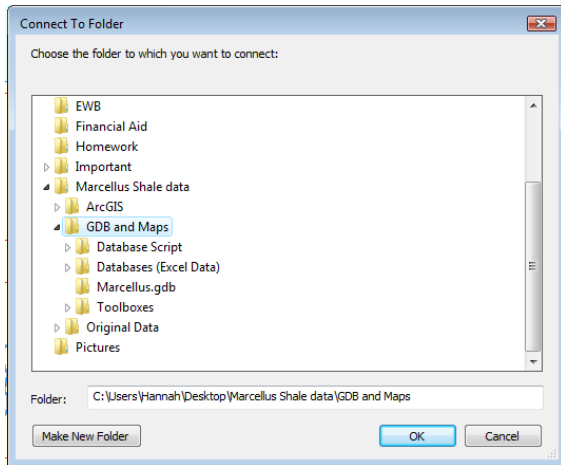
## A.2.4 Geo-database

The geodatabase contains information from all of the databases in layer format, so they can be easily dragged and dropped onto the map.

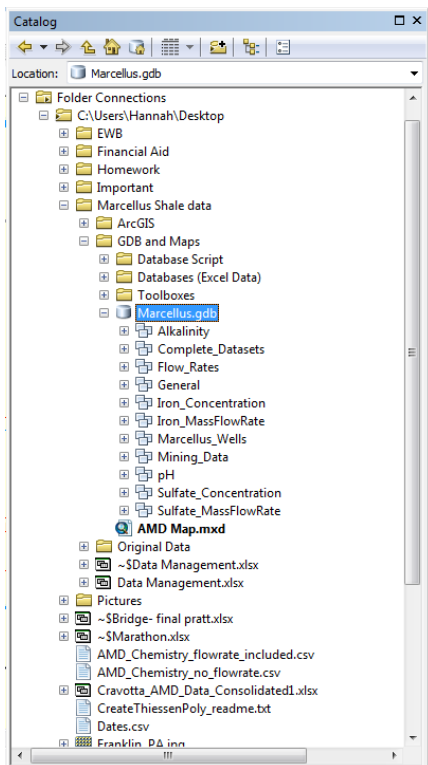
1. If the geodatabase has not been used on a particular computer yet, a folder connection needs to be made. Open ArcCatalog from the toolbar, and click “Connect to Folder” in the ArcCatalog panel.



2. When Connect to Folder opens, navigate to the folder in which the Marcellus.gdb is located, and click Ok



3. Marcellus.gdb can now be viewed in the ArcCatalog panel by navigating to it under “Folder Connections”



4. The geodatabase contains data from each of the databases in layer format, clipped to show the locations of a particular sample parameter on the map. After dragging a dropping a layer onto the map, it displays in the map's table of contents. The value of a particular attribute



(i.e. sulfate concentration, alkalinity, flow rate, etc) can be displayed using the same method described in section II.

